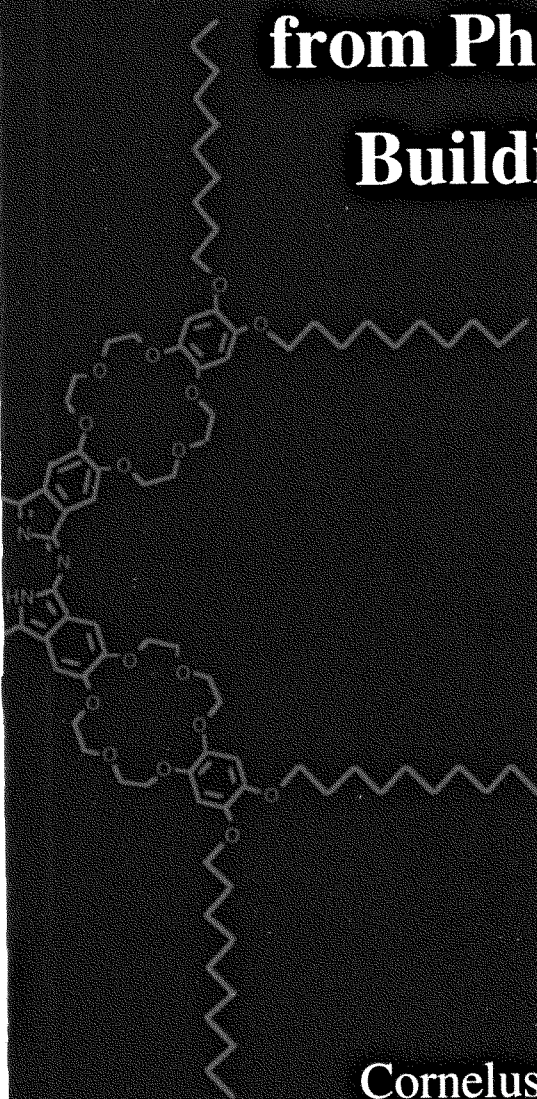


# **Supramolecular Assemblies from Phthalocyanine Building Blocks**



**Cornelus F. van Nostrum**



# **Supramolecular Assemblies from Phthalocyanine Building Blocks**

**EEN WETENSCHAPPELIJKE PROEVE OP HET GEBIED VAN DE  
NATUURWETENSCHAPPEN**

**PROEFSCHRIFT**

**TER VERKRIJGING VAN DE GRAAD VAN DOCTOR AAN DE KATHOLIEKE  
UNIVERSITEIT NIJMEGEN, VOLGENS BESLUIT VAN HET COLLEGE VAN  
DECANEN IN HET OPENBAAR TE VERDEDIGEN OP DINSDAG 21 MAART 1995,  
DES NAMIDDAGS TE 3.30 UUR PRECIES**

**DOOR**

**CORNELUS FRANCISCUS VAN NOSTRUM  
GEBOREN OP 28 MAART 1966 TE VINKEVEEN EN WAVERVEEN**

**Promotor:** Prof. Dr. R.J.M. Nolte  
**Copromotor:** Dr. A.J. Schouten (RUG)

Het onderzoek beschreven in dit proefschrift werd gefinancierd door het Innovatiegerichte Onderzoekprogramma Polymeercomposieten en Bijzondere Polymeren (IOP-PCBP) van het Ministerie van Economische Zaken (projectnummer BP-204).



## VOORWOORD

Het is mij de afgelopen jaren gebleken dat het bedrijven van fysisch-organische chemie niet kan zonder de hulp van vele personen. Er zijn bedenkers en makers nodig van nieuwe molekulen en er zijn mensen nodig voor het bestuderen van de eigenschappen van deze creaties. Allen die mij daarbij geholpen hebben, en zonder wie dit proefschrift onmogelijk tot stand kon komen, wil ik in dit voorwoord dank zeggen.

Allereerst wil ik mijn ouders bedanken. Meer dan 15 jaar geleden heb ik hen al verteld dat ik scheikunde wilde gaan "doen", en zij hebben er mede voor gezorgd dat ik vele jaren later aan de studie kon beginnen. Hun interesse in mijn promotieonderzoek heb ik altijd gewaardeerd.

Mijn promotor, Prof. R. Nolte, wil ik bedanken voor zijn inspirerende ideeën en aanstekelijke enthousiasme. Beste Roeland, ik vond het fijn dat je vrijwel altijd tijd voor me had tussen je drukke werkzaamheden door.

Onmisbaar zijn de studenten geweest, wiens resultaten een groot deel van dit boekje hebben kunnen vullen: Max Fusari, Hugo Brussaard, Peter ten Have, Tonny Bosman, Frank Benneker en Gerwin Gelinck. Daarnaast wil ik bedanken: Hendriët "biosensor" Wanders, Herbert van de Voort voor zijn scriptie en Anneke Schoneveld, die de leemte tussen mij en mijn opvolger probeert te vullen.

Dankzij mijn collega's van practicumzaal VII en omgeving heb ik altijd met plezier op het lab vertoeft. Hein Coolen, Jan van Esch, Gerben Gieling, Patricia Gosling, Rudi Hafkamp, Bert Klein Gebbink, Kees Koopal, Stan Martens, Hanny van Nunen, Joost Reek, Alan Rowan, Albert Schenning, Ruud Schuurman, Rint Sijbesma, Nico Sommerdijk, Gino van Strijdonck en Fokke Venema: allemaal bedankt. Rudi wil ik bedanken voor zijn hulp bij elektronenmicroscopie. Patricia ben ik zeer erkentelijk voor het corrigeren van het Engels. Natuurlijk mag ik Martin Feiters hier niet vergeten. Ik bedank hem voor het opnemen van de EPR-spectra, en vooral voor de experimenten die op het allerlaatste moment nog snel uitgevoerd moesten worden, maar die voor hoofdstuk 7 van wezenlijk belang bleken te zijn.

De vaste staf van ons laboratorium wil ik graag bedanken voor hun (technische) ondersteuning: Helene Amatdjais, Peter van Galen, Chris Kroon, Wim van Luyn, Pieter van der Meer, Ad Swolfs en Sandra Tijdink.

De overige mensen van de KUN die ik graag wil bedanken voor hun bijdragen aan dit onderzoek zijn: Marijn Devillers (ellipsometrie), Huub Geurts (elektronenmicroscopie) en Arno Kentgens en zijn medewerkers (vaste-stof-NMR).

Niet alleen vanuit Nijmegen kreeg ik de nodige hulp. Vanwege het multidisciplinaire karakter van het onderzoek mocht ik vaak mijn toevlucht zoeken bij andere laboratoria, wat voor de nodige afwisseling zorgde. Met plezier kijk ik terug naar de weken die ik in Groningen heb doorgebracht. Dankzij mijn collega's van de afdeling Polymeerchemie van de RUG voelde ik me daar prima thuis. Zij zorgden tevens voor verstrooiing gedurende de bezoeken aan buitenlandse congressen in Bangor (Wales) en Denver (VS). Met name wil ik de volgende personen noemen: paranimf Marcel Teerenstra, die mij altijd met raad en daad bijstond en me de beginselen van het LB-werk bijbracht; co-promotor Arend-Jan Schouten voor zijn verhelderende kijk op de resultaten; Ulrich Sohling voor zijn kritische blik op hoofdstuk 4 en zijn bereidheid röntgen-diffractie-metingen uit te voeren in Mainz; Gert Oostergetel voor het produceren van een aantal mooie elektronenmicroscopie-opnamen; en Prof. George Hadzioannou voor zijn belangstelling in ons werk en hulp bij STM-opnamen.

Een zeer prettige samenwerking had ik ook met de mensen van het IRI te Delft. De volgende personen wil ik bedanken voor hun welwillende medewerking, boeiende discussies en het veraangename van diverse IOP- en SON-bijeenkomsten: paranimf Leo Schouten, John Warman en Thijs de Haas. John wil ik nog extra bedanken voor het beoordelen van het manuscript.

Zeer dankbaar ben ik Stephen Picken (Akzo Nobel), die mij de afgelopen vier jaar vele malen op een plezierige wijze heeft geholpen met polarisatiemicroscopie en de interpretatie van röntgendiffractie-metingen (uitgevoerd door Rob van Puijenbroek - ook bedankt). Stephen ben ik tevens erkentelijk voor zijn zitting in de manuscriptcommissie.

De afdeling kristal- en structuurchemie van de Rijksuniversiteit Utrecht heb ik een aantal keren "lastig" mogen vallen met het verzoek tot opheldering van kristalstructuren. Ton Spek, Huub Kooijman en met name contactpersoon Nora Veldman dank ik hartelijk voor hun hulp en het kritisch doornemen van hoofdstuk 7. Ook uit Utrecht wil ik bedanken: Andries Meijerink (luminescentie), Erik Keegstra (DSC) en Jan Zwikker (discussies en tellen van stereoisomeren).

I am grateful to John Wright. Dear John, I enjoyed the visit during my holidays and the two weeks' stay in Canterbury. Your hospitality and unceasing

enthusiasm were very inspiring to me. I would like to thank Ann and Sally-Ann for their help and company.

Van de Technische Universiteit Delft wil ik graag Prof. J. Schoonman en Rob van Landschoot bedanken voor hun adviezen en hulp bij de impedantie-metingen die ik bij hen mocht uitvoeren. Voor het verkrijgen en het bespreken van CD-resultaten ben ik mijn dank verschuldigd aan respectievelijk Joost van Dongen (TUE) en Harry Dekkers (RUL). I would like to thank Prof. W. Ford for useful discussions and for selling me his indispensable Mac. De leden van het IOP, en met name het tweemanschap von Morgen en Wapenaar, ben ik dankbaar voor hun interesse en aanmoedigingen.

Tenslotte, maar zeker niet als minste, bedank ik Mariëlle, de steun en toeverlaat bij wie ik me altijd thuis zal blijven voelen.

# CONTENTS

## CHAPTER 1

<i>General Introduction</i>	1
1.1 Molecular materials	1
1.2 Phthalocyanines	4
1.3 Outline of this thesis	5

## CHAPTER 2

<i>Literature Survey: Supramolecular Chemistry of Phthalocyanines</i>	7
2.1 Introduction	7
2.2 Liquid-crystalline phthalocyanines	8
2.2.1 Structure and dynamics of the mesophase	8
2.2.2 Energy and charge migration	11
2.3 Crown-ether phthalocyanines	13
2.4 Phthalocyanine polymers	16
2.5 Langmuir-Blodgett films of phthalocyanines	17
2.5.1 Monolayer formation and deposition	17
2.5.2 Applications	22

## CHAPTER 3

<i>Monolayer Behavior of a Side-Chain Phthalocyaninatopolymethacrylate</i>	31
3.1 Introduction	31
3.2 Experimental section	32
3.3 Results	33
3.3.1 Monolayer properties and deposition	33
3.3.2 FT-IR spectroscopy	36
3.3.3 UV/Vis spectroscopy	39
3.3.4 Electron microscopy	39
3.3.5 Electron diffraction	40
3.3.6 Ellipsometry	42
3.4 Discussion	44

## CHAPTER 4

<i>Structure and Properties of a Chiral Liquid-Crystalline Phthalocyanine</i>	47
4.1 Introduction	47

4.2 Experimental section	48
4.3 Results	50
4.3.1 Phase behavior	50
4.3.2 Solid-state NMR	54
4.3.3 Luminescence	59
4.3.4 Microwave conductivity	62
4.3.5 Monolayers and LB films	63
4.3.6 Circular dichroism	70
4.4 Discussion	71
 <b>CHAPTER 5</b>	
<i>Synthesis and Properties of a Novel Amphotropic Phthalocyanine</i>	77
5.1 Introduction	77
5.2 Experimental section	79
5.3 Results and discussion	82
5.3.1 Synthesis	82
5.3.2 Thermotropic properties	84
5.3.3 Lyotropic properties	86
5.3.4 Monolayer properties	88
5.4 Conclusions	92
 <b>CHAPTER 6</b>	
<i>Liquid-Crystalline Crown-Ether Substituted Phthalocyanines</i>	95
6.1 Introduction	95
6.2 Experimental section	97
6.3 Results and discussion	103
6.3.1 Synthesis and characterization	103
6.3.2 Solid state and mesophase structure	107
6.3.3 Aggregation in solution: UV/Vis spectroscopy	111
6.3.4 Aggregation in solution: electron microscopy	114
6.3.5 Formation of monolayers and LB films	116
6.3.6 Binding of alkali metal ions in monolayers	119
6.4 Concluding remarks	121
 <b>CHAPTER 7</b>	
<i>Dithiacrown-ether Substituted Porphyrazines</i>	125
7.1 Introduction	125

7.2 Experimental section	126
7.3 Results	130
7.3.1 Synthesis	130
7.3.2 Single-crystal X-ray structures	131
7.3.3 Electronic absorption spectra	139
7.3.4 Electron paramagnetic resonance	144
7.4 Discussion	147
Appendix	150
 <b>CHAPTER 8</b>	
<b><i>Phthalocyanines as Gas Sensing Materials</i></b>	<b>153</b>
8.1 Introduction	153
8.2 Surface plasmon resonance	155
8.3 Experimental section	158
8.4 Characterization of the spin coated films	159
8.5 SPR results	161
8.5.1 Compound (S)-Pc(8,2) (1)	161
8.5.2 Compound (R,S)-Pc(12,3) (2)	163
8.5.3 Crown-ether phthalocyanine (3)	164
8.5.4 Crown-ether porphyrazine (4)	166
8.6 Conclusions	166
 <i>Summary</i>	<b>169</b>
 <i>Samenvatting</i>	<b>171</b>
 <i>Curriculum Vitae</i>	<b>175</b>

## *General Introduction*

### **1.1 Molecular materials**

For a long time scientists have been puzzled by the existence of order in a world that, according to classical thermodynamics, tends toward chaos. In recent decades new theories have been developed about the "spontaneous" formation of ordered structures including the concept of *self organization*. Without self organization life would be impossible. Some examples of the huge number of self-organized structures in biology are cell membranes, DNA, the photosynthetic reaction center, ion pumps, and the less known, but nevertheless illustrative example of the tobacco mosaic virus [1].

Chemists are exploring the phenomenon of self organization for practical applications. Within this context Simon introduced the term *molecular materials* some years ago [2]. Molecular materials are constituted of molecular units which can be separately synthesized and which are, in a second step, organized into some condensed phase. The first step in this sequence comprises the field of synthetic chemistry, *i.e.* the chemistry of the formation of covalent bonds, the second step is part of *supramolecular chemistry*, or the chemistry of the intermolecular (noncovalent) bond [3].

The formation of supramolecules is based on molecular recognition phenomena. These phenomena make use of molecular information such as shape, flexibility, polarizability, polarity, and the possibility of hydrogen bond formation and aromatic  $\pi$ -stacking. The strength of a noncovalent bond is a factor 10 to 1000 weaker than a covalent bond and comparable to thermal energies. Supramolecules can, therefore, only be stable if many noncovalent interactions or large interacting areas are involved. Moreover, these interactions must be stronger than interactions with solvents and energetically more favorable than the entropic advantages of dissociation.

Supramolecular chemistry can be divided into two large and partly overlapping areas. One is the area of host-guest chemistry, which involves the association

of two or more complementary molecules. The discovery of cation-binding crown ethers by Pedersen in 1967 had a great impact on host-guest chemistry [4]. Since then hundreds of receptors that can selectively bind substrate molecules have been designed and synthesized [5]. This binding, based on molecular recognition, can be followed by a chemical reaction, a transport process, or a detectable signal, *i.e.* a change in conformation or a change in electronic, ionic, or optical properties. The second area in supramolecular chemistry concerns the formation of larger molecular aggregates [2,6]. Four kinds of molecular aggregates are shown in Figure 1.1 and listed below.

I. *The solid state* is a familiar aggregation state in molecular chemistry and includes single crystals, polycrystalline materials, and amorphous states.

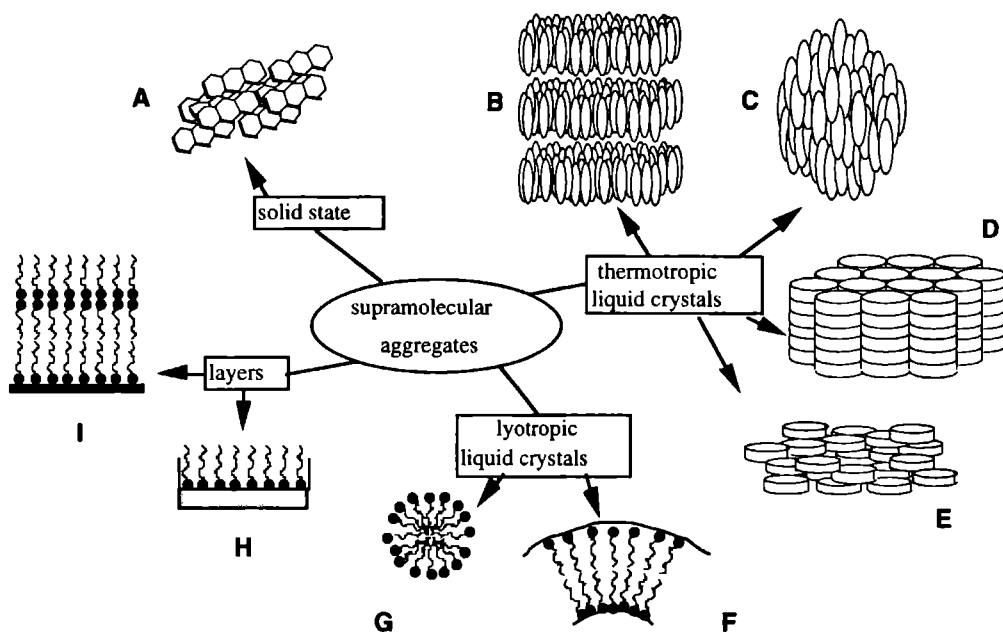


**Figure 1.1** Different types of supramolecular aggregates: crystalline phase (A); smectic mesophase (B); nematic mesophase (C); columnar mesophase (D); nematic discotic mesophase (E); bilayers and vesicles (F); micelles (G); monolayers (H); Langmuir-Blodgett multilayers (I).



II. *Thermotropic liquid crystals*. The liquid crystalline state combines the order of crystals with the fluidity of liquids. The term thermotropic indicates that the presence of a liquid crystalline phase or mesophase is dependent on the temperature. The structure of the mesophase is mainly determined by the shape of the molecule (called mesogen) and the flexibility of the substituents present. Subdivisions can be made according to the shape of the mesogen, *i.e.* rod-like or disc-like, or to the level of order: nematic for directional order but no positional order, and smectic for both directional and positional order. The smectic-analogous phase for disc-like molecules is called the columnar phase.

III. *Lyotropic liquid crystals*. This state is induced in an assembly of molecules by a solvent. Usually the building blocks are amphiphilic molecules, which consist of a soluble and an insoluble part (lyotropic mesogens). Examples of aggregates that can be formed are bilayers, micelles, and vesicles.

IV. *Monolayers at interfaces*. These are closely related to lyotropic liquid crystals, and have a great potential for molecular materials. Amphiphiles can form monolayers at an interface, usually a water surface: their polar head groups are dissolved in the aqueous phase and their apolar parts extend away from it. Monolayers can often be transferred onto a solid substrate to give well-defined multilayer structures or Langmuir-Blodgett (LB) films. Very promising in this respect are amphotropic molecules, *i.e.* molecules with lyotropic as well as thermotropic liquid crystalline behavior [6]. Certain non-amphiphilic molecules are also known to form stable, transferrable monolayers.

Currently, most of the research in molecular materials is focussed on molecular electronics, opto-electronics, and iono-electronics [3,7-11]. Molecular electronics is currently an area of intense study and includes the investigation of electronic processes in low dimensional systems (for example charge transfer salts, conducting polymers, or LB films), and the study of the electronic properties of single molecules or clusters of molecules. Devices that are a goal of this research are organic rectifiers, switches, transistors, optical memories for data storage, photodiodes, and chemical sensors. Photoinduced electron or energy transport, photoluminescence, and nonlinear optical effects are examples of the type of research in the field of molecular photonics and are extensively studied with the help of supramolecular systems [3,7]. Finally, molecular ionics is concerned with the treatment and the storage of information in which the active species is an ion

[10,12]. The disadvantage of the low mobility of ions is partly compensated by the fact that a great diversity of ions can be set in to construct a device. Examples of research topics in the area of molecular ionics are the development of switchable ion receptors (by light or electrons), ion carriers, and ion channels, often based on polyethers and crown ethers.

## 1.2 Phthalocyanines

Since the accidental discovery of a phthalocyanine (Pc) in 1907 [13], this class of compounds has been extensively studied. Pcs are structurally related to porphyrins and are highly stable, both thermally and (photo)chemically. The extended conjugated  $\pi$ -system in these molecules leads to remarkable electronic and optical properties (see next chapter) [14]. Pcs are interesting building blocks for the construction of molecular materials [9], especially liquid-crystalline (or mesomorphic) Pcs (Figure 1.2A), which were first synthesized approximately ten years ago [15]. Electron and energy transport in these systems have been extensively investigated [16,17]. With crown-ether substituted Pcs (Figure 1.2B), first synthesized by our group and independently by a Japanese and a Turkish group [18], the field of molecular ionics was also opened [10,19].

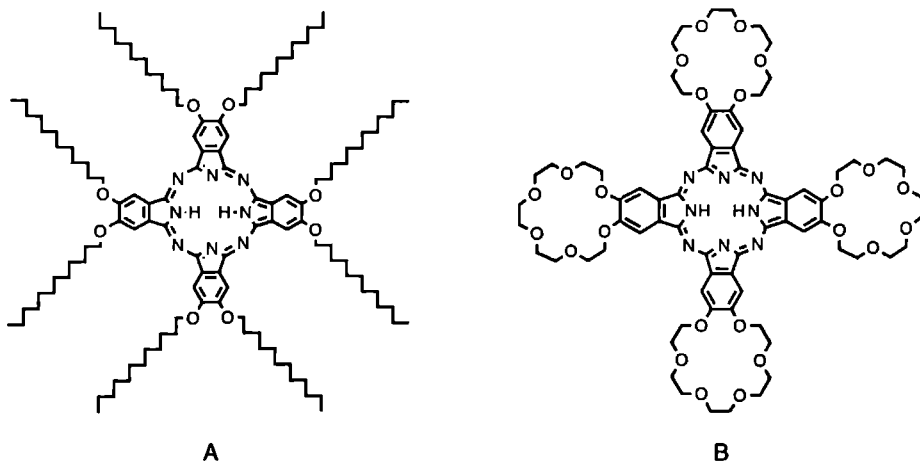


**Figure 1.2** Examples of a liquid-crystalline phthalocyanine (A) and a crown-ether substituted phthalocyanine (B).

### 1.3 Outline of this thesis

This thesis describes the synthesis of some new Pc derivatives and the organization of these molecules into supramolecular structures. In chapter 2 a literature survey is given on this subject, including LB films of phthalocyanines.

Chapter 3 describes the remarkable conformational changes that occur in a Langmuir monolayer of a Pc side chain polymer. This chapter also includes structural investigations on transferred multilayers of this polymeric Pc.

The synthesis and phase behavior of a novel chiral liquid-crystalline Pc is presented in chapter 4. X-ray diffraction studies and polarization microscopy reveal that this compound forms a so far unknown chiral discotic mesophase. Solid state NMR studies and energy and charge transport measurements have been carried out to characterize this new mesophase. The formation of highly ordered monolayers and multilayers of the chiral Pc is described. Circular dichroism experiments show that the multilayers have a chiral superstructure.

In chapter 5 the synthesis of an amphotropic Pc is presented. The thermotropic and lyotropic liquid-crystalline properties of this novel compound are described, as well as some monolayer studies.

Chapter 6 deals with the synthesis of a novel thermotropic liquid-crystalline crown-ether Pc. This compound shows a surprising aggregation behavior in chloroform. Stacks of molecular thickness and micrometer length are formed which can be seen by electron microscopy. A dihydroxysilicon derivative of this phthalocyanine can be spread on a water surface to give a stable and transferrable monolayer.

In chapter 7 a novel crown-ether substituted porphyrazine is described. The single-crystal X-ray structure and silver ion binding properties of this macrocycle are presented.

This thesis concludes with a preliminary study on the application of Pcs as gas-sensor materials.

## References

- [1] D.J. Kushner, *Bacteriological Rev.* **33** (1969) 302.
- [2] J. Simon, J.-J. André, A. Skoulios, *New J. Chem.* **10** (1986) 295.
- [3] J.-M. Lehn, *Angew. Chem.* **100** (1988) 91; *Ibid, Int. Ed. Engl.* **27** (1988) 89.
- [4] C.J. Pedersen, *J. Am. Chem. Soc.* **89** (1967) 7017.
- [5] See for example: J.L. Atwood, J.E.D. Davies, D.D. MacNicol (eds.), *Inclusion Compounds*, Volume 2; Academic Press: London (1984).
- [6] H. Ringsdorf, B. Schlarb, J. Venzmer, *Angew. Chem.* **100** (1988) 117; *Ibid, Int. Ed. Engl.* **27** (1988) 113.
- [7] J.-M. Lehn, *Angew. Chem.* **102** (1990) 1347; *Ibid, Int. Ed. Engl.* **29** (1990) 1304.
- [8] R.M. Metzger, C.A. Panetta, *New J. Chem.* **15** (1991) 209.
- [9] J. Simon, C. Sirlin, *Pure Appl. Chem.* **61** (1989) 1625.
- [10] J. Simon, M.K. Engel, C. Soulié, *New J. Chem.* **16** (1992) 287.
- [11] D. Bloor, *Mol Cryst. Liq. Cryst.* **234** (1993) 1.
- [12] T. Toupance, V. Ahsen, J. Simon, *J. Am. Chem. Soc.* **116** (1994) 5352.
- [13] A. Braun, J. Tchernivac, *Ber.* **40** (1907) 2709.
- [14] C.C. Leznoff, A.B.P. Lever (eds.), *Phthalocyanines, Properties and Applications*, Volumes 1-3; VCH: New York (1989-1993).
- [15] C. Piechocki, J. Simon, A. Skoulios, D. Guillon, P. Weber, *J. Am. Chem. Soc.* **104** (1982) 5245.
- [16] J.F. van der Pol, *thesis*, Utrecht (1990).
- [17] J. Simon, P. Bassoul, in ref. 14, Vol. 2, pp. 223-299.
- [18] (a) R. Hendriks, O.E. Sielcken, W. Drenth, R.J.M. Nolte, *J. Chem. Soc. Chem. Commun.* (1986) 1464. (b) A.R. Koray, V. Ahsen, Ö Bekâroglu, *Ibid* (1986) 932. (c) N. Kobayashi, Y. Nishiyama, *Ibid* (1986) 1462.
- [19] O.E. Sielcken, *thesis*, Utrecht (1990).

# *Literature Survey: Supramolecular Chemistry of Phthalocyanines*

## 2.1 Introduction

In the previous chapter some characteristic features of self-organization were described. Aromatic  $\pi$ -stacking was mentioned as one of the driving forces for this process. Examples of  $\pi$ - $\pi$  stacking interactions can be found in a wide variety of systems, *e.g.* in molecular crystals, DNA, proteins, and host-guest systems. Phthalocyanines (Pcs) and porphyrins owe their self-organizing properties mainly to the strong attracting forces between their aromatic rings.

Overlap between the  $\pi$ -orbitals within a stack of Pcs may result in interesting one-dimensional conducting properties [1-4], a feature that has been extensively studied since 1948 [5]. The conducting properties are usually discussed in terms of a tight-binding band model with a characteristic energy gap between extended valence and conduction bands. Good electrical conductivities are expected when a large overlap between the  $\pi$ -orbitals exists. Hunter and Sanders have used a simple model to describe  $\pi$ - $\pi$  interactions in general [6]. They concluded that van der Waals interactions are the major driving force for overlap. The geometry of the system is determined by electrostatic effects. A favorable geometry is a tilted stacking, which is found in the solid state of Pcs and porphyrins (Figure 2.1a) [7,8]. This geometry is unfavorable for obtaining good electrical conductivities. In fact, the conductivities of solid Pcs are lower than  $10^{-10} \text{ S}\cdot\text{m}^{-1}$ , which makes these molecules insulators [1]. Maximum  $\pi$ - $\pi$  overlap is achieved when the stacks are untilted (Figure 2.1b). Such a stacking is favored by van der Waals interactions and solvophobic effects [6]. The amount of  $\pi$ - $\pi$  overlap, and hence the charge-carrier mobility, depends on the staggering angle  $\phi$  [9-11].

Untilted cofacial stacks are formed when the Pcs are oxidized (*e.g.* with iodine) [12]. Electron holes which are created in this process are very mobile. Conductivities as high as  $3.10^5 \text{ S}\cdot\text{m}^{-1}$  at 55 K have been reported for Ni(Pc)I [13]. Other

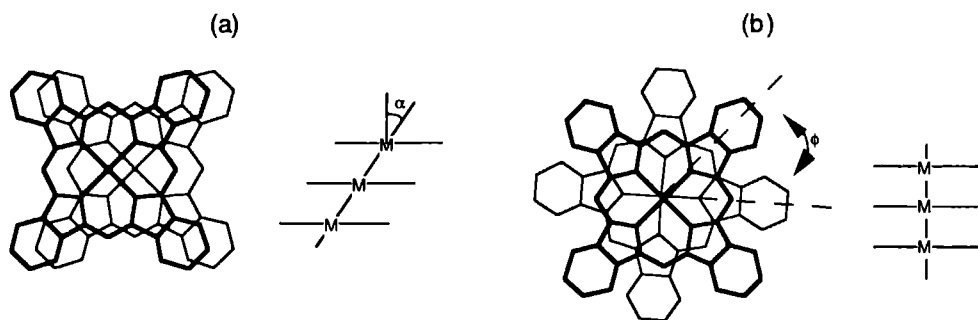


**Figure 2.1** Cofacial stacking of phthalocyanine molecules: tilted stack with tilt angle  $\alpha$  (a); untitled stack with staggering angle  $\phi$  (b).

examples of untitled Pc stacks will be discussed in the next sections. They include complexes of crown-ether Pcs, axial polymers, and mesogenic Pcs. These stacked compounds - when properly processed - are interesting building blocks for semiconducting materials. One way to realize this processing is with the help of Langmuir-Blodgett films. This will also be reviewed in this chapter.

## 2.2 Liquid-crystalline phthalocyanines

### 2.2.1 Structure and dynamics of the mesophase

Since the first discovery of a discotic liquid-crystalline phase by Chandrasekhar in 1977 [14], a large number of molecules have been reported to display this mesophase structure. Among the most studied examples are truxenes, triphenylenes, and phthalocyanines [15]. In general, molecules forming a discotic mesophase are built up from a disc-shaped rigid core which is substituted with long flexible hydrocarbon chains. The first mesogenic Pc was synthesized by Piechocki *et al.* in 1982 [16]. Since then, we and others have investigated the mesophase structure of a wide variety of Pcs and porphyrins. Some typical examples and literature references are presented in Figure 2.2.

The most investigated mesogenic Pcs are the ones that are substituted with eight linear alkyl, alkoxyethyl, or alkoxy chains at their  $\beta$ -positions. All these compounds display a transition from the solid phase to the mesophase at elevated temperatures. Powder X-ray diffraction measurements have revealed that in the

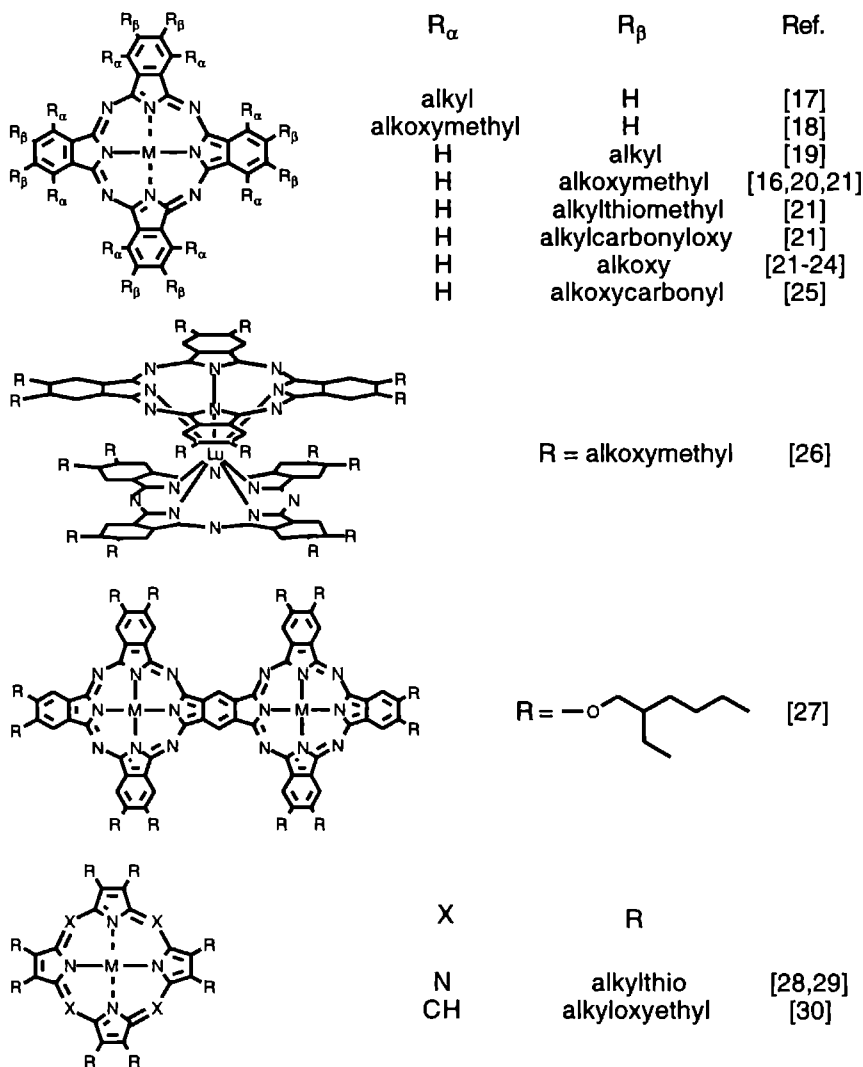
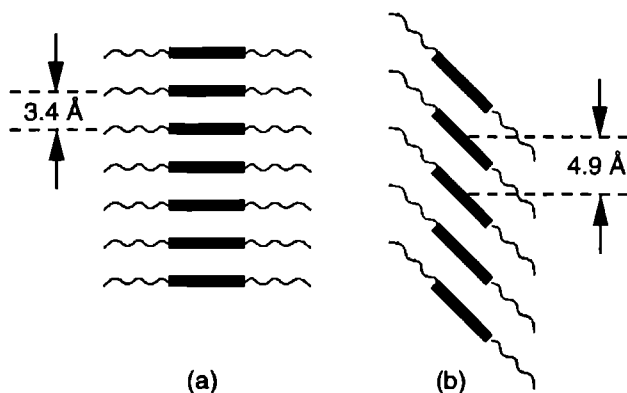


**Figure 2.2** Examples of liquid-crystalline phthalocyanines and porphyrins.

solid phase the macrocycles are stacked in columns. The Pc molecules are tilted with respect to the columnar axis and have a center to center distance along this axis of 4.3 Å [31]. In the mesophase the Pc molecules are also arranged in columns. The structure of the octaalkoxy substituted Pcs differs, however, from that of the octaalkyl and octaalkoxymethyl derivatives [19,31-33]. The planes of the former

**Figure 2.3** Schematic representation of different types of columnar mesophases:  $D_h$  phase (a);  $D_t$  phase (b).



molecules are perpendicular to the columnar axis, whereas those of the latter are not. The columns are hexagonally ordered and the Pc center to center distance is *ca* 3.4 Å. The mesophase is classified as a  $D_h$  phase (Figure 2.3a) [22,32]. The mesophase structure of the alkyl and alkoxyethyl derivatives is still a matter of discussion in the literature. The large angle X-ray reflection found at 4.9 Å has been attributed to the intracolumnar stacking period, with the molecules tilted by an angle of 46° (Figure 2.3b) [19,33–35]. More information from X-ray on aligned samples, *e.g.* as carried out on mesogenic triphenylenes and truxenes [36,37], is required to definitively establish the structure.

A characteristic change occurring at the solid to mesophase transition, which can be observed by X-ray measurements, is the melting of the hydrocarbon chains. In the solid phase a number of sharp hydrocarbon reflections are visible. In the mesophase only a very broad and diffuse reflection is present indicative of disordered aliphatic chains. The melting of the hydrocarbon chains has also been studied by temperature dependent solid state  $^{13}\text{C}$  NMR, *viz.* in the case of octaundecyloxy Pc [38]. At -70 °C broad lines in the aliphatic region of the NMR spectrum are found, which suggests that the chains are rigid. On increasing the temperature a gradual increase in side chain motion takes place as followed from the analysis of the NMR signals. At the phase transition the spectrum changes dramatically: the aliphatic region becomes well-resolved, which means that the side chains have a liquid-like order. These NMR measurements revealed another interesting feature, *viz.* that the molecules in the mesophase rotate around their columnar axes. From an analysis of the spectra an upper limit for the frequency of rotation was derived, *viz.* 6.3 kHz. Similar results were obtained from solid state NMR measurements on a mesogenic triphenylene [39].



### 2.2.2 Energy and charge migration

One-dimensional energy (exciton) migration in mesogenic Pcs has been studied by different groups. Excitation of metal-free Pc by absorption of light was found to be followed by luminescence at higher wavelengths [40-42]. This luminescence can be quenched by impurities, for example copper-Pc. It has been calculated that at room temperature the exciton migration length is in the order of a micrometer [41,42]. A large decrease in luminescence intensity was found to take place at the solid to mesophase transition for both alkoxyethyl [40,42] and alkoxy [41] Pcs. This was explained from the fact that in the mesophase energy migration is more efficient.

Charge carriers, *i.e.* free electrons and holes, in Pcs can be generated in different ways: thermally (intrinsic), chemically by doping (extrinsic), photochemically, or by high energy electron irradiation. Charge-carrier transport has been studied by dc, ac, and the time-resolved microwave conductivity (TRMC) techniques. Pure, undoped metal-free alkoxy and alkoxyethyl Pcs are insulators when measured by ac at low frequencies because the rate of charge migration is then limited by domain boundary effects [43]. At higher frequencies ( $\omega > 100$  Hz) the conductivity follows the relationship  $\sigma(\omega) = A(T)\omega^{n(T)}$ , where  $T$  is the temperature. For alkoxy Pcs in the mesophase  $n(T)$  is 0.5, whereas for alkoxyethyl Pcs this value amounts to 0.8. It has been proposed that  $n(T)$  is related to the degree of order within the columns [43]. For octadecyloxy Pc a slight decrease in ac conductivity was observed at the solid to mesophase transition ( $T = 83$  °C) [22]. The conductivity of this compound at 175 °C is in the same range as that of the unsubstituted Pc at this temperature, *i.e.*  $7 \times 10^{-8}$  S·m<sup>-1</sup>. However, the activation energy of conduction is much lower (0.5 eV) for the former compound than for the latter (1.4 eV), which may be related to the fact that the extent of  $\pi$ - $\pi$  overlap in the stacks of the two compounds is different. Doping with iodine increases the ac conductivity of octadecyloxy Pc by five orders of magnitude [22].

Bis(phthalocyaninato)lutetium (Pc<sub>2</sub>Lu) is a real intrinsic semiconductor, as a consequence of its free-radical nature [44]. Undoped single-crystals of Pc<sub>2</sub>Lu show a room temperature conductivity of  $6 \times 10^{-3}$  S·m<sup>-1</sup>. The conductivity of the mesogenic octasubstituted analogue (see Figure 2.2 for the structural formula) is much lower, due to a lower amount of intrinsic charge carriers [43,45,46]. It was found that the ac conductivity of the latter Pc increases at the solid to mesophase transition and also at the mesophase to isotropic phase transition. This is in contrast with the behavior of the above-mentioned substituted metal-free Pcs.

An interesting and useful tool to obtain information about intra- and intercolumnar charge transport is the TRMC technique, which makes use of high microwave frequencies (about 30 MHz) to monitor the conductivity in a material. These high frequencies have certain advantages [47,48] as no field-induced drift of charge carriers to domain boundaries or polarization of the sample takes place. Moreover, the TRMC technique is a contactless method and therefore excludes electrode interface effects.

The dark (background) microwave conductivity of alkoxy Pcs shows a sudden increase at the solid to mesophase transition [49]. This effect was initially attributed to an improved  $\pi$ -stacking of the Pc molecules in the mesophase, but was later explained in terms of a dipolar relaxation mechanism related to the increased motion of the ether linkage in the side chains of the Pcs [50].

Chemical doping is commonly used to increase the number of charge carriers in a material, but this process is often accompanied with structural changes [2]. To overcome this problem the pulse-radiolysis (PR) TRMC technique was developed [51,52]. Ionization with short (nanosecond) pulses of high energy electrons is used to create charge carriers in the bulk material. Microwaves are then applied to monitor the change in conductivity of the medium. In the case of octaalkoxy Pcs the so-called end-of-pulse conductivity decreases sharply at the solid to mesophase transition [51]. This effect was explained from an increase of the molecular motion in the mesophase, which more than counteracted the *a priori* expected increase in charge migration due to the better  $\pi$ - $\pi$  overlap between the Pc rings. At the mesophase to isotropic phase transition the conductivity drops to zero, supporting the idea that a columnar structure is necessary for charge transport [52]. In the PR-TRMC experiments the conductivity decays after the pulse with high energy electrons [51-53]. From the observation that the lifetime of the conductivity transients is exponentially dependent on the length of the alkoxy side chains it was concluded that intercolumnar charge transport occurs, probably via a tunneling mechanism through the hydrocarbon mantles.

A number of applications of mesomorphic Pc and porphyrin materials have been suggested, based on the anisotropic properties of the materials [54]. Worth mentioning are the interesting photovoltaic effects observed with photoconductive liquid-crystalline porphyrins [55,56].

## 2.3 Crown-ether phthalocyanines

In this section we will present a short summary of the initial studies of Sielcken *et al.* and some other groups on crown-ether phthalocyanines, and a review of new structures that have been synthesized more recently. A comprehensive review of this type of compounds has been published in the literature [57].

Porphyrins containing pendant crown-ether macrocycles have been described by Thanabal [58] and by Kobayashi [59]. Pcs  $\beta$ -substituted with four oxacrown-ether rings (Figure 2.4-A) were reported independently by the groups of Nolte [60], Bekâroglu [61], and Kobayashi [62]. These phthalocyanines display solvent and metal-salt induced aggregation behavior [63-65]. Complexes of crown-ether Pcs with different alkali metal picrates have been isolated and studied by Sielcken *et al.* [66]. These materials consist of untitled stacks of eclipsed Pc molecules (Figure 2.5). With barium picrate non-cofacial aggregates are formed [67]. The conductivities of the complexes were measured by ac impedance spectroscopy [66-68]. The electrical conductivities of the  $K^+$ ,  $Rb^+$ , and  $Cs^+$  complexes of 18-crown-6 Pc were two to three orders of magnitude higher than that of the free host. A further increase was observed on doping with iodine. The conductivity of the  $Ba^{2+}$  complex was found to be much lower than the conductivities of the other complexes, which is in agreement with the non-cofacial structure of the former compound.

A 15-crown-5-lutetium Pc-dimer has been synthesized [69] and its electrochemistry studied [70]. When in contact with an aqueous solution containing a  $K^+$  or  $Na^+$  electrolyte, this compound shows both a reversible one electron reduction and an one electron oxidation, unlike other lutetium diphthalocyanines. A positive cooperative binding effect was observed when  $Rb^+$  was complexed to  $(18\text{-crown-6 Pc})_2Lu$ . Such a cooperativity has been suggested to be an important step towards the realization of a neural network and molecular switches [71]. Recently, a lutetium Pc-dimer radical has been synthesized, in which one of the Pc units is substituted with four 15-crown-5 rings. This molecule dimerizes in the presence of  $K^+$  ions to form a tetrameric phthalocyanine [72], which was demonstrated to possess a biradical state.

Other crown-ether substituted Pcs that have been published in recent years, are summarized in Figure 2.4. Several thiacrown-ether (Figure 2.4-B) and azacrown-ether Pcs (Figure 2.4-C) were synthesized by the group of Bekâroglu [73-77]. The solubility of the former compounds in organic solvents is low [77]. The azacrown derivatives can be made water soluble by quaternarization of the

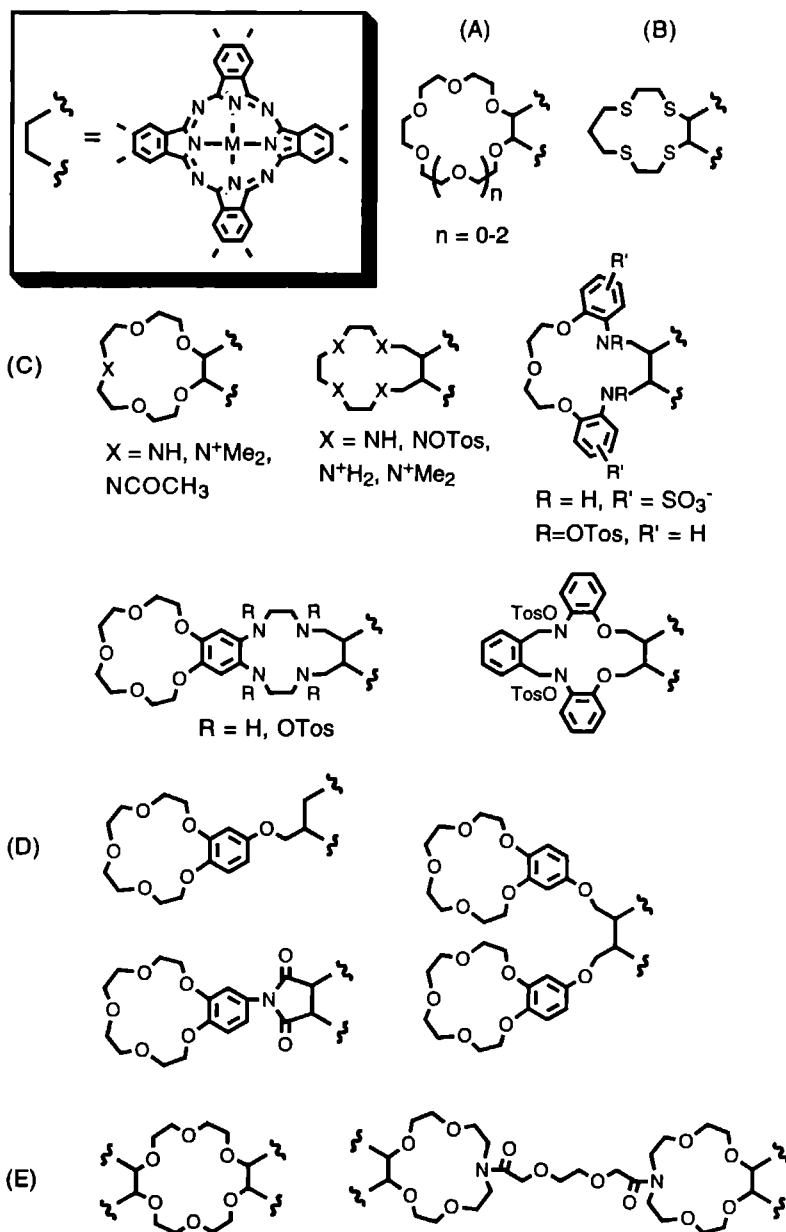
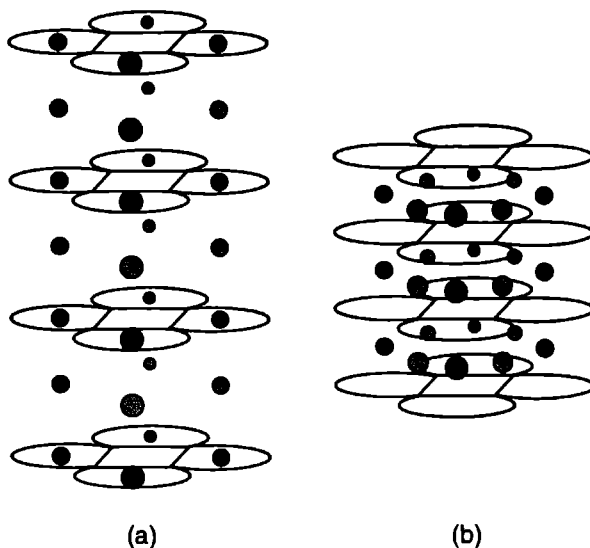


**Figure 2.4** Crown-ether substituted Pcs: oxacrowns (A); thiocrowns (B); azacrowns (C); flexibly connected crowns (D); lateral network polymers (E).

**Figure 2.5** Schematic representation of the complexes of 18-crown-6 Pc with  $K^+$  picrate (a) and with  $Rb^+$  and  $Cs^+$  picrate (b). The filled circles are the cations and the dotted circles the picrate anions.



nitrogen atoms. With the latter compounds it is possible to complex transition-metal ions like  $Co^{2+}$ ,  $Ni^{2+}$ ,  $Cu^{2+}$ , and  $Zn^{2+}$  [75]. The electrical properties of these complexes have been reported [74,78,79]. The dc conductivities in vacuum are rather low ( $10^{-10}$  -  $10^{-12}$  S·m $^{-1}$ ) but can be increased 10 to 1000× by doping, or by complexation of cations. Ac measurements suggest that the electron conduction proceeds by a hopping mechanism. Other compounds that have been synthesized by Bekâroglu's group are asymmetrical Pcs with single oxacrown- or azacrown-ether units [80], and two different lateral network polymers (Figure 2.4-E) [81-83]. An asymmetrical Pc substituted with three crown-ether rings has been synthesized by Simon and coworkers [84].

Most Pcs reported in the literature have their crown-ether rings directly attached to the  $\beta$ -positions of the macrocycles. Some examples are known where the crown-ether rings are connected to the Pc cores by flexible bridges (Figure 2.4-D) [85-87]. Except for the compound with eight crown-ether units per molecule, these phthalocyanines show metal-salt induced aggregation.

Only a few applications of crown-ether Pcs have been described so far in the literature. Ion selective membranes have been constructed from 15-crown-5 Pc [88]. Ion conducting channels present in crown-ether Pc polysiloxanes (see next section) may lead to interesting future applications, as may crown-ether Pcs in iono-electronic devices [89]. Very promising is the use of crown-ether Pcs in gas sensors, which will be discussed in Chapter 8 of this thesis.

## 2.4 Phthalocyanine polymers

A third way to achieve an untilted stacked arrangement of Pcs is by linking the central metal atoms M via bridging groups L (Figure 2.6). This method was first described by Kenney in 1962 [90]. He prepared a polysiloxane from a dihydroxysilicon Pc by a polycondensation reaction. In subsequent years a large number of unsubstituted Pc polymers have been prepared with different metal atoms M and different bridging ligands L. The molecular structures and electrical conductivities of these materials have been thoroughly investigated [3,91,92]. An iron Pc polymer with tetrazine as axial bridging ligand was reported to display an intrinsic conductivity as high as  $2 \text{ S} \cdot \text{m}^{-1}$  [93].

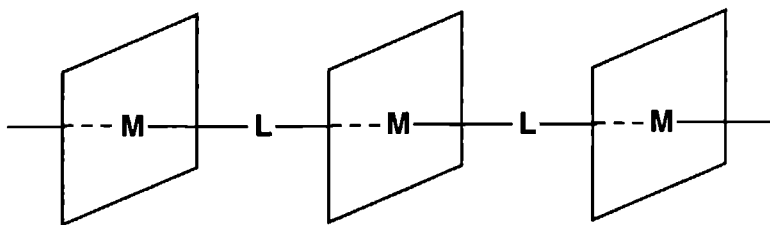


**Figure 2.6** Schematic representation of a linear chain of bridged phthalocyanines.

The unsubstituted Pc polymers are highly insoluble. Substitution of the Pc units increases, however, the solubility in organic solvents. Liquid-crystalline dihydroxysilicon and dihydroxytin Pcs, substituted with eight hydrocarbon chains, have been synthesized and polymerized [94-96] to high molecular weight polymers (degree of polymerization up to 100), which are soluble in organic solvents. X-ray investigations revealed that the structure of these polymers is similar to that of the metal-free Pcs in their mesophase, *viz.* a hexagonal arrangement of columns and an intracolumnar distance of  $3.4 \text{ \AA}$  [96,97]. Depending on the alkoxychain length the polysiloxanes display several phase transitions [97]. Those containing eight or less carbon atoms per side chain possess only a solid phase. The polymers with 8-12 carbon atoms in their side chains form columnar mesophases, while those with 16 or more carbon atoms yield isotropic phases at high temperatures. Solid-state NMR studies have been performed to obtain more insight into the temperature dependent molecular dynamics of these polymers [38,98]. With increasing temperature a gradual increase in the side chain motion is observed. Each of the Pc units rotates independently around the columnar axis. These rotations involve  $90^\circ$  jumps.

Energy migration in the octaalkoxy Pc-polysiloxanes appears to be very efficient as was concluded from the complete absence of luminescence down to 4 K [96]. The ac conductivity of the polymers was estimated to be in the order of  $10^{-8}$  S·m<sup>-1</sup> [99]. Pulse radiolysis TRMC measurements showed no abrupt changes in the end-of-pulse conductivity as observed in the case of the metal-free monomers (Section 2.2). Instead, a gradual increase of the conductivity with increasing temperature was found up to the same value as that of the monomer in the mesophase [51]. These results are consistent with an untilted stacking arrangement of the Pc units in the polymer over a wide temperature range.

Pc-polysiloxanes containing crown-ether substituents have been prepared by Sielcken *et al.* [100]. The degree of polymerization of the compounds was found to be rather low, *i.e.* between 6 and 18, depending on the size of the crown-ether rings. The dimeric and trimeric products are soluble in organic solvents and appeared to bind alkali metal ions. The electronic ac conductivities are of the order of  $10^{-8}$  S·m<sup>-1</sup> with activation energies of *ca.* 0.3 eV. The 21-crown-7 substituted polymer was shown to conduct sodium ions.

Two lateral network polymers containing crown-ether Pcs were mentioned in the previous section. A three-dimensional network polymer from a mesogenic Pc has been described by our group [101]: radical polymerization in the mesophases of a Pc substituted with eight alkoxy chains terminating in acryloyl functions, resulted in a network that retained the mesophase structure at room temperature. The intracolumnar energy migration in the network was found to be very efficient, just as in the case of the above-mentioned polysiloxanes. An ac conductivity of  $10^{-5}$  S·m<sup>-1</sup> at 175 °C and an activation energy of 0.4 eV was measured for this polymer. A side chain polymer containing mesogenic Pc units has also been reported (see chapter 3).

## 2.5 Langmuir-Blodgett films of phthalocyanines

### 2.5.1 Monolayer formation and deposition

Ordered monolayers can be formed by self-organization of amphiphilic molecules at an air-water interface. Film deposition is possible by first spreading the amphiphile onto the water surface, compressing the molecules into a condensed Langmuir monolayer, and successively transferring the film onto a substrate by vertical or horizontal dipping [102]. Three types of deposition are

possible: (i) Y-type when the deposition takes place during both upstroke and downstroke dipping, (ii) Z-type when this only occurs during upstroke dipping, and (iii) X-type when it only takes place during downstroke dipping. The resulting so-called Langmuir-Blodgett (LB) multilayers are characterized by the fact that they have a molecularly defined thickness and an anisotropic arrangement of the amphiphilic molecules. LB films can also be prepared from molecules which do not have amphiphilic properties, *e.g.* triphenylenes, porphyrins, and Pcs. The Pcs that have been described in the literature can be divided into five classes.

(i) *Unsubstituted Pcs*

The first experiments with Pc monolayers were carried out in 1937 and involved an unsubstituted magnesium Pc, but these monolayers turned out to be unstable [103]. Almost half a century later Baker *et al.* reported that stable but non-monomolecular films could be prepared from dilithium Pc [104]. In general, unsubstituted Pcs are not very suitable to construct LB films because the molecules have poor solubilities and aggregate strongly. In addition the monolayers are usually very rigid, which is unfavorable for deposition [104-106].

(ii) *Nonmesogenic substituted Pcs*

To overcome the solubility problems, substituted Pcs have been applied to form LB films, *e.g.* tetra-*tert*-butyl substituted metal-free Pc [104]. A monolayer of this compound was found to be less rigid than that of the unsubstituted phthalocyanine and gave a uniform Z-type transfer onto substrates. Since then many reports have been published dealing with LB-films of metallated or metal-free *t*-Bu Pcs. These Pc molecules were shown to be stacked in crystalline domains, which are disorderly arranged [107], but in some cases a preferred orientation of the stacks parallel to the dipping direction has been observed [108]. In general, the molecular planes are oriented almost perpendicularly to the substrate surface [108a,109]. Reports on the orientation of the Pb phthalocyanine derivative are contradictory. Both a perpendicular [110] and a parallel orientation [107] have been suggested in the literature. Different orientations, depending on the stearic acid content of the monolayer, have been reported for a triaza analogue of *t*-Bu Pc [111]

Other Pcs frequently used for LB-film preparation possess four ether-linked substituents. Examples are tetraphenoxy [112], tetra(alkylphenoxy) [113,114], tetra(cumylphenoxy) [110,112,113,115-118], and tetraalkoxy [110,112,119-121] Pcs. In some cases long-chain alcohols, carboxylic acids, or amides are added to improve the deposition. Cumylphenoxy Pc forms stacked multilayers at the air-water



interface. In most cases the molecules are oriented perpendicularly to the substrate surface, usually with a small tilt angle. Sometimes the suggested orientations are contradictory, *e.g.* in the case of cumylphenoxy Pc for which both parallel [112,118] and approximately perpendicular [116,117] orientations have been reported.

The majority of the Pcs used for LB film formation are substituted at their  $\beta$ -positions. LB-films from  $\alpha$ -substituted Pcs have also been prepared. Good results have been obtained with  $\alpha$ -octaalkoxy Pcs [122] and asymmetrically substituted Pcs [123-127] (Figure 2.7). The latter compounds contain carboxylic acid functions or hydroxyl groups at the end of two side chains, which gives the molecules more amphiphilic character. Uniform films are obtained with Y-type deposition. The carboxylic acid derivatives [125] and the isopentyloxy substituted compounds [127] give the highest degree of film organization. The Pc molecules are stacked in columns and aligned predominantly along the dipping direction. When heated, the crystalline films reorganize to yield a more compact multilayer structure. This reorganization is accompanied by a change from a herringbone stacking arrangement to an arrangement in which the Pcs are organized in cofacial stacks, which have a hexagonal pattern [124]. Remarkably, such a reorganization does not take place in the bulk material [128].

An even higher degree of organization has been achieved with Pcs substituted with two, four or eight alkoxy carbonyl side chains [129-132]. Via a Y-type deposition process films are obtained in which the molecular planes are oriented nearly perpendicularly to the substrate surface. The in-plane anisotropy is very high, as was evidenced by polarized UV/Vis spectroscopy, where dichroic ratios of 6-8 were measured. By thermal annealing this ratio could be further increased to 16 [130].

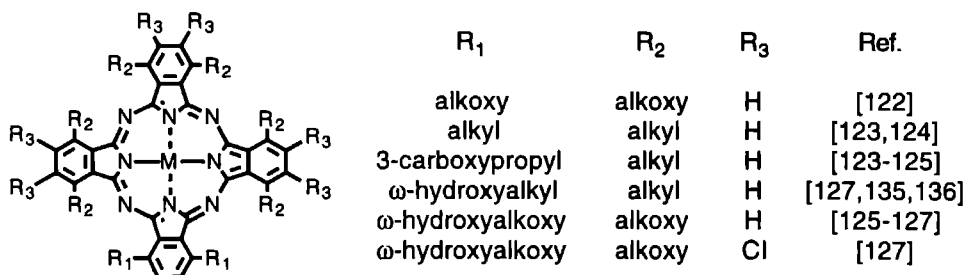


**Figure 2.7** Chemical structure of the symmetrically and asymmetrically  $\alpha$ -substituted Pcs used in LB-films.

## (iii) Mesogenic Pcs

It has been recognized that amphotropic molecules, *i.e.* molecules with both amphiphilic and thermotropic mesogenic properties, might be very suitable for the construction of stable and well-organized LB-films [133]. In view of this, discotic liquid crystals may be interesting as well [134]. In principle, a discotic liquid-crystalline molecule can adopt four types of arrangements on a water surface (Figure 2.8): (A) side on with the side chains randomly oriented. In this case the conformation of the molecules in the bulk columnar mesophase is preserved; (B) side on with the side chains oriented upwards. This will occur when the amphiphilic character of the molecule is the dominant factor; (C) edge on with the side chains in random orientation. This arrangement is likely when the cores have a strong interaction and the discotic liquid-crystalline character of the molecules dominates; (D) edge on with all side chains oriented upwards. This situation can be expected when both the amphiphilic and discotic character of the molecule are important. In this section we will refer to these four types of arrangements.

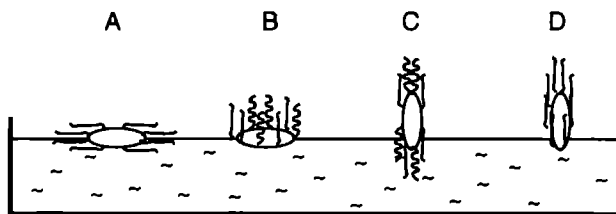


**Figure 2.8** Possible arrangements of a discotic liquid crystalline compound in a monolayer on a water surface (see text).

In only a few cases have mesogenic Pcs, substituted with eight long hydrocarbon side chains, been used in LB-films. Mesogenic  $\alpha$ -octaalkyl Pcs (Figure 2.7) form rigid films which cannot be deposited onto substrates [123]. However, when two chains at one side of the phthalocyanine are modified with hydroxy functions the molecule becomes amphiphilic and forms columnar monolayers and Y-type LB films [135,136]. Monolayers of  $\beta$ -octaalkyl Pcs can be transferred onto substrates by X-type deposition [137]. It has been suggested that in the transferred film the molecules are arranged as shown in Figure 2.8.B, *i.e.* the Pc planes parallel and the alkyl chains perpendicular to the substrate surface. The reported areas per molecule obtained from the pressure-area isotherms, *viz.* 80-110 Å<sup>2</sup>, however, are too low to account for this orientation. A monolayer of octaalkyloxymethyl Pc displays a molecular area of 180 Å<sup>2</sup> [138]. For this film also a type B arrangement has been

proposed. This is in contradiction with the observed polarized absorption spectra, which indicate a preferred orientation of the Pc planes perpendicular to the dipping direction (dichroic ratio is *ca.* 2). This is only possible when the molecules are arranged edge on. LB-films of a mesogenic Pc with eight (*R,S*)-3,7-dimethyloctoxy side chains have been prepared, but details about the film structure are not known [139]. In chapter 4 our results with this compound will be presented. Also relevant to mention here are mono- and multilayer studies performed with mesogenic alkylthioporphyrazines [140]. Good quality films have been obtained from an asymmetric derivative, and from the symmetrically octasubstituted compound mixed with stearic acid. A type C (edge on) arrangement was observed, with no orientation of the molecules with respect to the dipping direction.

(iv) *Amphiphilic Pcs*

Wöhrle and coworkers have prepared LB films from amphiphilic Pcs containing four alkyl chains which are connected to the Pc core via amido, pyridino or ammonium groups (Figure 2.9) [141]. These molecules are arranged parallel to the substrate surface with their alkyl chains pointing away from it (type B arrangement). The films on the water surface, however, are probably not real monolayers. Y-type LB-multilayers have been obtained from a Pc with dialkyl-dimethylammonium substituents (Figure 2.9) [142]. In this case the Pc molecules probably have a type D orientation (Figure 2.8).

A class of compounds closely related to Pcs are the tetrapyrridino porphyrans, in which one carbon atom in every Pc benzene ring is replaced by a nitrogen atom (Figure 2.9). Quaternization of these molecules with an alkylbromide results

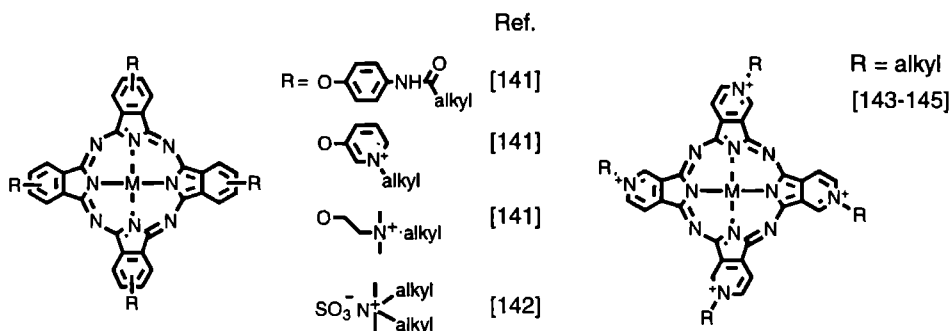


Figure 2.9 Chemical structures of amphiphilic Pcs used in LB-films.

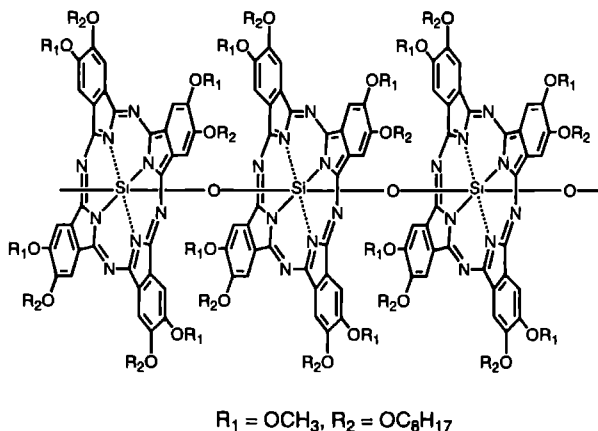
in charged species, which have been used by Palacin *et al.* to prepare LB-films [143-146]. The molecules in the film have a side-on arrangement (type B).

#### (v) Polymeric Pcs

The use of polymers for LB-films has the advantage that the Pc units are preorganized. Much work in this field has been carried out by Wegner and coworkers, who used tetra(methoxy)-tetra(octoxy)-Pc-polysiloxane as the building block (Figure 2.10) [147]. The structure of the LB film has been extensively studied [148-151]. The main conclusions are that the axes of the polymer molecules are oriented parallel to the substrate surface as well as to the dipping direction, the latter resulting in a dichroic ratio of 2.3, which can be increased to 5.8 by thermal annealing. The side chains are randomly distributed around the polymer axes. Theoretical studies suggest that the lateral orientation of the polymers is the result of monolayer flow during the dipping process [152].

Other related polymers that have been applied in LB-films are Pc-polysiloxanes with eight butoxy or decoxy side chains [153], and a Pc-polygermoxane with eight dodecoxycarbonyl substituents [154].

**Figure 2.10** Chemical structure of the Pc-polysiloxane used by Wegner to prepare LB-films.



### 2.5.2 Applications

LB-films of phthalocyanines are expected to find application in the field of molecular electronics [155-157]. In many papers, therefore, the electrical properties of the films are reported. It has been suggested that multilayer assemblies of Pcs can be used to construct a three-dimensional molecular memory device, *i.e.* by

controlling electron transfer through a well-organized film composed of alternating layers of isolating and conducting materials [158,159]. Rectifying behavior [160] has been reported to occur in LB-films of a tetra-*t*-Bu Pc [108a,161] and in films of Pc-polysiloxanes [162,163] which are sandwiched between ITO and metal electrodes. For the photovoltaic device constructed from the polysiloxane film a rectification ratio of 3 was found. This value could be increased to 20 by thermal annealing, probably because heating improves the order in the film. A bistable switching device was constructed using 4 layers of tris(isopropylaminomethyl) Pc between GaAs and gold electrodes [105].

In a number of cases the optical and electrical properties of Pcs have been combined to develop a device. Electroluminescent diodes were constructed from LB-films of tris(isopropylaminomethyl) Pc [105], and from LB-films of a tetra-*t*-Bu Pc [161]. It was shown that films of rare-earth-metal diphthalocyanines can display electrochromic behavior [164,165]: electrochemical oxidation resulted in a shift of the absorption maximum to higher wavelength, whereas reduction caused a shift to lower wavelength. In this way the color of the film could be changed from purple to blue, green, and red, depending on the applied potential. The third order nonlinear properties of LB films of Pc-polysiloxanes have been studied by Wegner and coworkers [166]. Second order NLO studies have been performed on LB-films of an asymmetrically substituted nitro-Pc [167].

A soluble Pc-polysiloxane has been modified with double bonds in its side chains. UV irradiation of a film of this material gave an insoluble network, which could be used to develop patterns by a negative photoresist technique [162].

Several reports deal with sensor applications of LB-films [168]. A membrane has been prepared from a LB film of a Pc-polysiloxane, which was used to construct a stable pH-sensitive field-effect transistor [169]. Gas sensor studies have been reported by several authors. Good results have been obtained with LB-films of Pcs on interdigital microelectrodes [114,161,170-174]. Exposure to oxidizing or reducing gases leads to changes in conductivities. Films of tetra(di(*tert*-amyl)phenoxy) CuPc were shown to detect selectively NH<sub>3</sub> (down to 2 ppm in air), and were insensitive to NO<sub>2</sub>, SO<sub>2</sub>, and H<sub>2</sub>S (up to 200 ppm), the response time being approximately 30-60 seconds and the recovery time <15 minutes [114]. LB-films of a similar compound were reported to operate as humidity sensor at ambient temperature and as a NH<sub>3</sub> sensor at elevated temperatures [173]. An LB-film of tris(isopropylaminomethyl) CuPc was found to be sensitive only to NO<sub>2</sub> with a similar response time and sensitivity as the above-mentioned tetra(di(*tert*-amyl)phenoxy) CuPc [170]. The substituents on the Pc ring therefore seem to determine the selectivity. LB-films

containing a 1:1 mixture of tetra(cumylphenoxy) Pc and stearyl alcohol have been reported to be sensitive to both  $\text{NH}_3$  (0.5 ppm) and  $\text{NO}_2$  (*ca* 1 ppm) [171]. The conductivities measured after exposure of these films to  $\text{NH}_3$  were found to be proportional to the number of monolayers in the film, which suggests that the gas adsorption is a bulk process. Other methods that have been applied to monitor gas adsorption on LB-films of Pcs are based on surface acoustic wave (SAW) [113,175] and surface plasmon resonance (SPR) measurements [113,176,177]. The sensor characteristics of the aforementioned amperometric devices are usually better than those of the SAW and SPR devices. With the help of surface-enhanced Raman scattering (SERS) and electronic absorption spectroscopy it has been possible to get insight in the mechanism of the adsorption of  $\text{NO}_2$  on Pc films [178]. The SERS spectra showed that especially the intensity of the pyrrole vibrations change when gas is adsorbed.

In summary, we may conclude that the possible applications of LB-films of Pcs are manifold. Especially the use of these materials in sensor devices is very promising. More about the latter subject will be presented in Chapter 8 of this thesis.

## References

- [1] J. Simon, J.-J. André, *Molecular Semiconductors*, Springer, Berlin (1985).
- [2] T.J. Marks, *Angew. Chem.* **102** (1990) 886; *Angew. Chem. Int. Ed. Engl.* **29** (1990), 857.
- [3] H. Schultz, H. Lehmann, M. Rein, M. Hanack, *Struct. Bonding* **74** (1991) 41.
- [4] D.D. Eley, *Mol. Cryst. Liq. Cryst.* **171** (1990) 1.
- [5] D.D. Eley, *Nature* **162** (1948) 819.
- [6] C.A. Hunter, J.K.M. Sanders, *J. Am. Chem. Soc.* **112** (1990) 5525.
- [7] D. Wöhrle, *Kontakte (Darmstadt)* **1** (1986) 24.
- [8] W.R. Scheidt, Y.J. Lee, *Struct. Bonding* **64** (1987).
- [9] W.J. Pietro, T.J. Marks, M.A. Ratner, *J. Am. Chem. Soc.* **107** (1985) 5387.
- [10] H. Konami, M. Hatano, A. Tajiri, *Chem. Phys. Lett.* **166** (1990) 605.
- [11] A. Rosa, E.J. Baerends, *Inorg. Chem.* **31** (1992) 4717.
- [12] B.M. Hoffman, J.A. Ibers, *Acc. Chem. Res.* **16** (1983) 15.
- [13] J. Martinsen, R.L. Greene, S.E. Palmer, B.M. Hoffman, *J. Am. Chem. Soc.* **105** (1983) 677.
- [14] S. Chandrasekhar, B.K. Sadashiva, K.A. Suresh, *Pramana* **9** (1977) 471.
- [15] For a recent review see: S. Chandrasekhar, G.S. Ranganath, *Rep. Prog. Phys.* **53** (1990) 57.
- [16] C. Piechocki, J. Simon, A. Skoulios, D. Guillon, P. Weber, *J. Am. Chem. Soc.* **104** (1982) 5245.
- [17] M.J. Cook, S.J. Cracknell, K.J. Harrison, *J. Mater. Chem.* **1** (1991) 703.
- [18] A.N. Cammidge, M.J. Cook, K.J. Harrison, N.B. McKeown, *J. Chem. Soc. Perkin Trans. I* (1991) 3053.
- [19] M.K. Engel, P. Bassoul, L. Bosio, H. Lehmann, M. Hanack, J. Simon, *Liq. Cryst.* **15** (1993) 709.
- [20] M. Hanack, A. Beck, H. Lehmann, *Synthesis* (1987) 703.
- [21] I. Cho, Y. Lim, *Mol. Cryst. Liq. Cryst.* **154** (1988) 9.
- [22] J.F. van der Pol, E. Neeleman, J.W. Zwikker, R.J.M. Nolte, W. Drenth, J. Aerts, R. Visser, S.J. Picken, *Liq. Cryst.* **6** (1989) 577.
- [23] W.T. Ford, L. Sumner, W. Zhu, Y.H. Chang, P.-J. Um, K.H. Choi, P.A. Heiney, N.C. Maliszewskyj, *New J. Chem.* **18** (1994) 495.
- [24] L.M. Severs, A.E. Underhill, D. Edwards, P. Wight, D. Thetford, *Mol. Cryst. Liq. Cryst.* **234** (1993) 235.
- [25] L. Dulog, A. Gittinger, *Mol. Cryst. Liq. Cryst.* **213** (1992) 31; *ibid* **237** (1993) 235.
- [26] C. Piechocki, J. Simon, J.-J. André, D. Guillon, P. Petit, A. Skoulios, P. Weber, *Chem. Phys. Lett.* **122** (1985) 124.
- [27] D. Lelièvre, L. Bosio, J. Simon, J.-J. André, F. Bensebaa, *J. Am. Chem. Soc.* **114** (1992) 4475.
- [28] P. Doppelt, S. Huille, *New J. Chem.* **14** (1990) 607.
- [29] F. Lelj, G. Morelli, G. Ricciardi, A. Roviello, A. Sirigu, *Liq. Cryst.* **12** (1992) 941.
- [30] B.A. Gregg, M.A. Fox, A.J. Bard, *J. Am. Chem. Soc.* **111** (1989) 3024.
- [31] K. Ohta, L. Jacquemin, C. Sirlin, L. Bosio, J. Simon, *New J. Chem.* **12** (1988) 751.
- [32] J.F. van der Pol, E. Neeleman, J.W. Zwikker, R.J.M. Nolte, W. Drenth, *Recl. Trav. Chim. Pays-Bas* **107** (1988) 615.
- [33] P. Weber, D. Guillon, A. Skoulios, *Liq. Cryst.* **9** (1991) 3.

- [34] D. Guillon, A. Skoulios, C. Piechocki, J. Simon, P. Weber, *Mol. Cryst. Liq. Cryst.* **100** (1983) 275.
- [35] P.G. de Gennes, *J. Phys. Lett. France* **44** (1983), L-657.
- [36] P.A. Heiney, E. Fontes, W.H. de Jeu, A. Riera, P. Carroll, A.B. Smith III, *J. Phys. France* **50** (1989) 461.
- [37] E. Fontes, P.A. Heiney, M. Ohba, J.N. Haseltine, A.B. Smith III, *Phys. Rev.* **37** (1988) 1329.
- [38] A.P.M. Kentgens, B.A. Markies, J.F. van der Pol, R.J.M. Nolte, *J. Am. Chem. Soc.* **112** (1990) 8800.
- [39] J. Leisen, M. Werth, C. Boeffel, H.W. Spies, *J. Chem. Phys.* **97** (1992) 3749.
- [40] B. Blanzat, C. Barthou, N. Tercier, J.-J. André, J. Simon, *J. Am. Chem. Soc.* **109** (1987) 135.
- [41] G. Blasse, G.J. Dirksen, A. Meijerink, J.F. van der Pol, E. Neeleman, W. Drenth, *Chem. Phys. Lett.* **154** (1989) 420.
- [42] D. Markovitsi, I. Lécuyer, J. Simon, *J. Phys. Chem.* **95** (1991) 3620.
- [43] Z. Belarbi, C. Sirlin, J. Simon, J.-J. André, *J. Phys. Chem.* **93** (1989) 8105.
- [44] P. Turek, P. Petit, J.-J. André, J. Simon, R. Even, B. Boudjema, G. Guillaud, M. Maitrot, *J. Am. Chem. Soc.* **109** (1987) 5119.
- [45] Z. Belarbi, M. Maitrot, K. Ohta, J. Simon, J.-J. André, P. Petit, *Chem. Phys. Lett.* **143** (1988) 400.
- [46] Z. Belarbi, *J. Phys. Chem.* **94** (1990) 7334.
- [47] J.M. Warman, M.P. de Haas, in *Pulse radiolysis of irradiated systems*, ed. Y. Tabata, CRC, Boca Raton, 1991, pp. 101-133.
- [48] J.M. Warman, M.P. de Haas, *Radiat. Phys. Chem.* **34** (1989) 581.
- [49] J.F. van der Pol, M.P. de Haas, J.M. Warman, W. Drenth, *Mol. Cryst. Liq. Cryst.* **183** (1990) 411.
- [50] J.F. van der Pol, M.P. de Haas, J.M. Warman, W. Drenth, *Mol. Cryst. Liq. Cryst.* **195** (1991) 307.
- [51] P.G. Schouten, J.M. Warman, M.P. de Haas, J.F. van der Pol, J.W. Zwikker, *J. Am. Chem. Soc.* **114** (1992) 9028.
- [52] P.G. Schouten, J.M. Warman, M.P. de Haas, M.A. Fox, H.-L. Pan, *Nature* **353** (1991) 736.
- [53] J.M. Warman, M.P. de Haas, J.F. van der Pol, W. Drenth, *Chem. Phys. Lett.* **164** (1989) 581.
- [54] J. Simon, C. Sirlin, *Pure Appl. Chem.* **61** (1989) 1625.
- [55] B.A. Gregg, M.A. Fox, A.J. Bard, *J. Phys. Chem.* **94** (1990) 1586.
- [56] Y. Shimizu, A. Ishikawa, S. Kusabayashi, M. Miya, A. Nagata, *J. Chem. Soc. Chem. Commun.* (1993) 656.
- [57] H. An, J.S. Bradshaw, R.M. Izatt, Z. Yan, *Chem. Rev.* **94** (1994) 939.
- [58] V. Thanabal, V. Krishnan, *J. Am. Chem. Soc.* **104** (1982) 3643.
- [59] N. Kobayashi, T. Osa, *Heterocycles* **15** (1981) 675.
- [60] R. Hendriks, O.E. Sielcken, W. Drenth, R.J.M. Nolte, *J. Chem. Soc. Chem. Commun.* (1986) 1464.
- [61] A.R. Koray, V. Ahsen, Ö. Bekâroglu, *J. Chem. Soc. Chem. Commun.* (1986) 932.
- [62] N. Kobayashi, Y. Nishiyama, *J. Chem. Soc. Chem. Commun.* (1986) 1462.
- [63] O.E. Sielcken, M.M. van Tilborg, M.F.M. Roks, R. Hendriks, W. Drenth, R.J.M. Nolte, *J. Am. Chem. Soc.* **109** (1987) 4261.



- [64] N. Kobayashi, A.B.P. Lever, *J. Am. Chem. Soc.* **109** (1987) 7433.
- [65] V. Ahsen, E. Yilmazer, M. Ertas, Ö. Bekâroglu, *J. Chem. Soc. Dalton Trans.* (1988) 401.
- [66] O.E. Sielcken, H.C.A. van Lindert, W. Drenth, J. Schoonman, J. Schram, R.J.M. Nolte, *Ber. Bunsenges. Phys. Chem.* **93** (1989) 702.
- [67] O.E. Sielcken, W. Drenth, R.J.M. Nolte, *Rec. Trav. Chim. Pays-Bas* **109** (1990) 425.
- [68] O.E. Sielcken, R.J.M. Nolte, J. Schoonman, *Rec. Trav. Chim. Pays-Bas* **109** (1990) 230.
- [69] T. Toupance, V. Ahsen, J. Simon, *J. Chem. Soc. Chem. Commun.* (1994) 75.
- [70] M. Bardin, E. Bertounesque, V. Plichon, J. Simon, V. Ahsen, Ö. Bekâroglu, *J. Electroanal. Chem.* **271** (1989) 173.
- [71] T. Toupance, V. Ahsen, J. Simon, *J. Am. Chem. Soc.* **116** (1994) 5352.
- [72] N. Ishikawa, Y. Kaizu, *Chem. Phys. Lett.* **203** (1993) 472.
- [73] E. Musluoglu, V. Ahsen, A. Gül, Ö. Bekâroglu, *Chem. Ber.* **124** (1991) 2531.
- [74] G. Gümüş, Z.Z. Öztürk, V. Ahsen, A. Gül, Ö. Bekâroglu, *J. Chem. Soc. Dalton Trans.* (1992) 2485.
- [75] (a) A. Gürek, V. Ahsen, A. Gül, Ö. Bekâroglu, *J. Chem. Soc. Dalton Trans.* (1991) 3367; (b) N. Tan, A. Gürek, Ö. Bekâroglu, F. Kadirgan, *J. Electroanal. Chem.* **374** (1994) 45.
- [76] (a) M. Koçak, A.I. Okur, Ö. Bekâroglu, *J. Chem. Soc. Dalton Trans.* (1994) 323; (b) E. Hamuryudan, Ö. Bekâroglu, *J. Chem. Res. (S)* (1993) 460.
- [77] A.G. Gürek, Ö. Bekâroglu, *Helv. Chim. Acta* **77** (1994) 1616.
- [78] Z.Z. Öztürk, E. Musluoglu, V. Ahsen, A. Gül, Ö. Bekâroglu, *J. Mater. Sci.* **27** (1992) 6183.
- [79] Z.Z. Öztürk, A. Altindal, A. Gürek, Ö. Bekâroglu, *Synth. Metals* **52** (1992) 291.
- [80] E. Musluoglu, A. Gürek, V. Ahsen, A. Gül, Ö. Bekâroglu, *Chem. Ber.* **125** (1992) 2337.
- [81] V. Ahsen, E. Yilmazer, A. Gül, Ö. Bekâroglu, *Makromol. Chem. Rapid Commun.* **8** (1987) 243.
- [82] V. Ahsen, E. Yilmazer, Ö. Bekâroglu, *Makromol. Chem.* **189** (1988) 2533.
- [83] E. Musluoglu, Z.Z. Öztürk, V. Ahsen, A. Gül, Ö. Bekâroglu, *J. Chem. Res. (S)* (1993) 6.
- [84] J. Vacus, G. Memetzidis, P. Doppelt, J. Simon, *J. Chem. Soc. Chem. Commun.* (1994) 697.
- [85] A.I. Okur, A. Gül, A. Cihan, N. Tan, Ö. Bekâroglu, *Synth. React. Inorg. Met.-Org. Chem.* **20** (1990) 1399.
- [86] S. Sarigül, Ö. Bekâroglu, *Chem. Ber.* **122** (1989) 291.
- [87] N. Kobayashi, T. Ohya, M. Sato, S.-I. Nakajima, *Inorg. Chem.* **32** (1993) 1803.
- [88] J.-I. Anzai, C.-C. Liu, N. Kobayashi, *Polym. Commun.* **31** (1990) 223.
- [89] J. Simon, M.K. Engel, C. Soulié, *New J. Chem.* **16** (1992) 287.
- [90] R.D. Joyner, M.E. Kenney, *Inorg. Chem.* **1** (1962) 717.
- [91] T.J. Marks, *Science* **227** (1985) 881.
- [92] T.J. Marks, *Angew. Chem.* **102** (1990) 886.
- [93] M. Dreier, M. Hanack, A. Hirsch, R. Thies, *Synth. Met.* **41-43** (1991) 2609.
- [94] C. Sirlin, L. Bosio, J. Simon, *J. Chem. Soc. Chem. Commun.* (1987) 379.
- [95] W. Caseri, T. Sauer, G. Wegner, *Makromol. Chem. Rapid Commun.* **9** (1988) 651.

- [96] J.F. van der Pol, J.W. Zwikker, J.M. Warman, M.P. de Haas, *Rec. Trav. Chim. Pays-Bas* **109** (1990) 208.
- [97] T. Sauer, *Macromolecules* **26** (1993) 2057.
- [98] S. Schwiegk, M. Werth, J. Leisen, G. Wegner, H.W. Spiess, *Acta Polym.* **44** (1993) 31.
- [99] J.F. van der Pol, *thesis*, Utrecht (1990).
- [100] O.E. Sielcken, L.A. van de Kuil, W. Drenth, J. Schoonman, R.J.M. Nolte, *J. Am. Chem. Soc.* **112** (1990) 3086.
- [101] J.F. van der Pol, E. Neeleman, J.C. van Miltenburg, J.W. Zwikker, R.J.M. Nolte, W. Drenth, *Macromolecules* **23** (1990) 155.
- [102] A. Ulman, *An introduction to ultrathin organic films, from Langmuir-Blodgett to self-assembly*, Academic Press: San Diego (1991)
- [103] A.E. Alexander, *J. Chem. Soc.* (1937) 1813.
- [104] S. Baker, M.C. Petty, G.G. Roberts, M.V. Twigg, *Thin Solid Films* **99** (1983) 53.
- [105] G.G. Roberts, M.C. Petty, S. Baker, M.T. Fowler, N.J. Thomas, *Thin Solid Films* **132** (1985) 113.
- [106] R.D. George, P.F. McMillan, V.A. Burrows, R. Hervig, *Thin Solid Films* **203** (1991) 303.
- [107] J.R. Fryer, C.M. McConnell, R.A. Hann, B.L. Eyres, S.K. Gupta, *Philos. Mag. B* **61** (1990) 843.
- [108] (a) E. Brynda, I. Koropec, L. Kalvoda, S. Nespurek, *Thin Solid Films* **199** (1991) 375. (b) Y.L. Hua, G.G. Roberts, M.M. Ahmad, M.C. Petty, M. Hanack, M. Rein, *Philos. Mag. B* **53** (1986) 105.
- [109] M.J. Cook, A.J. Dunn, A.A. Gold, A.J. Thomson, M.F. Daniel, *J. Chem. Soc. Dalton Trans.* (1988) 1583.
- [110] K. Nichogi, K. Waragai, A. Taomoto, Y. Saito, S. Asakawa, *Thin Solid Films* **179** (1989) 297.
- [111] Y. Fu, M. Forman, C.C. Leznoff, A.B.P. Lever, *J. Phys. Chem.* **98** (1994) 8985.
- [112] W.R. Barger, A.W. Snow, H. Wohltjen, N.L. Jarvis, *Thin Solid Films* **133** (1985) 197.
- [113] J. O'Donnell, C.L. Honeybourne, *J. Phys. Condens. Matter.* **3** (1991) S337.
- [114] D.P. Jiang, A.D. Lu, Y.J. Li, X.M. Pang, Y.L. Hua, *Thin Solid Films* **199** (1991) 173.
- [115] A.W. Snow, N.L. Jarvis, *J. Am. Chem. Soc.* **106** (1984) 4706.
- [116] W. Barger, J. Dote, M. Klusty, R. Mowery, R. Price, A. Snow, *Thin Solid Films* **159** (1988) 369.
- [117] J.J. Burack, J.D. LeGrange, J.L. Markham, W. Rockward, *Langmuir* **8** (1992) 613.
- [118] A. Suzuki, H. Awano, M. Hikosaka, H. Ohigashi, *Thin Solid Films* **216** (1992) 283.
- [119] J.-H. Kim, T.M. Cotton, R.A. Uphaus, C.C. Leznoff, *Thin Solid Films* **159** (1988) 141.
- [120] J. Ouyang, A.B.P. Lever, *J. Phys. Chem.* **95** (1991) 5272.
- [121] Y. Fu, A.B.P. Lever, *J. Phys. Chem.* **95** (1991) 6979.
- [122] M.J. Cook, A.J. Dunn, M.F. Daniel, R.C.O. Hart, R.M. Richardson, S.J. Roser, *Thin Solid Films* **159** (1988) 395.
- [123] N.B. McKeown, M.J. Cook, A.J. Thomson, K.J. Harrison, M.F. Daniel, R.M. Richardson, S.J. Roser, *Thin Solid Films* **159** (1988) 469.

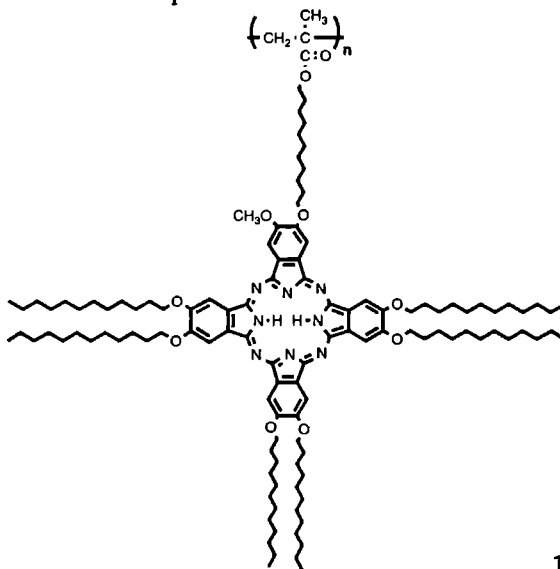
- [124] M.J. Cook, N.B. McKeown, J.M. Simmons, A.J. Thomson, M.F. Daniel, K.J. Harrison, R.M. Richardson, S.J. Roser, *J. Mater. Chem.* **1** (1991) 121.
- [125] M.A. Chesters, M.J. Cook, S.L. Gallivan, J.M. Simmons, D.A. Slater, *Thin Solid Films* **210/211** (1992) 538.
- [126] S. Mukhopadhyay, A.K. Ray, M.J. Cook, J.M. Simmons, C.A. Hogarth, *J. Mater. Sci. Mater. Electr.* **3** (1992) 139.
- [127] M.J. Cook, J. McMurdo, D.A. Miles, R.H. Poynter, J.M. Simmons, S.D. Haslam, R.M. Richardson, K. Welford, *J. Mater. Chem.* **4** (1994) 1205.
- [128] N.B. McKeown, I. Chambrier, M.J. Cook, *J. Chem. Soc. Perkin Trans. I* (1990) 1169.
- [129] K. Ogawa, S.-I. Kinoshita, H. Yonehara, H. Nakahara, K. Fukuda, *J. Chem. Soc. Chem. Commun.* (1989) 477.
- [130] K. Ogawa, H. Yonehara, T. Shoji, S.-I. Kinoshita, E. Maekawa, H. Nakahara, K. Fukuda, *Thin Solid Films* **178** (1989) 439.
- [131] H. Itoh, T. Koyama, K. Hanabusa, E. Masuda, H. Shirai, T. Hayakawa, *J. Chem. Soc. Dalton Trans.* (1989) 1543.
- [132] P.A. Albouy, *J. Phys. Chem.* **98** (1994) 8543.
- [133] H. Ringsdorf, B. Schlarb, J. Venzmer, *Angew. Chem.* **100** (1988) 117; *Ibid, Int. Ed. Engl.* **27** (1988) 113.
- [134] A. Laschewsky, *Adv. Mater.* **1** (1989) 392.
- [135] G.C. Bryant, M.J. Cook, C. Ruggiero, T.G. Ryan, A.J. Thorne, S.D. Haslam, R.M. Richardson, *Thin Solid Films* **243** (1994) 316.
- [136] R.H. Poynter, M.J. Cook, M.A. Chesters, D.A. Slater, J. McMurdo, K. Welford, *Thin Solid Films* **243** (1994) 346.
- [137] H. Nakahara, K. Fukuda, K. Kitahara, H. Nishi, *Thin Solid Films* **178** (1989) 361.
- [138] D.W. Kalina, S.W. Crane, *Thin Solid Films* **134** (1985) 109.
- [139] W.J. Schutte, M. Sluyters-Rehbach, J.H. Sluyters, *J. Phys. Chem.* **97** (1993) 6069.
- [140] (a) F. Bonosi, G. Ricciardi, F. Lelj, G. Martini, *J. Phys. Chem.* **97** (1993) 9181; (b) *Ibid*, **98** (1994) 10613.
- [141] M.A. Mohammed, P. Ottenbreit, W. Prass, G. Schnurpfeil, D. Wöhrle, *Thin Solid Films* **213** (1992) 285.
- [142] M. Fukui, N. Katayama, Y. Ozaki, T. Araki, K. Iriyama, *Chem. Phys. Lett.* **177** (1991) 247.
- [143] S. Palacin, P. Lesieur, I. Stefanelli, A. Barraud, *Thin Solid Films* **159** (1988) 83.
- [144] S. Palacin, A. Barraud, *Coll. Surf.* **52** (1991) 123.
- [145] F. Porteu, S. Palacin, A. Ruau-del-Teixier, A. Barraud, *Mol. Cryst. Liq. Cryst* **211** (1992) 193.
- [146] S. Palacin, A. Ruau-del-Teixier, A. Barraud, *J. Phys. Chem.* **93** (1989) 7195.
- [147] E. Orthmann, G. Wegner, *Angew. Chem.* **98** (1986) 1114; *Ibid, Int. Ed. Engl.* **25** (1986) 1105.
- [148] T. Sauer, T. Arndt, D.N. Batchelder, A.A. Kalachev, G. Wegner, *Thin Solid Films* **187** (1990) 357.
- [149] R.G.M. Crockett, A.J. Campbell, F.R. Ahmed, *Polymer* **31** (1990) 602.
- [150] K. Yase, S. Schwiegk, G. Lieser, G. Wegner, *Thin Solid Films* **210/211** (1992) 22; *ibid* **213** (1992) 130.
- [151] V.K. Gupta, J.A. Kornfield, A. Ferencz, G. Wegner, *Science* **265** (1994) 940.

- [152] S. Schwiegk, T. Vahlenkamp, Y. Xu, G. Wegner, *Macromolecules* **25** (1992) 2513.
- [153] Z. Ali-Adib, K. Davidson, H. Nooshin, R.H. Tredgold, *Thin Solid Films* **201** (1991) 187.
- [154] L. Dulog, A. Gittinger, S. Roth, T. Wagner, *Makromol. Chem.* **194** (1993) 493.
- [155] B. Tieke, *Adv. Mater.* **2** (1990) 222; *ibid.* **3** (1991) 532.
- [156] I.R. Peterson, *J. Phys. D: Appl. Phys.* **23** (1990) 379.
- [157] H. Tachibana, M. Matsumoto, *Adv. Mater.* **5** (1993) 796.
- [158] P.E. Burrows, K.J. Donovan, E.G. Wilson, *Thin Solid Films* **179** (1989) 129.
- [159] K.J. Donovan, R. Paradiso, K. Scott, R.V. Sudiwala, E.G. Wilson, R. Bonnett, R.F. Wilkins, D.A. Batzel, T.R. Clark, M.E. Kenney, *Thin Solid Films* **210/211** (1992) 253.
- [160] J.R. Sambles, A.S. Martin, *Phys. Scripta* **T49** (1993) 718.
- [161] Y.L. Hua, D.P. Jiang, Z.Y. Shu, M.C. Petty, G.G. Roberts, M.M. Ahmad, *Thin Solid Films* **192** (1990) 383.
- [162] S. Schwiegk, H. Fischer, Y. Xu, F. Kremer, G. Wegner, *Makromol. Chem. Macromol. Symp.* **46** (1991) 211.
- [163] G. Wegner, *Thin Solid Films* **216** (1992) 105.
- [164] M. Petty, D.R. Lovett, J.M. O Connor, J. Silver, *Thin Solid Films* **179** (1989) 387.
- [165] Y. Liu, K. Shigehara, M. Hara, A. Yamada, *J. Am. Chem. Soc.* **113** (1991) 440.
- [166] C. Bubeck, D. Neher, A. Kaltbeitzel, G. Duda, T. Arndt, T. Sauer, G. Wegner, *NATO ASI Ser., Ser. E, Nonlinear Opt. Eff. Org. Polym.* **162** (1989) 185.
- [167] Y. Liu, Y. Xu, D. Zhu, T. Wada, H. Sasabe, L. Liu, W. Wang, *Thin Solid Films* **244** (1994) 943.
- [168] For recent reviews, see (a) ref. 143; (b) T. Moriizumi, *Thin Solid Films* **160** (1988) 413; (c) A. Barraud, *Vacuum* **41** (1990) 1624; (d) A.W. Snow, W.R. Barger, in *Phthalocyanines, properties and applications*, eds. C.C. Leznoff and A.B.P. Lever, Vol. 1, VCH, New York (1989), 341-392.
- [169] T. Sauer, W. Caseri, G. Wegner, A. Vogel, B. Hoffmann, *J. Phys D: Appl. Phys.* **23** (1990) 79.
- [170] S. Baker, G.G. Roberts, M.C. Petty, *IEE Proc., Part 1* **130** (1983) 260.
- [171] H. Wohltjen, W. Barger, A. Snow, N.J. Jarvis, *IEEE Trans. Electron Devices* **32** (1985) 1170.
- [172] A. Chyla, J. Sworakowski, A. Szczurek, E. Brynda, S. Nespurek, *Mol. Cryst. Liq. Cryst.* **230** (1993) 1.
- [173] C. Gu, L. Sun, T. Zhang, T. Li, M. Hirata, *Thin Solid Films* **244** (1994) 909.
- [174] J. Souto, R. Aroca, J.A. DeSaja, *J. Phys. Chem.* **98** (1994) 8998.
- [175] B. Holcroft, G.G. Roberts, *Thin Solid Films* **160** (1988) 445.
- [176] J.P. Lloyd, C. Pearson, M.C. Petty, *Thin Solid Films* **160** (1988) 431.
- [177] D.G. Zhu, M.C. Petty, M. Harris, *Sens. Actuators B* **2** (1990) 265.
- [178] D. Battisti, R. Aroca, *J. Am. Chem. Soc.* **114** (1992) 1201.

# *Monolayer Behavior of a Side-Chain Phthalocyaninatopolymethacrylate*

## 3.1 Introduction

So far, main-chain polysiloxanes are the only type of phthalocyanine polymers that have been studied by the Langmuir-Blodgett (LB) technique (see previous chapter, section 2.5.1, sub (v)). Recently, van der Pol *et al.* synthesized a polymethacrylate with dodecoxy-substituted phthalocyanine side chains (**1**, see below) [1]. This polymer is more flexible than the aforementioned phthalocyaninatopolysiloxane. It has a molecular weight of 47,000, which corresponds to a degree of polymerization of  $\approx 24$ . The phthalocyanine units in the polymer are stacked in columns due to strong intramolecular interactions. We studied the monolayer properties of this methacrylate polymer at the air-water interface and the subsequent deposition of the monolayer film onto various solid substrates. The results are presented in this chapter.



### 3.2 Experimental section

The synthesis of poly[2-[[11-(methacryloyloxy)undecyl]oxy]-3-methoxy-9,10,16,17,23,24-hexakis(dodecyloxy)phthalocyanine] (**1**) has been reported elsewhere [1].

The monolayer properties were studied by measuring pressure-area isotherms on a computer-controlled Lauda Film Balance (FW 2) with water, purified by a Milli-Q filtration system, as the subphase. The polymer was dissolved in chloroform (spectroscopic quality, about 1 mg·mL<sup>-1</sup>) and isotherms were recorded at a compression speed of 10 Å<sup>2</sup>·(repeating unit)<sup>-1</sup>·min<sup>-1</sup>. The stability curves were obtained by measuring the surface area as a function of time at 20 °C using a constant pressure.

Transmission electron microscopy (TEM) and electron diffraction (ED) were performed on monolayers, picked up from the water surface by horizontally touching the monolayer with a Formvar/carbon coated grid at a surface pressure of 20 mN·m<sup>-1</sup> and a temperature of 20 °C. The samples were blotted dry by touching the edge of the grid with filter paper and subsequently dried in air. For the TEM experiments part of the specimens were shadowed with platinum at an angle of 20°. Electron micrographs of the shadowed specimens were recorded on a JEOL 1200EX electron microscope at 80 kV and a magnification of 5,000× or 10,000×. Electron diffractograms of unshadowed specimens were recorded on a Philips CM20-FEG microscope at 200 kV and a camera length of 500 mm, using a Gatan 626 cryo-specimen holder at -170 °C.

Glass and silicon substrates were cleaned ultrasonically with chloroform, treated with concentrated sulfochromic acid at 80 °C for 2 h, washed several times with Milli-Q water, cleaned again ultrasonically in acetone and in chloroform, and finally stored in methanol. Before use the substrate was rinsed with chloroform, partially hydrophobized by treatment with a boiling mixture of chloroform and hexamethyldisilazane and finally rinsed with chloroform. Gold substrates were obtained by sputtering a gold layer 500 Å thick onto the cleaned glass slides. Zinc sulfide plates, also used as substrates, were cleaned by washing thoroughly with chloroform. Deposition was performed by spreading a mixture of polymer **1** and arachidic acid in chloroform on the LB trough and subsequently dipping the substrate through the monolayer at a constant surface pressure with a speed of 4-10 mm·min<sup>-1</sup>.

Transmission (TM) and grazing incidence reflection (GIR) Fourier-transform infrared (FT-IR) spectra were recorded on a Bruker IFS-88 FT-IR spectrometer at 4

cm<sup>-1</sup> resolution by the method of Arndt [2], cycles of 1000 scans were used UV/vis spectra were recorded on a Unicam SP-8 spectrophotometer

Ellipsometry experiments were carried out with a Gaertner L117-C single-wavelength ellipsometer ( $\lambda = 632.8$  nm) The measured parameters  $\Delta$  and  $\Psi$  had a relative accuracy of  $2 \times 10^{-4}$  deg and an absolute reproducibility of  $10^{-3}$  deg For the measurements at the air-water interface a monolayer was spread on demineralized water in a Teflon Petri dish with a diameter of 8 cm The amount of polymer solution that had to be spread to obtain a monolayer was calculated from the pressure-area isotherms

### 3.3 Results

#### 3.3.1 Monolayer properties and deposition

The pressure-area isotherm of polymer 1, measured directly after spreading the solution, is shown in Figure 3.1, curve A. By extrapolation to zero pressure an occupied area per repeating unit of  $67 \text{ \AA}^2$  is obtained This value is very close to the areas per repeating unit reported in the literature for tetrakis(decyloxy)-substituted phthalocyaninatopolysiloxanes [3] In monolayers of the latter polymers the planes

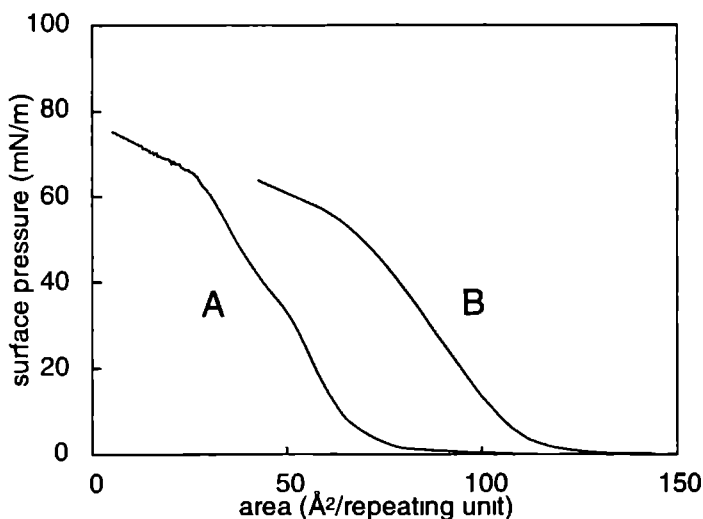


**Figure 3.1** Isotherms of pure polymer 1 at  $T = 20 \text{ }^{\circ}\text{C}$  directly after spreading the solution (A), after 1 night expansion at zero pressure (B)

of the closely packed phthalocyanine rings are oriented perpendicular to the water surface. Because one alkoxy chain in our polymer **1** occupies an area of at least  $\approx 20 \text{ \AA}^2$ , the seven alkoxy groups in one unit of the polymer cannot all contribute to the occupied area. Therefore, some of them must lie between the phthalocyanine unit and the subphase. This will cause unfavorable contact of the hydrophobic chains with the water phase. This can be compensated for if a strong intramolecular interaction exists between the phthalocyanine units. It is most probable that the side of the phthalocyanine ring bearing the methoxy and methacrylate functions will face the subphase, because of the hydrophilic nature of these functions.

Stabilization experiments revealed that a very unusual effect took place. As is shown in Figure 3.2 the total area of the monolayer gradually increased with time after an initial small decrease. This increase took place against the applied pressure of  $15 \text{ mN}\cdot\text{m}^{-1}$ . Even after 16 hours this process was continuing. The rate of area increase depended on the applied pressure, as can be seen in Figure 3.3.

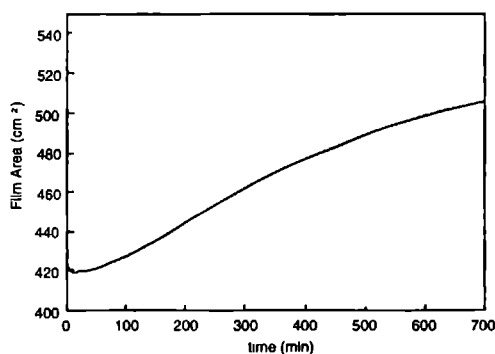


**Figure 3.2** Film area as a function of time recorded during stabilization experiments with a film of polymer **1**. The surface pressure was kept constant at  $15 \text{ mN}\cdot\text{m}^{-1}$ .

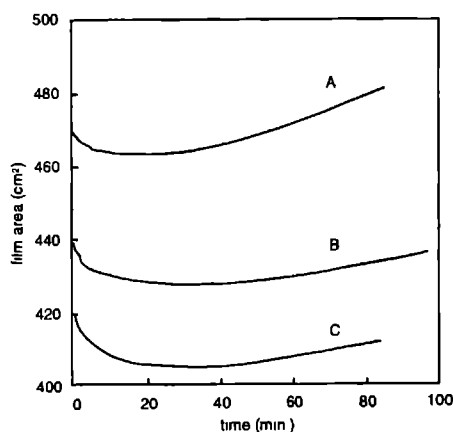


**Figure 3.3** Film area as a function of time recorded during stabilization experiments with polymer **1** at different surface pressures:  $7.5 \text{ mN}\cdot\text{m}^{-1}$  (A);  $15 \text{ mN}\cdot\text{m}^{-1}$  (B);  $20 \text{ mN}\cdot\text{m}^{-1}$  (C).

To obtain some information about what was happening during the expansion of the monolayer, we spread a solution of the polymer on the subphase and allowed the layer to expand at zero pressure overnight. Subsequently, the isotherm shown in Figure 3.1, curve B, was recorded. As one can see, the calculated area per repeating unit is appreciably higher than in case of curve A, *i.e.*  $120 \text{ \AA}^2$ . When the



film was fully compressed directly after spreading, a rigid and bright green collapsed monolayer was obtained. However, when this compression was carried out after 1 night expansion, the green color was less bright and the rigidity of the collapsed film had diminished.

At this point these results can be explained in three ways: (i) It is possible that the phthalocyanine units in the polymer slowly change from an "edge on" to a "side on" orientation with regard to the water subphase. (ii) The phthalocyanine units may retain their edge-on arrangement, but the hydrophobic alkoxy chains rise up from the water surface and become aligned beside the phthalocyanine units. (iii) Another unknown deaggregation process is taking place.

Information about the arrangement of the phthalocyanine units in polymer 1 can be obtained by studying transferred LB multilayers of 1 by spectroscopic methods. However, attempts to transfer the monolayer before expansion onto substrates resulted in only a partial and irregular deposition. This suggests that the polymer molecules are strongly aggregated, resulting in a rigid film. Also after overnight expansion the monolayer could not be transferred uniformly. Therefore, it was necessary to mix the polymer with a transfer promotor, *viz.*, arachidic acid. It is known that the latter compound reduces the rigidity of LB films [4]. One has to take into account, however, that the promotor may also influence the film morphology [5].

Various mixtures of polymer 1 and arachidic acid ranging from 2:1 to 1:4 (= repeating units:arachidic acid) were prepared and isotherms were recorded at 20 °C (Figure 3.4 and Table 3.I). As can be seen in Table 3.I, the presence of arachidic acid hardly changes the calculated area per polymer repeating unit. This indicates that the arachidic acid probably has no influence on the arrangement of the phthalocyanine units and that the arachidic acid and the polymer phases are segregated. Moreover, the mixed monolayers showed the same properties as discussed above; *i.e.*, the monolayer area increased gradually with time, and after overnight expansion the isotherms showed higher areas per repeating unit than before expansion.

Transfer of the mixed monolayers onto glass, gold, silicon, and zinc sulfide substrates was found to be possible with the 1:2 polymer-arachidic acid mixture at a pressure of 20 mN·m<sup>-1</sup> and was carried out directly after spreading as well as after overnight expansion. Unlike the pure polymer films this mixture gave good transfer results. The first downward movement of the substrate gave almost no transfer, but after that a Y-type transfer with a transfer ratio close to unity was possible. At least 59 layers could be deposited in this way.

**Figure 3.4** Isotherms at 20 °C of various polymer 1 - arachidic acid mixtures: pure polymer (A); 2:1 (B); 1:1 (C); 1:2 (D); 1:4 mixture (E).

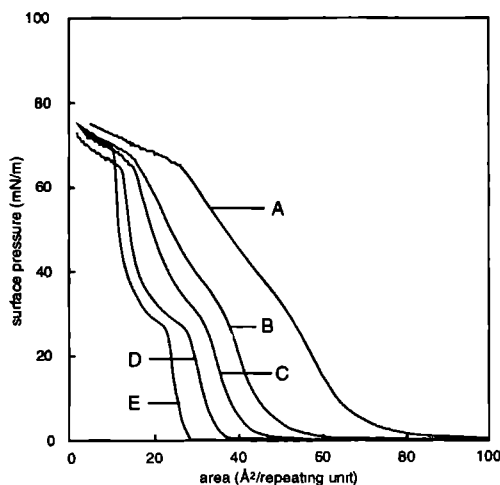


**Table 3.I** Calculated Areas from Pressure-Area Isotherms of Polymer-Arachidic Acid Mixtures

Ratio [a]	Measured area [b] / Å <sup>2</sup>	Area per repeating unit [c] / Å <sup>2</sup>
pure polymer	67	67
2 : 1	48	62
1 : 1	40	60
1 : 2	34	62
1 : 4	28	60

[a] Polymer 1 repeating unit . arachidic acid.

[b] Obtained by extrapolation of the isotherms to zero pressure

[c] Calculated assuming an area of 20 Å<sup>2</sup> for one arachidic acid molecule.

### 3.3.2 FT-IR spectroscopy

A total of 39 layers of the polymer-arachidic acid (1:2) mixture was built on zinc sulfide and gold substrates. For transmission (TM) and grazing incidence reflection (GIR) FT-IR measurements spectra were recorded with polarized incident light. This allowed us to obtain the absorbances in the film in three perpendicular directions. The spectra of multilayers, prepared directly after spreading, were compared with those of samples that had been prepared after 1 night of expansion. This was done to see if the orientation of the phthalocyanine units had changed during monolayer expansion (see Figure 3.5).

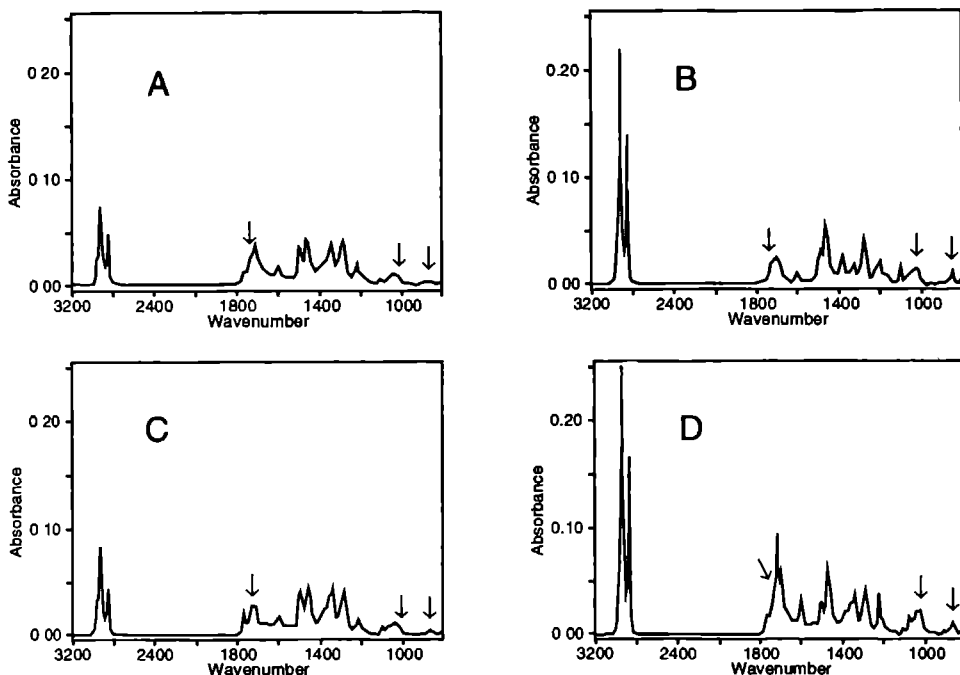


**Figure 3.5** IR spectra of polymer 1-arachidic acid (1:2) mixed films consisting of 39 layers: GIR spectrum of a nonexpanded film on a gold substrate (A); TM spectrum with polarization parallel to the dipping direction of a nonexpanded film on a zinc sulfide substrate (B); GIR spectrum of a film expanded overnight (C); TM spectrum with polarization parallel to the dipping direction of a film expanded overnight (D). Peaks at 1735, 1020, and 870  $\text{cm}^{-1}$  are indicated by arrows.

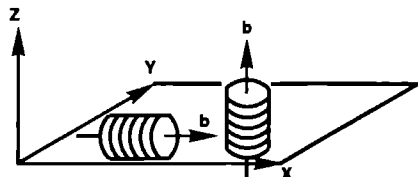
In order to be able to compare the TM spectra with the GIR spectra, we calculated a reflection spectrum from the TM spectrum in Figure 3.5D according to the procedure of Brinkhuis *et al.* [6]. This was possible because the thickness of the film was exactly known from ellipsometry measurements (*vide infra*). The calculated spectrum was almost identical with the measured one, so no dispersion effects were present in the GIR spectra.

The largest difference between the TM and the GIR spectra is the higher absorbance in the C-H stretching region between 2800 and 3000  $\text{cm}^{-1}$  in the former spectrum. This is due to the orientation of the phthalocyanine side chains and the arachidic acid molecules perpendicular to the film plane. These two cannot be distinguished from each other.

**Table 3.II** Orientations of the Phthalocyanine Ring which Can Be Derived from the Occurrence or Absence of In-Plane (i.p.) or Out-of-Plane (o.o.p.) Vibrational Modes in the Polarized FT-IR Spectra [a]

Direction of electric field vector $E$	i.p.	o.o.p.	i.p. + o.o.p.
$z$ (GIR)	edge-on	side-on	tilted
$y$ (TM)	edge-on ( $b \parallel x$ ) or side-on	edge-on ( $b \parallel y$ )	edge-on or tilted
$x$ (TM)	edge-on ( $b \parallel y$ ) or side-on	edge-on ( $b \parallel x$ )	edge-on or tilted

[a] Direction of the columnar axis  $b$  with respect to the substrate plane ( $x, y$ ) with the edge-on and the side-on arrangement being as follows:



The phthalocyanine vibrational modes can be divided into two different classes: in-plane (i.p.) and out-of-plane (o.o.p.) vibrations. Table 3.II shows the possible orientations that can be derived from the appearance of one or two of these classes of vibrational modes in single spectra, if the electric field vector  $E$  is polarized in one of the three different directions.

The only o.o.p. vibrations that occur in the measured range are the C-H and N-H vibrations at 870 and 1020  $\text{cm}^{-1}$ , respectively. In the GIR spectra of the nonexpanded (Figure 3.5A) and expanded (Figure 3.5C) films, these o.o.p. vibrations are practically absent. However, in the TM spectra of parts B and D of Figure 3.5 these bands are clearly present. According to Table 3.II, this suggests that the phthalocyanine rings in majority have an edge-on arrangement, which does not change during monolayer expansion.

We recorded TM spectra with polarizations in two different directions: perpendicular and parallel to the dipping direction  $t$ . Only one of these is depicted in Figure 3.5, because we observed almost no difference between the two spectra. From this we may conclude that the columnar axis of **1** is not oriented relative to the dipping direction. This result is in contrast with the results obtained for LB films of phthalocyaninatopolysiloxanes and some other rigid-rod polymers, where a flow-induced orientation during the transfer process was observed [7].

There are some small differences between the IR spectra of the transferred films obtained before (Figure 3.5, spectra A and B) and after (Figure 3.5, spectra C and D) monolayer expansion. Especially in the carbonyl region differences are observed due to either the polymeric ester carbonyl vibration at  $1735\text{ cm}^{-1}$  or the arachidic acid vibrations at  $1715$  and  $1750\text{ cm}^{-1}$ . Also in the region between  $1100$  and  $1600\text{ cm}^{-1}$  some differences can be seen. It is very difficult and rather premature to draw conclusions from these findings.

### **3.3.3 UV/Vis spectroscopy**

The results presented above indicate that the orientation of the phthalocyanine units has not changed after monolayer expansion. The question now arises as to what effect causes the color change of the monolayer during expansion. To study this we transferred nine layers of the nonexpanded mixed monolayer and nine layers of the expanded mixed monolayer to separate hydrophobic glass substrates and recorded the visible absorption spectra of the multilayers. As expected, a dramatic difference between the two spectra was visible (results not shown). The spectrum of the nonexpanded film was very similar to the solution spectrum of the polymer [1]. A broad Q-band was visible in the  $610\text{--}650\text{ nm}$  region, suggesting strong interactions between the phthalocyanine rings [1], and weak shoulders were visible at  $664$  and  $700\text{ nm}$ . In contrast, the spectrum of the expanded film showed a large decrease in intensity over the whole spectral range. The maximum of the Q-band had shifted to the red. This result indicates that the number of absorption sites within the same area had decreased and that the interaction between the phthalocyanine units had become weaker after expansion.

### **3.3.4 Electron microscopy**

The IR and visible spectroscopic investigations were carried out on transferred mixed multilayers of polymer 1 and arachidic acid. To get information about the structure of the monolayer on the water surface in the absence of arachidic acid, we recorded electron micrographs and diffractograms of nonexpanded and expanded pure polymer monolayers that were picked up from the water surface by a Formvar/carbon coated grid (see the Experimental Section). During the preparation of these specimens we observed that the surface of the monolayer facing the water

phase was relatively hydrophobic before monolayer expansion and hydrophilic after expansion. This was evidenced by a larger contact angle of the water droplet on the grid during blotting before expansion than after expansion [8].

Electron micrographs of the nonexpanded monolayer showed distinct smooth domains of different sizes and homogeneous thickness (Figure 3.6A). These domains were mostly separated by narrow boundaries. The expanded monolayer displayed much smaller domains that had a rough, grainy and more irregular surface (Figure 3.6B). In addition to these small irregular domains, smooth domains were visible similar to those in the nonexpanded films, suggesting that the expansion had not been fully completed.

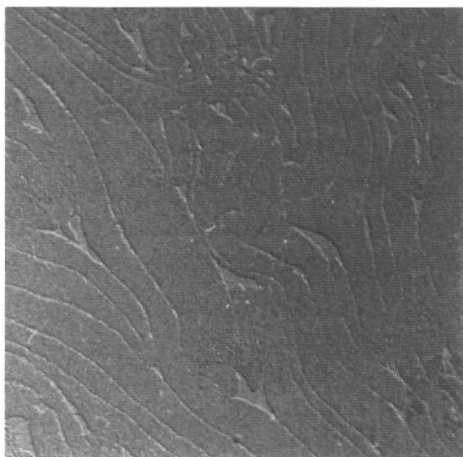
As the nonexpanded domains are homogeneous in thickness, we may conclude that the polymer on the water surface is not present in the form of multilayers. As a consequence, the expansion can not be the result of a spreading out of stacked multilayer aggregates.

### 3.3.5 Electron diffraction

To further characterize the different types of domains, we recorded electron diffractograms of both the nonexpanded and the expanded polymer monolayer, in the absence of arachidic acid. The specimens were cooled to  $-170\text{ }^{\circ}\text{C}$  to decrease the radiation sensitivity. Figure 3.7 shows an electron diffractogram from a nonexpanded film. From the displayed pattern a rectangular unit cell of  $3.9 \times 16.6\text{ }\text{\AA}$  can be derived. Assuming one polymer repeating unit per unit cell, the occupied area per polymer repeating unit is  $64.7\text{ }\text{\AA}^2$ , which is very close to the value calculated from the pressure-area isotherms. The  $3.9\text{-}\text{\AA}$  periodicity probably corresponds to the stacking distance of the phthalocyanine units and the distance of  $16.6\text{ }\text{\AA}$  to the lateral packing of the phthalocyanine stacks.

The expanded film showed much less crystalline order. Only at a few positions of the sample a diffraction pattern was observed, which may be ascribed to nonexpanded areas as the diffraction pattern was indistinguishable from the pattern of the nonexpanded film. From these results it can be concluded that crystalline order is present before expansion and is lost when the monolayer of polymer molecules expands at constant pressure.

(A)



(B)

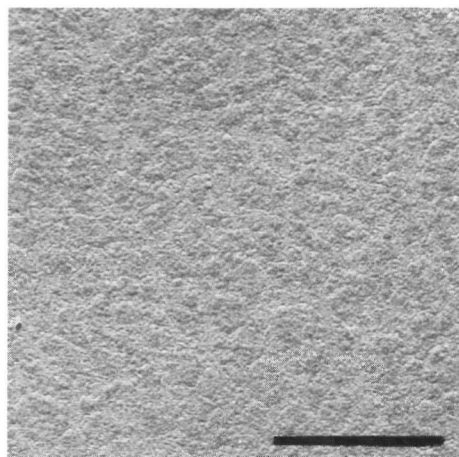


**Figure 3.6** Electron micrographs of pure polymer monolayers, picked up on a Formvar/carbon coated grid at a surface pressure of  $20 \text{ mN}\cdot\text{m}^{-1}$ : picked up directly after spreading (A); picked up after overnight expansion at zero pressure (B). Scale bar =  $1 \mu\text{m}$ .

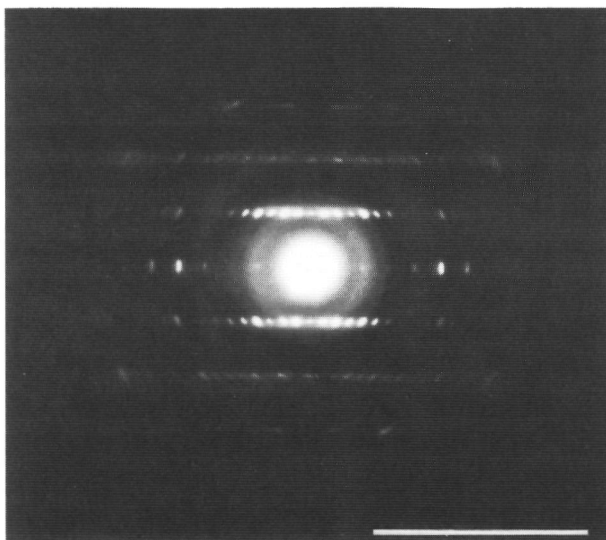


**Figure 3.7** Electron diffractogram of a nonexpanded pure polymer monolayer. Scale bar =  $1 \text{ \AA}^{-1}$ .

## 3.3.6 Ellipsometry

The observed monolayer expansion may be due to a change in the orientation of the alkoxy chains on the phthalocyanine rings, which increases the monolayer area and decreases the monolayer thickness. To investigate this, we studied the monolayer thickness by ellipsometry [9].

In principle, the film thickness  $d$  and the refractive index  $n$  of the film can be determined by ellipsometry [10]. Each measurement at a given  $\lambda$  results in two ellipsometric parameters  $\Delta$  (the phase difference between the light components perpendicular and parallel to the plane of incidence) and  $\Psi$  ( $\tan \Psi$  is the ratio of the amplitudes of the perpendicular and parallel components), whereas there are three unknown quantities:  $n_1$  (the real part of  $n$ ),  $n_2$  (the imaginary part of  $n$ ) and the film thickness  $d$ . Furthermore, the dielectric constant  $\epsilon_s$  of the substrate (+ interfacial layers) is unknown, resulting in two additional quantities that must be determined. Four LB multilayer samples each containing a well-defined layer of different total thickness  $Nd_0$  ( $d_0$  is the monolayer thickness) provide eight experimental values for  $\Delta$  and  $\Psi$ , enough to solve for  $n_1$ ,  $n_2$ , and  $d_0$ . Samples of these compositions were prepared on silicon substrates as well as on gold substrates. Deposition was carried out after overnight expansion of the polymer-arachidic acid monolayer (1:2 mixture). We did not study nonexpanded samples because the monolayer expansion during transfer would result in films that are not fully uniform. The results are shown in Table 3.III. Silicon substrates gave the most accurate results for  $n$  and  $d_0$  at  $\lambda = 632.8$  nm. For this substrate we obtained a monolayer thickness of  $d_0 = 28.8 \pm 0.5$  Å. However, we should mention that the in-plane refractive index probably differs from the refractive index perpendicular to the substrate surface, but we did not take this into account in our calculations. We performed measurements with the laser beam oriented parallel and perpendicular

**Table 3.III** Monolayer Thickness ( $d_0$ ) and Refractive Index ( $n$ ) of Polymer-Arachidic Acid (1:2) Multilayers as Determined by Ellipsometry Measurements <sup>[a]</sup>

	Sample 1	Sample 2	Sample 3
Substrate	Au	Si	Au
$N$	0/19/59	0/21/39/59	39
$\lambda$ / nm	632.8	632.8	500
$d_0$ / Å	$29.0 \pm 1.0$	$28.8 \pm 0.5$	28.5
$n_1$	$1.46 \pm 0.04$	$1.46 \pm 0.02$	1.450
$n_2$	$0.08 \pm 0.01$	$0.08 \pm 0.01$	0.018

[a]  $N$  is number of monolayers deposited on the substrate.



to the dipping direction of the substrate. No difference was observed between these two measurements, which is in agreement with the FT-IR results. Apparently, the crystalline monolayer domains with dimensions of the order of 1  $\mu\text{m}$  (see Figure 3.6A) are randomly oriented. The beam spot of the ellipsometer has a diameter of at least 1 mm and therefore includes a large number of domains. As a result the sample seen by the ellipsometer is optically isotropic.

Measurements were also carried out directly at the air-water interface. Two types of experiments were performed. First, an amount of a solution of the polymer in chloroform was spread on a water surface. This amount was calculated to be such that the whole surface could be covered with a "nonexpanded" monolayer. In a second experiment, the same water surface was only partly covered. This allowed the layer to become fully expanded after standing.

Ellipsometry measurements were carried out at a number of time intervals after the dissolved material had been spread on the water surface. From the  $\Delta$  and  $\Psi$  data the product of  $n$  and  $d_0$  was calculated using the standard three-phase model assuming temperature-corrected indexes of refraction for demineralized water of  $n_1 = 1.332$  and  $n_2 = 0.000$ .

In experiments of the second type we observed directly after spreading domains that floated in and out of the narrow detection window of the ellipsometer on the water surface. These domains had the same value of  $nd_0$  as the LB films in the first type of experiment. After a few hours we observed in the former case additional domains with a lower  $nd_0$ , and after 1 night we could only detect domains with this lower  $nd_0$ . Taking for this "expanded" film the same values for  $n_1$  and  $n_2$  as determined for our deposited LB films, *i.e.*,  $n_1 = 1.46$  and  $n_2 = 0.08$  at  $\lambda = 632.8$  nm, we can calculate a film thickness of  $29 \pm 3$  Å. This number is in good agreement with the number determined for the multilayer deposited on silicon, *viz.*,  $d_0 = 28.8 \pm 0.5$  Å. Apparently, the presence of arachidic acid in the multilayer sample does not have a great influence on the results.

The higher  $nd_0$  value measured for the nonexpanded film in the first type of experiment can be a result of a different  $n$ -value or a higher film thickness  $d_0$ . If we assume that the latter is the case and if we take for  $n_1$  and  $n_2$  the same values as from the expanded film, we may calculate a film thickness of  $49 \pm 5$  Å. This number is an approximate value, as we observed a large change in the absorption spectrum of the LB-film during expansion, as was outlined before (*vide supra*). The value of  $n_2$  is therefore expected to be larger for the nonexpanded film than for the expanded film. However, our calculations revealed that a change in  $n_2$  has only a

minor influence on the ellipsometry parameters. So the 49-Å film thickness will be a good estimate.

### 3.4 Discussion

The phthalocyanine polymer discussed in this paper has a rather flexible backbone and differs in this respect from the rigid-rod phthalocyaninatopolysiloxanes reported in the literature [3,7a]. Its monolayer properties are unusual. The observed monolayer expansion is unprecedented. Our phthalocyanine polymer does not show any flow-induced orientation during monolayer transfer. This could be due to the fact that we are dealing with a polymer with a relatively low degree of polymerization, *viz.*, only 24. The phthalocyaninatopolysiloxanes in the literature are more stiff and have a higher length/thickness aspect ratio than our polymer, resulting in a better possibility for alignment in the transfer direction.

The UV/vis and FT-IR measurements reveal that before expansion the phthalocyanine units are closely packed with their planes perpendicular to the water surface. From the surprisingly good quality of the electron diffractogram we may conclude that there is a high degree of crystallinity in the nonexpanded film. Electron micrographs show that in this film no multilayer aggregates are present. The dimension of the unit cell calculated from the electron diffractogram is in very good agreement with the area per repeating unit derived from the pressure-area isotherms: 16.6 Å is the diameter of the phthalocyanine core [3b], 3.9 Å is the interplanar distance. From these results a molecular conformation for the non-expanded monolayer can be derived as schematically depicted in Figure 3.8B. The interplanar distance is somewhat larger than the value of 3.32 Å derived from solid-state X-ray diffraction measurements [1]. This can be explained by the fact that in the solid state the alkoxy chains in the polymer are stretched out in all directions (figure 3.8A). In this state the phthalocyanine planes are stacked with a staggering angle of 45° to minimize the interplanar distance [11]. In the nonexpanded monolayer the alkoxy chains are forced to be closely aligned in vertical position (Figure 3.8B). This will cause steric repulsion between neighboring units, which explains the larger interplanar distance. The estimated 49-Å thickness of the monolayer from ellipsometry measurements on the nonexpanded film and the 67-Å<sup>2</sup> mean molecular area from the pressure-area isotherm are in line with the conformation proposed in Figure 3.8B.

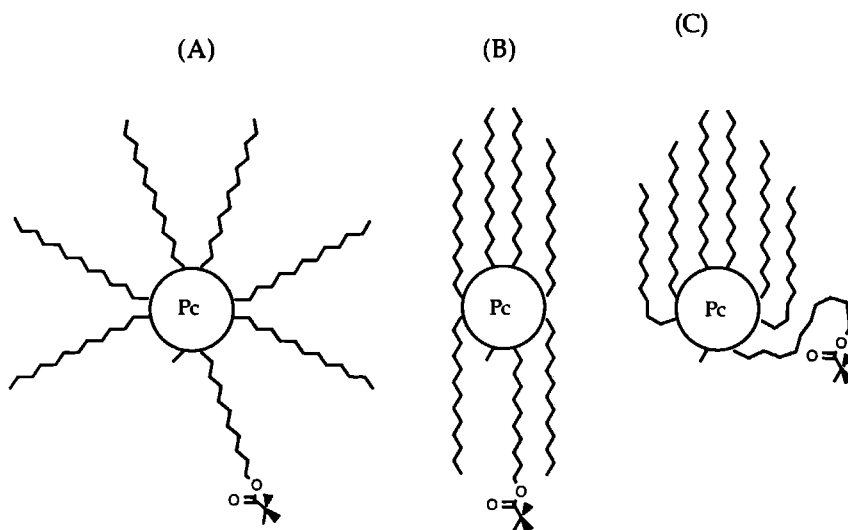


**Figure 3.8** Schematic representations of the proposed molecular conformations of one polymer repeating unit: in the solid state (A); in a monolayer at the air-water interface directly after spreading and subsequent compression (B); in a monolayer at the air-water interface after full expansion (C).

FT-IR measurements indicated that the orientation of the phthalocyanine units does not change during monolayer expansion. The observed expansion therefore must be explained by a change in the orientation of the peripheral alkoxy chains, resulting in a loss of crystallinity and a decrease in interaction between the phthalocyanine units. The latter is possible because the spacer connection with the polymeric backbone is flexible. Ellipsometry measurements revealed that  $nd_0$  decreased during expansion. From the calculated film thickness ( $d_0 = 28.8 \pm 0.5 \text{ \AA}$ ) we may derive a conformation of the expanded monolayer as depicted in Figure 3.8C. The areas per repeating unit before and after expansion are 67 and  $120 \text{ \AA}^2$ , respectively. The ratio of these numbers is 4:7, which corresponds to the number of alkoxy chains that probably contribute to the total area per repeating unit.

Our polymer is flexible and has asymmetrically substituted phthalocyanine units. As a consequence, the polymer molecules may initially orient themselves with their backbones toward the water surface. Apparently, this conformation is thermodynamically unfavorable, resulting in a very slow reorientation of the alkoxy chains away from the water surface. As a consequence the more hydrophilic phthalocyanine core becomes partly exposed to the water surface. This process will be slow because the reorientation requires a concerted movement of all the alkoxy chains in the polymer.

## References

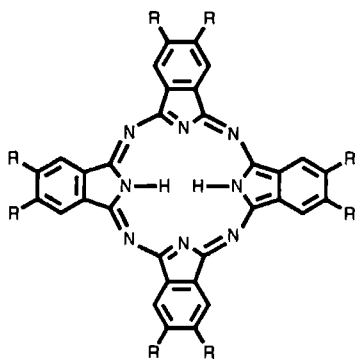
- [1] J.F. van der Pol, E. Neeleman, R.J.M. Nolte, J.W. Zwikker, W. Drenth, *Makromol. Chem.* **190** (1989) 2727.
- [2] T. Arndt, C. Bubeck, A.J. Schouten, G. Wegner, *Mikrochim. Acta* **2** (1988) 7.
- [3] (a) E. Orthmann, G. Wegner, *Angew. Chem.* **98** (1986) 1114; *Angew. Chem. Int. Ed. Engl.* **25** (1986) 1105. (b) R.G.M. Crockett, A.J. Campbell, F.R. Ahmed, *Polymer* **31** (1990) 602.
- [4] A.W. Snow, W.R. Barger, in *Phthalocyanines, Properties and Applications*, Vol. 1 (Eds: C.C. Leznoff, A.B.P. Lever); VCH Publishers: New York (1989), pp. 341-392.
- [5] See, for example: Y. Fu, M. Forman, C.C. Leznoff, A.B.P. Lever, *J. Phys. Chem.* **98** (1994) 8985.
- [6] R.H.G. Brinkhuis, A.J. Schouten, *Macromolecules* **24** (1991) 1496.
- [7] (a) T. Sauer, T. Arndt, D.N. Batchelder, A.A. Kalachev, G. Wegner, *Thin Solid Films* **187** (1990) 357. (b) M.N. Teerenstra, E.J. Vorenkamp, A.J. Schouten, R.J.M. Nolte, *Thin Solid Films* **196** (1991) 153.
- [8] R.M. Glaeser, A. Zilker, M. Radermacher, H.E. Gaub, T. Hartmann, W. Baumeister, *J. Microsc.* **161** (1991) 21.
- [9] For recent literature on ellipsometry measurements on polymer monolayers at the air-water interface and on phthalocyanines, see: (a) J. Mårtensson, H. Arwin, *Thin Solid Films* **188** (1990) 181. (b) M.K. Debe, D.R. Field, *J. Vac. Sci. Technol. A* **9** (1991) 1265. (c) M. Kawaguchi, M. Tohyama, Y. Mutoh, A. Takahashi, *Langmuir* **4** (1988) 407. (d) H. Motschmann, R. Reiter, R. Lawall, G. Duda, M. Stamm, G. Wegner, W. Knoll, *Langmuir* **7** (1991) 2743.
- [10] R.M.A. Azzam, N.M. Bashara, *Ellipsometry and Polarized Light*; North Holland Physics Publishing: Amsterdam, The Netherlands (1979).
- [11] P. Weber, D. Guillon, A. Skoulios, *Liq. Cryst.* **9** (1991) 369.

## CHAPTER 4

# Structure and Properties of a Chiral Liquid-Crystalline Phthalocyanine

### 4.1 Introduction

Most of the Pcs studied so far become liquid-crystalline only at elevated temperatures. The few Pcs that are liquid-crystalline at room temperature have branched hydrocarbon substituents [1]. Branching probably introduces disorder and hence a decrease in the transition temperature [2]. Schouten *et al.* recently synthesized the branched phthalocyanine (*R,S*)-Pc(8,2) (Chart 4.1), and studied the liquid-crystalline properties of this compound (Table 4.I) [1e]. At room temperature (*R,S*)-Pc(8,2) has a supercooled mesophase which crystallizes in a couple of hours. This compound was prepared from a racemic starting material, and the product therefore is a mixture of a large number of stereoisomers, *viz.* 43 (16 pairs of enantiomers and 11 meso compounds). Such a mixture is unfavorable for studying the relation between the molecular structure of the compound and its material properties. Therefore we synthesized the optically active phthalocyanine, with the eight chiral centers in the side chains all in the (*S*)-configuration ((*S*)-Pc(8,2)). Only



Pc(*n*) : R = O(CH<sub>2</sub>)<sub>*n*</sub>H

(*R,S*)-Pc(8,2) : R =

(*S*)-Pc(8,2) : R =

Chart 4.1

a few examples of optically active discotic mesogens are known. Destrade *et al.* have described the synthesis of chiral esters of triphenylenes and truxenes that exhibit a columnar mesophase [3]. An aligned sample of one of the former compounds was studied by X-ray diffraction, which indicated that the columns were helically distorted [4]. Ringsdorf and coworkers have suggested that films of polymers of chiral triphenylenes contain helical superstructures [5]. An optically active mesogenic dibenzopyrene has been reported which displays ferroelectrical switching [6]. One example of an optically active mesogenic Pc has been published in the literature [1b]. No evidence of a chiral superstructure was reported in this case. Noteworthy also are the recently reported optically active binaphthol substituted Pcs, which are not liquid-crystalline, but show interesting circular dichroism activity in solution [7].

In this chapter we report on the structure and physical properties of optically active (S)-Pc(8,2). X-ray and solid state NMR studies are presented as well as studies of intramolecular energy and charge transport. The results are compared with those obtained with (R,S)-Pc(8,2). In addition to this we will show that Langmuir-Blodgett (LB) films of excellent quality can be prepared from (S)-Pc(8,2).

## 4.2 Experimental Section

**Synthesis.** Metal-free 2,3,9,10,16,17,23,24-octa(R,S-3,7-dimethyloctoxy)phthalocyanine, (R,S)-Pc(8,2), was prepared as described before [1e]. The optically active derivative, (S)-Pc(8,2), was synthesized analogous to this procedure, starting from optically pure (S)-citronellol, which was purchased from Aldrich and used without further purification. The spectroscopic data of (S)-Pc(8,2) were similar to that of (R,S)-Pc(8,2) [1e]. Thermogravimetric analyses (TGA) showed that decomposition of (S)-Pc(8,2) starts at 280 °C in air, and at 350 °C under an inert atmosphere.  $[\alpha]_{546}^{20} = -1200^{\circ}$  ( $c = 0.001$  in  $\text{CHCl}_3$ );  $\text{C}_{112}\text{H}_{178}\text{N}_8\text{O}_8$  (1764.7): calcd C 76.23, H 10.17, N 6.35; found C 76.15, H 10.11, N 6.31%.

**Measurements.** Differential scanning calorimetry (DSC) data were obtained with a Mettler DSC 12E and a Perkin Elmer 7 Series Thermal Analysis System. The measurements were carried out under an inert atmosphere using 3-7 mg samples and heating and cooling rates of 1-20 °C·min<sup>-1</sup>. TGA was carried out on a Perkin Elmer 7 Series Thermal Analysis System as well as on a Perkin Elmer System 4 under ambient and inert atmospheres. For polarization microscopy (PM) a Leitz Orthoplan polarization microscope was used, equipped with a Mettler FP80/FP82

Hot Stage. Small angle X-ray scattering (SAXS) measurements were taken with a Kiessig Camera (focal distance 8.01 cm, Cu K $\alpha$  source with a wavelength of 1.5418 Å).

High-resolution solid-state NMR spectra were obtained on a Bruker AM 500 spectrometer (proton frequency 500.14 MHz, carbon frequency 125.7 MHz) equipped with a Doty 5 mm MAS probe. Magic angle spinning speeds of *ca* 4200 Hz were employed. Temperatures were measured with a Bruker VT 100 instrument. Spectra were recorded using single pulse excitation and high power proton decoupling. The spectra below -10 °C were obtained with cross-polarization (CP) with 3 ms contact time, a relaxation delay of 4 s, and a proton pulse of 5.1  $\mu$ s. 500-4000 FID's were accumulated per spectrum. Adamantane was used as secondary reference with respect to TMS for the calibration of the spectra.

Luminescence measurements were carried out using a Spex Fluorolog 2 spectrofluorometer equipped with a Xe lamp, a red-sensitive photomultiplier (Hamamatsu R928), a liquid helium flow cryostat (Oxford CF1204), and a home-made high-temperature cell. Emission spectra were recorded after excitation in the Q-band at 560 nm at temperatures between 4 and 400 K.

The pulse-radiolysis time-resolved microwave conductivity (PR-TRMC) measurements were carried out as described elsewhere [8].

**Langmuir-Blodgett film formation and characterization.** Monolayers at the air-water interface were studied by measuring pressure-area isotherms on a computer-controlled Lauda Film Balance (FW 2) with water, purified by a Milli-Q filtration system, as the subphase. The samples were dissolved in chloroform (spectroscopic quality, *ca* 1 mg·mL<sup>-1</sup>), spread on the water surface, and isotherms were recorded at a compression speed of *ca* 10 Å<sup>2</sup>·molecule<sup>-1</sup>·min<sup>-1</sup>.

Substrates were prepared as described in chapter 3. Deposition was performed by vertically dipping the substrate through a stabilized monolayer at a constant surface pressure and temperature with a speed of 5-10 mm·min<sup>-1</sup>.

UV/Vis measurements were carried out with a SLM-Aminco 3000 diode array spectrophotometer. Transmission (TM) and grazing incidence reflection (GIR) Fourier-transform infrared (FT-IR) spectra were recorded on a Bruker IFS-88 FT-IR spectrometer at 4 cm<sup>-1</sup> resolution by the method of Arndt [9]; cycles of 1000 scans were used. The TM spectra were taken from a 10-layer film on both sides of zinc sulfide substrates, and the GIR spectra were taken from a 20-layer film on gold substrates. The films were studied with polarization microscopy using the microscope that was described above. Film thicknesses and refractive indices were measured using a Gaertner L117-C single-wavelength ellipsometer ( $\lambda$  = 632.8 nm).

Small angle X-ray diffraction was performed with a Siemens D-500 powder diffractometer equipped with a graphite monochromator at the detector side, using copper  $K\alpha$ -radiation with a wavelength of 1.542 Å.

Circular dichroism (CD) spectra were recorded on a JASCO J-600 spectropolarimeter at temperatures between -10 °C and 100 °C. The molecular ellipticity,  $[\Theta]$ , is defined as [10]:

$$[\Theta] = \frac{[\Psi] \cdot M}{100} \quad (4.1)$$

with  $M$  = molecular mass and

$$[\Psi] = \frac{\Psi}{L \cdot d} \quad (4.2)$$

where  $\Psi$  = measured ellipticity (degrees),  $L$  = film thickness (dm), and  $d$  = density ( $\text{g} \cdot \text{mL}^{-1}$ ). The product of  $L$  and  $d$  in (4.2) can be calculated to be

$$L \cdot d = \frac{M \cdot n}{6 \times 10^8 \cdot A} \quad (4.3)$$

where  $n$  = number of monolayers in the film, and  $A$  = area per molecule ( $\text{\AA}^2$ ) from the pressure-area isotherm. Combination of formulas (4.1)-(4.3) gives

$$[\Theta] = \Psi \cdot \frac{6 \times 10^6 \cdot A}{n} \quad (4.4)$$

Formula (4.4) can be generally applied for the calculation of the molecular ellipticity of LB-films.

## 4.3 Results

### 4.3.1 Phase behavior

DSC measurements were performed to study the phase behavior of (S)-Pc(8,2). The phase transition temperatures and enthalpy changes are given in Table 4.I. On heating a freshly precipitated sample of (S)-Pc(8,2) a broad endothermic peak was



observed between 45 and 65 °C. This peak did not appear in the second and further heating scans. (R,S)-Pc(8,2) is known to display a similar behavior, *viz.* an irreversible transition at 70 °C, which was attributed to a crystalline (K) to mesophase (M) transition [1e]. However, in the case of (S)-Pc(8,2) the peak is less sharp and the transition enthalpy much lower, which makes a K→M transition less likely. On further heating a second small transition was found at 111 °C. The reverse transition occurs slowly, as only occasionally a weak and broad DSC peak was observed between 95 and 75 °C. At 295 °C the transition to the isotropic phase took place. On cooling (S)-Pc(8,2) below room temperature a reversible phase transition was found at 3 °C (in heating run at 14 °C), which was accompanied by a small enthalpy effect. The second and further DSC runs were similar to the first one, except that the transition between 45 and 65 °C was absent.

**Table 4.1** Phase Transition Temperatures and Enthalpy Changes Determined by DSC, and Structural Assignments from X-ray Diffraction and Polarization Microscopy [a]

Compound	Transition	T / °C [b]	ΔH / kJ mol <sup>-1</sup>
(R,S)-Pc(8,2)	K→D <sub>h</sub> [c]	70	54.6
	D <sub>h</sub> ↔I	295(293)	8.3
(S)-Pc(8,2)	A→D <sub>h</sub> * [d]	45-65	8.2
	D <sub>7</sub> ↔D <sub>h</sub> *	14(3)	6.4
	D <sub>h</sub> *↔D <sub>r</sub>	111(95-75)	3.1
	D <sub>r</sub> ↔I	295(295)	10.9

[a] A: amorphous phase, K: crystalline phase, D<sub>h</sub>: hexagonal columnar mesophase, D<sub>h</sub>\*: chiral D<sub>h</sub>-phase, D<sub>7</sub>: unknown mesophase, D<sub>r</sub>: rectangular mesophase, I: isotropic phase

[b] Temperatures as observed in heating and cooling (between brackets) DSC runs

[c] The reverse transition to the crystalline phase was not observed by DSC, but other experiments (see text) show that crystallization takes place at room temperature in a couple of hours

[d] Irreversible phase transition, only observed on heating a freshly precipitated sample

When (S)-Pc(8,2) was slowly cooled down from the isotropic phase a mosaic texture appeared under the polarization microscope, which is characteristic of a columnar mesophase (Figure 4.1a). When the material was further cooled down slowly to 70 °C, small cracks appeared in this texture, indicating a transition to a more ordered mesophase. However, when the material was quickly cooled down from the isotropic phase to room temperature a very characteristic texture was observed with spiralized concentric rings (Figure 4.1b). This result is a first

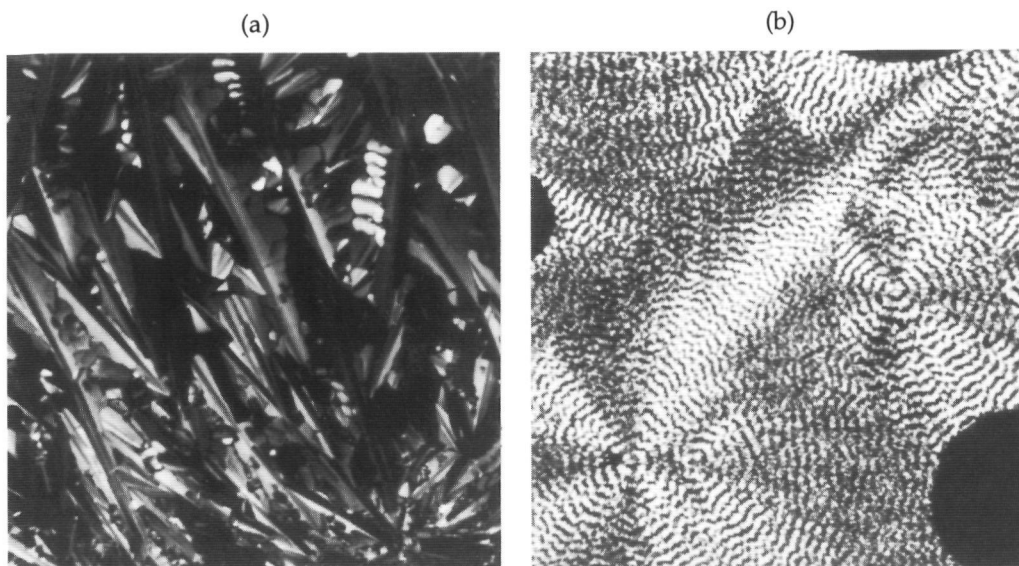


**Figure 4.1** Textures of (S)-Pc(8,2) observed between crossed polarizers at 250 °C after slowly cooling from the isotropic phase (a). Idem at room temperature after quickly cooling (b).

indication of the presence of a chiral mesophase. Spiral textures have also been reported for chiral triphenylenes [11].

The structures of two of the stable phases of (S)-Pc(8,2) were determined by powder X-ray diffraction measurements at 80 °C and at 180 °C. Due to restrictions of the apparatus, the structure of the phase below room temperature could not be determined. The results are shown in Table 4.II. A number of reflections of (S)-Pc(8,2) at 80 °C are similar to those of (R,S)-Pc(8,2), indicating that both compounds have a  $D_h$  phase. The additional, weak reflections on both sides of the 3.4 Å reflection observed in the case of (S)-Pc(8,2) indicate the presence of an extra periodicity along the columnar axis. The columnar structure can be described using the superspace approach of de Wolff, Janner, and Janssen [12], in which the periodicity is described mathematically in a higher dimensional Euclidean space. In the case of a single modulation, the set  $(hklm)$  expresses the components of a reciprocal wave vector  $\mathbf{K}$  in terms of four fundamental periodicities. In three dimensions  $\mathbf{K} = h\mathbf{a}^* + k\mathbf{b}^* + l\mathbf{c}^* + m\mathbf{q}$ , with  $\mathbf{a}^*$ ,  $\mathbf{b}^*$ , and  $\mathbf{c}^*$  referring to the basic structure and  $\mathbf{q}$  being the wave vector of the modulation. For  $m = 0$  the unmodulated structure is obtained, *i.e.* a hexagonal pattern of columns and an average intracolumnar stacking distance of 3.4 Å. The satellite reflections around 3.4 Å,  $S_1$

**Table 4.II** Spacings from X-ray Diffraction Data (Å) and Assigned Miller Indices (hklm) of (R,S)-Pc(8,2) and (S)-Pc(8,2) at Various Temperatures [a]

(hklm)	(R,S)-Pc(8,2)	(S)-Pc(8,2)	
	20 °C	80 °C	180 °C
0002	-	27 44	-
1000	24 64	24 01	26 06
0100	24 64	24 01	23 13
0003	-	18 76	-
1100	15 59	15 32	-
2000	13 87	-	13 41
2100	10 44	10 16	-
3000	9 47	9 59	-
0011	-	3 63	-
0010	3 39	3 43	3 55
001-1	-	3 22	-
<i>D</i>	31 98	31 63	-
<i>P</i>	-	57	-

[a] *P* = helical periodicity

The largest *d*-spacings are the most inaccurate ones, due to large experimental errors. They were not included in the calculation of the values of the intercolumnar distance *D*.

and  $S_2$ , are the result of the reciprocal summation of two independent periodicities. In formula,  $1/S_{1,2} = 1/34 + q/m$ . Regarding them as first order satellites ( $m = \pm 1$ ), the extra periodicity along the columnar axis can be calculated to be  $57 \pm 4$  Å. Each periodicity includes approximately 16 molecules. The extra reflections at low angles, viz. 27.4 and 18.8 Å, can be indexed as (0002) and (0003), respectively. The columnar modulation is probably the result of a helical superstructure (*vide infra*). We denote this chiral phase as a  $D_h^*$  phase.

The X-ray diffraction measurements at 180 °C gave only a few reflections. The ones that were assigned to the columnar modulation at 80 °C, had disappeared. The few low angle reflections could not be indexed according to a hexagonal lattice. They were in line with a rectangular lattice, suggesting that a  $D_r$  phase is present above 111 °C. A similar phase transition has been reported for triphenylene hexa(dodecanoate) by Safinya *et al.* [13].

## 4.3.2 Solid-state NMR

Solid-state NMR experiments were carried out to obtain insight into the structural and dynamic changes that occur at the phase transitions of (S)-Pc(8,2). For comparison, experiments were also performed with octa(dodecoxy)phthalocyanine, Pc(12).

*Aromatic core signals*  $^{13}\text{C}$  MAS NMR spectra of the aromatic core signals of (S)-Pc(8,2) showed a temperature dependence that could be correlated to the transitions found by DSC. Below  $-10\text{ }^{\circ}\text{C}$  strong cross-polarization signals were recorded for all the core carbon atoms (see Figure 4 2a). The spectra were, however, significantly broader than the corresponding spectra of Pc(12) and the previously studied Pc(11) [14]. This indicates that the structure of (S)-Pc(8,2) differs from the crystalline structure of Pc(11) and Pc(12) and is probably less ordered. Kentgens *et al* previously reported that the chemical shifts of the core carbons of Pc(11) are influenced by intermolecular ring current effects leading to well-resolved crystallographic splittings in the  $^{13}\text{C}$  MAS NMR spectra of the crystalline state [14]. In the present case such well-resolved splittings are absent, which indicates that there is a large distribution of different crystallographic sites. It is of interest to note that for carbon atom C4 in (S)-Pc(8,2) the observed chemical shift difference between the solution spectrum and the spectrum in the solid state (see Table 4 III) is much larger than for the corresponding carbon atoms in Pc(11) [14] and Pc(12) [results not shown]. This suggests that in (S)-Pc(8,2) the shielding due to neighboring molecules is larger than in Pc(12) and Pc(11), which in turn points to a more slipped and/or eclipsed molecular stacking in the former compound than in the latter ones.

**Table 4.III** Observed  $^{13}\text{C}$  Chemical Shifts (ppm) for (S)-Pc(8,2) in  $\text{CDCl}_3$  Solution and in the Solid State at Various Temperatures [a]

	C1	C2	C3	C4	C5	C6	C7	C7'	C8
$\text{CDCl}_3$	149	130.2	105.3	152.0	68.0	36.5	30.2	19.9	37.6
155 $^{\circ}\text{C}$	144.3	127.3	103.0	148.8	-	-	-	-	-
115 $^{\circ}\text{C}$	143.2	126.4	102.1	148.3	65.7	35.8	29.0	18.1	37.1
25 $^{\circ}\text{C}$	-	-	-	-	63	-	28	17	-
-15 $^{\circ}\text{C}$	-	126	-	146	-	-	-	-	-
-35 $^{\circ}\text{C}$	-	126	-	144	63	-	-	17	-
-60 $^{\circ}\text{C}$	-	127	-	144	-	-	-	-	-

[a] For the labeling of the carbon atoms see Figure 4 2

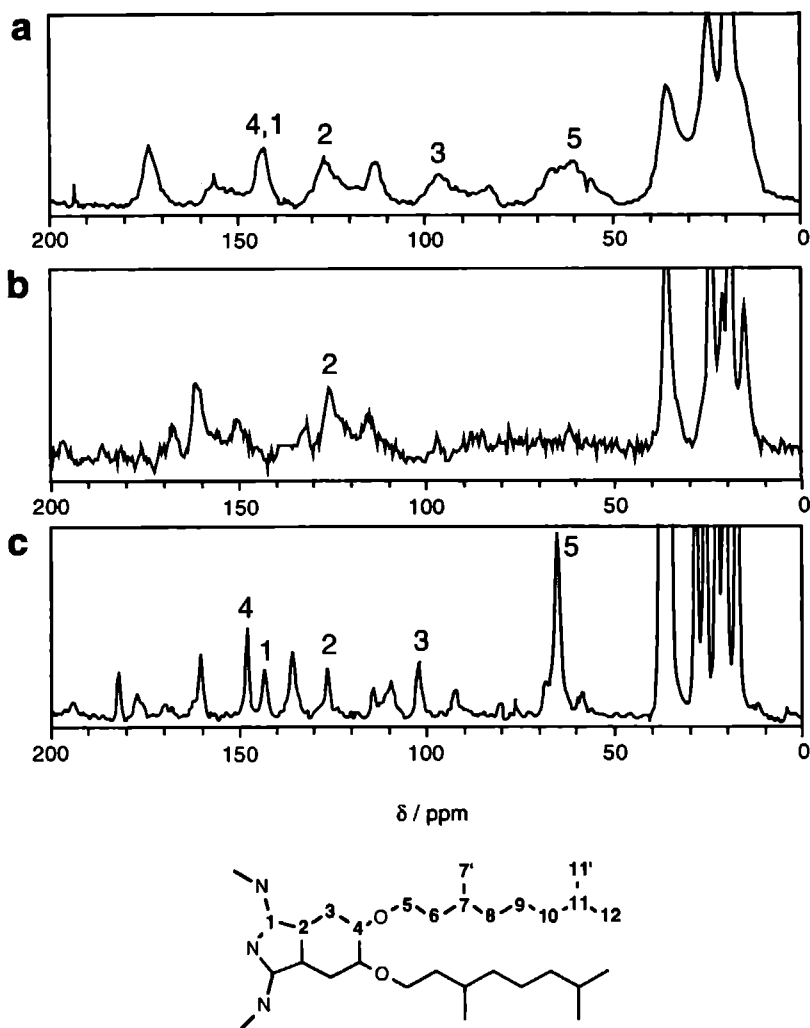


**Figure 4.2** Solid state  $^{13}\text{C}$  NMR spectra of (S)-Pc(8,2) at -60 °C with cross polarization (a), at 25 °C with cross polarization (b), and at 140 °C with direct pulse excitation (c). The labels used for spectral assignment are shown underneath. Peaks that are not numbered are spinning side bands.

At temperatures above -10 °C, close to the transition to the  $\text{D}_{\text{h}}^*$  phase, a gradual broadening of the carbon signals of the Pc core was observed. In fact, above room temperature no well-resolved spectrum could be obtained either with cross polarization or single pulse excitation (Figure 4.2b). This line broadening may indicate that the structural disorder in the sample has increased or that the

molecular motions become larger on the NMR timescale. The latter explanation seems to be the most likely, given the fact that the lines gradually disappeared. If, for instance, the molecules start to move laterally, every carbon will experience a different chemical shift as a function of time due to the ring current effects of neighboring molecules. Depending on the timescale and the amplitude of these motions this phenomenon can spread out the resonances of the carbon atoms of the core to such an extent that they become unobservable.

When the temperature was raised above 85 °C, near the  $D_h^* \rightarrow D_r$  transition, the signals of the carbon core reappeared and well-resolved lines were observed for every carbon (Figure 4.2c). At these temperatures cross polarization was no longer effective, and the single pulse excitation technique had to be applied. Similar observations were made at the crystalline to mesophase transition of Pc(11) [14] and Pc(12) [results not shown]. We attribute the sudden decrease of the cross polarization and the well resolved character of the spectra to the formation of a phase that has an organized columnar structure and a high molecular mobility. It is thought that the Pc molecules rotate rapidly around the columnar axes. Evidence for this interpretation comes from the determination of the chemical shift anisotropy using Herzfeld's and Berger's spinning side band analysis [15]. Table 4. IV shows the obtained chemical shift tensor (CST) for the C4 atom of (S)-Pc(8,2) at different temperatures. At elevated temperatures the principal values  $\sigma_{11}$  and  $\sigma_{22}$  of this tensor, which lie in the plane of the molecule, are equal, demonstrating that the system has axial symmetry. At low temperatures the tensor is clearly non-axial. This averaging of the chemical shift anisotropy in the plane of the molecule when entering the mesophase, was also observed for Pc(12).

**Table 4.IV** Principal Values (in ppm) of the Chemical Shift Tensor of the C4 Carbon of (S)-Pc(8,2) at Various Temperatures [a]

	$\sigma_{11}$	$\sigma_{22}$	$\sigma_{33}$
180 °C	184	184	75
155 °C	182	182	76
-15 °C	210	162	61
-60 °C	211	161	60

[a] The  $\sigma_{11}$ ,  $\sigma_{22}$  axes are parallel with the molecular plane, the  $\sigma_{33}$  axis is perpendicular to the molecular plane.

*Side chain signals* The linear chain phthalocyanine Pc(11) shows a sudden change in the high field (alkane) region of the solid state NMR spectrum around the  $K \rightarrow D_h$  transition, as we reported previously [14]. Broad peaks are observed in

the crystalline phase, indicating that the side chains are rigid, but they appear liquid-like (sharp lines) in the mesophase. A similar behavior was observed for Pc(12). Such a sudden change did not occur in the case of (S)-Pc(8,2). Below 0 °C the lines are also broad (Figure 4.3a), and above 85 °C also sharp (Figure 4.3c), but - in contrast to Pc(11) and Pc(12) - the peak widths change gradually in between these two temperatures. Very striking is the observation that the temperature at which each side chain carbon atom of (S)-Pc(8,2) becomes mobile increases with decreasing distance of the atom from the core, which was not so clearly observed for the linear chain Pcs. The signals of the three terminal carbon atoms C11, C11' and C12 of (S)-Pc(8,2) already are sharp at -30 °C, suggesting that this part of the side chains is mobile at this temperature. Above 10 °C the peaks of atoms C7', C9, and C10 become sharper (see Figure 4.3b), and above 60 °C the mobility of atoms C7 and C8 increases. Finally, atom C6 becomes mobile above 85 °C. A similar stepwise change in side chain mobility was found by Leisen *et al.* in their NMR studies of a liquid-crystalline triphenylene [16].

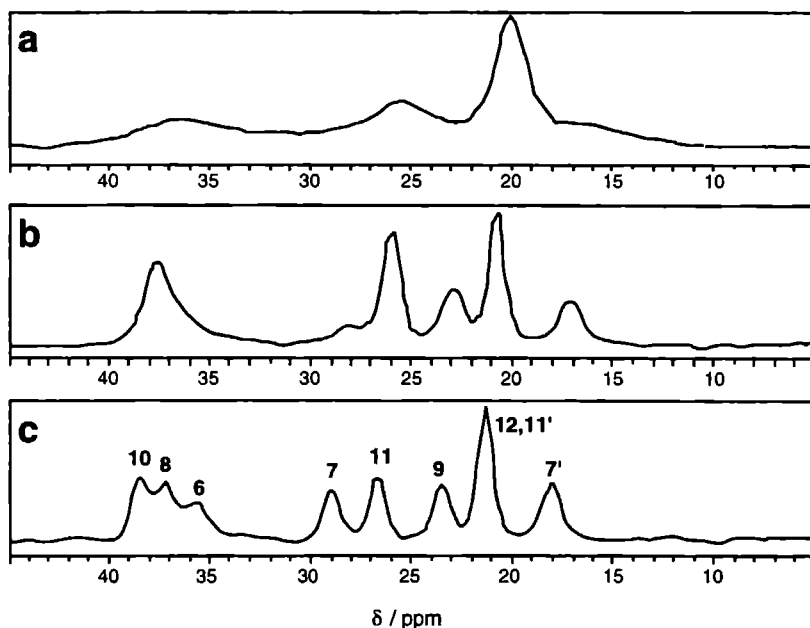


**Figure 4.3** Aliphatic regions of the solid state  $^{13}\text{C}$  NMR spectra of (S)-Pc(8,2) at -60 °C with cross polarization (a), at 25 °C with cross polarization (b), and at 115 °C with direct pulse excitation (c).

The signals of the side chain carbon atoms in the solid state spectrum at different temperatures are summarized in Table 4.III. They are shifted upfield as compared to the solution spectrum. This effect is most pronounced for carbon atoms C5 and C7', especially at lower temperatures. This result provides information about the conformation of the side chains of the phthalocyanines. It is known that a  $\gamma$ -substituent causes a shielding of 5 ppm on a carbon atom when it is in a gauche conformation with respect to this carbon atom [17]. The side chain conformation that is in line with a  $\gamma$ -effect on both C5 and C7' - and only on these carbon atoms - is shown in Figure 4.4a. The other possible conformations (Figures 4.4b,c) are unlikely as these would lead to an upfield shift on carbon atom C8. Taking for C5 the most stable arrangement (in-plane with the Pc core and C5-O *syn* with C3-C4 of the aromate) [16,18], we may derive what the conformation of the side chains is, at least at temperatures below 60 °C, see Figure 4.4d. Thus, the methyl groups at the chiral centers are positioned alternately above and under the molecular plane. Such an arrangement may result in an overall chiral molecular shape, which could be the origin of the helical superstructure in the  $D_h^*$  phase.

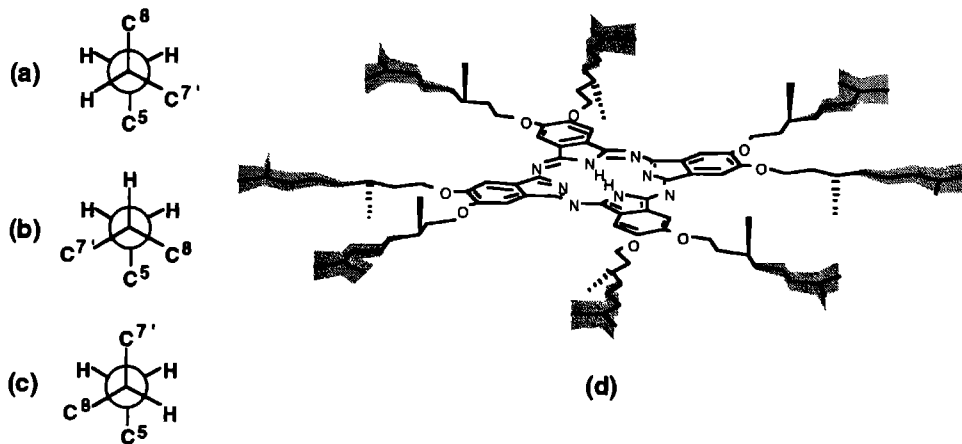


**Figure 4.4** Newman representation of the three possible side chain conformations of (S)-Pc(8,2) around the bond between C6 and C7 (a-c), and representation of the most probable molecular conformation of the phthalocyanine (d). The ends of the side-chains have no fixed conformation (shaded areas).



**Proton spectra.** The solid state  $^1\text{H}$ -NMR spectrum of Pc(12) in its mesophase displayed three peaks (not shown): a large one at 1.5 ppm due to the side chain protons, a small peak at 4.1 ppm resulting from the protons at C5, and a peak at 5.8 ppm from the aromatic protons. The latter one is shifted 3 ppm upfield as compared to the solution spectrum, because of intermolecular ring current effects [14]. On cooling, line-broadening was found to take place at the transition to the crystalline phase near 85 °C, probably because the axial symmetry phases out. This change takes place within a temperature range of 5 °C. A similar line-broadening of the proton signals was observed on cooling (S)-Pc(8,2) (results not shown). However, with the latter compound this change took place over a larger temperature range, *i.e.* between 82 and 70 °C, which is in line with the DSC data.

#### 4.3.3 Luminescence

Energy migration in the columns of (S)-Pc(8,2) and (R,S)-Pc(8,2) was studied by carrying out luminescence experiments in the temperature range of 4 to 400 K. Blasse *et al.* have performed similar experiments with the linear side chain phthalocyanine Pc(12) [19]. They discussed their results using a model in which mobile excitons decay, after excitation in the Q-band, at different sites in the columnar stacks: at intrinsic sites (positionally undisturbed Pc molecules, radiative decay), at extrinsic sites (strongly disturbed molecules, radiative decay), and at quenching sites (nonradiative decay). The wavelengths of emission were reported to be 795 nm for the intrinsic sites and approximately 820 nm for the extrinsic sites.

Luminescence spectra of (S)-Pc(8,2) and (R,S)-Pc(8,2) were recorded during a heating and cooling cycle starting at 4 K. Some spectra of (S)-Pc(8,2) at different temperatures are given in Figure 4.5. Figure 4.6 shows the intensity at the wavelength of the emission maximum,  $I_{\text{max}}$ , as a function of temperature for the two compounds. The intensity is seen to decrease gradually with increasing temperature until a plateau is reached at approximately 200 K. This loss of intensity was also observed for Pc(12), and can be explained from the fact that excitons migrate faster through the stacks at higher temperatures, and can reach quenching sites (copper phthalocyanine molecules left from the synthesis) more easily. At *ca* 345 K, the luminescence drops to almost zero for both (S)-Pc(8,2) and (R,S)-Pc(8,2). In the case of the latter compound this sudden change in intensity coincides with the  $\text{K} \rightarrow \text{D}_\text{H}$  transition; it occurs within a temperature range of 10 °C. This behavior is

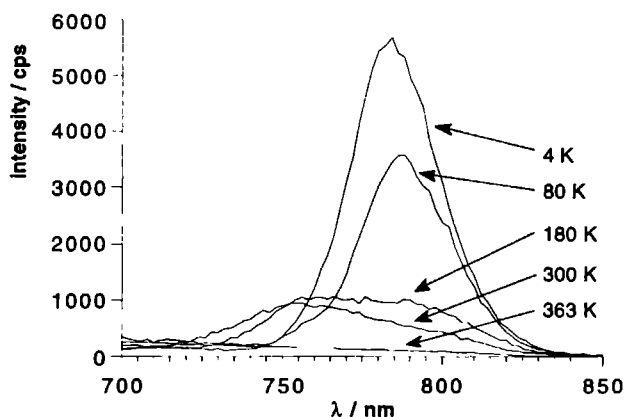


**Figure 4.5** Emission spectra of (S)-Pc(8,2) at different temperatures. Excitation is in the Q-band at 560 nm.

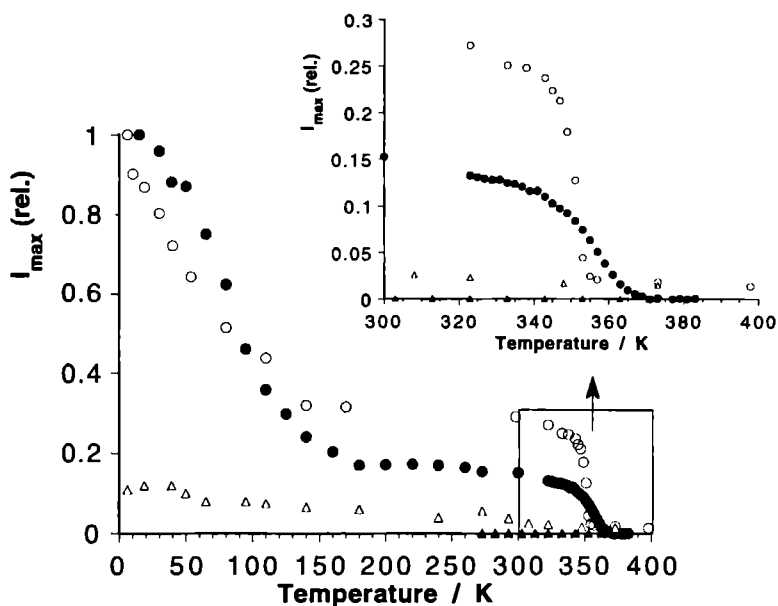


**Figure 4.6** Normalized emission intensity at the wavelength of maximum emission measured for (R,S)-Pc(8,2) during heating (open circles) and cooling (open triangles). Idem for (S)-Pc(8,2) during heating (closed circles) and cooling (closed triangles). Inset: enlargement of the temperature range 300 - 400 K.

similar to that found for Pc(12). In the mesophase - unlike the crystalline phase - the Pc molecules are oriented perpendicular to the columnar axes, which leads to a faster migration of the excitons and a more rapid trapping at quenching sites [19]. The drop in luminescence intensity observed for (S)-Pc(8,2) cannot be due to a  $K \rightarrow D_h$  transition, because such a transition is not found by DSC. Moreover, the disappearance of the luminescence is much slower for (S)-Pc(8,2) than for (R,S)-Pc(8,2), as it occurs over a temperature range of *ca* 25 °C. Although it does not coincide exactly, this change may be related to the slow transition found by DSC between 45 and 65 °C. The latter probably involves the transformation of a distorted columnar mesophase to an undistorted one. In the undistorted phase energy migration will be more efficient. Other experiments corroborate this hypothesis (*vide infra*).

For both (S)-Pc(8,2) and (R,S)-Pc(8,2) the initial emission intensity does not reappear on cooling, not even at 4 K. Apparently, at low temperatures the mesophase is frozen, and fast exciton migration can still occur through the well organized, stacked Pc cores. Van der Pol *et al.* observed a similar fast energy migration at low temperatures for phthalocyanines in which the mesophase was fixed by polymerization [20].

Phthalocyanine (S)-Pc(8,2) differs in an interesting way from (R,S)-Pc(8,2) and Pc(12). For the latter two compounds a gradual shift in the wavelength of the emission maximum was observed with increasing temperature, *viz.* from *ca* 790 nm at 4 K to *ca* 820 nm above 80 K. This phenomenon was explained previously by a change in the radiative decay mechanism, *viz.* from a decay *via* intrinsic sites to decay *via* extrinsic sites [19]. The emission of (S)-Pc(8,2) was found to shift to shorter wavelengths with increasing temperature, *viz.* from 788 nm at 4 K to 756 nm above 200 K (see Figure 4.5). This contrasting behavior must be due to the helical columnar structure of (S)-Pc(8,2). At low temperatures (R,S)-Pc(8,2) and Pc(12) are crystalline, whereas (S)-Pc(8,2) is probably in a distorted helical mesophase, *i.e.* the molecules are more or less cofacially stacked, but the length of the columns is limited. At 4 K fast energy migration is therefore still possible for (S)-Pc(8,2), but trapping takes place more frequently at the large number of distorted (extrinsic) sites. On increasing the temperature thermal detrapping occurs, and emission from the undistorted (intrinsic) sites at shorter wavelength is now predominant. Above 70 °C the columnar stacking improves slowly, and energy migration to quenching sites is so efficient that only nonradiative quenching takes place.

## 4.3.4 Microwave conductivity

In a recent paper we discussed the effect of structural modifications on charge migration, as measured by the TRMC technique, in several mesogenic Pcs [8]. The results obtained with (S)-Pc(8,2) and (R,S)-Pc(8,2) are summarized in this section.

Figure 4.7 shows the temperature dependence of the dose normalized end-of-pulse conductivity,  $\Delta\sigma_{\text{eop}}/D$ , of the two phthalocyanines. The initial value of  $\Delta\sigma_{\text{eop}}/D$  measured in the crystalline phase of (R,S)-Pc(8,2) at 25 °C is close to that found in the crystalline phase of *n*-alkoxy Pcs [8]. The sudden decrease of the conductivity by a factor of 5 at the  $K \rightarrow D_h$  transition is also observed with *n*-alkoxy Pcs. This decrease is ascribed to the fact that the molecular motions in the mesophase are stronger than in the crystalline phase, causing the path for charge migration to be less efficient [8]. On cooling,  $\Delta\sigma_{\text{eop}}/D$  of (R,S)-Pc(8,2) does not immediately return to its initial value, as found for the *n*-alkoxy compounds. This feature is in line with the absence of a  $D_h \rightarrow K$  phase transition in the DSC cooling runs. The conductivity eventually returns, however, to the starting level after standing at room temperature for a period of several hours. During this time the material slowly reassumes the initial solid state structure. The small increase in

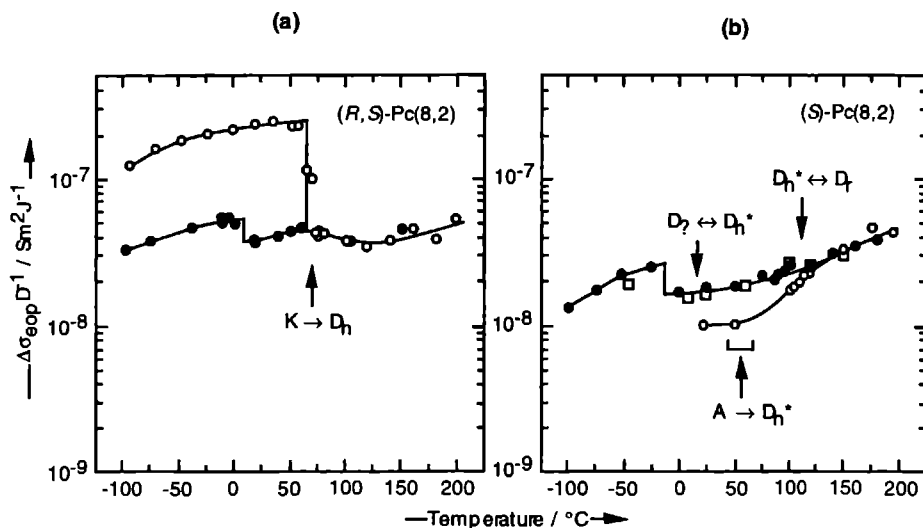


**Figure 4.7** Dose normalized radiation induced end-of-pulse conductivity versus temperature for (R,S)-Pc(8,2) (a) and (S)-Pc(8,2) (b) on heating (open circles) and cooling (filled circles). For (S)-Pc(8,2) the open squares represent the values during the second heating. The arrows indicate the phase transition temperatures.

$\Delta\sigma_{\text{eop}}/D$  observed at *ca* 0 °C, is probably the result of a phase transition that is not seen by DSC.

In contrast to the mixture of stereoisomers, (S)-Pc(8,2) does not show a sudden decrease in  $\Delta\sigma_{\text{eop}}/D$  upon heating, which is in agreement with the absence of a  $K \rightarrow D_h$  transition for the latter compound. Remarkably, the  $D_h^* \rightarrow D_r$  transition at 111 °C has no influence on the charge migration. Above 150 °C both (S)-Pc(8,2) and (R,S)-Pc(8,2) have the same  $\Delta\sigma_{\text{eop}}/D$  value. Figure 4.7b shows that upon cooling, the conductivity of the optically active phthalocyanine does not return to its starting value but remains higher by a factor of approximately 2. This result suggests that the stacking of the molecules in a sample of (S)-Pc(8,2) that is freshly precipitated from solution, is unfavorable for charge migration, and that this stacking improves irreversibly upon heating. The same conclusion was drawn from the energy migration experiments. This observation corroborates the idea (*vide supra*) that the irreversible endothermic peak observed by DSC between 45 and 65 °C is not a real phase transition but a slow reorganization of the phthalocyanine molecules.

Upon further cooling, (S)-Pc(8,2) displayed a slight increase in  $\Delta\sigma_{\text{eop}}/D$  at approximately 0 °C, which coincides with the phase transition found by DSC. A second heating trajectory was found to correspond with the first cooling trajectory (see Figure 4.7b). The low starting value recorded for the freshly precipitated sample at room temperature was never observed again after the first heating trajectory.

The values of  $\Delta\sigma_{\text{eop}}/D$  of (S)-Pc(8,2) below 150 °C are lower than those of (R,S)-Pc(8,2). This indicates that the molecular packing in the former compound is less favorable for one-dimensional charge migration than in the latter compound. We will return to this below.

#### 4.3.5 Monolayers and LB films

The construction of LB-films from discotic molecules that are liquid-crystalline at room temperature has not been reported in the literature. Because such liquid-crystalline behavior is thought to be favorable for the construction of well-organized and stable Langmuir-Blodgett (LB)-films [21], we performed monolayer studies on (S)-Pc(8,2) and (R,S)-Pc(8,2). [\*]

[\*] Schutte *et al.* reported that (R,S)-Pc(8,2) can be used for deposition as LB-films [22].

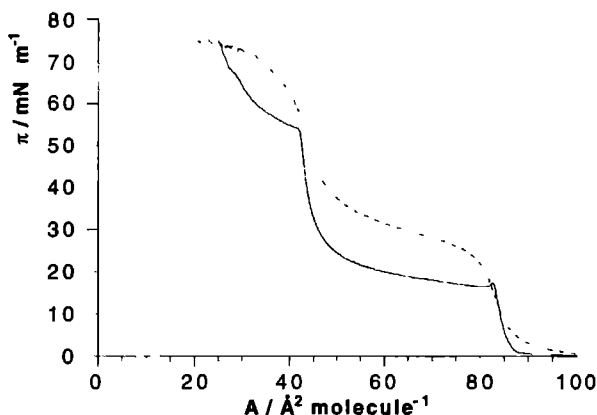


**Figure 4.8** Surface pressure versus surface area isotherms for (R,S)-Pc(8,2) (broken line) and (S)-Pc(8,2) (solid line) at a subphase temperature of 20 °C.

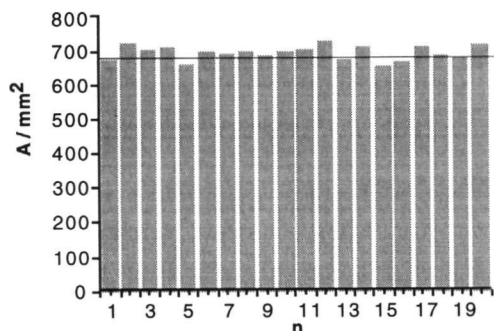
Figure 4.8 shows the pressure-area isotherms of (R,S)-Pc(8,2) and (S)-Pc(8,2) at 20 °C. The two isotherms are very similar and indicate that phase transitions occur when the films are compressed. For (S)-Pc(8,2) a first rise in surface pressure is found at an area of 85 Å<sup>2</sup> per molecule. This small number suggests that the planes of the phthalocyanine molecules are oriented perpendicularly to the water surface. Four side chains are bent towards the air-water interface, while the other side chains extend into the air. Similar values of the molecular areas have been reported for other phthalocyanines (see chapter 3 and reference 23). Upon further lowering the surface area, a second pressure increase can be seen at 45 Å<sup>2</sup> per molecule. Interestingly, this value is approximately half the value of the area where the first increase takes place, suggesting that a bilayer is formed (see also below). At higher subphase temperatures even a third rise in pressure (not shown) was observed at one third of the area of the first increase, which may point to the formation of a triple layer.

Stability is a prerequisite if one wants to transfer a monolayer uniformly onto a substrate. We therefore studied the change in surface area as a function of time when the surface pressure was kept constant. The decays of the surface area per hour for (S)-Pc(8,2) at various surface pressures and temperatures are reported in Table 4.V. At a surface pressure of 8 mN·m<sup>-1</sup> the monolayer was unstable at elevated temperatures and weakly stable at low temperatures. In contrast, at a surface pressure of 30 mN·m<sup>-1</sup>, *i.e.* when probably a bilayer is present, a stable film was obtained at 20 °C. This was found to hold for both (S)-Pc(8,2) and (R,S)-Pc(8,2).

**Table 4.V** Decay of the Surface Area of (S)-Pc(8,2) Films at the Air-Water Interface as a Function of the Surface Pressure ( $\pi$ ) and the Temperature (T)

$\pi$ / $\text{mN}\cdot\text{m}^{-1}$	T / $^{\circ}\text{C}$	decay / ( $\text{\AA}^2\cdot\text{molecule}^{-1}\cdot\text{hr}^{-1}$ )
8	5	0.966
8	35	2.66
30	20	0.298

**Figure 4.9** Transferred area versus layer number measured for the deposition of a bilayer of (S)-Pc(8,2) on a gold substrate at a surface pressure of  $30 \text{ mN}\cdot\text{m}^{-1}$  and a temperature of  $20^{\circ}\text{C}$ . The first layer is from downstroke deposition. The horizontal line indicates the covered area on the substrate.



Transfer of the (S)-Pc(8,2) film turned out to be very irregular and troublesome in the monolayer phase, even at lower temperatures. However, in the bilayer phase transfer was possible with a constant transfer ratio close to unity, as can be seen in Figure 4.9. Transfer was observed during both upstroke and downstroke dipping, *i.e.* Y-type multilayers were obtained. Up to 20 bilayers were assembled onto hydrophobized glass, quartz, silicon, gold, and zinc sulfide substrates.

The anisotropy of the LB-films was clearly visible by polarization microscopy. When a glass substrate containing 10 bilayers was placed between crossed polarizers no light was transmitted if the transfer direction of the LB-film was parallel to the analyzer or polarizer. Intermediate orientations of the glass gave a structureless bright field. The anisotropic properties of the material were studied by polarized absorption spectroscopy on quartz slides with 10 bilayers on both sides of the substrate. Figure 4.10 shows the absorption spectra of a freshly prepared film and those of the same film after annealing for one hour at  $100^{\circ}\text{C}$ , with the light polarized parallel and perpendicular to the transfer direction. For the freshly prepared sample the maximum of the Q-band is found at a wavelength of 617 nm. The blue-shift of this band, as compared to the solution spectrum, indicates that the molecules in the LB-film are stacked in columns; the spectrum is similar to the

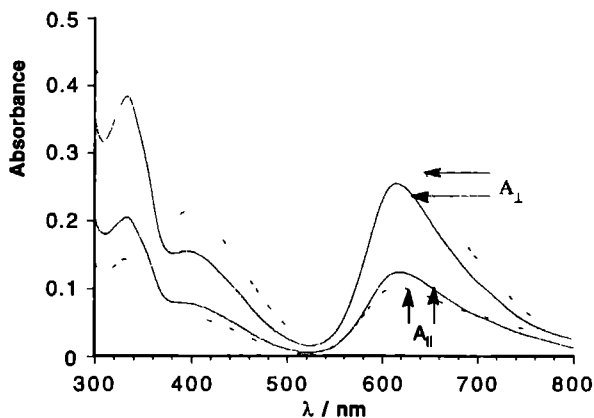


**Figure 4.10** Electronic absorption spectra of 2x10 bilayers of (S)-Pc(8,2) on quartz slides directly after preparation of the LB films (solid lines) and after one night annealing at 100 °C (broken lines). The spectra were recorded with the light polarized parallel ( $\parallel$ ) and perpendicular ( $\perp$ ) to the dipping direction.

spectra of alkoxymethyl Pc [24] and of alkoxy Pc [own work] in their mesophases. The wavelength of the absorption maximum decreases to 612 nm after annealing of the film, which suggests that the number of molecules in the stacks is increased. The highest absorption is found when the polarized light is perpendicular to the transfer direction, which means that the columns are predominantly aligned in the dipping direction. The dichroic ratio,  $R$ , can be determined using the formula [25]:

$$(A_{\perp})_i = R (A_{\parallel})_i + (a - Rb) \quad (4.5)$$

where  $(A_{\perp})_i$  and  $(A_{\parallel})_i$  are the absorptions measured at the  $i$ th wavenumber based on the given baselines, and  $a$  and  $b$  are the differences between the given baselines and the true baseline. Table 4.VI shows the values of  $R$  that were calculated by fitting the datapoints to eqn. (4.5). A dichroic ratio of 1.85 was found for the freshly prepared film, and a value of 3.32 for the film that had been annealed for one hour. Longer annealing times did not further increase this number. The two-dimensional order parameter,  $S$ , for the cofacial stacks, and the mean deviation angle of the columnar axis from the transfer direction,  $\psi$ , can be calculated from the following equations [26]:

$$S = \frac{R - 1}{R + 1} \quad (4.6)$$



$$\langle \sin^2 \psi \rangle = \frac{1}{R + 1} \quad (4.7)$$

As can be seen in Table 4.VI,  $S$  increases and  $\psi$  decreases on thermal annealing, which clearly demonstrates the beneficial effect of this treatment on the organization of the molecules in the LB-films.

**Table 4.VI** Dichroic Ratio ( $R$ ), Two Dimensional Order Parameter ( $S$ ), Mean Deviation Angle ( $\psi$ ), and Real ( $n_r$ ) and Imaginary ( $n_{im}$ ) Parts of the Refractive Index, Both Parallel and Perpendicular to the Transfer Direction, of an LB-Film of (S)-Pc(8,2) Before and After Annealing for One Hour at 100 °C [a]

	Before annealing	After annealing
$R$	1.85	3.32
$S$	0.29	0.54
$\psi$ / degrees	36	29
$n_{r,  }$	1.68	1.63
$n_{r,\perp}$	1.78	1.83
$n_{im,  }$	0.02	0.01
$n_{im,\perp}$	0.08	0.08

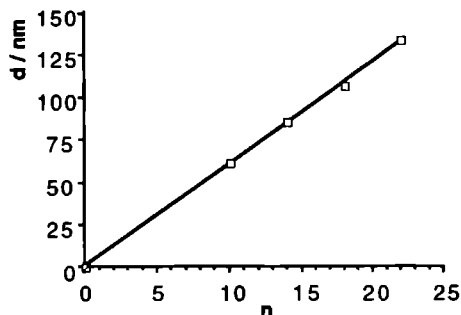
[a] The refractive indices are derived from ellipsometry measurements, the other parameters are obtained from spectroscopic studies.

In the LB trough the molecules of (S)-Pc(8,2) are probably oriented perpendicularly to the water surface. The same is true for the bilayer phase at a surface pressure of 30 mN·m<sup>-1</sup>. FT-IR spectroscopy revealed that this molecular orientation is retained in the transferred LB-films (results not shown). The out-of-plane vibrations at 850 (=C-H) and 740 cm<sup>-1</sup> (Pc ring deformation) are practically absent in the grazing incidence reflection (GIR) spectrum (the field vector of the IR beam is oriented perpendicularly to the substrate surface), whereas they are very distinct in the transmission (TM) spectrum when the field vector is parallel to the transfer direction. In the TM spectrum recorded with the polarized light perpendicular to the transfer direction, these out-of-plane vibrations are only weak. This difference in the two TM spectra is due to the anisotropic arrangement of the molecules within the layers. The perpendicular orientation of the Pc molecular planes with respect to the substrate surface, did not change after thermal annealing of the film.

In order to confirm the presence of bilayers, ellipsometry experiments were carried out on LB-films deposited on a silicon substrate. The ellipsometric parameters  $\Delta$  and  $\Psi$  were measured for parallel and perpendicular orientations of the sample with respect to the plane of incidence of the laser beam. These values were

fitted using an anisotropic model [27], in such a way that for both orientations the thickness of the film was equal. The calculated film thickness as a function of the number of transferred layers is displayed in Figure 4.11. From this figure a layer thickness of 60.4 Å can be derived. This high value can only be explained if indeed bilayers are transferred onto the substrate: half the thickness is close to the diameter of one molecule, *viz.* 31.63 Å as derived from X-ray measurements (Table 4.II). Thermal annealing did not affect the film thickness within experimental error, but the real and imaginary refractive indices became more anisotropic, as can be judged from the values in Table 4.VI.

**Figure 4.11** Film thickness, as calculated from ellipsometry measurements, versus the number of transferred bilayers of (S)-Pc(8,2). The measurements indicated that a 6 nm SiO<sub>2</sub> layer was present on the bare silicon substrate. The measured values are corrected for this 6 nm layer.



The layer structure of the film was studied by small angle X-ray scattering measurements, using a sample containing 10 bilayers of (S)-Pc(8,2) on a glass slide. As can be seen in Figure 4.12, the scattering curve of the freshly prepared sample at 20 °C shows three broad peaks, which correspond with *d* spacings of 31.9, 25.5, and 21.1 Å. It is not possible to derive an unequivocal structure from this result. The 31.9 and 25.5 Å spacings may be related to a rectangular and a hexagonal arrangement of the cylindrical columns, respectively, with the latter spacing being approximately equal to the (1000) reflection of the bulk sample (see Table 4.II). Probably both arrangements are present in the film. The 21.1 Å spacing might be some higher order reflection. Alternatively, there could be a coexistence of different phases probably with different orientations. The film then consists of domains with different structures and lattice periodicities. This is in line with the low number of Kiessig fringes at small angles, which indicates that the overall film thickness is not well defined.

When the film is heated to 100 °C, only one of the Bragg peaks is left, *viz.* the one at 25.4 Å (Figure 4.12). Moreover, the number of Kiessig fringes is increased, which is a result of a decreased roughness of the film surface. It can be concluded

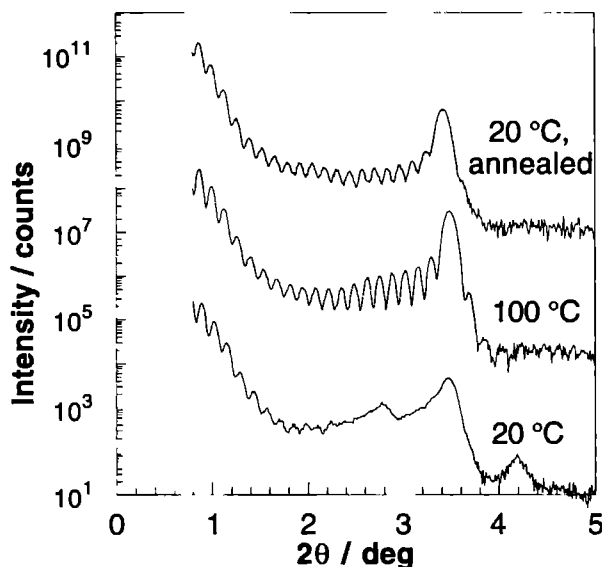


**Figure 4.12** X-ray scattering curves at different temperatures of a sample containing 10 bilayers of (S)-Pc(8,2) on glass. The curves are displaced along the y-axis to avoid overlapping.

that a reorganization has taken place to a hexagonal packing. At the same time the thickness of the film has become more homogeneous. From the periodicity of the Kiessig fringes the overall film thickness can be calculated to be 659 Å. This value is not equal to the product of the layer spacing and the number of layers, *i.e.*  $20 \times 25.4 = 508$  Å. The molecular area of the film at the air-water interface and the constant and well-defined transfer ratio (*vide supra*) indicate that bilayers must have been deposited. It is possible that the bilayers rearrange on the solid support, which lead to a thicker film with defects. It is also imaginable that only parts of the film are responsible for the Kiessig fringes. Such parts could fail to give a Bragg reflection due to a disordered structure. More experiments are required to solve this problem. The overall film thickness calculated from ellipsometry (604 Å) deviates somewhat from the X-ray results (659 Å), which is due to the larger inaccuracy of the former technique.

When the film was cooled back to 20 °C its structure remained unchanged, even after a period of 10 days (see Figure 4.12). The layer spacing was found to increase slightly to 25.8 Å by this treatment.

## 4.3.6 Circular dichroism

Circular dichroism (CD) spectroscopy is a powerful tool to obtain structural information related to optical activity [10]. We studied phthalocyanine (S)-Pc(8,2) with the help of this technique. Spectra were recorded in solution and were also taken from LB-films.

A solution of (S)-Pc(8,2) in chloroform did not give a CD spectrum. A similar negative result was obtained in the case of a freshly prepared LB-film. However, when the temperature was raised above 60 °C this film displayed CD activity (Figure 4.13). When the sample was subsequently cooled to room temperature, this activity was retained, even after standing for one night. Further cooling down to -10 °C did not change the spectrum. The calculated molecular ellipticity  $[\theta]$  is very high. Under the same experimental conditions a LB-film of (R,S)-Pc(8,2) did not show any CD activity at room temperature, or at elevated temperatures. Apparently, the thermal annealing of the LB-film of (S)-Pc(8,2) leads to a more ordered structure (as discussed above) and consequently to the observed strong CD activity. As a solution of (S)-Pc(8,2) does not give a CD spectrum, the CD activity of the film must be the result of a chiral superstructure.

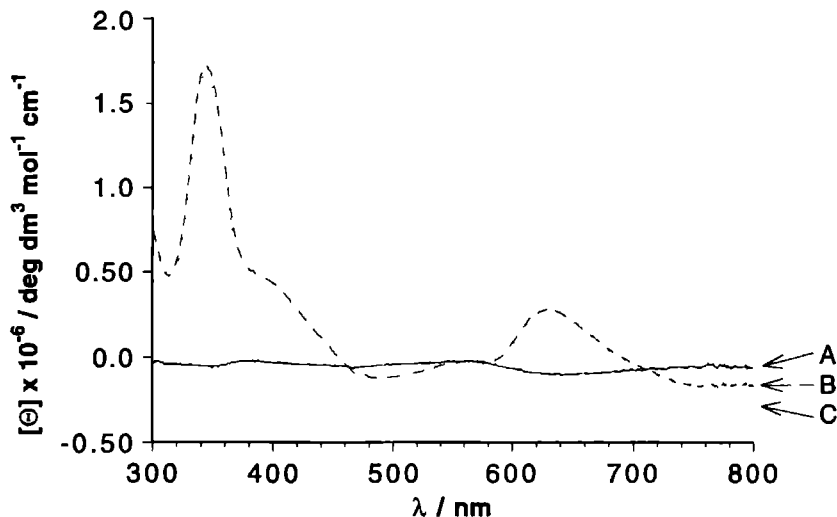


**Figure 4.13** Circular dichroism spectra of 2x10 bilayers of (S)-Pc(8,2) on quartz: freshly prepared sample at 20 °C (A); sample at 100 °C (B), and sample after cooling to 20 °C (C).

When measuring the CD spectrum of an anisotropic solid medium, one should be aware of artefacts due to linear dichroism (LD) [28]. A method to check for such artefacts is to record spectra at sample orientations differing by 90° [29]. We observed no appreciable difference when the LB film of (S)-Pc(8,2) was measured in horizontal or vertical position. Another argument against a LD contribution in our CD spectra is the absence of CD activity in the freshly prepared LB film of (S)-Pc(8,2) and in the film of (R,S)-Pc(8,2), although LD was clearly observed in the two samples.

Figure 4.13 clearly shows a negative exciton effect in the Q-band region, especially for the sample that was cooled to 20 °C after annealing. This feature indicates that the  $\pi$ - $\pi^*$  transition dipoles of the Pc molecules are coupled in a left-handed chiral arrangement [10]. It is possible to derive the exact orientations of the molecules with respect to each other by comparing the measured CD spectrum with the calculated one, but because of the complexity of the system this is not easily performed. We plan to do CD calculations in the near future.

#### 4.4 Discussion

From the results presented in the foregoing section a rather complete picture emerges of the structure and dynamical properties of optically active phthalocyanine (S)-Pc(8,2) in its various phases. One of the striking results is that this compound lacks a crystalline phase, unlike (R,S)-Pc(8,2). This was not *a priori* expected. Because (S)-Pc(8,2) is only one stereoisomer, it was thought to crystallize more readily than the mixture of (R,S)-Pc(8,2), which contains 43 stereoisomers. The reason for this curious behavior is not yet clear.

A freshly precipitated sample of (S)-Pc(8,2) is in a type of distorted mesophase, which slowly reorganizes to a more ordered mesophase on heating above 65 °C. This reorganization - which is irreversible - is evident from the following experimental results: (i) DSC, which shows a broad peak with a low transition enthalpy in the first heating scan only, (ii) the disappearance of luminescence, indicating that energy migration is very efficient in the more ordered mesophase, (iii) an increase of the microwave conductivity, (iv) the improvement of the anisotropy and the layer structure of the LB-films of the compound, and (v) the development of a very strong CD activity in the LB-films. The difference between the distorted mesophase in the freshly precipitated sample and the ordered mesophase after annealing may be the number of kinks in the columnar stacks, which are probably

larger in the former case than in the latter. This is concluded from luminescence experiments, which show that in freshly precipitated (S)-Pc(8,2) at low temperatures energy trapping predominantly occurs at extrinsic sites.

The ordered mesophase of (S)-Pc(8,2) has a unique structure. From X-ray diffraction experiments, polarization microscopy, and CD measurements we may conclude that a chiral superstructure is present in this phase. We will compare three possible limiting structures (Figure 4.14). Destrade and coworkers postulated the presence of a spiral staircase-like structure in the mesophase of an optically active triphenylene, where the molecules are displaced perpendicularly to the columnar axis (Figure 4.14a) [11]. Such a molecular arrangement is unlikely for (S)-Pc(8,2) since it would lead to an intercolumnar distance that is larger than the distance between the columns in the mesophase of (R,S)-Pc(8,2). Our X-ray results show that the intercolumnar distance of (S)-Pc(8,2) is slightly smaller than that of (R,S)-Pc(8,2) (Table 4.II). Levelut *et al.* proposed that the above mentioned chiral triphenylene molecules are aligned in a way as is shown in Figure 4.14b [4]: moving along the columnar axis the staggering angle of two neighboring molecules is constant and always in the same direction. In our case such a superstructure can make that the dipoles of the aromatic cores of the Pc molecules are arranged in the form of a left-handed helix, and can give a negative CD effect. It is, however, difficult to understand how such a staggered arrangement can give rise to the characteristic X-ray diffraction pattern shown in Table 4.II. We, therefore, propose a

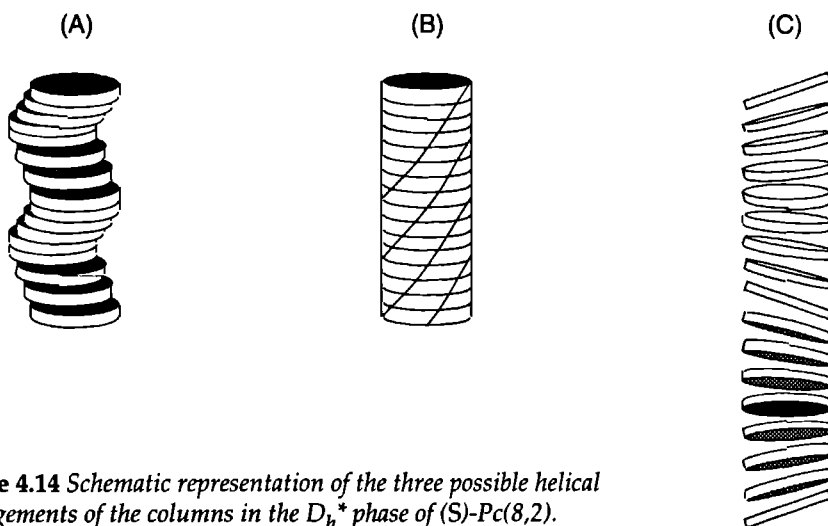


**Figure 4.14** Schematic representation of the three possible helical arrangements of the columns in the  $D_h^*$  phase of (S)-Pc(8,2).

third superstructure, which is schematically represented in Figure 4.14c. The molecules of (S)-Pc(8,2) are slightly tilted and, moving along the columnar axis, the normal of the Pc-plane gradually rotates around the columnar axis forming a left-handed helix. We denote this novel mesophase as a  $D_h^*$  phase. The columnar modulation giving rise to the X-ray diffraction pattern is now more obvious. CD calculations and X-ray diffraction studies as well as NMR experiments on aligned samples will give more conclusive information about the actual structure. Such experiments are under way.

No solid state NMR signals from the aromatic cores of the Pc molecules are observed in the  $D_h^*$  phase, probably because of line broadening due to the helical displacement of the Pc macrocycles and because of exchange broadening due to molecular motions. The mobility of the side chains increases gradually with increasing temperature. From the signals in the NMR spectra it follows that the side chains adopt an overall chiral molecular conformation, as illustrated in Figure 4.4, at least at temperatures below 60 °C. The presence of such a chiral conformation may be the reason why a helix is formed. The helical distortion of the columns appears to be unfavorable for intracolumnar charge migration. This can be concluded from the fact that for (S)-Pc(8,2) a lower microwave conductivity is observed at room temperature than for (R,S)-Pc(8,2).

On heating (S)-Pc(8,2) from the  $D_h^*$  phase a small transition is observed by DSC at 111 °C. The hexagonal arrangement of the columns is lost and a new phase appears, probably a  $D_r$  phase. A dramatic change near this phase transition is recorded by solid state  $^{13}\text{C}$  NMR: the Pc molecules start to rotate around their columnar axes and the side chains become completely liquid-like. Interestingly, these changes have hardly any influence on the charge migration, as the microwave conductivity shows no sudden change around this transition. The reverse transition from the  $D_r$  to the  $D_h^*$  phase appears to be slow, according to DSC and solid state  $^1\text{H}$  NMR.

On cooling (S)-Pc(8,2) from the  $D_h^*$  phase another transition occurs at 3 °C. The precise structure of the phase that is entered, could not be elucidated. The transition enthalpy is very low, which suggests that no major structural change takes place at the transition. NMR measurements indicate that the aromatic core as well as the side chains of the Pc molecules become almost completely immobile on the NMR timescale below 3 °C. TRMC measurements reveal a slight increase in the microwave conductivity. We believe that at  $T < 3$  °C, the structure of the  $D_h^*$  phase becomes frozen in, resulting in a slightly better intracolumnar charge

migration. The columnar stacking is not changed, since energy migration remains very efficient and the CD activity is still present.

Our experiments indicate that intracolumnar charge migration is faster in the crystalline phase than in the mesophase. Apparently, transport of electrons and electron holes is very much dependent on the molecular motions that occur in the mesophase and on the columnar deformations that are present (columnar kinks and helical superstructure). Even in the supercooled, frozen mesophase charges do not migrate very efficiently. On the contrary, energy migration appears to be faster in the mesophase than in the crystalline phase and is not affected by molecular motions. It is disfavored by the noncofacial stacking of the molecules in the crystalline phase and by columnar kinks in the mesophase. For efficient energy migration close contact, whether permanently or incidentally, between the molecules in one column seems to be essential. For hopping of electrons or holes an undistorted, rigid stacking is required.

We have shown that it is possible to prepare an excellent quality LB-film from our mesogenic Pc [<sup>\*</sup>]. Very striking is the observation that a bilayer, and perhaps even a multilayer, of (S)-Pc(8,2) can be formed at the air-water interface. The bilayer is more stable and can be better transferred than the monolayer. So far, only few examples are known of compounds that form multilayers on a water surface [31]. Rapp *et al.* described a liquid-crystalline compound displaying this behavior [31b]. Multilayer formation was explained from the fact that (i) the mesogens have only weak interactions with the water surface, and (ii) they do not collapse to an undefined state but rather form highly ordered structures, guided by the interactions between the molecules forming a liquid-crystalline phase. In a similar way, the formation of stable bilayers by (S)-Pc(8,2) (and also by (R,S)-Pc(8,2)) can be explained from the occurrence of a mesophase at ambient temperature.

The ability to form well-organized LB-films, the rich phase behavior, and the optically active properties, make (S)-Pc(8,2) an interesting compound for future applications, *e.g.* in electronic and ferroelectrical devices, and in optical data storage systems.

---

[<sup>\*</sup>] Recently, Cook and coworkers described the formation of LB-films from a phthalocyanine that is mesogenic at elevated temperatures [30].



## References

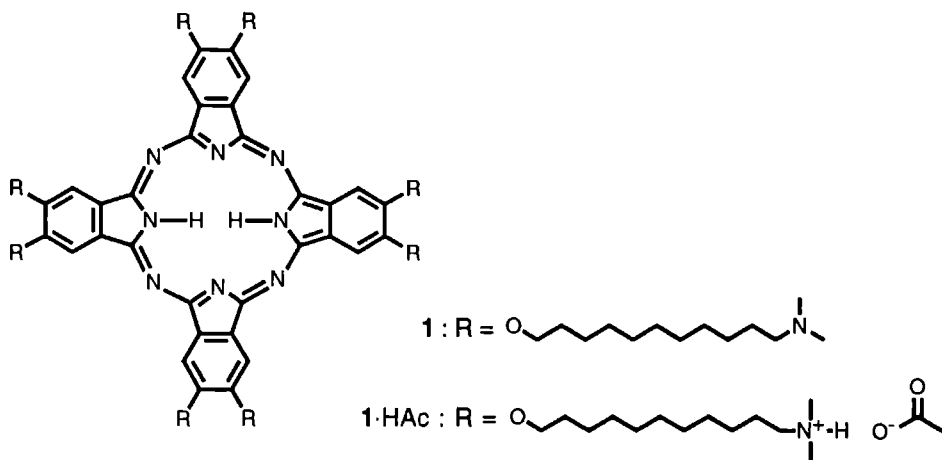
- [1] (a) A.N. Cammidge, M.J. Cook, K.J. Harrison, N.B. McKeown, *J. Chem. Soc. Perkin Trans. I* (1991) 3053. (b) I. Cho, Y. Lim, *Mol. Cryst. Liq. Cryst.* **154** (1988) 9. (c) W.T. Ford, L. Sumner, W. Zhu, Y.H. Chang, P.-J. Um, K.H. Choi, P.A. Heiney, N.C. Maliszewskyj, *New J. Chem.* **18** (1994) 495. (d) D. Lelièvre, L. Bosio, J. Simon, J.-J. André, F. Bensebaa, *J. Am. Chem. Soc.* **114** (1992) 4475. (e) P.G. Schouten, J.F. van der Pol, J.W. Zwikker, W. Drenth, S.J. Picken, *Mol. Cryst. Liq. Cryst.* **195** (1991) 291; *ibid.* **208** (1991) 109.
- [2] D.M. Collard, C.P. Lillya, *J. Am. Chem. Soc.* **113** (1991) 8577.
- [3] C. Destrade, N.H. Tinh, J. Malthête, J. Jacques, *Phys. Lett. A* **79** (1980) 189.
- [4] A.M. Levelut, P. Oswald, A. Ghanem, J. Malthête, *J. Physique* **45** (1984) 745.
- [5] M.M. Green, H. Ringsdorf, J. Wagner, R. Wüstefeld, *Angew. Chem.* **102** (1990) 1525. *Angew. Chem. Int. Ed. Engl.* **29** (1990) 1478.
- [6] H. Bock, W. Helfrich, *Liq. Cryst.* **12** (1992) 697.
- [7] N. Kobayashi, Y. Kobayashi, T. Osa, *J. Am. Chem. Soc.* **115** (1993) 10994.
- [8] P.G. Schouten, J.M. Warman, M.P. de Haas, C.F. van Nostrum, G.H. Gelink, R.J.M. Nolte, M.J. Copyn, J.W. Zwikker, M.K. Engel, M. Hanack, W.T. Ford, *J. Am. Chem. Soc.* **116** (1994) 6880.
- [9] T. Arndt, C. Bubeck, A.J. Schouten, G. Wegner, *Mikrochim. Acta* **2** (1988) 7.
- [10] N. Harada, K. Nakanishi, *Circular Dichroic Spectroscopy - Exciton Coupling in Organic Chemistry*, Oxford University Press, Oxford (1983).
- [11] J. Malthête, J. Jacques, N.H. Tinh, C. Destrade, *Nature* **298** (1982) 46.
- [12] (a) P.M. de Wolff, *Acta Crystallogr. Sect. A* **30** (1974) 777. (b) A. Janner, T. Janssen, *Phys. Rev. B* **15** (1977) 643.
- [13] C.R. Safinya, N.A. Clark, K.S. Liang, W.A. Varady, L.Y. Chiang, *Mol. Cryst. Liq. Cryst.* **123** (1985) 205.
- [14] A.P.M. Kentgens, B.A. Markies, J.F. van der Pol, R.J.M. Nolte, *J. Am. Chem. Soc.* **112** (1990) 8800.
- [15] J. Herzfeld, A.E. Berger, *J. Chem. Phys.* **73** (1980) 6021.
- [16] J. Leisen, M. Werth, C. Boeffel, H.W. Spiess, *J. Chem. Phys.* **97** (1992) 3749.
- [17] A.E. Tonelli, F.C. Schilling, *Acc. Chem. Res.* **14** (1981) 233.
- [18] J.F. van der Pol, E. Neeleman, J.W. Zwikker, R.J.M. Nolte, W. Drenth, *Recl. Trav. Chim. Pays-Bas* **107** (1988) 615.
- [19] G. Blasse, G.J. Dirksen, A. Meijerink, J.F. van der Pol, E. Neeleman, W. Drenth, *Chem. Phys. Lett.* **154** (1989) 420.
- [20] (a) J.F. van der Pol, E. Neeleman, J.C. van Miltenburg, J.W. Zwikker, R.J.M. Nolte, W. Drenth, *Macromolecules* **23** (1990) 155. (b) J.F. van der Pol, J.W. Zwikker, J.M. Warman, M.P. de Haas, *Recl. Trav. Chim. Pays-Bas* **109** (1990) 208.
- [21] (a) H. Ringsdorf, B. Schlarb, J. Venzmer, *Angew. Chem.* **100** (1988) 117; *Angew. Chem. Int. Ed. Engl.* **27** (1988) 113. (b) T.L. Penner, J.S. Schildkraut, H. Ringsdorf, A. Schuster, *Macromolecules* **24** (1991) 1041. (c) A. Laschewsky, *Adv. Mater.* **1** (1989) 392.
- [22] W.J. Schutte, M. Sluyters-Rehbach, J.H. Sluyters, *J. Phys. Chem.* **97** (1993) 6069.
- [23] (a) W.R. Barger, A.W. Snow, H. Wohltjen, N.L. Jarvis, *Thin Solid Films* **133** (1985) 197. (b) Y. Fu, A.B.P. Lever, *J. Phys. Chem.* **95** (1991) 6979. (c) H. Nakahara, K. Fukuda, K. Kitahara, H. Nishi, *Thin Solid Films* **178** (1989) 361.

- (d) E. Orthmann, G. Wegner, *Angew. Chem.* **98** (1986) 1114; *Angew. Chem. Int. Ed. Engl.* **25** (1986) 1105. (e) G.G. Roberts, M.C. Petty, S. Baker, M.T. Fowler, N.J. Thomas, *Thin Solid Films* **132** (1985) 113. (f) Y.L. Hua, D.P. Jiang, Z.Y. Shu, M.C. Petty, G.G. Roberts, M.M. Ahmad, *Thin Solid Films* **192** (1990) 383.
- [24] D. Markovitsi, I. Lécuyer, J. Simon, *J. Phys. Chem.* **95** (1991) 3620.
- [25] S. Schwiegk, T. Vahlenkamp, Y. Xu, G. Wegner, *Macromolecules* **25** (1992) 2513.
- [26] T. Sauer, T. Arndt, D.N. Batchelder, A.A. Kalachev, G. Wegner, *Thin Solid Films* **187** (1990) 357.
- [27] R.M.A. Azzam, N.M. Bashara, *Ellipsometry and Polarized Light*; North Holland Physics Publishing, Amsterdam (1979), p. 354.
- [28] J. Schellman, H.P. Jensen, *Chem. Rev.* **87** (1987) 1359.
- [29] M.J. Tunis-Schneider, M. Maestre, *J. Mol. Biol.* **52** (1970) 521.
- [30] M.J. Cook, J. McMurdo, D.A. Miles, R.H. Poynter, J.M. Simmons, S.D. Haslam, R.M. Richardson, K. Welford, *J. Mater. Chem.* **4** (1994) 1205.
- [31] (a) M. VandeAuweraer, C. Catry, L. Feng Chi, O. Karthaus, W. Knoll, H. Ringsdorf, M. Sawodny, C. Urban, *Thin Solid Films* **210/211** (1992) 39. (b) B. Rapp, M. Eberhardt, H. Gruler, *Makromol. Chem. Macromol. Symp.* **46** (1991) 439. (c) P.A. Albouy, *J. Phys. Chem.* **98** (1994) 8543. (d) F. Takeda, M. Matsumoto, T. Takenaka, Y. Fujiyoshi, N. Uyeda, *J. Coll. Interf. Sci.* **91** (1983) 267. (e) M.N. Teerenstra, E.J. Vorenkamp, A.J. Schouten, R.J.M. Nolte, C.A. van Walree, J.F. van der Pol, J.W. Zwikker, *Thin Solid Films* **210/211** (1992) 496.

## Synthesis and Properties of a Novel Amphotropic Phthalocyanine

### 5.1 Introduction

It has been suggested that amphotropic molecules, *i.e.* molecules which have both lyotropic and thermotropic mesogenic properties, would be very suitable for the construction of stable and well-organized Langmuir-Blodgett (LB) films [1]. Only one recent example of an amphotropic phthalocyanine (Pc) has been described in the literature, *viz.* a Pc which is substituted with oligoethylene chains [2]. We have designed a novel amphotropic Pc which is substituted with eight hydrophobic alkoxy chains terminating in a polar (1) or - after protonation - a charged group (1·HAc). Benzenes and triphenylenes containing similar side chains have been reported to form lyotropic mesophases in water [3]. Pcs with amino or ammonium groups, attached to shorter (propyl) side chains have been synthesized previously [4], but the liquid-crystalline properties of these molecules are unknown.



In view of their structural resemblance with mesogenic alkoxy Pcs and their amphiphilic character, we anticipated that compounds **1** and **1-HAc** will form both thermotropic and lyotropic liquid-crystalline phases. These features have been investigated and the results are presented in this chapter. The presence of hydrophilic groups at the outer end of the side chains may allow the molecules of **1** and **1-HAc** to adopt a completely flat orientation on a water surface, *i.e.* with both the Pc core and the side chains parallel to the interface. Deposition of molecules that have such orientations may result in LB films, in which the Pc units are cofacially stacked in columns of well-defined length. These columns will be oriented perpendicular to the substrate surface (see Figure 5.1 for different possible orientations of the Pc molecules).

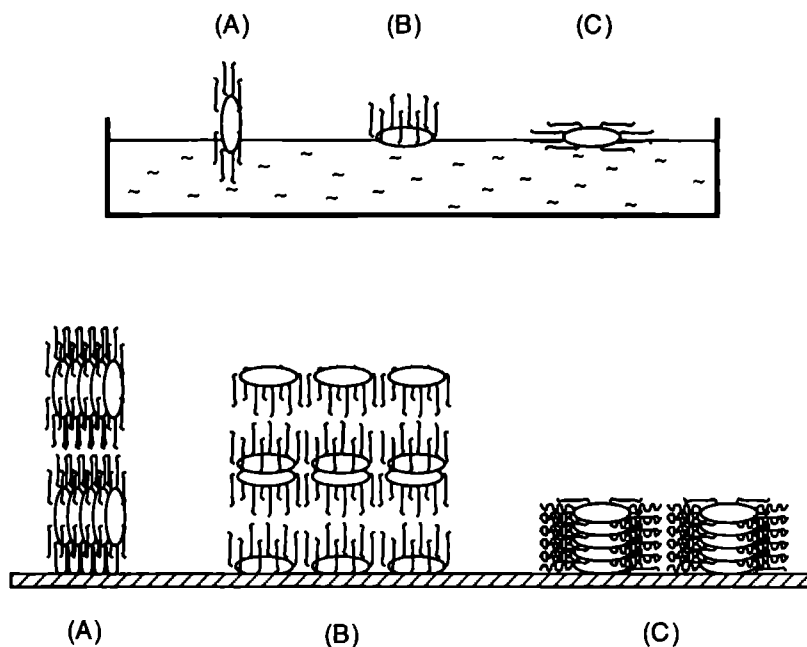


**Figure 5.1** Schematic representation of three possible molecular arrangements of substituted Pcs on a water surface (top), and the corresponding structures of multilayers deposited on a solid substrate (bottom).

## 5.2 Experimental Section

**Materials and methods.** All solvents were dried before use. Catechol was recrystallized from toluene. All other reagents were used as supplied without further purification.

Melting points were determined with a Reichert hot-stage microscope and are uncorrected. Infrared (IR) spectra were recorded with a Perkin Elmer 1720-X Infrared Fourier Transform Spectrophotometer. UV/Vis spectra were obtained with a Perkin Elmer Lambda 5 Spectrophotometer.  $^1\text{H}$  NMR spectra were recorded with Bruker WH-90, AC-100, and WM-400 instruments, and  $^{13}\text{C}$  NMR spectra were obtained with the latter instrument. Chemical shifts are reported in ppm downfield from internal TMS standard. Abbreviations used are: s = singlet, t = triplet, br = broad. Electronic Ionization (EI) and Chemical ionization (CI) mass spectra (MS) were obtained with a VG-7070E apparatus. Elemental analysis were carried out with an EA 1108 Carlo Erba instrument.

Differential scanning calorimetry (DSC) data were obtained with a Perkin Elmer 7 Series Thermal Analysis System. The measurements were carried out under an inert atmosphere with heating and cooling rates of  $10\text{ }^\circ\text{C}\cdot\text{min}^{-1}$ . For polarizing microscopy a Leitz Orthoplan polarizing microscope was used, equipped with a Mettler FP80/FP82 Hot Stage. Recordings were taken with a video camera and a Mitsubishi Color Video Copy Processor. Recordings from powder small angle X-ray scattering (SAXS) measurements were taken with a Kiessig Camera with a focal distance of 8.01 cm, using a  $\text{Cu K}\alpha$  source with a wavelength of  $1.5418\text{ \AA}$ .

Monolayers at the air-water interface were studied by measuring pressure-area isotherms on a computer-controlled Lauda Film Balance (FW 2) using water that was purified by a Milli-Q filtration system as the subphase. Samples of 25-150  $\mu\text{L}$ , dissolved in chloroform (spectroscopic quality, *ca*  $1\text{ mg}\cdot\text{mL}^{-1}$ ), were spread on the water surface, and isotherms were recorded using a compression time of 15 min (corresponding to speeds of  $15\text{-}90\text{ \AA}^2\cdot\text{molecule}^{-1}\cdot\text{min}^{-1}$ ) at  $20\text{ }^\circ\text{C}$ . Deposition of monolayers onto hydrophobized glass was carried out by vertically dipping the substrate through the monolayer after equilibration at a surface pressure of  $7.5\text{ mN}\cdot\text{m}^{-1}$  and using a dipping speed of  $10\text{ mm}\cdot\text{min}^{-1}$ . Intermissions of 0.5 and 2 min were applied after immersion and draw up, respectively.

**Syntheses.** **4,5-Dibromocatechol (2).** Catechol (38.8 g, 0.35 mol) was suspended in tetrachloromethane (400 mL) and cooled on ice. Molecular bromine (56 g, 0.70 mol), dissolved in tetrachloromethane (50 mL), was slowly added from a dropping

funnel, while stirring. Escaping HBr gas was caught in an aqueous NaOH solution. After complete addition, the reaction mixture was stirred for 16 h at room temperature. The solid was filtered, washed with tetrachloromethane, dried, and stored under nitrogen atmosphere. Yield: 86.3 g (91%). White solid, mp 119 °C. IR (KBr)  $\lambda^{-1}$  [ $\text{cm}^{-1}$ ] = 651 (ArBr), 1268 (ArO), 3443 (OH).  $^1\text{H}$  NMR ( $\text{CDCl}_3$ , 90 MHz)  $\delta$  [ppm] 5.30 (s, 2H, OH), 7.06 (s, 2H, ArH).

**1,2-Bis(11'-hydroxyundecoxy)-4,5-dibromobenzene (3).** 4,5-Dibromocatechol (25.4 g, 0.095 mol) and 11-bromoundecanol (49.9 g, 0.20 mol) were dissolved in DMF (400 mL). The flask was evacuated and filled with nitrogen gas (3x).  $\text{K}_2\text{CO}_3$  (89.3 g, 0.35 mol) was added and the mixture was stirred at 100 °C under a nitrogen atmosphere for 24 h. After cooling, water (400 mL) was added and the product was extracted with chloroform (3x100 mL). The combined extracts were washed with water (3x50 mL), dried over  $\text{MgSO}_4$ , filtered, and the solvent was evaporated under vacuum. The resulting solid was recrystallized from dichloromethane. Yield: 50.1 g (87%). White solid, mp 86 °C. IR (KBr)  $\lambda^{-1}$  [ $\text{cm}^{-1}$ ] = 654 (Ar-Br), 1203, 1251 (Ar-O-C), 3262 (OH).  $^1\text{H}$  NMR ( $\text{CDCl}_3$ )  $\delta$  [ppm] 1.30 (s, 36H,  $\text{CH}_2$ ), 3.64 (t, 4H,  $\text{CH}_2\text{OH}$ ), 3.94 (t, 4H,  $\text{CH}_2\text{OAr}$ ), 7.02 (s, 2H, ArH). MS (EI)  $m/z$  608 ( $\text{M}^+$ ). Anal. Calcd for  $\text{C}_{28}\text{H}_{48}\text{Br}_2\text{O}_4$ : C, 55.27; H, 7.95. Found: C, 55.87; H, 7.85.

**1,2-Bis(11'-chloroundecoxy)-4,5-dibromobenzene (4).** Compound 3 (16.0 g, 0.026 mol) and triethylamine (5.34 g, 0.053 mol) were dissolved in 1,2-dichloroethane (200 mL). Thionyl chloride (25.1 g, 0.211 mol) in 1,2-dichloroethane (25 mL) was added very slowly, while vigorously stirring. After the addition was complete, the mixture was refluxed for 1 h. The solvent was evaporated under vacuum, and chloroform was added. The solution was washed with 1 N aqueous HCl (2x) and with water (2x), dried over  $\text{MgSO}_4$ , and concentrated. The product was pure on TLC and used without further purification. Yield: 16.6 g (98%). Yellow solid, mp 35 °C. IR (KBr)  $\lambda^{-1}$  [ $\text{cm}^{-1}$ ] = 652 (Ar-Br), 830 (C-Cl), 1202, 1251 (Ar-O-C).  $^1\text{H}$  NMR ( $\text{CDCl}_3$ )  $\delta$  [ppm] 1.30 (s, 36H,  $\text{CH}_2$ ), 3.64 (t, 4H,  $\text{CH}_2\text{Cl}$ ), 3.94 (t, 4H,  $\text{CH}_2\text{O}$ ), 7.06 (s, 2H, ArH).

**1,2-Bis(11'-N,N-dimethylaminoundecoxy)-4,5-dibromobenzene (5).** Dimethylamine was expelled from a 40% aqueous solution by addition of KOH, and transferred with a stream of nitrogen to a condenser, which was cooled to -78 °C and mounted above an ice-cooled 100 mL reaction vessel. Finely powdered 4 (16.5 g, 0.026 mol) was added in small portions to the condensed dimethylamine (75 mL), while vigorously stirring. The vessel was completely filled with dimethylamine, and placed in an autoclave. The latter was closed and the reaction mixture was stirred at 100 °C for 48 h. After this period the autoclave was carefully opened, and the mixture was stirred for 2 h at room temperature to evaporate the solvent.

Chloroform was added, and the solution was washed with 1 N aqueous NaOH (1x) and with water (2x), dried over MgSO<sub>4</sub>, and evaporated under vacuum. Yield: 16.8 g (99%) of a yellow, viscous oil. IR (KBr)  $\lambda^{-1}$  [cm<sup>-1</sup>] = 652 (Ar-Br), 1190, 1250 (Ar-O-C), 2777, 2823 (C-N). <sup>1</sup>H NMR (CDCl<sub>3</sub>)  $\delta$  [ppm] 1.30 (s, 36H, CH<sub>2</sub>), 2.26 (t, 4H, CH<sub>2</sub>N), 2.26 (s, 12H, CH<sub>3</sub>N), 3.94 (t, 4H, CH<sub>2</sub>O), 7.06 (s, 2H, ArH). MS (CI)  $m/z$  661 (M<sup>+</sup>-1). Anal. Calcd for C<sub>32</sub>H<sub>58</sub>Br<sub>2</sub>N<sub>2</sub>O<sub>2</sub>: C, 58.00; H, 8.82; N, 4.23. Found: C, 57.52; H, 9.35; N, 4.18. The product is not entirely pure (see Results section).

**1,2-Bis(11'-N,N-dimethylaminoundecoxy)-4,5-dicyanobenzene (6).** A mixture of compound 5 (16.8 g, 0.025 mol), CuCN (22.7 g, 0.252 mol), and pyridine (20.0 g, 0.253 mol) in DMF (200 mL) was refluxed under a nitrogen atmosphere for approximately 48 h. After the reaction was complete (as checked by TLC), the mixture was cooled to room temperature and poured into 25% aqueous ammonia (500 mL). Air was bubbled through the mixture for 2 h. Subsequently, the reaction mixture was extracted with chloroform (4x150 mL). The extracts were washed with diluted aqueous ammonia (2x100 mL) and water (4x100 mL), dried over MgSO<sub>4</sub>, and concentrated. The product was partially purified by chromatography on basic alumina (activity 5) with ethyl acetate as the eluent. Yield: 2.94 g (21%). Yellow solid, mp 76 °C. IR (KBr)  $\lambda^{-1}$  [cm<sup>-1</sup>] = 1173, 1268 (Ar-O-C), 2231 (C≡N), 2777, 2823 (C-N). <sup>1</sup>H NMR (CDCl<sub>3</sub>)  $\delta$  [ppm] 1.30 (s, 36H, CH<sub>2</sub>), 2.24 (s, 12H, CH<sub>3</sub>N), 2.26 (t, 4H, CH<sub>2</sub>N), 4.04 (t, 4H, CH<sub>2</sub>O), 7.11 (s, 2H, ArH). MS (CI)  $m/z$  556 (M<sup>+</sup>+1). Anal. Calcd for C<sub>34</sub>H<sub>58</sub>N<sub>4</sub>O<sub>2</sub>: C, 73.60; H, 10.54; N, 10.10. Found: C, 72.69; H, 10.10; N, 10.28. The compound is not entirely pure (see Results section).

**2,3,9,10,16,17,23,24-octakis(11'-N,N-dimethylaminoundecoxy)phthalocyanine (1).** An electrolysis cell as described by Petit *et al.* [5] was filled with 0.3 M LiCl/EtOH. Compound 6 (554 mg, 1 mmol) was placed in the cathodic compartment of the cell. The system was brought under a nitrogen atmosphere and thermostated at 70 °C. A constant current of 3 mA was run through the mixture for 4.5 h, while stirring the cathodic and anodic compartments. After the reaction was complete, the mixture was poured into 0.2 M aqueous H<sub>2</sub>SO<sub>4</sub> (30 mL), stirred for 30 min, and washed with chloroform (2x). The aqueous solution containing the phthalocyanine was neutralized with 1 N aqueous NaOH (12 mL), and extracted with chloroform (3x). The combined organic solutions were washed with water (2x) and saturated aqueous NaCl (1x), and the solvent was evaporated under vacuum. The resulting solid was washed with boiling acetone until the washings were clear. Yield: 221 mg (40%). Dark green solid, K→M 80 °C. IR (CHCl<sub>3</sub>)  $\lambda^{-1}$  [cm<sup>-1</sup>] = 861 (Pc-H), 895, 1032, 1100 (Pc), 1278 (Pc-O-C), 1490, 1603 (Pc), 2781, 2844 (C-N), 3299 (N-H). <sup>1</sup>H NMR (CDCl<sub>3</sub>)  $\delta$  [ppm] -2.00 (br s, 2H, NH), 1.36 (s, 144H, CH<sub>2</sub>), 2.23 (s, 48H, CH<sub>3</sub>N), 2.23 (t,

16H, CH<sub>2</sub>N), 4.52 (br s, 16H, CH<sub>2</sub>O), 8.49 (s, 8H, PcH). <sup>13</sup>C NMR (CDCl<sub>3</sub>) δ [ppm] 26.0-29.8 (CH<sub>2</sub>), 45.4 (CH<sub>3</sub>N), 59.9 (CH<sub>2</sub>N), 69.5 (CH<sub>2</sub>O), 105.2, 130.0, 148.4, 151.7 (Pc). UV/Vis (CHCl<sub>3</sub>) λ<sub>max</sub> [nm] (log ε [L·mol<sup>-1</sup>·cm<sup>-1</sup>]) 702.5 (5.03), 664.8 (4.98), 645 (4.67), 604.9 (4.44). Anal. Calcd for C<sub>136</sub>H<sub>234</sub>N<sub>16</sub>O<sub>8</sub>: C, 73.53; H, 10.62; N, 10.09. Found: C, 72.97; H, 11.32; N, 9.66.

**Octaacetic acid salt of 1 (1·HAc).** Phthalocyanine 1 (40 mg, 18 μmol) was dissolved in 10% aqueous acetic acid (25 mL). The solvent and excess acetic acid were removed by evaporation under vacuum. Yield: 48.8 mg (100%). Dark green solid, K→M 74 °C. IR (KBr) λ<sup>-1</sup> [cm<sup>-1</sup>] = 1101 (Pc), 1278 (Pc-O-C), 1575 (C=O). <sup>1</sup>H NMR (D<sub>2</sub>O) δ [ppm] 1.58 (s, 144H, CH<sub>2</sub>), 1.89 (s, 24H, CH<sub>3</sub>CO<sub>2</sub><sup>-</sup>), 2.83 (t, 16H, CH<sub>2</sub>N<sup>+</sup>), 2.90 (s, 24H, CH<sub>3</sub>N<sup>+</sup>), 4.11 (br s, 16H, CH<sub>2</sub>O). <sup>13</sup>C NMR (D<sub>2</sub>O/dioxane) δ [ppm] 23.5 (CH<sub>3</sub>CO<sub>2</sub><sup>-</sup>), 25.9-31.3 (CH<sub>2</sub>), 43.9 (CH<sub>2</sub>N<sup>+</sup>), 58.9 (CH<sub>3</sub>N<sup>+</sup>), 69.2 (CH<sub>2</sub>O), 105.0, 127.9 (Pc), 180.5 (CO<sub>2</sub><sup>-</sup>). UV/Vis (H<sub>2</sub>O) λ<sub>max</sub> [nm] (log ε [L·mol<sup>-1</sup>·cm<sup>-1</sup>]) 609 (4.38). Anal. Calcd for C<sub>152</sub>H<sub>266</sub>N<sub>16</sub>O<sub>24</sub>: C, 66.08; H, 9.92; N, 8.29. Found: C, 66.08; H, 9.13; N, 8.62.

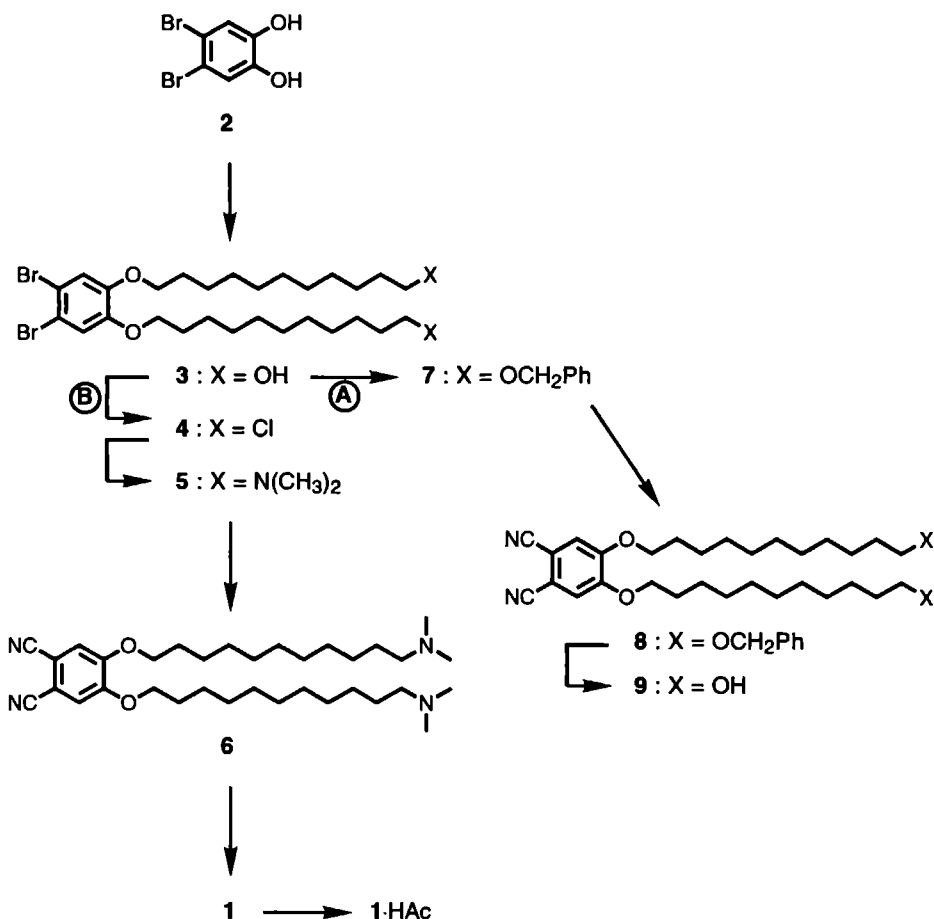
## 5.3 Results and Discussion

### 5.3.1 Synthesis

We evaluated different synthetic routes to obtain the target compound 1 (Scheme 5.1). One possibility is to use octakis(11'-hydroxyundecoxy)Pc as an intermediate. Our previously published procedure for the synthesis of this compound is tedious, since it involves the direct cyanation of 3 to 9; the yield of this reaction is very low [6]. An alternative method is via the protected dicyano derivative 8, which could be synthesized in good yield using standard procedures (Scheme 5.1.A) [7,8]. Subsequent removal of the benzylic functions with trimethylsilyl iodide was almost quantitative [9]. We have shown previously that compound 9 can be converted to the corresponding octa(11'-hydroxyundecoxy)phthalocyanine [6]. The hydroxy functions of the latter compound must be replaced by chlorine atoms and subsequently by dimethylamino functions to obtain Pc 1. This procedure involves the complicated purification of the intermediate Pcs. The next route, which prevents these problems, was chosen (Scheme 5.1.B).

First, 4,5-dibromocatechol was alkylated with 11-bromoundecanol in DMF in the presence of K<sub>2</sub>CO<sub>3</sub> to give 3 in 87% yield. The hydroxy groups of the latter compound were subsequently replaced by chlorine atoms with the help of thionyl-





Scheme 5.1

chloride and triethylamine. The resulting compound (4) was converted into the diamine 5 by reaction with dimethylamine under elevated pressure. Substitution of the two bromine atoms of 5 by cyano groups to obtain compound 6 was carried out *via* the Rosenmund-von Brown reaction [10]. A large excess of copper cyanide was required in this reaction because this reagent coordinates to the amino functions of 5. Despite several attempts, the compounds 4-6 could not be purified completely by extraction, recrystallization, or column chromatography. Therefore, they were all used directly without purification, which turned out to be harmless, since impurities could be removed easily in the last stage of the synthesis. Phthalocyanine 1 was obtained from dicyanide 6 by electrosynthesis, as first

described by Petit *et al.* [5]. Other, more common methods, *e.g.* reaction of **6** with *N,N*-dimethylaminoethanol or lithium pentanolate, gave the product in low yields, probably because of interference of the amino functions. Starting from dibromocatechol the overall yield of **1** was 7%. The acetate of **1**, **1**·HAc, could be obtained quantitatively by dissolving **1** in 10% aqueous acetic acid, and subsequently removing the solvent and the excess acetic acid. The Pcs were characterized by IR, NMR, and elemental analysis (see Experimental Section).

Phthalocyanine **1** is highly soluble in organic solvents such as chloroform and methanol, and in diluted aqueous acetic acid (see above). Remarkably, it is not soluble in diluted aqueous sulfuric acid or hydrochloric acid. Compound **1**·HAc is soluble in water and methanol, and insoluble in chloroform. The  $^1\text{H}$  and  $^{13}\text{C}$  NMR spectra of **1**·HAc in  $\text{D}_2\text{O}$  showed broad peaks, and some of the protons and carbon atoms of the Pc core were even invisible. These features suggest that compound **1**·HAc aggregates in aqueous solutions, as will be discussed below.

Phthalocyanine **1** turned out to be unstable when stored for several days in air and light, especially at elevated temperatures, forming an insoluble polymeric product. In the IR spectrum of the latter the amino functions had disappeared, probably because they were eliminated or oxidized. Because of its insolubility, this polymer could not be further characterized. The degradation process could be prevented by storing **1** in the dark in the refrigerator. Compound **1**·HAc was found to be completely stable for several months.

### 5.3.2 Thermotropic properties

The mesogenic properties of phthalocyanines **1** and **1**·HAc were studied with the help of polarizing microscopy (PM) and differential scanning calorimetry (DSC). Both compounds displayed two liquid-crystalline phases. The transition temperatures and enthalpies are given in Table 5.I.

Powder X-ray diffraction experiments were carried out on both compounds at 100 °C. Unfortunately, compound **1** was not able to withstand this temperature and decomposed during the long X-ray exposure time of *ca.* three days. Compound **1**·HAc, however, was stable under the measuring conditions, and gave nice reflections which could be indexed according to a hexagonal pattern. The results are presented in Table 5.II. The broad and diffuse band at approximately 4.3 Å is characteristic of disordered aliphatic chains [8]. A sharp and intense reflection is

**Table 5.I** Phase Transition Temperatures and Enthalpy Changes of Phthalocyanines 1 and 1 HAc as Determined by DSC and Polarizing Microscopy [a]

		1	1 HAc
K→M <sub>1</sub>	T	80 (49)	73 (39)
	ΔH	98.1	80.0
M <sub>1</sub> →M <sub>2</sub>	T	168 (153)	89 (47)
	ΔH	6.42	2.87
M <sub>2</sub> →I	T	265 [b]	270 [b]

[a] T and ΔH are obtained from heating runs and are given in °C and kJ mol<sup>-1</sup>, respectively. The values in parentheses are obtained from cooling runs.

[b] Only observed under the polarizing microscope. The transition is accompanied with decomposition.

**Table 5.II** Relative Intensity, Spacings, and Assigned Miller Indices (hkl) Derived from X-ray Diffraction Experiments on Phthalocyanine 1 HAc at 100 °C.

Intensity [a]	Spacing / Å	Index
vs	38.02	100
vs	21.52	110
vs	18.76	200
m	14.26	210
vw	11.06	220
vw	8.71	320
vw,br	7.2	330
m,vbr	4.3	L [b]
s	3.34	001

[a] vs = very strong, m = medium, vw = very weak, br = broad, vbr = very broad, s = strong

[b] L = average interatomic distance between the side chains

observed at a spacing of 3.34 Å, which corresponds to the stacking period of the molecules within one column [8]. From the small angle reflections, which are related to the hexagonal arrangement of the columns, an intercolumnar distance of 43.65 Å can be calculated. The latter value is 8 Å larger than that measured for octakis(dodecoxy)Pc [8]. This difference is equal to twice the dimension of the acetate ion, which suggests that these ions are aligned with the ends of the hydrocarbon chains.

### 5.3.3 Lyotropic properties

**UV/Vis spectroscopy.** The electronic absorption spectra of diluted solutions of **1** in chloroform and in 10% aqueous acetic acid are displayed in Figure 5.2. The former solution shows a split Q-band with absorption maxima at 702 and 664 nm, which is characteristic of a mononuclear Pc species. Spectra of **1** in methanol and in 10% aqueous acetic acid are broad and the Q-band is shifted to the blue. This behavior is characteristic of columnar aggregated Pcs (see Chapters 4 and 6, and Ref. 11). The maximum of the Q-band of **1** in aqueous acetic acid is located at 609 nm. This value turned out to be practically independent of the concentration of the Pc (0.3  $\mu$ M to 0.3 mM) and of the temperature (25 to 55  $^{\circ}$ C at 3  $\mu$ M).

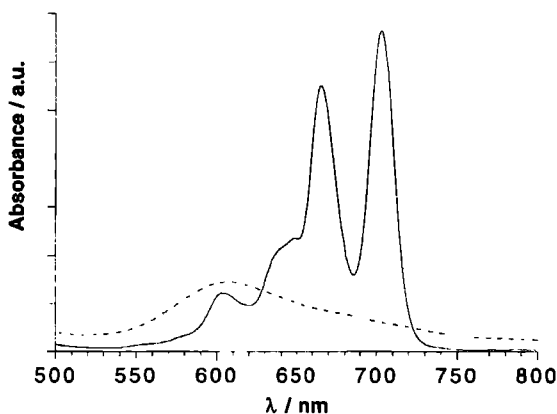


**Figure 5.2** Electronic absorption spectra of **1** in chloroform (solid line) and in 10% aqueous acetic acid (broken line).

The aggregation number,  $N$ , of the phthalocyanine can be estimated from the Q-band shift using the following equation [11a]:

$$\frac{1}{N} = 1 - \frac{\Delta E(N)}{\Delta E(N \rightarrow \infty)} \quad (5.1)$$

where  $\Delta E(N)$  is the observed exciton shift, and  $\Delta E(N \rightarrow \infty)$  is the exciton shift for an infinite stack of molecules. Following the studies of Fujiki *et al.* [11a], we can take for the latter shift the value that is found for a cast film, assuming that the structure of the stacks in solution is similar to that of the stacks in the solid state, *i.e.* with the same interplanar distance, tilt angle, and torsion angle. The spectral

envelope of a cast film of **1** was similar to that of the spectrum in solution, making this assumption plausible. The absorption maximum of the film was found to lie at 603 nm. From the value of the exciton shift (Table 5.III) the aggregation number of **1** in aqueous acetic acid solution was calculated to be  $N = 12$ . Likewise, the aggregation number of **1** in methanol and that of **1**·HAc in pure water were found to be 4.3 and 24, respectively. These values are similar to the ones reported for aggregates of tetra(octadecylamide)Pc in chlorobenzene [11a]. The sodium salt of tetrasulfonato phthalocyanine forms aggregates in water consisting of 2-20 molecules [12].

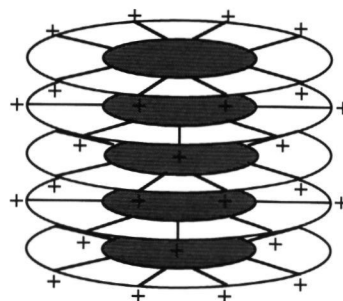
The most probable structure of the aggregates of **1** in acetic acid and **1**·HAc in aqueous solution is shown in Figure 5.3. The hydrophobic cores of the phthalocyanines are organized in columns, and the ammonium groups form hydrophilic shells, which makes the aggregates soluble in water.

**Table 5.III** Wavelengths ( $\lambda_{\max}$ ) and the Corresponding Energies ( $E$ ) of the Q-Band Absorption Maxima, Exciton Shift Values ( $\Delta E$ ), and the Calculated Aggregation Numbers ( $N$ ) for Pcs **1** and **1**·HAc

Compound	Solvent	$\lambda_{\max}$	$E$	$\Delta E$	$N$
<b>1</b>	chloroform	683 [a]	14641	-	1
<b>1</b>	cast film	603	16584	1943	$\infty$
<b>1</b>	10% aqueous acetic acid	609	16420	1779	12
<b>1</b>	methanol	620	16129	1488	4.3
<b>1</b> ·HAc	water	606	16502	1861	24

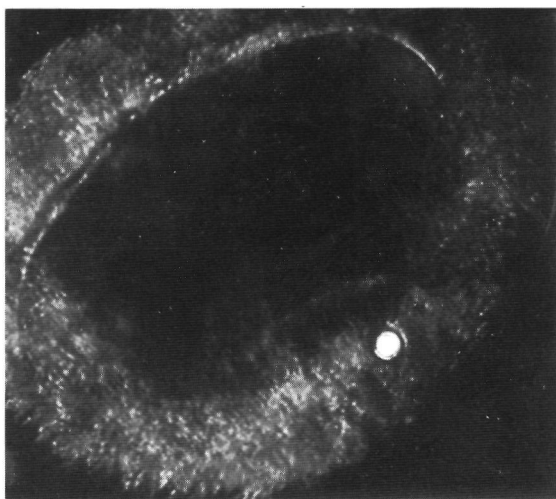
[a] Average of the two absorption maxima of the split Q-band.

**Figure 5.3** Schematic representation of the columnar aggregates formed by **1** in diluted aqueous acetic acid and by **1**·HAc in water.



*Polarizing microscopy.* The presence of a lyotropic liquid crystalline phase can be detected with the help of polarizing microscopy [2,3]. A sample of **1** was placed between a microscope slide and a cover slip. A drop of 10% aqueous acetic acid was put at the edge of the cover slip, and the solvent was allowed to diffuse between the glass plates. In this way a gradient was created with the highest concentration of phthalocyanine in the middle of the sample. Figure 5.4 shows a typical picture. The dark regions in the central and outer parts of the sample are due to the crystalline and isotropic phases, respectively. In between, birefringence is observed, which obviously points to the formation of a mesophase. Unfortunately, no textures were seen, making it impossible to assign a structure to the mesophase.

**Figure 5.4** Photomicrograph of a concentration gradient of compound **1** in 10% aqueous acetic acid at ambient temperature, observed between crossed polarizers.



#### 5.3.4 Monolayer properties

Figure 5.5 (solid line) shows the surface pressure - surface area isotherm of a monolayer of compound **1**, recorded at 20 °C on pure water. Three plateau regions are visible, *viz.* at 5, 11, and 53 mN·m<sup>-1</sup>. Extrapolation of the steepest part of the first pressure increase to zero pressure gives a very large area of 780 Å<sup>2</sup> per molecule. The diameter of the extended molecule is *ca* 35 Å, and that of the Pc core including the oxygen atoms 16.8 Å [13]. These values correspond to areas of 962 Å<sup>2</sup> and 220 Å<sup>2</sup>, respectively. We may conclude from the above numbers that the

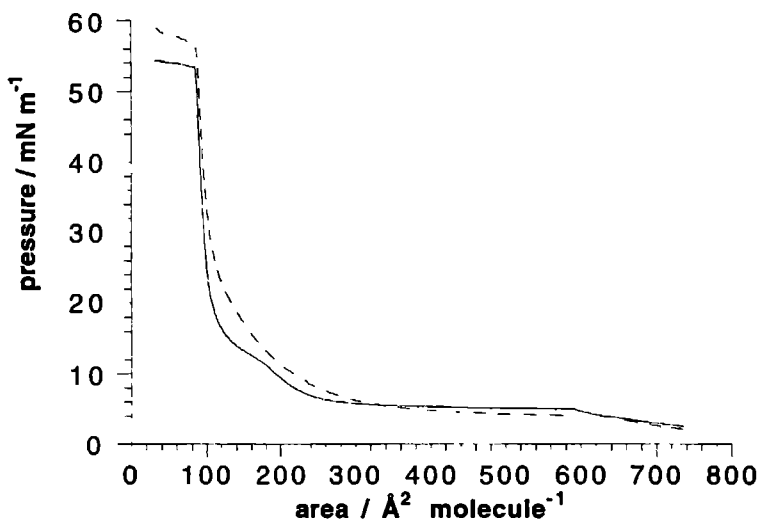


**Figure 5.5** Surface pressure - surface area isotherms of **1** recorded at 20 °C on various subphases: pure water (solid line); 0.1 N NaOH (broken line); 0.1 N H<sub>2</sub>SO<sub>4</sub> (dotted line).

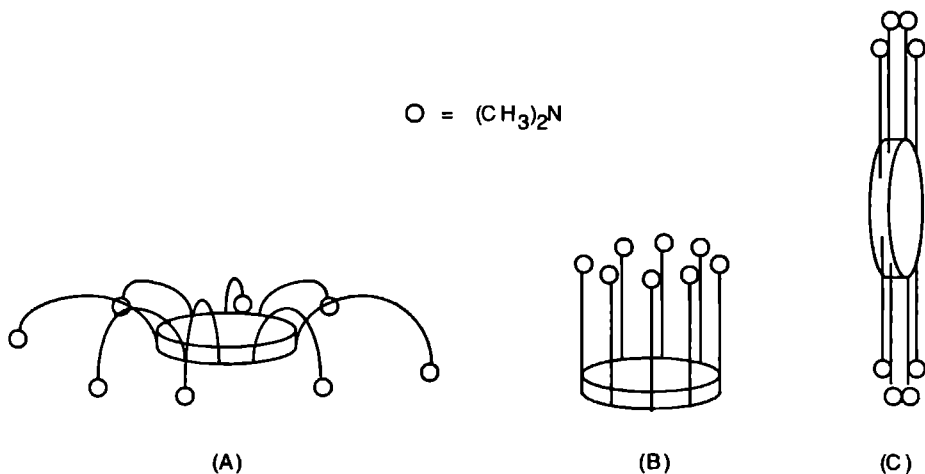
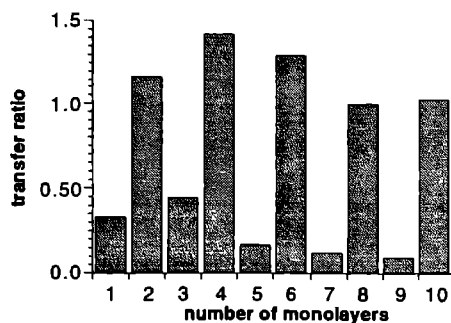


**Figure 5.6** Schematic representations of the proposed conformations of molecules of **1** in a monolayer on pure water at different surface pressures (see text). The areas per molecule are 780 (A), 240 (B), and 108 Å<sup>2</sup> (C).

molecules lie almost entirely flat on the water surface. The Pc core as well as the hydrophilic amino functions are in contact with the water; each molecule floats on the surface like a "crane fly" (Figure 5.6A). This conformation is not stable, as can be judged from the fact that already at a low surface pressure of *ca.*  $5 \text{ mN}\cdot\text{m}^{-1}$  a phase transition takes place. Moreover, if the surface pressure is maintained at a value of  $3 \text{ mN}\cdot\text{m}^{-1}$ , a gradual decrease in the surface area is observed, which also indicates instability of the monolayer.

The second rise of the surface pressure is found at an area of  $240 \text{ \AA}^2$  per molecule, which is close to the area of the plane of a single Pc ring including the oxygen atoms (see above). Space filling models reveal that the area of one tertiary amino group amounts to *ca.*  $30 \text{ \AA}^2$ . This is one eighth of the calculated area per molecule at the second pressure increase. We propose that the Pc rings are still parallel to the water surface, but now with their side chains and amino functions pointing outwards as shown in Figure 5.6B. The amino functions are probably not located under the Pc rings and in contact with the water as will be discussed below. The monolayer with the molecules in the conformation of Figure 5.6B was found to be very stable. When the surface pressure was maintained at a value of  $8 \text{ mN}\cdot\text{m}^{-1}$ , the surface area reached a constant value after an equilibration period of *ca.* 30 min. This monolayer could be transferred onto hydrophobized glass. Figure 5.7 shows the transfer ratios (ratio of monolayer area decrease and covered substrate area) that were obtained during several dipping cycles of the substrate in the LB trough. It can be seen that after three cycles a nice Z-type deposition takes place. This result is of interest given the above-mentioned problem of whether the molecules are positioned with their amino functions or with their Pc rings in contact with the water surface. In the former case it is difficult to understand why only upstroke dipping would give transfer of the monolayer (see Figure 5.8A), as deposition during downstroke dipping would result in a more favorable inter-

**Figure 5.7** Transfer ratio versus layer number for the deposition of a monolayer of 1 on hydrophobic glass at a surface pressure of  $7.5 \text{ mN}\cdot\text{m}^{-1}$ . The first layer corresponds to downstroke deposition.





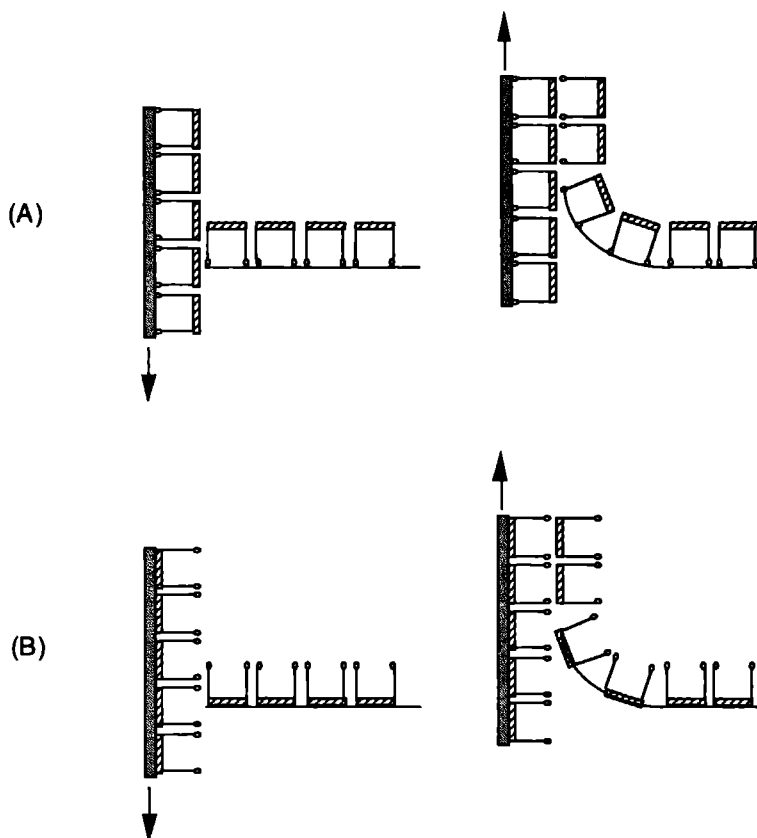


**Figure 5.8** Z-type deposition of a monolayer with the molecules of **1** in two possible orientations: with the amino groups in contact with the water surface (A); with the amino groups pointing away from the water surface (B). The latter orientation is more probable (see text).

action between the Pc units in neighboring layers. We, therefore, believe that the situation as illustrated in Figure 5.8B is more likely to occur. A non-centrosymmetric multilayer structure is obtained with the Pc planes parallel to the substrate surface and the side chains directed away from it.

When the monolayer on the water surface is further compressed, a second phase transition takes place at a surface pressure of  $11 \text{ mN}\cdot\text{m}^{-1}$ , eventually reaching a limiting area of  $108 \text{ \AA}^2$  per molecule. The Pc units are now forced to orient themselves perpendicularly to the water surface. Four side chains are directed towards the water surface, and four point away from it (Figure 5.6C). The monolayer collapses when a surface pressure of *ca.*  $53 \text{ mN}\cdot\text{m}^{-1}$  is reached.

The isotherm of a monolayer of **1** on a subphase of 0.1 N aqueous NaOH is shown in Figure 5.5 (broken line). It can be seen from this figure that the surface pressure at which the first phase transition takes place is slightly lower ( $4 \text{ mN}\cdot\text{m}^{-1}$ ) than that of the monolayer on pure water ( $5 \text{ mN}\cdot\text{m}^{-1}$ ). This suggests that the parallel orientation of the molecules as depicted in Figure 5.6A is less stable in the former case than in the latter. Apparently, the high pH-value of the subphase results in a decreased interaction between the amino groups and the subphase. On the contrary, when an isotherm of **1** is recorded on 0.1 N aqueous  $\text{H}_2\text{SO}_4$  (Figure 5.5, dotted line), the surface pressure of the first plateau region increases, *viz.* to *ca*  $15 \text{ mN}\cdot\text{m}^{-1}$ . The amino groups are protonated in this case, which leads to a strong interaction with the water surface. This is probably also the reason why the phase transition, at which the side chains are lifted from the water surface, is not observed in the isotherm. The second increase in the surface pressure starts near an area of  $100 \text{ \AA}^2$  per molecule, which means that the molecules directly change their orientation into the perpendicular mode. Remarkably, no collapse is observed, even not when the area is decreased to a very low value per molecule. When the surface pressure was maintained at a constant value of  $10 \text{ mN}\cdot\text{m}^{-1}$ , the monolayer area was found to decrease slowly in a linear fashion with time. Probably the solubility of **1** in aqueous  $\text{H}_2\text{SO}_4$  is large enough to allow the protonated molecules to dissolve gradually into the subphase. As a result the formation of a stable monolayer is prevented.

## 5.4 Conclusions

The octaacetic acid salt of octakis(*N,N*-dimethylaminoundecoxy)Pc (**1**·HAc) is structurally related to the previously reported [13,14] thermotropic liquid-crystalline octaalkoxy Pcs. The side chains of this molecule resemble the classical amphiphiles. This may explain why compound **1**·HAc displays amphotropic behavior forming not only a hexagonal columnar mesophase at elevated temperatures, but also highly stable columnar aggregates in aqueous solution. The latter aggregates may be classified as cylindrical micelles [1,3].

The multipolar amphiphilic character of the free-base phthalocyanine **1** endows this molecule with unique monolayer behavior. The entirely flat orientation found at low surface pressures is not very stable on pure water, and therefore uniform deposition is not possible. We expect however, that by carefully controlling the pH of the subphase this problem can be solved. The structure of the Z-type

LB-multilayer that we were able to built from **1** is quite unique. The non-centro-symmetric arrangement of the Pc molecules, with their planes oriented parallel to the substrate surface and their side-chains perpendicular to it, might be interesting for applications in, for example, nonlinear optics. Future studies will focus on the detailed elucidation of the structures of the mono and multilayers of **1**, and on applications.

## References

- [1] H Ringsdorf, B Schlarb, J Venzmer, *Angew Chem* **100** (1988) 117, *Angew Chem Int Ed Engl* **27** (1988) 113
- [2] N B McKeown, J Painter, *J Mater Chem* **4** (1994) 1153
- [3] R Keller-Griffith, H Ringsdorf, A Vierengel, *Coll Polym Sci* **264** (1986) 924
- [4] (a) N Kobayashi, F Ojima, T Osa, S Vigh, C C Leznoff, *Bull Chem Soc Jpn* **62** (1989) 3469 (b) C C Leznoff, S Vigh, P I Svirskaya, S Greenberg, D M Drew, E Ben-Hur, I Rosenthal, *Photochem Photobiol* **49** (1989) 279
- [5] (a) M A Petit, V Plichon, H Belkacemi, *New J Chem* **13** (1989) 459 (b) M A Petit, T Thami, C Sirlin, D Lelièvre, *New J Chem* **15** (1991) 71
- [6] J F van der Pol, E Neeleman, J C van Miltenburg, J W Zwikker, R J M Nolte, W Drenth, *Macromolecules* **23** (1990) 155
- [7] G Coudert, M Mpassi, G Guillaumet, C Selve, *Synth Commun* **16** (1986) 19
- [8] J F van der Pol, E Neeleman, J W Zwikker, R J M Nolte, W Drenth, *Recl Trav Chim Pays-Bas* **107** (1988) 615
- [9] M E Jung, M A Lyster, *J Org Chem* **42** (1977) 3761
- [10] G P Ellis, T M Romney-Alexander, *Chem Rev* **87** (1987) 779
- [11] (a) M Fujiki, H Tabei, T Kurihara, *J Phys Chem* **92** (1988) 1281 (b) O E Sielcken, M M van Tilborg, M F M , Roks, R , Hendriks, W Drenth, R J M Nolte, *J Am Chem Soc* **109** (1987) 4261 (c) W J Schutte, M Sluyters-Rehbach, J H Sluyters, *J Phys Chem* **97** (1993) 6069 (d) D Markovitsi, I Lécuyer, J Simon, *J Phys Chem* **95** (1991) 3620 (e) E S Dodsworth, A B P Lever, P Seymour, C C Leznoff, *J Phys Chem* **89** (1985) 5698
- [12] O Kratky, H Olschlager, *J Coll Interface Sci* **31** (1969) 490
- [13] J F van der Pol, E Neeleman, J W Zwikker, R J M Nolte, W Drenth, J Aerts, R Visser, S J Picken, *Liq Cryst* **6** (1989) 577
- [14] (a) I Cho, Y Lim, *Mol Cryst Liq Cryst* **154** (1988) 9 (b) C Piechocki, J Simon, J -J André, D Guillon, P Petit, A Skoulios, P Weber, *Chem Phys Lett* **122** (1985) 124 (c) W T Ford, L Sumner, W Zhu, Y H Chang, P -J Um, K H Choi, P A Heiney, N C Mahszewsky, *New J Chem* **18** (1994) 495

# ***Liquid-Crystalline Crown-Ether Substituted Phthalocyanines***

## **6.1 Introduction**

The study of nanometer-sized, self-organized structures is of great interest for the construction of devices that are small and fast and for devices that can store information with high-density [1]. Molecular electronics and molecular ionics are new scientific fields dealing with this subject [2,3]. In the latter case the information storage and processing is achieved with the help of ions. An important step in this process is the non-linear complexation of ions, which allows for reliable switching between on and off states [3d]. Furthermore, the construction of supramolecular wires and channels, capable of transporting electrons and ions, is a great challenge [4].

In this chapter we describe the synthesis and self-organizing properties of the metal free and silicon Pcs **1a** and **1b**. These compounds contain a central Pc core, four 18-crown-6 rings, and a total of eight decoxy chains linked via benzene units to the crown-ether rings. They were designed to develop systems that combine the properties of electron conduction, ion conduction, and liquid crystallinity. CPK molecular models show that molecules **1a** and **1b** display a high degree of shape anisotropy, which is favorable for the formation of a (columnar) mesophase. Taking as the thickness of the molecules a value of 4.2 Å [5], the length over thickness ( $L/d$ ) aspect ratio is in the range of 9.5 to 15, depending on the conformation of the peripheral decoxy chains (see Figure 6.1). We will show in this chapter that **1a** indeed forms a thermotropic mesophase. Moreover, this compound self-assembles in chloroform solution to yield an extremely long supramolecular cable. Phthalocyanine **1b** forms stable monolayers at the air-water interface. Those monolayers can bind alkali metal ions from the subphase, and can be transferred onto solid substrates, giving a Langmuir-Blodgett (LB) film. Preliminary results indicate that **1b** can be polymerized to form an axial polysiloxane.

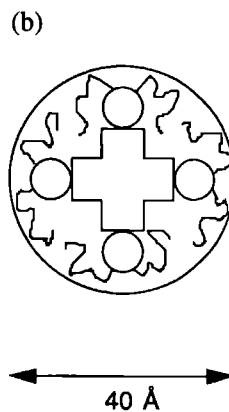
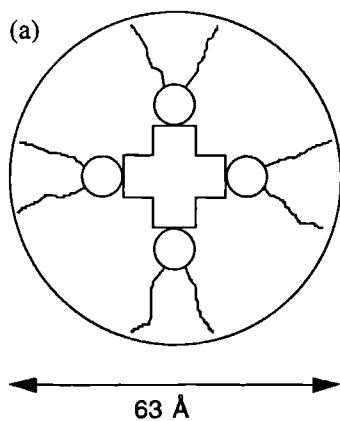
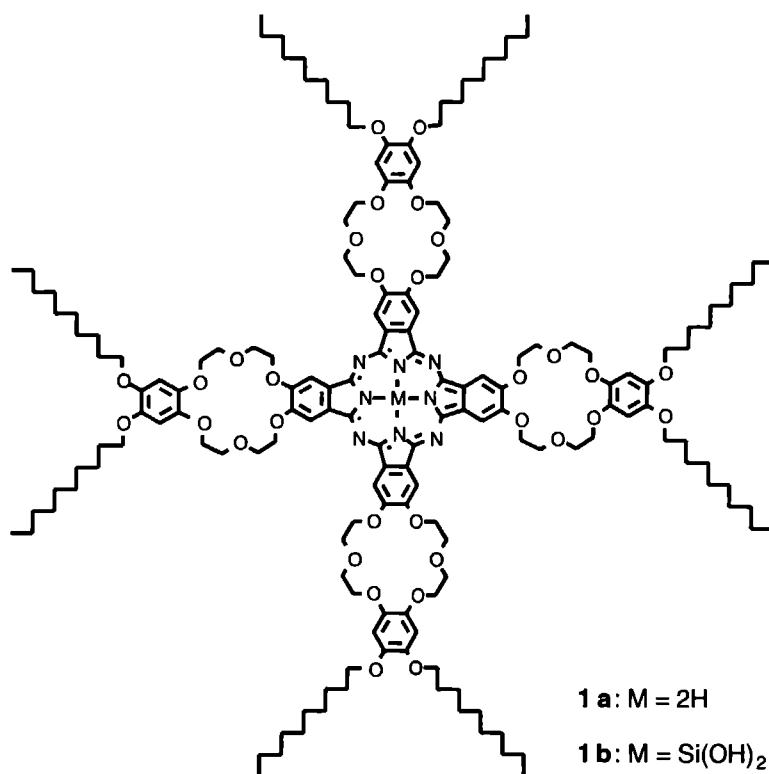


**Figure 6.1** Schematic representation of the disc-like molecules **1** showing the two limiting diameters  $L$ , as estimated from CPK molecular models: fully elongated decyloxy chains (a); decyloxy chains bending back (b).

## 6.2 Experimental section

**Materials and methods.** All solvents were dried before use. Merck Kieselgel 60H was used for chromatography. 3,4-Dihydroxybenzaldehyde was recrystallized twice from *o*-xylene.  $K_2CO_3$  was dried in an oven before use. Potassium nitrosodisulfonate (Fremy's radical) was prepared by the method of Zimmer *et al.* [6]. The synthesis of 4,5-dibromocatechol is described in chapter 5. The tetrahydropyranyl ether of 2-(2'-chloroethoxy)ethanol was synthesized following the procedure of Kyba *et al.* [7]. *p*-Toluenesulphonyl chloride was recrystallized from hexane. *N,N*-dimethylaminoethanol and  $SiCl_4$  were freshly distilled before use. Quinoline was freshly distilled from barium oxide. Tetrakis(acetonitrile)copper(I) triflate was prepared by the method of Caseri *et al.* [8]. All other reagents were used as supplied, without further purification.

Melting points were determined with a Reichert hot-stage microscope and are uncorrected. Infrared (IR) spectra were recorded with a Perkin Elmer 28 Infrared Spectrophotometer or a Perkin Elmer 1720-X Infrared Fourier Transform Spectrophotometer. UV/Vis spectra were obtained with a Perkin Elmer Lambda 5 Spectrophotometer.  $^1H$  NMR spectra were obtained with Varian EM 390, Bruker AC-100, or Bruker WM-400 instruments. Chemical shifts are reported in ppm downfield from internal TMS standard. Abbreviations used are as follows: s = singlet, d = doublet, t = triplet, m = multiplet, br = broad. Electronic ionization (EI), chemical ionization (CI), and fast atom bombardment (FAB) mass spectra (MS) were obtained with a VG-7070E apparatus. Elemental analysis were carried out on an EA 1108 Carlo Erba instrument.

Differential scanning calorimetry (DSC) data were obtained with a Mettler DSC 12E instrument. The measurements were carried out under an inert atmosphere with heating and cooling rates of  $10\text{ }^\circ\text{C}\cdot\text{min}^{-1}$ . Thermogravimetric analysis (TGA) was carried out on a Perkin Elmer System 4 under inert atmosphere. For polarization microscopy a Leitz Orthoplan polarization microscope was used, equipped with a Mettler FP80/FP82 Hot Stage. Small angle X-ray scattering (SAXS) curves were recorded using a Siemens D5000 reflection diffractometer with a HTK oven, and a  $Cu\ K_\alpha$  source with a wavelength of  $1.5406\text{ \AA}$ .

Transmission electron microscopy was carried out with a Philips TEM 201 instrument. Small drops of the samples were placed on carbon-coated grids, the material was allowed to adsorb for one minute, and then the grids were blotted dry by touching the edges with filter paper. Finally, the structures were visualized by shadowing with platinum at an angle of approximately  $45^\circ$ .

Monolayers at the air-water interface were studied by measuring pressure-area isotherms on a computer-controlled Lauda Film Balance (FW 2) and a home-built film balance both using water that was purified by a Milli-Q filtration system as the subphase. A sample was dissolved in chloroform (spectroscopic quality, *ca* 1 mg·mL<sup>-1</sup>), spread on the water surface, and isotherms were recorded at a compression speed of *ca.* 30 Å<sup>2</sup>·molecule<sup>-1</sup>·min<sup>-1</sup> at 20 °C. The water surface was visualized during compression with a Brewster Angle Microscope (NFT BAM-1) equipped with a 10 mW He-Ne laser with a beam diameter of 0.68 mm operating at 632.8 nm. Reflections were detected using a CCD camera. Glass substrates were prepared as described in chapter 3. Deposition was carried out by vertically dipping the substrate with a speed of 10 mm·min<sup>-1</sup> through the monolayer, which was equilibrated for 1.5 h at constant surface pressure and temperature. UV/Vis spectroscopy on the resulting film was carried out with an SLM-Aminco 3000 diode array spectrophotometer.

**Syntheses. 3,4-Bis(decoxy)benzaldehyde (3).** 3,4-Dihydroxybenzaldehyde (10.6 g, 0.077 mol) and 1-bromodecane (35.6 g, 0.161 mol) were dissolved in DMF (100 mL). Nitrogen gas was bubbled through the solution for 10 min. Then K<sub>2</sub>CO<sub>3</sub> (23.8 g, 0.172 mol) was added and the mixture was stirred at 100 °C under a nitrogen atmosphere for 16 h. After cooling, water (200 mL) was added and the product was extracted with chloroform (4x50 mL). The combined extracts were washed with water (40 mL), dried over MgSO<sub>4</sub>, and filtered, and the solvent was evaporated under high vacuum. The resulting solid was recrystallized from acetone at 4 °C. Yield: 27.1 g (84%). White solid, mp 64 °C. IR (KBr) 810, 865 (Ar-H), 1230, 1270 (Ar-O-C), 1505, 1585 (Ar), 1685, 2750 (H-C=O) cm<sup>-1</sup>. <sup>1</sup>H NMR (CDCl<sub>3</sub>, 90 MHz) δ 0.88 (t, 6H, CH<sub>3</sub>), 1.0-2.0 (m, 32H, CH<sub>2</sub>), 4.0 (t, 4H, CH<sub>2</sub>O), 6.88-7.52 (m, 3H, ArH), 9.85 (s, 1H, HC=O). MS (EI) *m/z* 418 (M<sup>+</sup>). Anal. (C<sub>27</sub>H<sub>46</sub>O<sub>3</sub>): found (calcd) C, 77.42 (77.46); H, 11.18 (11.07).

**3,4-Bis(decoxy)phenol (4).** Benzaldehyde 3 (31 g, 0.074 mol) was dissolved in chloroform (100 mL). Methanol (100 mL), 35% H<sub>2</sub>O<sub>2</sub> (9.5 g, 0.098 mol), and concentrated H<sub>2</sub>SO<sub>4</sub> (1 mL) were added, and the mixture was stirred at room temperature for 5 h. Water was added until two phases separated. The aqueous fraction was extracted with chloroform (2x25 mL). The combined organic solutions were washed with water (50 mL), dried over MgSO<sub>4</sub>, filtered, and rotary evaporated. The product was recrystallized from petroleum ether 40/60. Yield: 19.6 g (65%). Slightly brown solid, mp 78 °C. IR (KBr) 800, 825 (Ar-H), 1225, 1280 (Ar-O-C), 1510, 1605 (Ar), 3300 (OH) cm<sup>-1</sup>. <sup>1</sup>H NMR (CDCl<sub>3</sub>, 90 MHz) δ 0.88 (t, 6H, CH<sub>3</sub>), 1.0-1.9



(m, 32H, CH<sub>2</sub>), 3.9 (t, 4H, CH<sub>2</sub>O), 4.67 (br s, 1H, OH), 6.22-6.85 (m, 3H, ArH). MS (EI) *m/z* 406 (M<sup>+</sup>). Anal. (C<sub>26</sub>H<sub>46</sub>O<sub>3</sub>): found (calcd) C, 76.60 (76.80); H, 11.38 (11.40).

**4,5-Bis(decoxy)-1,2-benzoquinone (5).** The following solutions were prepared: tetrabutylammonium chloride (2 g, 7 mmol) in water (370 mL), KH<sub>2</sub>PO<sub>4</sub> (1.5 g, 11 mmol) in water (100 mL), and phenol **4** (7.5 g, 18 mmol) in THF (1250 mL). Potassium nitrosodisulfonate (10 g, 44 mmol) and the KH<sub>2</sub>PO<sub>4</sub> solution were quickly added to the stirred solution of Bu<sub>4</sub>N<sup>+</sup>Cl<sup>-</sup>. The resulting mixture was added immediately, while vigorously stirring, to the solution of **4** in THF. After stirring for 2 h at room temperature, the solution was saturated with NaCl and stirred for another h while keeping the solution saturated with NaCl. The organic layer was separated, the THF was evaporated under vacuum, and chloroform was added to the resulting paste. The chloroform solution was washed with water, dried over MgSO<sub>4</sub>, filtered, and evaporated under vacuum. The product was recrystallized from acetone at 4 °C. Yield: 6.0 g (80%). Orange solid, mp 128 °C. IR (KBr) 850 (C=C-H), 1590 (C=C), 1665 (C=O), 2800-3000 (CH<sub>2</sub>/CH<sub>3</sub>), 3060 (C=C-H) cm<sup>-1</sup>. <sup>1</sup>H NMR (CDCl<sub>3</sub>, 90 MHz) δ 0.95 (t, 6H, CH<sub>3</sub>), 1.2-2.1 (m, 32H, CH<sub>2</sub>), 4.00 (t, 4H, CH<sub>2</sub>O), 5.75 (s, 2H, C=C-H). MS (CI) *m/z* 422 (M<sup>+</sup>). Anal. (C<sub>26</sub>H<sub>44</sub>O<sub>4</sub>): found (calcd) C, 73.87 (74.24); H, 10.75 (10.54).

**1,2-Bis(decoxy)-4,5-bis(acetoxy)benzene (6).** Powdered zinc (5 g, 76 mmol) was added with stirring to a refluxing mixture of benzoquinone derivative **5** (8.4 g, 20 mmol), concentrated acetic acid (35 mL), and acetic anhydride (35 mL). This mixture was subsequently refluxed for 30 min. The product crystallized on cooling. The solvent was removed under vacuum and the resulting solid was dissolved in chloroform. This solution was filtered and concentrated under vacuum. The resulting product was recrystallized from acetone at 0 °C. Yield: 8.9 g (88%). White solid, mp 89 °C. IR (KBr) 1180, 1230 (Ar-O-C), 1510, 1605 (Ar), 1760 (C=O), 2800-3000 (CH<sub>2</sub>/CH<sub>3</sub>) cm<sup>-1</sup>. <sup>1</sup>H NMR (CDCl<sub>3</sub>, 100 MHz) δ 0.88 (t, 6H, CH<sub>3</sub>), 1.2-1.9 (m, 32H, CH<sub>2</sub>), 2.26 (s, 6H, CH<sub>3</sub>C=O), 3.94 (t, 4H, CH<sub>2</sub>O), 6.68 (s, 2H, ArH). MS (CI) *m/z* 506 (M<sup>+</sup>). Anal. (C<sub>30</sub>H<sub>50</sub>O<sub>6</sub>): found (calcd) C, 71.42 (71.11); H, 9.82 (9.95).

**1,2-Bis[2'-(2''-hydroxyethoxy)ethoxy]-4,5-dibromobenzene (9).** Dibromocatechol (**8**) (134 g, 0.5 mol) was added to 1-butanol (1400 mL), and nitrogen gas was bubbled through this mixture for 10 min. NaOH (40 g, 1 mol) was then added and dissolved by stirring and refluxing under a nitrogen atmosphere. The tetrahydropyranyl ether of 2-(2'-chloroethoxy)ethanol (208 g, 1 mol) was added dropwise to this solution, while stirring. The reaction mixture was refluxed under nitrogen for 16 h. After cooling, concentrated HCl (28 mL) was added, and the mixture was stirred for 1 h at room temperature. NaHCO<sub>3</sub> (140 g, 1.67 mol) was added, the mixture was

filtered, and the residue was extracted with dichloromethane. The combined organic solutions were washed with 1 M aqueous NaOH and with water, dried over  $\text{MgSO}_4$ , filtered, and concentrated under vacuum. The resulting liquid was distilled under vacuum. Yield: 109 g (49%). Clear, viscous oil, which slowly solidifies in the refrigerator, bp 240 °C (0.4 mm Hg). IR ( $\text{CHCl}_3$ ) 650 (Ar-Br), 1050, 1120 (C-O-C), 1190, 1240 (Ar-O-C), 2800-3000 ( $\text{CH}_2/\text{CH}_3$ ), 3200-3600 (OH)  $\text{cm}^{-1}$ .  $^1\text{H}$  NMR ( $\text{CDCl}_3$ , 100 MHz)  $\delta$  3.47 (s, 2H, OH), 3.6-4.2 (m, 16H,  $\text{CH}_2$ ), 7.09 (s, 2H, ArH). MS (CI)  $m/z$  444 ( $\text{M}^+$ ).

**1,2-Bis[2'-(2''-*p*-toluenesulphonyloxyethoxy)ethoxy]-4,5-dibromobenzene (10).**

A solution of compound 9 (68.4 g, 0.154 mol) in pyridine (125 mL) was cooled to -10 °C and a solution of *p*-toluenesulphonyl chloride (70 g, 0.367 mol) in pyridine (125 mL) was added dropwise, while stirring. This mixture was stirred for 2 h at -5 °C, and then for one night at 0 °C. The reaction mixture was poured over ice (400 g), acidified with 6 M aqueous HCl and extracted with dichloromethane (2x250 mL). The combined extracts were washed with water (2x250 mL), dried over  $\text{MgSO}_4$ , filtered, and concentrated under vacuum. Yield: 108 g (93%) of a very viscous oil. The product was chromatographed on silica gel using 1:1 (v/v) ethyl acetate/hexane as the eluent, in portions that were sufficient for the next reaction step. A small amount was recrystallized from  $\text{CDCl}_3$  to afford white needles, mp 87 °C. IR ( $\text{CHCl}_3$ ) 655 (Ar-Br), 1135 (C-O-C), 1170, 1350 ( $\text{SO}_3$ ), 1190, 1245 (Ar-O-C), 1595 (Ar)  $\text{cm}^{-1}$ .  $^1\text{H}$  NMR ( $\text{CDCl}_3$ , 90 MHz)  $\delta$  2.38 (s, 6H,  $\text{CH}_3$ ), 3.6-4.25 (m, 16H,  $\text{CH}_2$ ), 7.03 (s, 2H, ArH), 7.25 (d, 4H, ArH), 7.73 (d, 4H, ArH). MS (FAB)  $m/z$  752 ( $\text{M}^+$ ).

**{4',5'-Bis(decoxy)-4'',5''-dibromo}dibenzo[1',2'-b:1'',2''-k]-1,4,7,10,13,16-hexaoxa-cyclooctadeca-2,11-diene (11).** Compound 6 (9 g, 18 mmol) was suspended in 1-butanol (75 mL) and nitrogen gas was bubbled through the suspension for 10 min. Subsequently, NaOH (2.9 g, 72 mmol) was added and dissolved by stirring and refluxing under a nitrogen atmosphere. Compound 10 (13.5 g, 18 mmol) was added dropwise to the vigorously stirred solution (the addition can be facilitated by warming the viscous ditosylate 10 with a heatgun). The reaction mixture was refluxed with vigorous stirring under nitrogen for 16 h. After the reaction was complete, the mixture was acidified with concentrated HCl and the solvent was removed by evaporation under reduced pressure. The resulting solid was dissolved in chloroform, and the solution was washed with water (3x), dried over  $\text{MgSO}_4$ , and concentrated. The product was recrystallized from acetone (ca. 750 mL). Yield: 8.7 g (58%). White powder, mp 129 °C.  $^1\text{H}$  NMR ( $\text{CDCl}_3$ , 100 MHz)  $\delta$  0.88 (t, 6H,  $\text{CH}_3$ ), 1.2-1.9 (m, 32H,  $\text{CH}_2$ ), 3.8-4.2 (m, 20H,  $\text{CH}_2\text{O}$ ), 6.57 (s, 2H, ROArH), 7.05 (s, 2H,

BrArH). MS (CI)  $m/z$  830 ( $M^+$ ). Anal. ( $C_{40}H_{62}Br_2O_8$ ): found (calcd) C, 57.21 (57.83); H, 7.59 (7.52).

**{4',5'-Bis(decoxy)-4'',5''-dicyano}dibenzo[1',2'-b:1'',2''-k]-1,4,7,10,13,16-hexaoxacyclooctadeca-2,11-diene (12).** A mixture of dibromocrown-ether 11 (8.3 g, 10 mmol), CuCN (2.7 g, 30 mmol), and pyridine (0.5 mL) in DMF (100 mL) was refluxed under a nitrogen atmosphere for approximately 40 h. After the reaction was complete (as checked by TLC), the mixture was cooled to room temperature and poured into 25% aqueous ammonia (200 mL). Air was bubbled through the mixture for 2 h. Subsequently, the reaction mixture was extracted with chloroform (4x50 mL). The extracts were washed with water (4x100 mL), dried over  $MgSO_4$ , filtered, and concentrated. The resulting solid was chromatographed (silica gel, chloroform), and finally recrystallized from ethanol. Yield: 5.4 g (75%). White powder, mp 135 °C. IR ( $CHCl_3$ ) 869 (Ar-H), 1055, 1139 (C-O-C), 1288 (Ar-O-C), 1517, 1592 (Ar), 2233 (CN), 2856, 2928 ( $CH_2$ ), 3013 (Ar-H)  $cm^{-1}$ .  $^1H$  NMR ( $CDCl_3$ , 100 MHz)  $\delta$  0.88 (t, 6H,  $CH_3$ ), 1.1-1.9 (m, 32H,  $CH_2$ ), 3.8-4.3 (m, 20H,  $CH_2O$ ), 6.56 (s, 2H, ROArH), 7.11 (s, 2H, NCArH). MS (CI)  $m/z$  722 ( $M^+$ ). Anal. ( $C_{42}H_{62}N_2O_8$ ): found (calcd) C, 69.45 (69.78); H, 8.70 (8.64); N, 3.71 (3.87).

**Tetrakis{4',5'-bis(decoxy)benzo[1',2'-k]-1,4,7,10,13,16-hexaoxacyclooctadeca-2,11-dieno}[2,3-b:2',3'-i:2'',3''-p:2''',3'''-w]phthalocyanine (1a).** A mixture of dicyanocrown-ether 12 (0.75 g, 1.03 mmol) and *N,N*-dimethylaminoethanol (1 mL) was stirred and refluxed under a nitrogen atmosphere for 40 h. After cooling, chloroform (5 mL) was added and the mixture was stirred for 3 h and then kept without stirring for 1 h. The precipitate was filtered off and recrystallized three times from chloroform. Yield: 0.245 g (30%). Dark green solid, K $\rightarrow$ M 148 °C. IR ( $CHCl_3$ ) 863 (Ar-H), 909, 954 (Pc), 1022 (N-H), 1101 (Pc), 1134 (C-O-C), 1280 (Ar-O-C), 1529, 1603 (Ar/Pc), 2853, 2925 ( $CH_2$ ), 3294 (N-H)  $cm^{-1}$ .  $^1H$  NMR ( $CDCl_3$ , 400 MHz, 53 °C)  $\delta$  0.89 (br s, 24H,  $CH_3$ ), 1.2-1.8 (m, 128H,  $CH_2$ ), 3.6-4.9 (m, 80H,  $CH_2O$ ), 6.64 (s, 8H, ArH). Anal. ( $C_{168}H_{250}N_8O_{32} \cdot CHCl_3$ ): found (calcd) C, 67.18 (67.36); H, 8.28 (8.40); N, 3.74 (3.72).

**{4',5'-Bis(decoxy)benzo[1',2'-k]-1,4,7,10,13,16-hexaoxacyclooctadeca-2,11-dieno}[2,3-e]-1,3-diiminoisindoline (13).** Dicyanocrown-ether 12 (720 mg, 1 mmol) and sodium methoxide (100 mg, 1.9 mmol) were placed in a three-necked flask equipped with a gas inlet and reflux condenser. The flask was flushed with anhydrous ammonia and methanol (5 mL) and THF (5 mL) were added. The mixture was stirred at room temperature for 30 min and then refluxed for 4 h. During these periods a stream of anhydrous ammonia was slowly bubbled through the solution. After cooling, chloroform was added and the mixture was washed

with water and centrifugated (3x). The solvent was removed under vacuum. Chloroform was again added, the mixture was refluxed, cooled to room temperature, and finally filtered. The product was isolated after removal of the solvent under vacuum. Yield: 220 mg (30%). Light green solid. IR (CHCl<sub>3</sub>) 870 (Ar-H), 961 (Ar), 1015 (N-H) 1071, 1136 (C-O-C), 1285 (Ar-O-C), 1510, 1603 (Ar), 1658 (C=N), 2856, 2929 (CH<sub>2</sub>), 3275-3430 (N-H) cm<sup>-1</sup>. <sup>1</sup>H NMR (CDCl<sub>3</sub>, 100 MHz) δ 0.88 (t, 6H, CH<sub>3</sub>), 1.2-1.9 (m, 32H, CH<sub>2</sub>), 3.7-4.3 (m, 20H, CH<sub>2</sub>O), 6.57 (s, 2H, ArH), 7.2 (br s, ArH).

**(Tetrakis[4',5'-bis(decoxy)benzo[1',2'-k]-1,4,7,10,13,16-hexaoxacyclooctadeca-2,11-dieno][2,3-b:2',3'-i:2'',3''-p:2''',3'''-w]phthalocyaninato)silicondihydroxide (1b).** Diiminoisindoline **13** (220 mg, 0.3 mmol) and quinoline (1 mL) were placed in a dry vessel. After flushing with nitrogen gas, SiCl<sub>4</sub> (0.5 mL) was added and the mixture was quickly brought to 190 °C and kept at this temperature for 1 h. Subsequently, the mixture was stirred for 16 h at 160 °C under a nitrogen atmosphere. After cooling, the resulting dichlorosiliconphthalocyanine was hydrolyzed by addition of water (10 mL), and the product was filtered off, washed with methanol and acetone, and subsequently extracted in a Soxhlett apparatus with methanol for 16 h to remove impurities. The product was obtained from the residue by Soxhlett extraction with chloroform and purified by chromatography (silica gel, chloroform-methanol 9:1, v/v). The first green fraction contained **1b**. The compound was recrystallized twice from chloroform by addition of acetone. Yield: 38 mg (17%). Dark green solid, decomp 178 °C. IR (CHCl<sub>3</sub>) 864 (Ar-H), 910, 948 (Pc), 1099 (Pc), 1135 (C-O-C), 1285 (Ar-O-C), 1509, 1607 (Ar/Pc), 2856, 2928 (CH<sub>2</sub>), 3500 (OH) cm<sup>-1</sup>. <sup>1</sup>H NMR (CDCl<sub>3</sub>, 100 MHz) δ 0.87 (t, 24H, CH<sub>3</sub>), 1.1-2.0 (m, 128H, CH<sub>2</sub>), 3.8-4.9 (m, 80H, CH<sub>2</sub>O), 6.65 (s, 8H, ArH), 8.93 (s, 8H, PcH). Anal. (C<sub>168</sub>H<sub>250</sub>N<sub>8</sub>O<sub>34</sub>Si): found (calcd) C, 67.76 (68.31); H, 8.50 (8.53); N, 3.69 (3.79).

**Poly[(tetrakis[4',5'-bis(decoxy)benzo[1',2'-k]-1,4,7,10,13,16-hexaoxacyclooctadeca-2,11-dieno][2,3-b:2',3'-i:2'',3''-p:2''',3'''-w]phthalocyaninato)siloxane] (poly-1b).** Method A: Phthalocyanine **1b** (30 mg, 10 μmol) was heated in a Schlenck-vessel under vacuum at 200 °C for 24 h. This afforded a purple insoluble polymer. Method B: A mixture of phthalocyanine **1b** (50 mg, 17 μmol) and tetrakis(acetonitrilo)copper(I) triflate (25 mg, 59 μmol) in toluene (0.2 mL) was stirred at 110 °C for 24 h. Methanol was added, and the mixture was sonicated for 5 min. The product was filtered off, and the residue was dissolved in chloroform and passed through a filter. Yield: 35 mg (70%) of a dark blue solid.

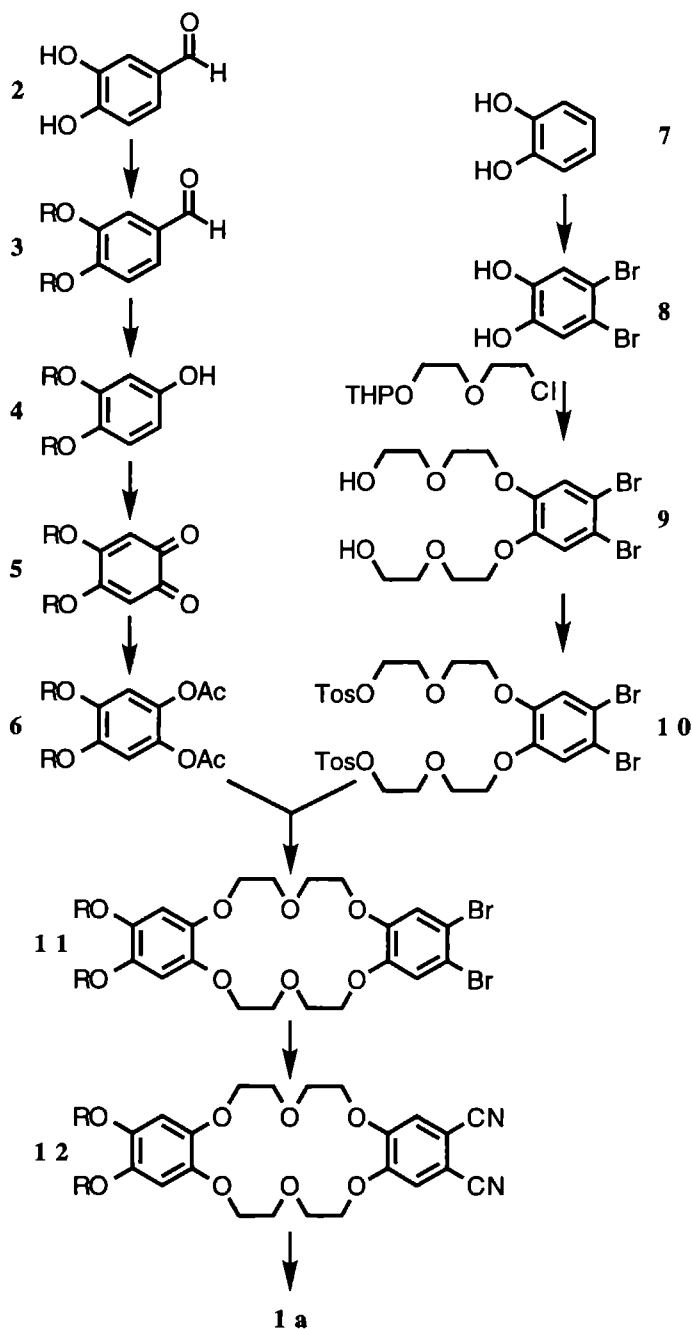
## 6.3 Results and discussion

### 6.3.1 Synthesis and characterization

Phthalocyanine **1a** was prepared according to Scheme 6.1. A key intermediate in the synthetic route is the dissymmetric dibenzocrown-ether **11**. This compound was prepared by coupling two fragments: the diacetate **6**, containing the decoxy chains, and the ditosylate **10** containing two bromine atoms. We used the protected *ortho*-dihydroxybenzene **6**, because this compound was much more stable than the corresponding extremely air-sensitive dihydroxide. The diacetate could be hydrolyzed and coupled to the ditosylate in a one pot reaction. Moreover, this compound could be synthesized very easily from *ortho*-benzoquinone **5** by reduction with zinc in the presence of acetic acid and acetic anhydride, in 88% yield [9]. Compound **5** was synthesized by the following procedure. The two decoxy chains were first introduced by alkylating the 3,4-dihydroxybenzaldehyde **2** with 1-bromodecane in DMF in the presence of  $K_2CO_3$ , to give **3** in 84% yield. The aldehyde group was subsequently converted into a hydroxy group by an acid catalyzed Baeyer-Villiger type of oxidation with hydrogen peroxide in 1:1 (v/v) chloroform-methanol (yield 65%) [10]. The resulting phenol **4** was reacted with Fremy's radical [6] under phase transfer conditions in THF/water to give **5** in 80% yield. The overall yield for the synthesis of **6** from **2** amounted to 38%.

The second fragment, ditosylate **10**, was prepared in three steps with an overall yield of 42% starting from catechol **7**. The latter compound was first brominated with molecular bromine in tetrachloro methane (yield 91%). The resulting dibromo catechol **8** was alkylated with tetrahydropyranyl (THP) protected diethyleneglycol monochloride in 1-butanol in the presence of NaOH. The THP groups were *in situ* removed by acidification of the reaction mixture. Compound **9** was obtained in 49% yield after distillation under reduced pressure. Its two hydroxy groups were converted into leaving groups by tosylation in pyridine (yield 93%) [11].

The two fragments **6** and **10** were coupled by first hydrolyzing **6** in 1-butanol in the presence of NaOH, followed by the *in situ* substitution of the tosylate groups of **10** by the formed dihydroxylate. This reaction afforded the dibenzocrown-ether **11** in 58% yield. The two bromine atoms of **11** were substituted by cyano groups

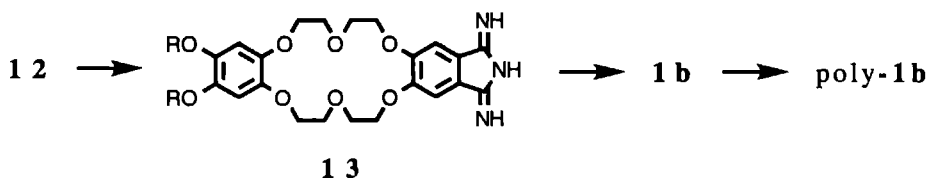


Scheme 6.1

according to a known procedure (yield 75%) [12]. The metal free Pc **1a** was obtained by cyclization of the dicyanide **12** with the help of *N,N*-dimethylaminoethanol [13]. After repeated recrystallization from chloroform the yield of this phthalocyanine amounted to 30%.

Surprisingly, the solubility of **1a** in organic solvents was extremely low. At room temperature the compound was found to be slightly soluble in chloroform and toluene only. The solubility in these solvents could be improved by heating. Pc **1a** was characterized by IR, NMR, and elemental analysis (see Experimental section). Because of the low solubility of the compound at room temperature, the  $^1\text{H}$  NMR spectrum was recorded in chloroform at elevated temperature. The NMR peaks were rather broad and the protons of the Pc core were invisible. As will be shown in the next section, this effect is due to strong aggregation of the molecules. Although the product had been dried extensively in high vacuum for several days, elemental analysis revealed that some chloroform was retained in the solid (molar ratio  $\text{CHCl}_3/\mathbf{1a} \approx 1$ ).

The dihydroxysilicon derivative **1b** was synthesized in two steps from dicyanide **12** (Scheme 6.2). The latter compound was first converted into the 1,3-diiminoisoindoline **13** by reaction with ammonia in 1:1 (v/v) THF-methanol (yield 30%). Subsequent cyclization of **13** in quinoline in the presence of  $\text{SiCl}_4$ , followed by hydrolysis of the resulting dichlorosilicon Pc, gave **1b** in 17% yield. In contrast to the metal free derivative **1a**, compound **1b** was found to be highly soluble in chloroform. A nicely resolved  $^1\text{H}$  NMR spectrum could be recorded, including the peaks of the Pc protons. This result suggests that aggregation of **1b** is prevented by the axial hydroxy substituents. The IR spectrum of **1b** is almost identical to that of **1a**, except for the N-H band at  $3294\text{ cm}^{-1}$  which is absent in **1b**, and the presence of a new band in **1b** at  $1361\text{ cm}^{-1}$ , which is probably related to the Si-O bond. The UV/Vis spectrum displays a strong Q-band at 679 nm (see Figure 6.2), which is in line with values found for other dihydroxysilicon Pcs [14].



Scheme 6.2

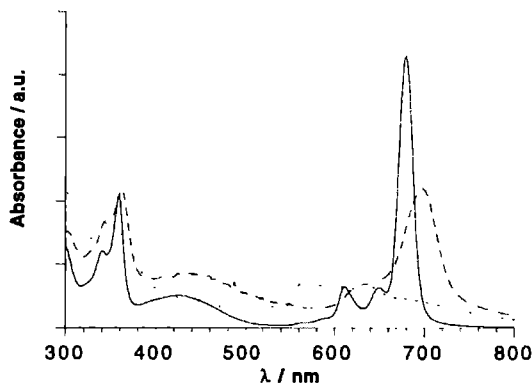


**Figure 6.2** Electronic absorption spectra of **1b** in chloroform (—), **1b** in a 2×10-layer LB film (---), and poly-**1b** in chloroform (...).

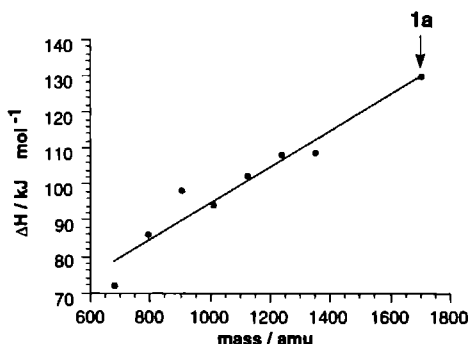
Phthalocyanine **1b** was polymerized using two different methods. Van der Pol described the synthesis of a high molecular weight polysiloxane from a liquid crystalline Pc by heating the corresponding dihydroxysilicon monomer in vacuum at 200 °C [14b]. A purple coloured polymer was obtained having a degree of polymerization of approximately 100. Using the same procedure for **1b** (method A), we obtained a purple polymer as well, but the material was insoluble in organic solvents. We also tried a method published by Caseri *et al.*, *viz.* a polycondensation reaction in refluxing toluene in the presence of copper triflate [8]. Using this method (method B) and a reaction time of 24 h a blue product was formed, which was soluble in chloroform. The Q-band in the UV/Vis spectrum of this product (Figure 6.2) showed an exciton shift of  $\Delta E(N) = 2909 \text{ cm}^{-1}$  (from 679 nm in the monomer to 567 nm in the product), confirming that the polycondensation reaction was successful. The degree of polymerization,  $N$ , can be derived from this Q-band shift according to formula (5.1) (chapter 5). For  $\Delta E(N \rightarrow \infty)$  in this formula we can take the value that has been reported by Sauer *et al.* for a high molecular weight Pc-polysiloxane, *i.e.*  $3609 \text{ cm}^{-1}$  [15]. With this value and (5.1) we can calculate that the degree of polymerization of poly-**1b**, synthesized by method B, is  $N = 5$ . The appearance of a shoulder in the UV/Vis spectrum at 680 nm suggests that some residual monomer is still present in the polymer.



### 6.3.2 Solid state and mesophase structure

The phase transition temperatures and enthalpies of compound **1a** were measured by DSC. One reversible transition was detected, with the peak onset in the heating run found at 148 °C. The transition enthalpy amounted to 130 kJ·mol<sup>-1</sup>. This value is *ca.* 20 kJ·mol<sup>-1</sup> larger than the value reported for the crystalline to mesophase transition of octa(dodecoxy)phthalocyanine [16]. This is due to the fact that the substituents of **1a** are larger than those of the aforementioned phthalocyanine. Figure 6.3 shows a plot of the transition enthalpies of octa(alkoxy)phthalocyanines, together with that of **1a**, *versus* the total mol mass of the flexible parts of the substituents. For the calculation of this mol mass the rigid benzene rings of **1a**, as well as the oxygen atoms connected to these benzene rings and those connected to the Pc cores of **1a** and the other octa(alkoxy)-Pcs, were excluded. The following linear relationship was found:  $\Delta H = 44.4 + 0.05 \times m_{\text{flex}}$ , with  $m_{\text{flex}}$  being the total flexible mass of the substituents in atomic mass units. At the crystalline to mesophase transition the side chains of the octa(alkoxy)phthalocyanines start to melt [17]. The second term in the above equation therefore is likely to be equal to the melting enthalpy of these chains, which appears to be proportional to their mass. It can be concluded from Figure 6.3 that **1a** exhibits melting behavior similar to the other liquid-crystalline phthalocyanines.

**Figure 6.3** Transition enthalpy versus the total mass of the side chains of octa(alkoxy)-Pcs (6 to 12 carbon atoms per chain, data taken from reference 16) and of **1a**. Only the flexible parts of the substituents are included in the calculation of the total mass (see text).



The mesophase of compound **1a** appears as a highly viscous mass, showing birefringence under the polarizing microscope. Large hysteresis was observed in the DSC cooling run, as the transition to the crystalline phase occurred at 105 °C. No transition to the isotropic phase could be observed below the decomposition temperature of the compound ( $T = 320$  °C). DSC measurements on compound **1b**

revealed no phase transition up to the temperature where the compound starts to polymerize, *i.e.* at 178 °C.

The structures of the crystalline phase and the mesophase of **1a** were determined by SAXS measurements at 20 °C and 170 °C, respectively. The results are shown in Figure 6.4. The crystalline phase gives rise to a large number of peaks that can be indexed according to a monoclinic lattice with eclipsed Pc units having a unit cell with the parameters  $a = 31.2$ ,  $b = 27.8$ ,  $c = 4.3$  Å, and  $\alpha = 96^\circ$ . With the help of molecular dimensions derived from CPK models, we propose a molecular arrangement as shown in Figure 6.5. The center-to-center distance of the Pc molecules along the  $a$ -axis is very close to the radius of a molecule with fully elongated decoxy chains, *i.e.* 31.5 Å (see Figure 6.1a). The fact that the  $a$ - and  $b$ -axes are unequal indicates that the molecules are tilted. The Pc cores and the benzene rings are probably tilted with respect to the  $c$ -axis by rotations around the molecular  $x$ -axes, as illustrated in Figure 6.5b. This makes the inter-Pc distance very close to the van der Waals distance, *i.e.* 3.4 Å, while the crown-ether rings and the alkoxy chains become oriented perpendicular to the  $c$ -axis and are stacked with a separating distance of 4.3 Å. The tilt angle of the Pc units is then calculated to be  $38^\circ$  ( $3.4/4.3 = \cos 38^\circ$ ). As can be noticed from Figure 6.5a, some empty space may be present in the crystalline structure. This space is probably occupied by solvent molecules, since elemental analysis reveals that chloroform is tightly bound in the solid material (*vide supra*). The density of the unit cell is calculated to be  $1.293 \text{ g}\cdot\text{cm}^{-3}$ . This value is quite reasonable and similar to the values found for other octa(alkoxy)-Pcs in the crystalline phase [16].

The SAXS measurements on **1a** at 170 °C confirmed the presence of a mesophase at this temperature. The scattering curve in Figure 6.4 shows an intense peak corresponding to a spacing of 35.3 Å which can be attributed to the (100) reflection of a hexagonal columnar ( $D_h$ ) mesophase. Small peaks observed at 17.3 and 13.4 Å are then related to the (200) and (210) reflections, respectively. These values correspond to an intercolumnar distance of 40.5 Å. This distance suggests that the decoxy chains are folded backwards as shown in Figure 6.1b, or what is more probable, are in an interlacing position, as illustrated in Figure 6.6. A very small band is observed around 3.34 Å (see Figure 6.4B), which can be assigned to the intracolumnar stacking period of the Pc cores. This reflection is somewhat diffuse, indicating that the stacking is disordered. A broad and diffuse band is visible at 4.4 Å, which is characteristic for disordered side chains [16]. This band is accompanied with a small reflection at approximately twice this spacing, *viz.* 8.7 Å.

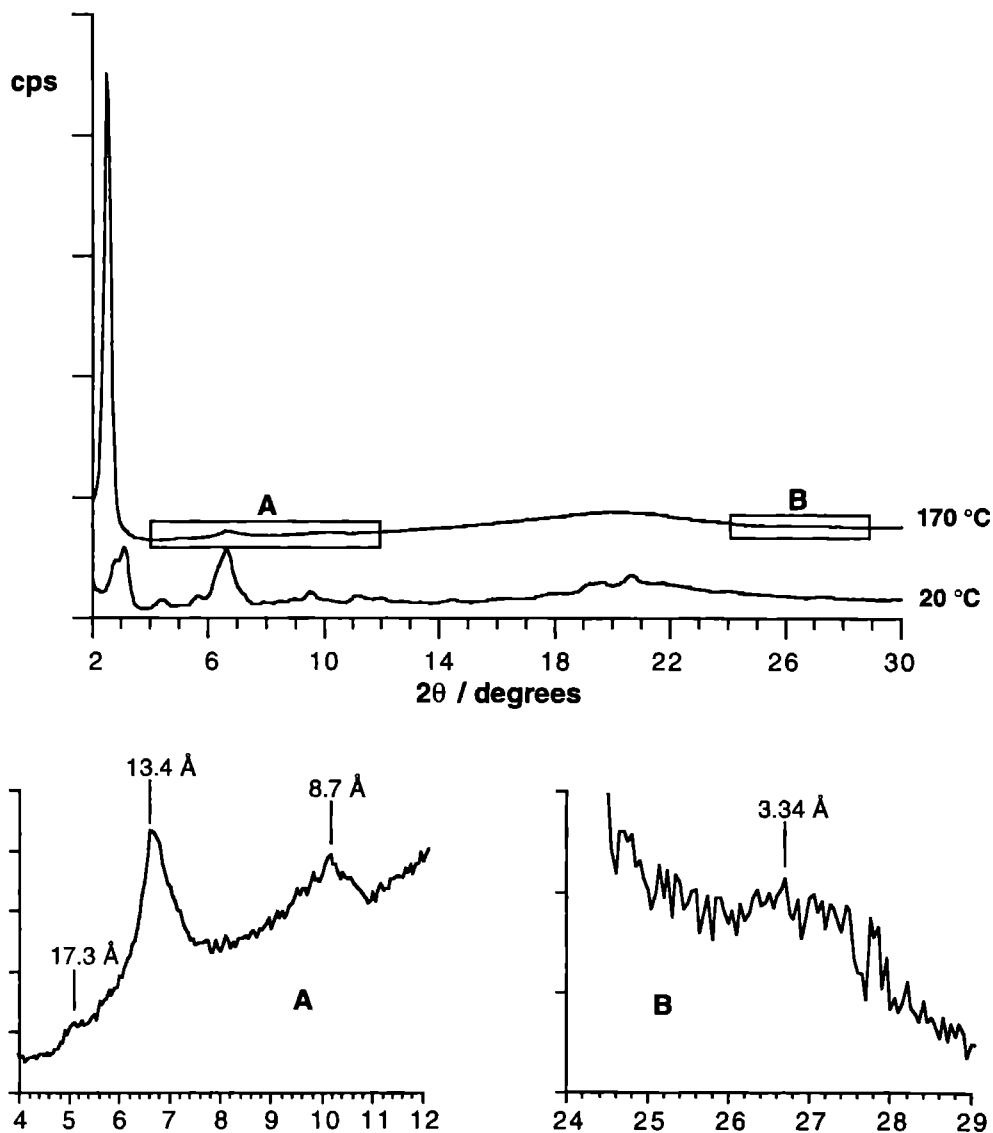


**Figure 6.4** X-ray scattering curves of **1a** in the crystalline phase at 20 °C and in the mesophase at 170 °C. The curves are displaced along the y-axis to avoid overlapping.

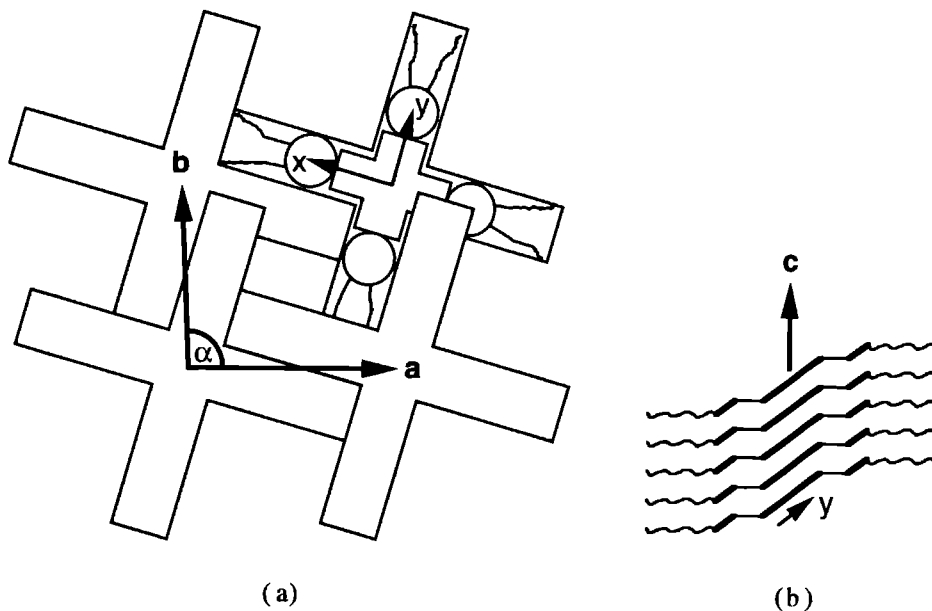


**Figure 6.5** Schematic representation of the proposed structure of the crystalline phase of **1a**: view along the normal on the  $Pc$   $xy$ -plane (a); view along the molecular  $x$ -axis (b).

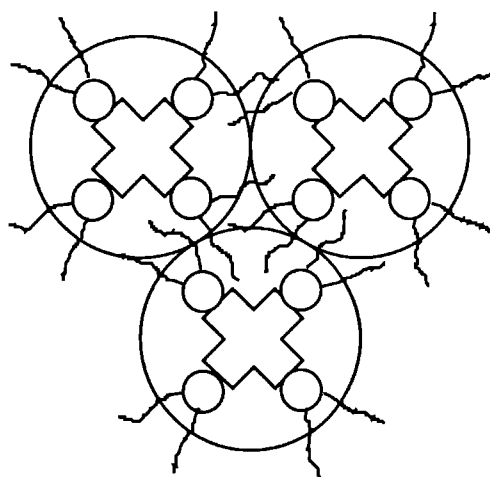


**Figure 6.6** Schematic representation of the proposed structure of the mesophase of **1a**.

These data suggest that the Pc molecules are stacked cofacially in a staggered conformation. A density of  $0.89 \text{ g}\cdot\text{cm}^{-3}$  can be calculated for the unit cell of the mesophase of **1a**, which is very close to the density of metal free octa(dodecoxy)-Pc in its mesophase [16].

The structural characteristics of the crystalline and mesophase of **1a** show some similarity with the corresponding phases of 15-crown-5 Pc [5b]. The most obvious difference is that the latter compound only exhibits a (metastable) mesophase when it is freshly purified, whereas compound **1a** forms a very stable recurrent mesophase.

An interesting feature of the structure of **1a** is the presence of ion channels: in the crystalline phase the molecules are in an eclipsed position, with the crown-ether rings superimposed. Also in the mesophase ion channels exist because the next-nearest crown-ether rings are superimposed. For future application of these channels as ion conducting pathways it is necessary to control the organization of the molecules over a long distance. In the next section we will demonstrate that this is possible by a process of self-assembly in solution.

### **6.3.3 Aggregation in solution: UV/Vis spectroscopy**

We noticed above that the metal free Pc derivative **1a** was hardly soluble in organic solvents, and that the NMR spectrum of this compound showed broad bands even at elevated temperature. These observations are indicative of strong aggregation in solution. This was corroborated by a study of the UV/Vis spectrum of **1a** in chloroform solution. Figure 6.7 shows the absorption spectra of a diluted solution ( $11 \mu\text{M}$ ) of **1a** recorded at room temperature and at  $50^\circ\text{C}$ . The high temperature spectrum displays the splitted Q-band that is characteristic for non-aggregated metal free Pcs, with maxima appearing at 661 and 700 nm. The spectrum recorded at room temperature is broadened and the maximum is blue-shifted to 614 nm. According to the molecular exciton theory [18], the blue shift points to stacking of the Pc molecules, the tilt angle being smaller than  $35.3^\circ$ . This result suggests that the structure of the aggregates is different from the structure in the crystalline solid for which a tilt angle of  $38^\circ$  was calculated. The exciton splitting,  $2\epsilon$ , which is due to the coupling of the  $\pi$ -systems including long range interactions, is given by [15]

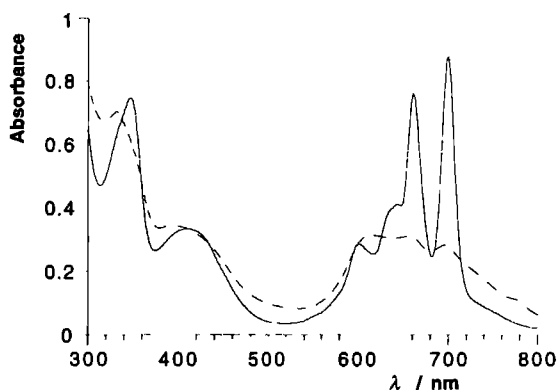


**Figure 6.7** Electronic absorption spectra of **1a** in chloroform (11  $\mu\text{M}$ ) at different temperatures: 25  $^{\circ}\text{C}$  (---); 50  $^{\circ}\text{C}$  (—)

$$2\varepsilon = 2[-(\Delta E_a - \Delta E_m) + \Delta D] = -4.8 \left[ \frac{N-1}{N} \cdot \frac{|\vec{M}|^2}{r^3} (\cos \alpha - 3\cos^2 \theta) \right] \quad (6.1)$$

where  $\Delta E_a$  and  $\Delta E_m$  are the energies corresponding to the aggregate and monomer Q-band maxima,  $\Delta D$  is the lowering of the difference between the ground and excited states due to van der Waals interaction ( $\Delta D = -615 \text{ cm}^{-1}$ ),  $N$  is the aggregation number,  $\vec{M}$  is the transition dipole moment,  $r$  is the center-to-center distance between the molecules,  $\alpha$  is the torsion angle between neighboring molecules, and  $\theta$  is the angle between the transition moment and the center-to-center line. The intercolumnar distance  $r$  is related to the angle  $\theta$  according to  $r = r_{\min}/\sin \theta$ , where the minimum van der Waals distance  $r_{\min} = 3.4 \text{ \AA}$ .  $|\vec{M}|^2$  can be calculated from the oscillator strength  $f$ . The latter value was determined by integration of the monomeric Q-band, resulting in  $f = 0.59 \text{ erg}\cdot\text{cm}^{-1}$ , from which a value of  $|\vec{M}|^2 = 2.17 \times 10^{-19} \text{ cm}^2$  could be derived. These values are very close to the literature values found for a substituted dihydroxysiliconphthalocyanine [15]. When the aggregation number  $N$  is considered to be large, which is justified as shown in the next section, then  $(N-1)/N$  can be taken as unity by good approximation. With the values of  $\Delta E_a$  and  $\Delta E_m$  being  $16287 \text{ cm}^{-1}$  and  $14695 \text{ cm}^{-1}$ , respectively, and taking an eclipsed conformation with  $\alpha = 0^{\circ}$ , a value of  $\theta = 60^{\circ}$  was calculated using formula (6.1). This value corresponds to a tilt angle of  $30^{\circ}$  and a center-to-center distance  $r$  of  $3.9 \text{ \AA}$ . If a staggered conformation is assumed with  $\alpha = 45^{\circ}$ , then a tilt angle of  $24^{\circ}$  and  $r$

= 3.7 Å are calculated. The latter structure cannot be ruled out, but the former is more plausible since the structural parameters are close to those of the  $\alpha$ -modification of solid unsubstituted Pcs [19].

The aggregation of **1a** was not only found to be temperature dependent, but also concentration dependent. The heat of association can be estimated from the temperature and concentration dependency of the UV/Vis spectrum. Figure 6.8a shows a plot of the ratio of the absorbances of the aggregate and the monomer *versus* the temperature, for four different concentrations of **1a** in chloroform. The aggregation number is related to this absorbance ratio: in other words at a fixed ratio the weight fraction of the monomer,  $m_1$ , is constant. For a constant  $m_1$  the following relationship holds [20]:

$$W_1 = R \cdot \frac{\Delta \ln c}{\Delta(1/T)} \quad (6.2)$$

where  $W_1$  is the heat of association,  $R$  is the gas constant,  $\Delta \ln c$  is the difference between two Pc concentrations, and  $\Delta(1/T)$  is related to the temperature difference that has to be applied to maintain a constant  $m_1$ . Formula (6.2) can be used for linear aggregates of uniform structure, making the following assumptions: the equilibrium constant  $K_i = c_i/c_1^i$  for the formation of the  $i$ -mer from  $i$  units depends only on  $T$ , and  $W_i = (i - 1)W_1$ , with  $W_1$  independent of  $i$ . The values of  $T$

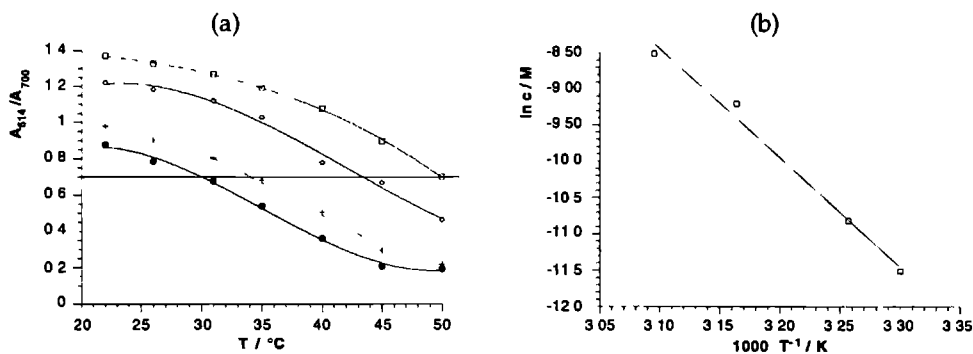


**Figure 6.8** (a) Ratio of the absorbances at 614 and 700 nm plotted versus the temperature for various concentrations of **1a** in chloroform: 0.202 mM (squares); 0.101 mM (lozenges); 0.020 mM (crosses); 0.010 mM (circles). The temperatures  $T$  at which the absorbance ratio equals 0.7 (horizontal line) were obtained by intra-polation of the data points at each concentration  $c$ , and plotted in (b) as  $\ln c$  versus  $1/T$ .

where the absorbance ratio has a constant but arbitrary chosen value (0.7 in this case) were obtained by intrapolation of the data points of Figure 6.8a at each concentration. The plot of  $\ln c$  versus the reciprocal temperature (Figure 6.8b) afforded a straight line, from which a value of  $W_1 = -125 \text{ kJ}\cdot\text{mol}^{-1}$  was derived. To our knowledge, such a high value has never been reported before in the literature for the aggregation of Pcs. For example, the heats of association of tetrasulfonato-phthalocyanines in water are 2.5 to 5 times lower [21]. The driving forces for aggregation in this literature example are  $\pi$ - $\pi$  interactions, van der Waals interactions, and in particular hydrophobic effects. The aggregation of Pc **1a** in chloroform is mainly the result of  $\pi$ - $\pi$  and van der Waals interactions. These interactions are exceptionally strong in our system because they can not only take place between the Pc cores, but also between the peripheral benzene units of different eclipsed molecules, resulting in a "five-points attachment". The existence of strong attraction between the molecules of **1a** leads to extremely long linear aggregates, as will be shown next.

#### 6.3.4 Aggregation in solution: electron microscopy

Interestingly, when a more concentrated solution of compound **1a** in hot chloroform was cooled to room temperature a firm gel was formed. This was observed at concentrations as low as  $7 \text{ mg}\cdot\text{mL}^{-1}$ . A sample having the latter concentration and a sample of  $1 \text{ mg}\cdot\text{mL}^{-1}$  were studied with the help of transmission electron microscopy (TEM). Some representative TEM pictures are shown in Figure 6.9. At a concentration of  $7 \text{ mg}\cdot\text{mL}^{-1}$  dense networks of large fibers are observed (micrograph (a)). Micrograph (b) was taken from the same sample with the same magnification but at another position. The latter picture clearly shows that the fibers consist of bundles of single parallel strands. Some isolated single strands can also be seen. The length of the fibers is of the order of a few micrometers. A magnification of micrograph (b) is shown in Figure 6.7c. The dimensions of the uncovered and platinum covered parts suggest that the strands are cylinders with a diameter of approximately  $60 \text{ \AA}$ , as illustrated in Figure 6.9d. This value matches very well with the diameter of a molecule of **1a** as estimated from CPK molecular models (see Figure 6.1a). At the lower concentration of  $1 \text{ mg}\cdot\text{mL}^{-1}$  fibers are also observed, but they are smaller in length and no network is formed (not shown).



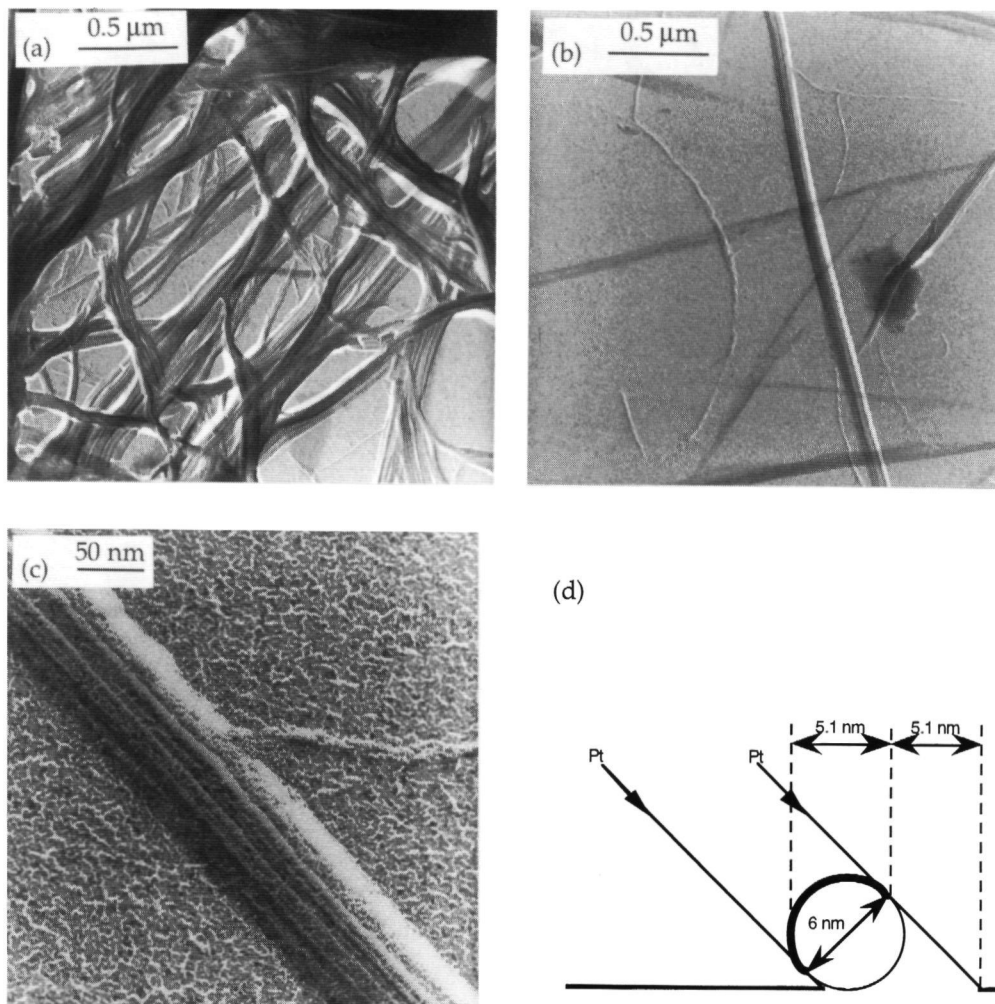
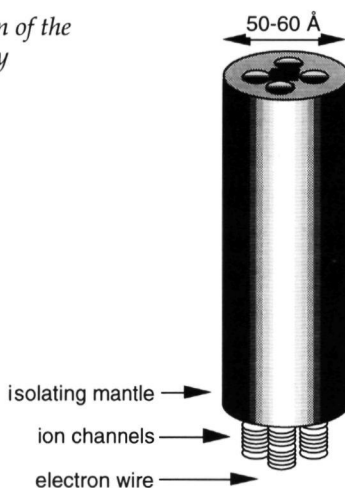


**Figure 6.9** Transmission electron micrographs (a-c) of a gel of **1a** in chloroform ( $7 \text{ mg} \cdot \text{mL}^{-1}$ ). Schematic illustration (d) showing how a cylindrical structure of  $60 \text{ \AA}$  diameter is covered when shadowed with platinum vapor at an angle of  $45^\circ$ . When viewed from the top this results in the appearance of a covered and an uncovered parallel stroke of  $51 \text{ \AA}$  width each, corresponding with the dimensions observed in the TEM micrographs.

From these results we may conclude that compound **1a** self-assembles in chloroform solution to produce linear aggregates. The stacks that are visualized by TEM have molecular thickness and are built up from *ca.*  $10^4$  molecules. Such a large aggregation number in solution is unprecedented and reflects the existence of large attracting forces between the molecules. It is reasonable to assume that at the

concentrations used (*i.e.* up to  $0.58 \text{ mg}\cdot\text{mL}^{-1}$ ), the aggregation number is sufficiently large to treat the observed exciton shifts in the UV/Vis spectra as resulting from infinitely large aggregates (*vide supra*). As discussed in the UV/Vis spectroscopy section, the molecules are most likely stacked in an eclipsed conformation. Such a conformation was also shown to be present in the crystalline state of **1a**. A (close to) eclipsed conformation places the peripheral benzene units in a favorable position for  $\pi$ - $\pi$  interaction. This has interesting consequences. The isolated strands of molecules **1a** can be considered as being molecular cables (Figure 6.10). Such cables contain a central electron conducting wire of stacked Pc molecules, four ion channels formed by the crown-ether rings, and a surrounding insulating hydrocarbon mantle. The electron and ion conducting properties of the solid and the mesophase, as well as of the aggregates in solution will be the subject of future studies.

**Figure 6.10** Schematic representation of the multiwired molecular cable formed by aggregation of **1a** in chloroform.



### 6.3.5 Formation of monolayers and LB films

We found that crown-ether substituted Pcs [5,14a,22] give unstable monolayers at the air-water interface and therefore can not be used to prepare multilayer films (unpublished results). We anticipated that the attachment of hydrocarbon chains to the crown-ether rings, as in compound **1a**, would be favorable for stabilizing the monolayers. Unfortunately, it was not possible to form monomolecular layers from **1a** due to the strong tendency of the molecules to aggregate. The dihydroxy-

silicon derivative **1b** does not aggregate in organic solution. This compound turned out to be suitable for the formation of LB films, as will be shown next.

A solution of **1b** in chloroform was spread on a water surface at 20 °C. After evaporation of the solvent the surface area  $A$  was slowly decreased while the surface pressure  $\pi$  was measured. Figure 6.11, curve A, shows the resulting  $\pi$ - $A$  isotherm. A continuous rise of the surface pressure with decreasing surface area was observed up to  $\pi = 53 \text{ mN}\cdot\text{m}^{-1}$ , whereupon the film collapsed. Extrapolation of the steepest part of the curve to zero pressure gave a very large area of  $313 \text{ \AA}^2$  per molecule. This value is too high for an edge-on arrangement of the molecules on the water surface. A side-on orientation of the Pc core with the substituents oriented away from the water surface fits well with the measured area per molecule. Assuming a circular projection of the molecule on the water surface, a diameter of  $20.0 \text{ \AA}$  can be derived from the measured area per molecule, which is in agreement with the dimensions of CPK molecular models of such a conformation (see Figure 6.12a). The four substituents occupy a total area of approximately  $180 \text{ \AA}^2$  when they are oriented perpendicular to the water surface. Therefore, they are probably randomly oriented above the Pc plane to fill the free space that would otherwise be present.

During the recording of the pressure-area isotherm we viewed the water surface with a Brewster Angle Microscope (BAM). Both the expanded ( $\pi = 0$ ) and the compressed monolayer ( $\pi > 0$ ) displayed a completely structureless surface. Only when the collapse pressure was reached, lines did appear due to the formation of multilayers. This behavior is in striking contrast with that of other

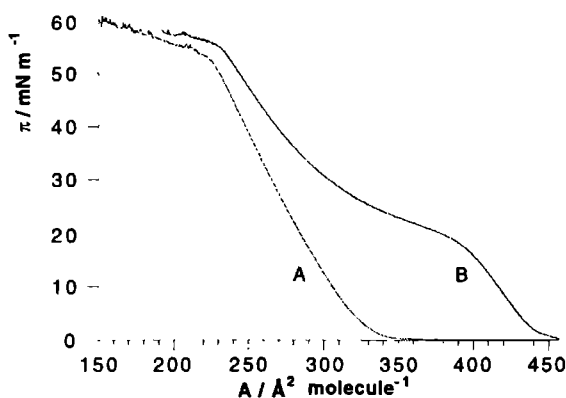


**Figure 6.11** Surface pressure - surface area isotherms for **1b** at a subphase temperature of 20 °C. Curve A: pure water; Curve B: 1 M KCl.

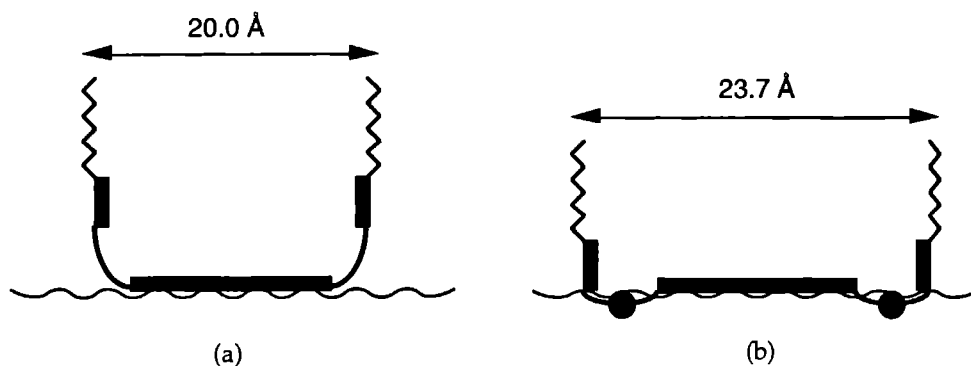


**Figure 6.12** Schematic representation of the conformation of a molecule of **1b** at the air-water interface: without KCl in the subphase (a); with KCl (b). The dark circles represent the  $K^+$  ions that are bound in the crown-ether rings.

monolayer forming Pcs and porphyrins. Usually "floating islands" are observed at the expanded monolayer, consisting of cofacially aggregated molecules, which collide on compression (see chapter 3 and reference 23). The absence of such islands in the case of Pc **1b** suggests that this molecule does not aggregate into large domains. This behavior is probably related to the axial hydroxy groups in the center of the molecule. These groups not only hinder the cofacial aggregation, but also increase the hydrophilicity of the molecular core of **1b**, which favors the side-on orientation of the molecules on the water surface.

We were able to transfer monolayers of **1b** onto a hydrophobic glass substrate by vertically dipping the substrate through the monolayer at a surface pressure of  $15 \text{ mN}\cdot\text{m}^{-1}$ . Y-type deposition occurred with a transfer ratio of *ca.* 1.0 with each upstroke transfer. The downstroke transfer resulted in a lower ratio of *ca.* 0.5, which might be the result of an incomplete transfer or a conformational change of the molecules during the deposition process. The UV/Vis spectrum of a  $2\times 10$  layer film is shown in Figure 6.2. The maximum of the Q-band is seen at 697 nm, which is red-shifted compared to the Q-band of a chloroform solution of **1b** (*vide infra*). An additional small peak is observed at 630 nm. These spectral changes can be attributed to exciton splitting due to a slipped cofacial stacking of the Pc units with a tilt angle larger than  $35.3^\circ$ . The smaller peak is the result of a transition that is only weakly allowed by the selection rules when the intermolecular torsion angle  $\alpha$  is larger than zero [18]. Similar spectral changes were observed in solid films of axially substituted silicon naphthalocyanines [24]. The observed energy difference between the allowed and partly forbidden transition,  $2\epsilon$ , amounts to  $1526 \text{ cm}^{-1}$ . We

can calculate the aggregation number  $N$  from this exciton splitting with the help of formula (6.1), taking for the center-to-center distance  $r$  the value that was previously measured for the dihydroxysilicon derivative of octa(alkoxy)Pc, *i.e.* 4.5 Å [25]. This value corresponds to  $\theta = 49.1^\circ$  or a tilt angle of  $40.9^\circ$ . The numerical factor in formula (6.1) has to be reduced to 4.0 to exclude longer range interactions. If we take for the torsion angle between the molecules the value  $\alpha = 0^\circ$  the upper limit of  $N$  can be calculated; for  $\alpha = 45^\circ$  the lower limit is found. These limits amount to 2.3 and 1.4, respectively. From these numbers we may conclude that the molecules in the LB film are present as dimers. This result is in line with the observed Y-type deposition, which results in an alternating "face-to-face" and "tail-to-tail" multilayer structure. Apparently, the slipped face-to-face interaction of the Pc-units is responsible for the observed "dimeric" UV/Vis spectrum of the LB-film.

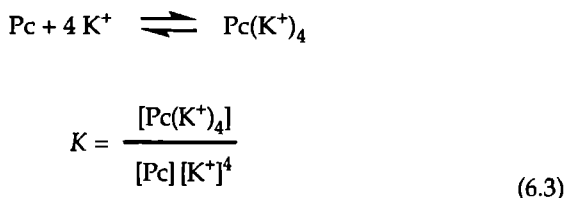
### **6.3.6 Binding of alkali metal ions in monolayers**

Several examples of monolayer forming crown-ethers are known in the literature [26,27]. In some studies the (selective) binding of alkali metal ions has been reported [27]. This binding can be observed by changes in the pressure-area isotherms or in the surface potential. We investigated the influence of potassium chloride in the subphase on the monolayer isotherms of compound **1b**.

Figure 6.11, curve B, shows the isotherm that was recorded with 1 M KCl as the subphase. It can be seen that a first rise of the surface pressure is found at an area of 440 Å<sup>2</sup> per molecule, which is much larger than the observed molecular area with pure water as the subphase. The increased area corresponds to a circle with a diameter of 23.7 Å. This value is very close to the diameter of the molecule when the Pc core as well as the four crown-ether rings lie completely flat on the water surface. In that conformation the benzene units and the decoxy chains are oriented away from the water surface. This situation is illustrated in Figure 6.12b. From this result it is obvious that the alkali metal ions induce a conformational change of the molecules of **1b** at the air-water interface. The binding of the metal ions in the crown-ether rings make these macrocycles more rigid and more hydrophilic, favoring their interaction with water. Figure 6.11 shows that a phase transition takes place when the monolayer area of **1b** on 1 M KCl is decreased. A second rise of the surface pressure is found at an area that is close to the molecular area on pure water. Collapse of the monolayer is observed at the same area per molecule and approximately the same surface pressure as on pure water. Probably

the decrease of the monolayer area forces the crown-ether rings to lift from the water surface. It is not clear at present whether or not this results in the release of the cation.

At intermediate KCl concentrations, isotherms were obtained that were inbetween the isotherms on pure water and on 1 M KCl. We recorded isotherms at various subphase concentrations between zero and 1 M KCl, and measured the area per molecule related to the first surface pressure rise. Figure 6.13 shows a plot of the area per molecule versus the potassium ion concentration. We assume the following equilibrium and the corresponding binding constant:



The concentrations of the complex and the free ligand can be calculated from the measured area per molecule,  $A$ , to be

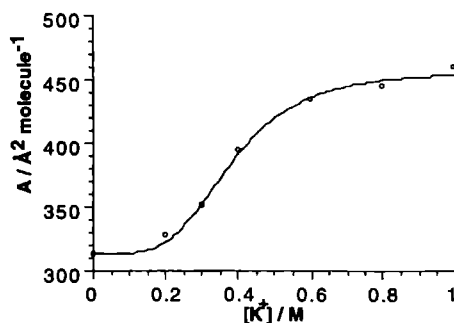
$$[\text{Pc}(\text{K}^+)_4] = \frac{A - A_0}{A_c - A_0} \times [\text{Pc}]_0 \quad (6.4)$$

and

$$[\text{Pc}] = \frac{A_c - A}{A_c - A_0} \times [\text{Pc}]_0 \quad (6.5)$$

where  $A_0$  is the area per molecule on pure water,  $A_c$  is the area per molecule when all complexation sites are occupied, and  $[\text{Pc}]_0$  is the total Pc concentration. By good approximation, the concentration of free potassium,  $[\text{K}^+]$ , is assumed not to be influenced by binding. This is true in our case because  $[\text{K}^+] \gg [\text{Pc}]_0$ . Combination of equations (6.3) - (6.5) results in the following relationship:

**Figure 6.13** Area per molecule of **1b** as a function of the potassium chloride concentration in the subphase. The open circles represent the measured data points. The solid line is the result of a computer fit of these points, leading to a binding constant of  $K = 48 \text{ M}^{-1}$  (see text).



$$K = \frac{A - A_0}{A_c - A} \times [K^+]^{-4} \quad (6.6)$$

Computer fitting of the datapoints of Figure 6.13 to this equation provides a binding constant of  $K = 48 \text{ M}^{-1}$ . This value is remarkably close to the value of the binding constant of dibenzo-18-crown-6 with potassium ions in aqueous solutions, *viz.*  $46.5 \text{ M}^{-1}$  [28].

## 6.4 Concluding remarks

We have described several ways to construct supramolecular structures from the novel phthalocyanine building blocks **1a** and **1b** by a process of self organization: in the solid state, in the liquid-crystalline state, in solution, and as monolayers and LB films. Two features are assumed to be mainly responsible for the spontaneous formation of the supramolecules: the high degree of shape anisotropy of the Pcs, which favors them to pack into columnar assemblies, and the fact that the molecules are strongly held together by van der Waals and  $\pi$ - $\pi$  interactions.

Very unexpected is the self organization of **1a** in chloroform solution leading to extremely long individual stacks of molecules. Aggregation of Pcs is usually observed in more polar solvents [12]. The very high association energy which we determined from UV/Vis spectroscopy experiments indicates that large attracting forces are responsible for this unique behavior. One-dimensional electron conducting wires and ion conducting channels are formed in the stacks, which are surrounded by an insulating hydrocarbon mantle. If it would be possible to isolate single strands or to align the strands all in one direction, these nanometer-sized

assemblies could find application as real molecular cables. It is noteworthy to mention that local motions in ion conducting materials have been recognized to be favorable for migration of large ions [3d]. Therefore, lyotropic or thermotropic liquid crystalline compounds are likely to be suitable building blocks in ion conducting materials. The electron and ion conductivities of our compound will be the subject of subsequent studies.

The limited stability of the self-assembled stacks in solution may be a problem for future applications. This problem can be solved by polymerization of the Pc building blocks, *e.g.* to give axial polysiloxanes. In that case the degree of polymerization has to be carefully controlled because of the insolubility of high molecular weight polymers. A second possibility is polymerization after the self-assembly process. This, for example, could be realized by introducing polymerizable groups in the side chains of the Pc molecules.

The formation of monolayers and LB films is a different way of making the Pc molecules suitable for future application. The ability of **1b** to bind cations in its crown-ether rings was demonstrated in monolayers of this compound. Interestingly, the obvious non-linearity of the "titration curve" of Figure 6.13 is suggestive of a positive cooperative effect in the complexation of potassium ions, *i.e.* a measurable change is only observed above a certain critical concentration of these ions. This result may be important for application in molecular switches based on the complexation of ions [29].



## References

- [1] G.M. Whitesides, J.P. Mathias, C.T. Seto, *Science* **254** (1991) 1312.
- [2] J.-M. Lehn, *Angew. Chem.* **100** (1988) 91; *Angew. Chem. Int. Ed. Engl.* **27** (1988) 89.
- [3] (a) J.-M. Lehn, *Angew. Chem.* **102** (1990) 1347; *Angew. Chem. Int. Ed. Engl.* **29** (1990) 1304. (b) R.M. Metzger, C.A. Panetta, *New J. Chem.* **15** (1991) 209. (c) J. Simon, C. Sirlin, *Pure Appl. Chem.* **61** (1989) 1625. (d) J. Simon, M.K. Engel, C. Soulié, *New J. Chem.* **16** (1992) 287.
- [4] M. Jørgensen, K. Bechgaard, T. Bjørnholm, P. Sommer-Larsen, L.G. Hansen, K. Schaumburg, *J. Org. Chem.* **59** (1994) 5877.
- [5] (a) O.E. Sielcken, H.C.A. van Lindert, W. Drenth, J. Schoonman, J. Schram, R.J.M. Nolte, *Ber. Bunsenges. Phys. Chem.* **93** (1989) 702. (b) C. Sirlin, L. Bosio, J. Simon, V. Ahsen, E. Yilmazer, Ö Bekaroğlu, *Chem. Phys. Lett.* **139** (1987) 362.
- [6] H. Zimmer, D.C. Lankin, S.W. Horgan, *Chem. Rev.* **71** (1971) 229.
- [7] E.P. Kyba, R.C. Helgeson, K. Madan, G.W. Gokel, T.L. Tarnowski, S.S. Moore, D.J. Cram, *J. Am. Chem. Soc.* **99** (1977) 2564.
- [8] W. Caseri, T. Sauer, G. Wegner, *Makromol. Chem. Rapid Commun.* **9** (1988) 651.
- [9] H.O. Huisman, *Recl. Trav. Chim. Pays-Bas* **69** (1950) 1133.
- [10] M. Matsumoto, H. Kobayashi, Y. Hotta, *J. Org. Chem.* **49** (1984) 4740.
- [11] B.P. Czech, B. Son, D.A. Babb, R.A. Bartsch, *Synthesis* (1985) 314.
- [12] O.E. Sielcken, M.M. van Tilborg, M.F.M. Roks, R. Hendriks, W. Drenth, R.J.M. Nolte, *J. Am. Chem. Soc.* **109** (1987) 4261.
- [13] P.J. Brach, S.J. Grammatica, O.A. Ossanna, L. Weinberger, *Heterocycl. Chem.* **7** (1970) 1403.
- [14] (a) O.E. Sielcken, L.A. van de Kuil, W. Drenth, J. Schoonman, R.J.M. Nolte, *J. Am. Chem. Soc.* **112** (1990) 3086. (b) J.F. van der Pol, J.W. Zwikker, J.M. Warman, M.P. de Haas, *Recl. Trav. Chim. Pays-Bas* **109** (1990) 208.
- [15] T. Sauer, W. Caseri, G. Wegner, *Mol. Cryst. Liq. Cryst.* **183** (1990) 387.
- [16] J.F. van der Pol, E. Neeleman, J.W. Zwikker, R.J.M. Nolte, W. Drenth, J. Aerts, R. Visser, S.J. Picken, *Liq. Cryst.* **6** (1989) 577.
- [17] A.P.M. Kentgens, B.A. Markies, J.F. van der Pol, R.J.M. Nolte, *J. Am. Chem. Soc.* **112** (1990) 8800.
- [18] (a) M. Kasha, H.R. Rawls, M. Ashraf El-Bayoumi, *Pure Appl. Chem.* **11** (1965) 371. (b) M. Kasha, in *Spectroscopy of the Excited State*, B. DiBartolo (ed.); Plenum Press: New York, 1976.
- [19] D. Wöhrle, *Kontakte (Darmstadt)* **1** (1986) 24.
- [20] H. Ölschläger, *J. Coll. Interface Sci.* **31** (1969) 503.
- [21] (a) O. Kratky, H. Ölschläger, *J. Coll. Interface Sci.* **31** (1969) 490. (b) R.D. Farina, D.J. Halko, J.H. Swinehart, *J. Phys. Chem.* **76** (1972) 2343.
- [22] P. Roisin, J.D. Wright, R.J.M. Nolte, O.E. Sielcken, S.C. Thorpe, *J. Mater. Chem.* **2** (1992) 131.
- [23] (a) J.M. Kroon, E.J.R. Sudhölter, A.P.H.J. Schenning, R.J.M. Nolte, *Langmuir*, in press. (b) G.H. Gelinck, C.F. van Nostrum, unpublished results.
- [24] M. Katayose, S. Tai, K. Kamijima, H. Hagiwara, N. Hayashi, *J. Chem. Soc. Perkin Trans. II* (1992) 403.

- [25] T. Sauer, G. Wegner, *Mol. Cryst. Liq. Cryst.* **162B** (1988) 97.
- [26] (a) J. Malthête, D. Poupinet, R. Vilanove, J.-M. Lehn, *J. Chem. Soc. Chem. Commun.* (1989) 1016. (b) C. Mertesdorf, T. Plesnivý, H. Ringsdorf, P.A. Suci, *Langmuir* **8** (1992) 2531 (c) Z. Zhang, H. An, X. Ma, X. Zhang, Y. Wu, Z. Zhu, *J. Incl. Phen. Mol. Recogn. Chem.* **13** (1992) 329. (d) S. Yoshida, Y. Okawa, T. Watanabe, S. Inokuma, T. Kuwamura, *Chem. Lett.* (1989) 243.
- [27] (a) J.M. Gold, D.M. Teegarden, K.M. McGrane, D.J. Luca, P.A. Falcigno, C.C. Chen, T.W. Smith, *J. Am. Chem. Soc.* **108** (1986) 5827. (b) J.Y. Fang, Z.H. Lu, S.P. Pan, Z.L. Chen, Y. Wei, J. Qin, M.C. Xie, *Solid State Commun.* **83** (1992) 1023. (c) H. Matsumura, T. Watanabe, K. Furusawa, S. Inokuma, T. Kuwamura, *Bull. Chem. Soc. Jpn.* **60** (1987) 2747.
- [28] E. Shchori, N. Nae, J. Jagur-Grodzinski, *J. Chem. Soc. Dalton Trans.* (1975) 2381.
- [29] T. Toupance, V. Ahsen, J. Simon, *J. Am. Chem. Soc.* **116** (1994) 5352.

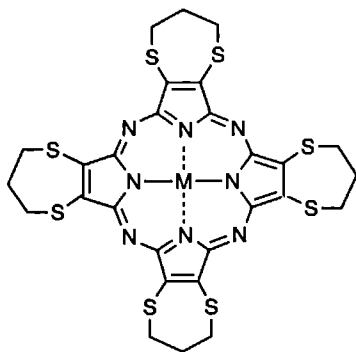
# ***Dithiacrown-ether Substituted Porphyrazines***

## **7.1 Introduction**

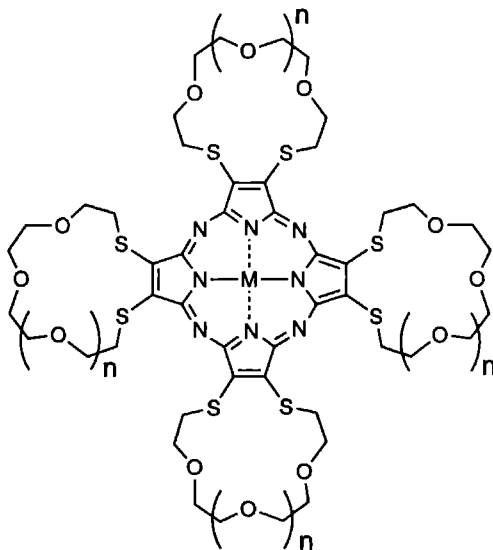
Molecular ionics is a rapidly developing area in chemistry. It is aimed at the development of molecular systems and devices that can handle and store information using ions as the basic species [1-3]. Crown-ethers, which are capable of selectively binding alkali metal ions, are important building blocks for constructing such devices because metal complexation can lead to a specific response, *e.g.* a change in electrical conductivity. In order to maximize the reliability, the response must be highly nonlinear, which can be achieved by introducing a cooperative effect in the binding process [2,3].

Phthalocyanines (Pcs), porphyrins (Pps), and porphyrazines (Pzs) are another class of compounds receiving great interest as components in molecular ionics. Of particular interest are phthalocyanines that are substituted with crown-ether rings [2,3]. In recent years we, Bekâroglu, and others have synthesized Pcs with different crown-ether substituents [5]. The metal binding properties of these molecules as well as their electron conducting behavior have been studied in detail [6]. Furthermore, linear and network polymers have been prepared [7,8].

In this chapter we describe the synthesis of novel porphyrazine derivatives to which four crown-ether rings of various sizes are connected: 7-crown-2 (MPz(7)), 15-crown-5 (MPz(15)), and 18-crown-6 rings (MPz(18)). Sulfur atoms are incorporated in the crown-ether rings for synthetic reasons. The presence of these atoms also gives the opportunity to bind soft transition-metal ions. We report the first single-crystal structure of a porphyrin/phthalocyanine derivative with peripheral crown-ether rings. Single-crystal structures are also presented of one free and one silver-ion complexed thiacycrown-ether. The affinities of the porphyrazines for silver and mercury ions have been measured and will be discussed.



MPz(7)  
(M = Mg)



MPz(15) : n = 1  
MPz(18) : n = 2  
(M = Mg, 2H, Cu)

## 7.2 Experimental section

**Materials and methods.** All solvents were dried before use. Silica gel used for chromatography (Kieselgel 60H) was obtained from Merck. Disodium *cis*-1,2-dicyano-1,2-ethylenedithiolate **1** was prepared by the method of Davison and Holm [9]. Tetraethyleneglycol dichloride and pentaethyleneglycol dichloride were prepared as described by Pedersen [10]. All other reagents were used as supplied without further purification.

$^1\text{H}$  and  $^{13}\text{C}$  NMR spectra were obtained using Bruker WH-90, AC-100, and WM-400 instruments. Chemical shifts are reported in ppm downfield from internal TMS standard. Abbreviations used are as follows: s = singlet; t = triplet; q = quartet; br = broad. Electronic ionization (EI) and fast atom bombardment (FAB) mass spectra (MS) were obtained using a VG-7070E apparatus and a Finnigan MAT 90 spectrometer. Elemental analyses were carried out on an EA 1108 Carlo Erba Instrument. Infrared (IR) spectra were obtained using a Perkin Elmer 1720-X Infrared Fourier-Transform Spectrometer. Electronic absorption spectra were recorded with a Perkin Elmer Lambda 5 Spectrophotometer. Melting points were determined with a Reichert hot-stage microscope and are uncorrected.

Single-crystal X-ray diffraction data were collected using an Enraf-Nonius CAD4-T/rotating anode (compounds MgPz(18) and 2(1)) or an Enraf-Nonius sealed-tube CAD4 (compound 2(2)) diffractometer. Suitable crystals were glued on a Lindemann-glass capillary and mounted on the diffractometer in a stream of cold nitrogen. Details on data collection and refinement will be published elsewhere [11].

Electron paramagnetic resonance (EPR) spectra were measured at X-band frequency (9 GHz) using a Bruker ESP 300 Instrument equipped with a helium continuous flow cryostat.

**Syntheses. 1,2-Dicyano-3,15-dithia-6,9,12-trioxacyclopentadecene (2(1)).** Dithiolate 1 (2.34 g, 12 mmol) was suspended in refluxing acetonitrile (150 mL) under a nitrogen atmosphere, and a solution of tetraethyleneglycol dichloride (1.92 g, 8 mmol) in acetonitrile (25 mL) was added dropwise during 1 h. The reaction mixture was refluxed for 48 h. The solvent was evaporated under reduced pressure, and the resulting orange oil was dissolved in dichloromethane (100 mL), washed with water (2x100 mL), and dried over MgSO<sub>4</sub>. The organic solvent was evaporated under reduced pressure and the product was purified by column chromatography (silica gel, eluent CHCl<sub>3</sub>-MeOH 1:1, v/v). The slightly yellow solid was recrystallized from hexane-benzene (1:1 v/v). Yield: 0.3 g (13%). White crystals, mp 131-132 °C (lit. [12] mp 125-127 °C). IR (KBr) 2210 (CN) cm<sup>-1</sup>. <sup>1</sup>H NMR (CDCl<sub>3</sub>, 100 MHz) δ 3.31 (t, 4H, CH<sub>2</sub>S), 3.61 (s, 8H, CH<sub>2</sub>O), 3.71 (t, 4H, CH<sub>2</sub>O). MS (EI) *m/z* 300 (M<sup>+</sup>). Anal. (C<sub>12</sub>H<sub>16</sub>N<sub>2</sub>O<sub>3</sub>S<sub>2</sub>): found (calcd) C, 47.92 (47.98); H, 5.24 (5.37); N, 9.23 (9.33); S, 21.83 (21.35).

**1,2-Dicyano-3,18-dithia-6,9,12,15-tetraoxacyclooctadecene (2(2)).** This compound was synthesized from 1 and pentaethyleneglycol dichloride as described for 2(1). Yield: 23%. Slightly yellow crystals, mp 84-85 °C (lit. [12] mp 64-66 °C). IR (KBr) 2210 (CN) cm<sup>-1</sup>. <sup>1</sup>H NMR (CDCl<sub>3</sub>, 100 MHz) δ 3.31 (t, 4H, CH<sub>2</sub>S), 3.67 (s, 12H, CH<sub>2</sub>O), 3.76 (t, 4H, CH<sub>2</sub>O). MS (EI) *m/z* 344 (M<sup>+</sup>). Anal. (C<sub>14</sub>H<sub>20</sub>N<sub>2</sub>O<sub>4</sub>S<sub>2</sub>): found (calcd) C, 48.95 (48.82); H, 5.76 (5.85); N, 8.09 (8.13); S, 18.74 (18.62).

**1,2-Dicyano-3,7-dithia-cycloheptene (3).** A suspension of dithiolate 1 (1.0 g, 5.3 mmol) in acetonitrile (10 mL) was added to a solution of 1,3-dibromopropane (10 g, 50 mmol) in acetonitrile (15 mL) under a nitrogen atmosphere. This mixture was stirred for 48 h at room temperature. The solvent was evaporated under reduced pressure, and the resulting orange oil was dissolved in dichloromethane (25 mL). The resulting solution was washed with water (2x50 mL), dried over MgSO<sub>4</sub>, and concentrated in vacuum. The product was purified by column chromatography

(silica gel, eluent  $\text{CHCl}_3$ -hexane 3:2, v/v). 1,10-Dibromo-5,6-dicyano-4,7-dithia-5-decene **4** was obtained as an oily side product in 33% yield. Compound **3** was collected as a white solid. Yield: 0.45 g (46%). Mp 104-106 °C. IR (KBr) 2210 (CN)  $\text{cm}^{-1}$ .  $^1\text{H}$  NMR ( $\text{CDCl}_3$ , 100 MHz)  $\delta$  2.26 (q, 2H, C- $\text{CH}_2$ -C), 3.71 (t, 4H,  $\text{CH}_2\text{S}$ ). MS (EI)  $m/z$  182 ( $\text{M}^+$ ). Anal. ( $\text{C}_7\text{H}_6\text{N}_2\text{S}_2$ ): found (calcd) C, 46.26 (46.13); H, 3.33 (3.32); N, 14.73 (15.37); S, 35.55 (35.18).

**{Tetrakis[1,5]dithiacyclohepteno}[6,7-*b*:6',7'-*g*:6'',7''-*l*:6''',7'''-*q*]porphyrazinato}-magnesium(II) (MgPz(7)).** Magnesium metal (0.67 g, 12.75 mmol) and a small crystal of  $\text{I}_2$  were added to *n*-propanol (30 mL) under a nitrogen atmosphere. The mixture was refluxed until the magnesium had completely reacted to form a suspension of magnesium propoxide. Dicyanocrown-ether **3** (1.0 g, 5.5 mmol) in *n*-propanol (30 mL) was added dropwise to the refluxing suspension during 1 h. After 24 h the reaction mixture was filtered while hot and the residue was washed with acetone (3x50 mL). The combined organic solutions were concentrated under vacuum. The resulting solid was purified by chromatography (silica gel, eluent  $\text{CHCl}_3$ -MeOH 93:7, v/v), and subsequently extracted in a Soxhlett apparatus with dichloromethane. After evaporation of the solvent the product was dissolved in hot benzene, and precipitated by adding hexane to this solution. Yield: 0.95 g (12%). Dark blue powder, mp >320 °C.  $^1\text{H}$  NMR (400 MHz,  $d_6$ -DMSO)  $\delta$  2.59 (q, 2H, C- $\text{CH}_2$ -C), 3.96 (t, 4H,  $\text{CH}_2\text{S}$ ).  $^{13}\text{C}$  NMR (400 MHz,  $d_6$ -DMSO)  $\delta$  31.3 (C-S), 32.3 (C- $\text{C}$ -C), 137.8 (C=C), 155.8 (C=N). MS (FAB)  $m/z$  753 ( $\text{M}^+$ ). Anal. ( $\text{C}_{28}\text{H}_{24}\text{MgN}_8\text{S}_8$ ): found (calcd) C, 45.35 (44.68); H, 3.57 (3.22); N, 14.79 (14.9); S, 33.76 (34.01).

**{Tetrakis[1,4,7,10,13]trioxadithiacyclopentadeceno}[11,12-*b*:11',12'-*g*:11'',12''-*l*:11''',12'''-*q*]porphyrazinato}magnesium(II) (MgPz(15)).** This compound was synthesized from **2(1)** as described for MgPz(7). The product was purified as follows. The hot reaction mixture was filtered and the residue was washed with dichloromethane until the washings were clear. The combined organic solutions were evaporated under reduced pressure, and the resulting solid was purified by column chromatography over NaBr impregnated silica gel. Impurities were first removed by elution with  $\text{CHCl}_3$ . The product was collected by elution with  $\text{CHCl}_3$ -MeOH (93:3, v/v). The product was finally washed with hot benzene. Yield: 32%. Dark blue powder, mp >320 °C.  $^1\text{H}$  NMR (400 MHz,  $\text{CDCl}_3$ )  $\delta$  3.28 (s, 4H,  $\text{CH}_2\text{O}$ ), 3.37 (s, 4H,  $\text{CH}_2\text{O}$ ), 3.86 (s, 4H,  $\text{CH}_2\text{O}$ ), 4.24 (s, 4H,  $\text{CH}_2\text{S}$ ).  $^{13}\text{C}$  NMR (400 MHz,  $\text{CDCl}_3$ )  $\delta$  35.0 (C-S), 70.0, 70.5, 70.6 (C-O), 140.1 (C=C), 157.1 (C=N). MS (FAB)  $m/z$  1225.5 ( $\text{M}^++1$ ), 1223.4 ( $\text{M}^+-1$ ). Anal. ( $\text{C}_{48}\text{H}_{64}\text{MgN}_8\text{O}_{12}\text{S}_8$ ): found (calcd) C, 47.09 (47.03); H, 5.34 (5.26); N, 9.04 (9.14); S, 20.36 (20.40).

**{Tetrakis[1,4,7,10,13,16]tetraoxadithiacyclooctadeceno}[14,15-*b*:14',15'-*g*:14'',15''-*l*:14''',15'''-*q*]porphyrazinato}magnesium(II) (MgPz(18)).** This compound was synthesized from 2(2) as described for MgPz(7). The product was purified as follows. The hot reaction mixture was filtered and the residue was washed with acetone until the washings were clear. The combined organic solutions were concentrated under reduced pressure, and the resulting solid was purified by chromatography (NaBr impregnated silica gel, eluent CHCl<sub>3</sub>-MeOH 9:1, v/v). The product was dissolved in hot benzene and precipitated by adding hexane to the solution. Yield: 52%. Dark blue powder, mp >320 °C. <sup>1</sup>H NMR (400 MHz, CDCl<sub>3</sub>) δ 3.32 (s, 8H, CH<sub>2</sub>O), 3.47 (s, 4H, CH<sub>2</sub>O), 3.85 (s, 4H, CH<sub>2</sub>O), 4.06 (br s, 4H, CH<sub>2</sub>S). <sup>13</sup>C NMR (400 MHz, CDCl<sub>3</sub>) δ 34.5 (C-S), 70.1, 70.2 (C-O), 140.0 (C=C), 157.2 (C=N). MS (FAB) *m/z* 1401.4 (M<sup>+</sup>+1), 1399.5 (M<sup>+</sup>-1). Anal. (C<sub>56</sub>H<sub>80</sub>MgN<sub>8</sub>O<sub>16</sub>S<sub>8</sub>): found (calcd) C, 48.03 (47.97); H, 5.80 (5.75); N, 7.99 (7.99); S, 18.09 (18.29).

**Tetrakis[1,4,7,10,13]trioxadithiacyclopentadeceno}[11,12-*b*:11',12'-*g*:11'',12''-*l*:11''',12'''-*q*]porphyrazine (H<sub>2</sub>Pz(15)).** MgPz(15) (0.10 g, 0.08 mmol) was dissolved in a minimum amount of trifluoroacetic acid and poured onto ice. The mixture was neutralized with concentrated ammonia, and extracted with chloroform. The chloroform solution was washed with water until the latter was neutral, dried over MgSO<sub>4</sub>, and concentrated in vacuum. Yield: 0.075 g (76%). Dark blue/purple powder, mp >320 °C. <sup>1</sup>H NMR (90 MHz, CDCl<sub>3</sub>) δ -1.6 (s, 2H, NH), 3.6 (s, 8H, CH<sub>2</sub>O), 3.95 (t, 4H, CH<sub>2</sub>O), 4.25 (t, 4H, CH<sub>2</sub>S). Anal. (C<sub>48</sub>H<sub>66</sub>N<sub>8</sub>O<sub>12</sub>S<sub>8</sub>): found (calcd) C, 47.45 (47.90); H, 5.46 (5.53); N, 9.16 (9.31); S, 22.22 (21.31).

**Tetrakis[1,4,7,10,13,16]tetraoxadithiacyclooctadeceno}[14,15-*b*:14',15'-*g*:14'',15''-*l*:14''',15'''-*q*]porphyrazine (H<sub>2</sub>Pz(18)).** This compound was synthesized from MgPz(18) as described for H<sub>2</sub>Pz(15). Yield: 85%. Dark blue/purple powder, mp >320 °C. <sup>1</sup>H NMR (100 MHz, CDCl<sub>3</sub>) δ -1.8 (s, 2H, NH), 3.3 (s, 8H, CH<sub>2</sub>O), 3.5 (s, 4H, CH<sub>2</sub>O), 3.85 (s, 4H, CH<sub>2</sub>O), 4.05 (br s, 4H, CH<sub>2</sub>S). Anal. (C<sub>56</sub>H<sub>82</sub>N<sub>8</sub>O<sub>16</sub>S<sub>8</sub>): found (calcd) C, 49.55 (48.75); H, 5.95 (5.99); N, 8.01 (8.12); S, 18.61 (18.59).

**{Tetrakis[1,4,7,10,13]trioxadithiacyclopentadeceno}[11,12-*b*:11',12'-*g*:11'',12''-*l*:11''',12'''-*q*]porphyrazinato}copper(II) (CuPz(15)).** H<sub>2</sub>Pz(15) (0.066 g, 0.055 mmol) was dissolved in chloroethanol (13.5 mL) at 100 °C. CuCl<sub>2</sub>·2H<sub>2</sub>O (0.046 g, 0.27 mmol) and sodium acetate (0.018 g, 0.22 mmol) were dissolved in hot ethanol (5 mL) and added to the hot solution of H<sub>2</sub>Pz(15). The mixture was refluxed for 15 min. The solvent was evaporated under reduced pressure, and water and chloroform were added. The chloroform layer was washed two times with water, dried over MgSO<sub>4</sub>, and concentrated in vacuum. The product was purified by chromatography (silica gel, eluent CHCl<sub>3</sub>-MeOH 96:4, v/v). Yield: 0.058 g (83%). Anal.

(C<sub>48</sub>H<sub>64</sub>CuN<sub>8</sub>O<sub>12</sub>S<sub>8</sub>·CH<sub>4</sub>O): found (calcd) C, 45.64 (45.37); H, 5.14 (5.28); N, 8.42 (8.64); S, 19.30 (19.77).

[Tetrakis[1,4,7,10,13,16]tetraoxadithiacyclooctadeceno][14,15-*b*:14',15'-*g*:14'',15''-*l*:14''',15'''-*q*]porphyrazinato)copper(II) (CuPz(18)). This compound was synthesized from H<sub>2</sub>Pz(18) as described for CuPz(15). The product was purified by chromatography (silica gel, eluent CHCl<sub>3</sub>-MeOH 95:5, v/v). Yield: 86%. Anal. (C<sub>56</sub>H<sub>80</sub>CuN<sub>8</sub>O<sub>16</sub>S<sub>8</sub>·CH<sub>4</sub>O): found (calcd) C, 46.68 (46.47); H, 5.57 (5.75); N, 7.34 (7.61); S, 16.79 (17.41).

**AgClO<sub>4</sub> complex of 2(1).** Crown-ether 2(1) and one equivalent of AgClO<sub>4</sub> were dissolved in dry methanol. Crystals were grown by slow evaporation of the solvent.

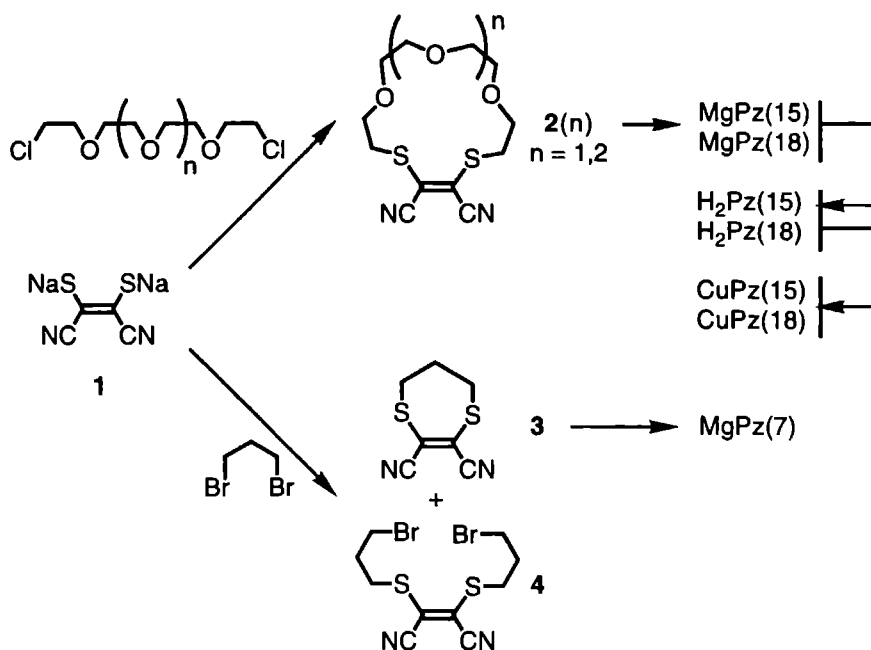
## 7.3 Results

### 7.3.1 Synthesis

The magnesium, copper, and metal-free derivatives of the dithiacrown-ether substituted porphyrazines were prepared starting from *cis*-1,2-dicyano-1,2-ethylene-dithiolate **1** as shown in Scheme 7.1. Reaction of the latter compound with tetraethyleneglycol dichloride or pentaethyleneglycol dichloride yielded the dicyanocrown-ethers **2(1)** and **2(2)**, respectively. These compounds were previously synthesized by Holdt and co-workers [12], but we improved the yield of this reaction by applying a high-dilution method in which we made use of the low solubility of the starting compound **1** in acetonitrile. The products were purified by column chromatography and by recrystallization. The yield of **2(2)** was twice as high as reported by Holdt. The smaller dicyanocrown-ether **3** was obtained in a yield of 46% by reaction of dithiolate **1** with a large excess of dibromopropane. The side product **4**, which was isolated after purification in 33% yield, is an interesting starting compound for the future synthesis of other crown-ethers.

From compounds **2(1)**, **2(2)**, and **3** we synthesized the corresponding magnesium Pzs according to the procedure described in the literature for the synthesis of alkylthio substituted Pzs [13]. The products were purified by column chromatography. We obtained the 15-crown-5 derivative MgPz(15) in 32% yield, the 18-crown-6 derivative MgPz(18) in 52% yield, and the 7-crown-2 derivative MgPz(7) in 12% yield, all as dark blue powders. MgPz(15) and MgPz(18) were quantitatively





Scheme 7.1

demetalated with trifluoroacetic acid [14] to give the metal-free derivatives  $\text{H}_2\text{Pz(15)}$  and  $\text{H}_2\text{Pz(18)}$  as dark blue to purple powders. The copper derivatives  $\text{CuPz(15)}$  and  $\text{CuPz(18)}$  were finally obtained by reaction of the metal-free compounds with copper chloride in the presence of sodium acetate in a mixture of ethanol and chloroethanol [14]. The yields of the dark blue CuPzs after purification by column chromatography amounted to approximately 85%. Elemental analysis showed that probably one molecule of methanol (from the eluent) is coordinated to the CuPzs. All products were soluble in chloroform.

### 7.3.2 Single-crystal X-ray structures

Crown-ethers containing 1,2-dicyano-1,2-dithioethene units, including crown-ethers 2(1) and 2(2), have been previously synthesized by Holdt and by Märkl [12,15]. The single-crystal structures of compounds 2(0) and 2(1) have been published in the literature [16], as well as the single-crystal structures of the  $\text{PdBr}_2$

and  $\text{HgCl}_2$  complexes of **2(2)**, which were determined by Holdt and by Sibert, respectively [17,18]. In this section we present the single-crystal structure of compound **2(2)**, and that of the  $\text{Ag}^+$  complex of crown-ether **2(1)**, which may serve as models for the structure of the crown-ether porphyrazines and their complexes. Additionally, we present below the single-crystal structure of porphyrazine  $\text{MgPz(18)}$ .

#### *Dicyanocrown-ether 2(2).*

Single-crystals of **2(2)** were grown from methanol and the X-ray structure of this compound was solved by standard methods. Crystal data are given in the Appendix. Selected torsion angles are listed in Table 7.I. Figure 7.1 shows a plot of the molecular conformation of compound **2(2)**. The density of the unit cell is close to the unit cells of **2(0)** and **2(1)** [16]. The most important conclusions that can be drawn from the structural data of **2(2)** are the following. (i) The angle between the least-squares planes through the dicyanodithioethene unit and the crown-ether unit amounts to  $131.74(4)^\circ$ . Holdt has reported angles of  $70.2^\circ$  and  $61.6^\circ$  for **2(0)** and **2(1)**, respectively. This difference is related to the size and flexibility of the macrocyclic rings. The 18-crown-6 ring of **2(2)** possesses more conformational freedom, which makes it easier for this ring to be stretched out in the plane of the dicyanodithioethene unit. (ii) As can be seen in Table 7.I, the torsion angles obey Wolf's rule for crown-ethers [19], *i.e.* the conformations around the C-S and the C-C bonds are *gauche* whereas those around the C-O bonds are *trans*. Exceptions are the conformations around the S2-C12 and C7-C8 bonds, which are *trans*, and the conformation around the O3-C9 bond, which is *gauche*. (iii) In the X-ray structures of crown-ethers the oxygen atoms are mostly oriented endodentate and the sulfur atoms exodentate [19], but in the structure of **2(2)** O3 is exodentate, and the two sulfur atoms are endodentate. The latter is very unusual and is related to the large angle between the dicyanodithioethene plane and the crown-ether segment.

#### *Silver perchlorate complex of dicyanocrown-ether 2(1)*

Binding of silver ions by thiacycrown-ethers is well documented in the literature [20]. In particular, crown-ethers containing both sulfur and oxygen atoms are known to be highly selective towards these ions and also towards  $\text{Hg}^{2+}$  [21]. The replacement of oxygen by sulfur in 15-crown-5 and 18-crown-6 macrocycles was shown to be favorable for the complexation of  $\text{Ag}^+$  and  $\text{Hg}^{2+}$ , but unfavorable for that of  $\text{Tl}^+$ ,  $\text{Pb}^+$ , and alkali metal ions [21a].

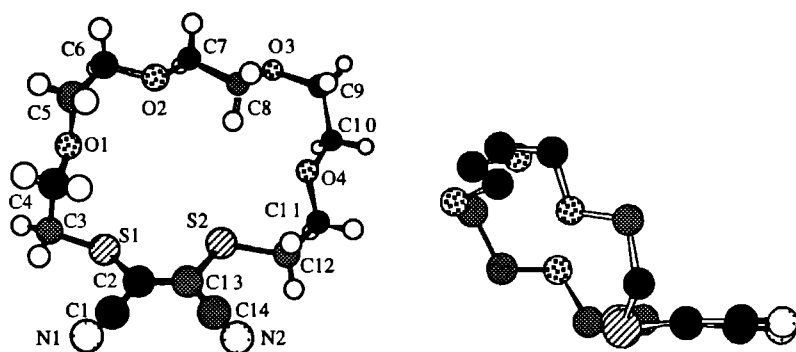


**Figure 7.1** Single crystal X-ray structure of crown-ether 2(2): top view (left), and side view (right)

**Table 7.1** Torsion Angles (degrees) of Selected Bonds for Crown-ether 2(2) and for the Different Crown-ether Rings A-D of MgPz(18) [a]

Atoms	2(2)	Ring A	Ring B	Ring C	Ring D
C3-S1-C2-C1	38.52(15)	115.2(8)	5.2(11)	74.7(9)	20.4(11)
C3-S1-C2-C13	-149.00(14)	-62.7(10)	-176.4(8)	-113.4(10)	-167.7(8)
C2-S1-C3-C4	81.79(14)	<u>166.3(7)</u>	80.0(9)	<u>148.7(10)</u>	71.3(9)
C13-S2-C12-C11	<u>178.50(15)</u>	<u>159.7(6)</u>	-77.2(7)	71.4(16)	-59.3(9)
C12-S2-C13-C2	175.24(15)	148.7(10)	124.6(9)	9.7(14)	159.0(9)
C12-S2-C13-C14	-5.74(17)	-42.5(10)	-65.9(8)	-173.3(10)	-31.5(10)
C5-O1-C4-C3	174.42(16)	-169.3(8)	177.9(9)	-176.1(13)	175.2(9)
C4-O1-C5-C6	160.05(17)	-179.0(8)	172.5(8)	<u>88.1(17)</u>	174.9(9)
C7-O2-C6-C5	166.76(19)	178.2(8)	<u>77.0(10)</u>	<u>94(2)</u>	164.0(10)
C6-O2-C7-C8	-172.51(18)	-179.4(8)	-177.4(8)	<u>98.7(18)</u>	177.4(10)
C9-O3-C8-C7	172.85(19)	-173.3(7)	-174.9(7)	<u>-99.3(15)</u>	<u>-84.3(15)</u>
C8-O3-C9-C10	<u>81.8(2)</u>	177.7(8)	<u>-69.0(10)</u>	159.1(12)	168(2)
C11-O4-C10-C9	-174.69(19)	-179.1(8)	<u>79.1(10)</u>	-173.5(13)	166.1(14)
C10-O4-C11-C12	-171.87(18)	-177.2(8)	158.9(7)	<u>-66(2)</u>	<u>103.6(18)</u>
S1-C3-C4-O1	58.58(18)	-79.0(9)	62.9(10)	54.7(14)	63.7(11)
O1-C5-C6-O2	-75.2(2)	-63.4(10)	-81.1(11)	<u>-168.2(14)</u>	-73.9(12)
O2-C7-C8-O3	<u>172.36(17)</u>	75.0(10)	72.6(10)	-67.7(17)	54.3(15)
O3-C9-C10-O4	-73.0(2)	-60.0(9)	-65.0(10)	-71.0(18)	50(3)
O4-C11-C12-S2	65.1(2)	66.0(9)	<u>170.5(6)</u>	<u>178.2(11)</u>	-56.6(11)

[a] Deviating torsion angles are underlined

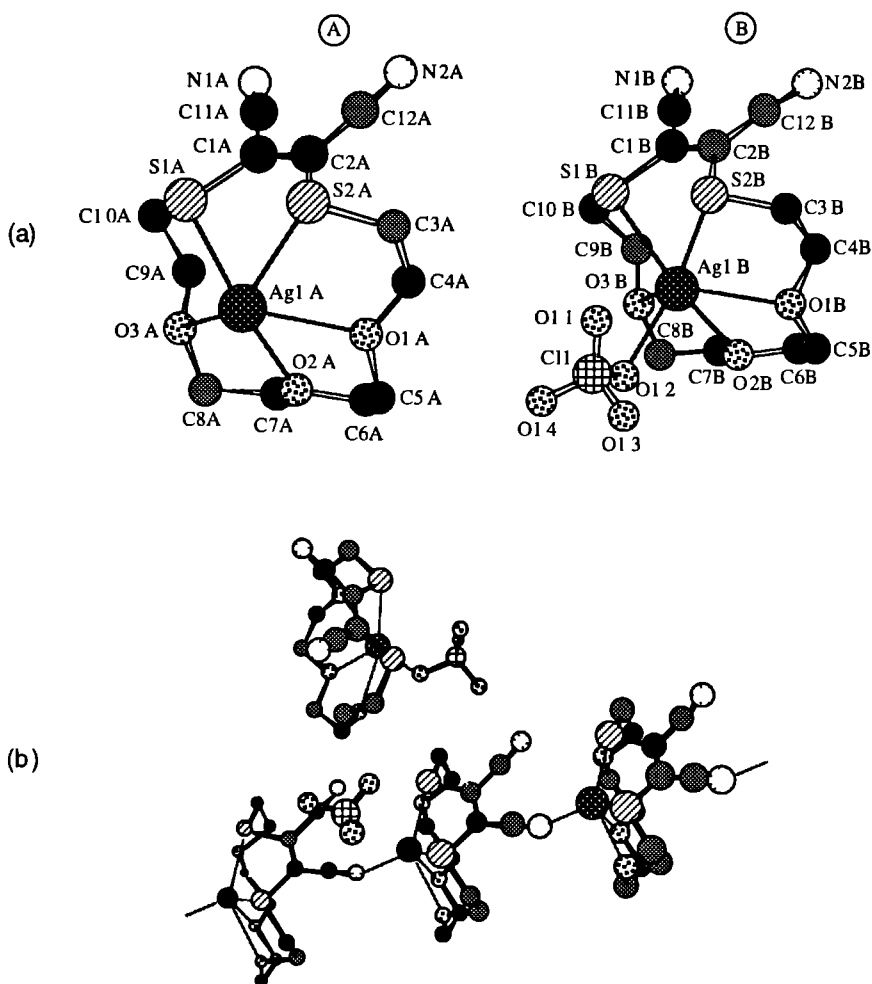


**Figure 7.2** Single crystal X-ray structure of the AgClO<sub>4</sub> complex of crown-ether 2(1) and the numbering of the atoms of the two species A and B (a), Representation of the arrangement of all species present in the unit cell, showing the polymeric structure formed by species A (b) For clarity the hydrogen atoms are omitted

Some single-crystal X-ray structures of metal ion complexes of 1,4-dithia-15-crown-5 and 1,4-dithia-18-crown-6 have been reported. Hg<sup>2+</sup>, Pd<sup>2+</sup> and Ru<sup>2+</sup> were shown to coordinate to the two sulfur atoms of the crown-ether rings [22], whereas Ag<sup>+</sup> appeared to be coordinated to the sulfur as well as to the oxygen atoms [23]. This could explain why these crown-ethers are so selective towards Ag<sup>+</sup> ions. The

dicyanocrown-ethers **2**(*n*) (*n*=0-2) are known to bind Ag<sup>+</sup>, Pd<sup>2+</sup>, and Hg<sup>2+</sup> ions [17,18]. The single crystal X-ray structures of the Pd(II) complexes of **2**(0) and **2**(2) revealed that the metal ion binds only to the sulfur atoms and not to the oxygen atoms, and that binding hardly induces a change in the conformation of the crown-ether rings [17]. On the contrary, Hg<sup>2+</sup> binds exclusively to the oxygen atoms of **2**(2) [18]. The latter is unusual and has been attributed to the fact that the affinity of the sulfur atoms for the Hg<sup>2+</sup> ion is reduced due to the electron withdrawing properties of the dicyanoethylene unit. However, in solution both S and O atoms were reported to interact with the metal ion [18].

The conformations of the complexes of **2**(*n*) with Ag<sup>+</sup> and the complexation sites are unknown. We have therefore grown crystals of a 1:1 complex of crown-ether **2**(1) and AgClO<sub>4</sub> from methanol solution, and have determined the single crystal X-ray structure of this complex. Crystal data are given in the Appendix. Two different species are present in the unit cell (Figure 7.2). Both contain a Ag<sup>+</sup> ion, which is coordinated to the sulfur atoms and the oxygen atoms of the crown-ether rings. In one complex the sixth coordination site is occupied by an oxygen atom of a disordered perchlorate ion. In the other complex this site is occupied by the cyano group of an adjacent ligand, while the perchlorate ion is not coordinating. This results in a polymeric chain of crown-ether molecules (Figure 7.2.b). Selected bond distances for the two complexes are summarized in Table 7.II.

The binding of the silver ion is similar to that reported for the complex between Ag<sup>+</sup> and 1,4-dithia-15-crown-5. The conformation of the ligand **2**(1) has changed on complexation in such a way that all the oxygen and sulfur donor sites point towards the metal center. This is most clearly seen in the conformations around the O1-C5 and O3-C8 bonds, which have changed from trans to gauche, and in the inversion of the S2-C3-C4-O1 and O3-C9-C10-S1 torsion angles (Table 7.III). This holds for both complexes found in the crystal structure. The angles between the least squares planes of the dicyanodithioethene units and the crown-ether rings

**Table 7.II** Selected Bond Distances For the Two Different Complexes of **2**(1) and AgClO<sub>4</sub>

Atoms	Distance / Å	Atoms	Distance / Å
Ag1A-S1A	2.6479(17)	Ag1B-S1B	2.6923(19)
Ag1A-S2A	2.7512(19)	Ag1B-S2B	2.7577(18)
Ag1A-O1A	2.651(6)	Ag1B-O1B	2.590(6)
Ag1A-O2A	2.523(6)	Ag1B-O2B	2.453(5)
Ag1A-O3A	2.814(5)	Ag1B-O3B	2.739(6)
Ag1A-N2B	2.281(6)	Ag1B-O12	2.379(15)

**Table 7.III** Torsion Angles (degrees) of Selected Bonds in the Free Ligand 2(1) and in the Two AgClO<sub>4</sub> Complexes A and B [a]

Atoms	2(1) [b]	Complex A	Complex B
C10-S1-C1-C2	-160.6(2)	-153.0(6)	-148.4(5)
C10-S1-C1-C11	26.8(2)	33.2(6)	34.4(5)
C1-S1-C10-C9	77.6(2)	80.4(6)	71.9(5)
C3-S2-C2-C1	160.1(2)	144.3(6)	150.7(5)
C3-S2-C2-C12	-28.1(2)	-43.8(6)	-33.0(6)
C2-S2-C3-C4	-76.8(2)	-77.6(6)	-73.6(7)
C5-O1-C4-C3	168.3(3)	-167.8(6)	-175.9(6)
C4-O1-C5-C6	172.5(3)	<u>-72.4(10)</u>	<u>-82.3(9)</u>
C7-O2-C6-C5	170.6(3)	-179.8(10)	176.7(8)
C6-O2-C7-C8	-169.1(3)	173.8(7)	-175.8(9)
C9-O3-C8-C7	-177.8(2)	<u>76.3(7)</u>	<u>80.9(11)</u>
C8-O3-C9-C10	-175.3(2)	174.9(5)	161.2(7)
S2-C3-C4-O1	58.6(3)	<u>-57.6(6)</u>	<u>-62.9(7)</u>
O1-C5-C6-O2	-70.8(4)	-61.2(12)	-58.2(11)
O2-C7-C8-O3	76.7(3)	58.0(8)	67.1(12)
O3-C9-C10-S1	-56.6(3)	<u>59.0(6)</u>	<u>57.9(6)</u>

[a] Deviating torsion angles are underlined.

[b] Data are taken from reference 16.

amount to 64.69(5)° and 71.91(14)° for complexes A and B, respectively. These values are close to the angle in the free ligand (61.6° [12]).

#### 18-Crown-6 porphyrazine MgPz(18).

Although several phthalocyanine and porphyrin derivatives with peripheral crown-ether rings directly attached to the aromatic core have been synthesized, no structural information has been reported so far from single-crystals. We were able to grow single-crystals of MgPz(18) from chloroform-methanol, which were of sufficient quality to determine the X-ray structure. Crystal data are listed in the Appendix. The molecular structure of the compound is shown in Figure 7.3(A). A water molecule is found to be present on the central magnesium ion of the porphyrazine ring. This water molecule is coordinated to one of the crown-ether

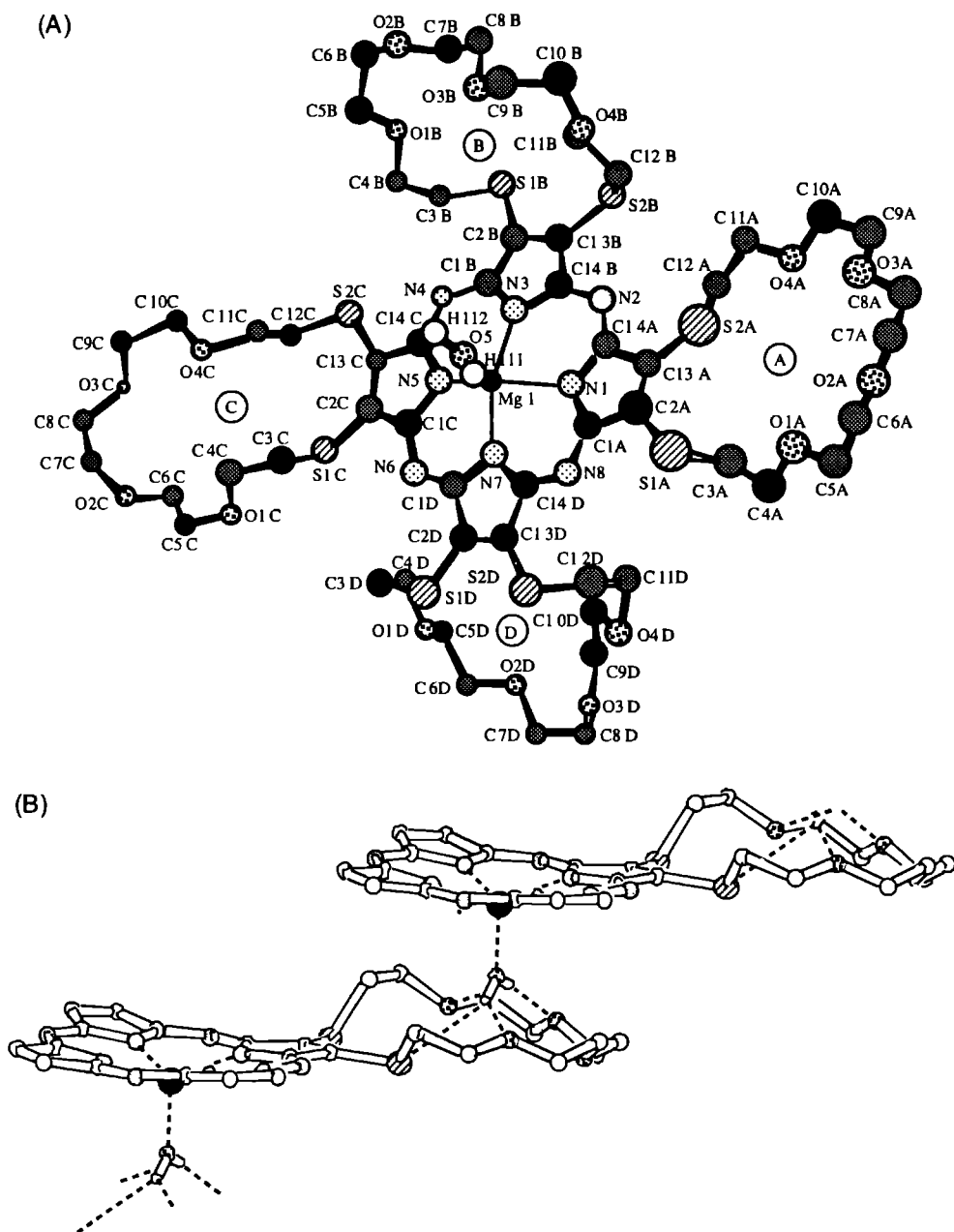


**Figure 7.3** Single crystal X-ray structure of porphyrazine  $\text{MgPz}(18) \cdot \text{H}_2\text{O}$ : top view of a molecule with the numbering of the atoms (A); side view showing the polymeric chain of molecules (for clarity only one crown-ether ring is shown and hydrogen atoms are omitted) (B).

rings (A) of a second porphyrzine molecule via two bifurcated hydrogen bonds to the oxygen and sulfur atoms. In this way a polymeric chain of molecules is formed as can be seen in Figure 7.3(B). As a result of the coordination of the water molecule, the aromatic core of the porphyrzine ring is not perfectly flat and the magnesium ion is displaced 0.570(40) Å from the N1-N3-N5-N7 plane. The least squares planes of crown-ether rings A and C make angles of 177.99(11)° and 176.39(17)°, respectively, with the least squares plane of the porphyrzine ring (defined by all its C, N, and Mg atoms). This is quite different from the single-crystal structures of the dicyanocrown-ethers 2(n) (*vide supra*). The least squares planes of crown-ether rings B and D are more tilted and make angles of 115.66(11)° and 110.02(13)°, respectively, with the porphyrzine plane, which is close to the angle found in compound 2(2). The sulfur atoms of rings A and D are oriented to one side of the Pz plane, those of rings B and C point to the other side. Crown-ether A is the most ordered ring, as would be expected because it is hydrogen bonded to the water molecule. As can be seen in Table 7.I, all C-C and C-O torsion angles of ring A obey Wolf's rule, *i.e.* the C-C bonds have a gauche conformation and the conformation around the C-O bonds is trans. The only exceptions from this rule are the S1-C3 and S2-C12 bonds which have almost trans instead of gauche conformations. The conformations of ring D deviates from the Wolf rule at the O3-C8 and O4-C11 bonds, which are gauche. Of the other two rings, ring C is the most deviating one: five out of the eight C-O bonds have a gauche conformation, and the conformations of the C5-C6 and C11-C12 bonds are trans instead of gauche.

Packing analysis [24] showed that MgPz(18) contains a small void, consistent with the presence of an additional water molecule, which is at hydrogen-bond distance between two crown-ether oxygens of adjacent, inversion related molecules. The site occupation factor of the tentative water molecule refined to 0.17. Both this water molecule and the magnesium coordinated water might add to the stability of the large and flexible porphyrzine complex in the crystalline phase.

The hydrogen bonded polymeric structure found for MgPz(18) is very similar to the structure that was previously reported for a chlorophyll *a* derivative [25]. In the latter case a one-dimensional chain is formed by water molecules, which link the magnesium centers of the chlorophyll *a* molecules to the carbonyl oxygen atoms of adjacent chlorophyll molecules. Water is known to play an important role in the dimerization of chlorophyll *a* in solution [26]. As will be shown in the next sections our compounds also display interesting dimerization properties in solution.



### 7.3.2 Electronic absorption spectra

#### Porphyrazines

The electronic spectral properties of porphyrazines have been less thoroughly investigated than those of the phthalocyanines. Some spectral data can however be found in the literature [27]. The electronic transitions are strongly dependent on the presence of substituents and on the type of central metal ion.

The absorption maxima and extinction coefficients of the novel porphyrazines MPz(7), MPz(15), and MPz(18), in chloroform solutions, are listed in Table 7.IV. The absorption spectra of these compounds are very similar to those reported for octa(alkylthio) substituted porphyrazines [13,28]. From the data of the magnesium derivatives MgPz(7), MgPz(15), and MgPz(18), it can be concluded that the size of the crown-ether ring has hardly any influence on the electronic properties. The spectra of the three 18-crown-6 derivatives are displayed in Figure 7.4. The metalated compounds MgPz(18) and CuPz(18) exhibit a single *Q*-band maximum at 675 nm, whereas the metal-free H<sub>2</sub>Pz(18) displays two broad bands with maxima at 714 nm and 640 nm. The broad band around 500 nm which is observed for the metalated as well as the metal-free porphyrazine has been attributed to an *n*- $\pi^*$  transition (*n* is non-bonding electron of sulfur) [28b,29]. The intense absorption at 350-380 nm (Table 7.IV) is due to the so-called *N*-band, which is strengthened with respect to the *B* (Soret) band because of configuration mixing with the latter [27,30]. It is of interest to note that the spectra are broad compared to the spectra of substituted phthalocyanines and most other porphyrazines. This phenomenon seems to be related to the presence of the sulfur substituents, since it is also observed for other alkylthioporphyrazines [28].

**Table 7.IV** Absorption Maxima and Molar Extinction Coefficients of the Porphyrazines [a]

Compound	$\lambda_{\max}$ / nm (log $\epsilon$ / l·mol <sup>-1</sup> ·cm <sup>-1</sup> )			
MgPz(7)	669 (4.98)	616 (sh)	542 (4.29)	371 (4.96)
MgPz(15)	675 (4.97)	619 (sh)	503 (4.07)	378 (4.89)
MgPz(18)	675 (4.97)	622 (sh)	503 (4.12)	377 (4.91)
H <sub>2</sub> Pz(15)	715 (4.63)	642 (4.48)	501 (4.30)	345 (4.67)
H <sub>2</sub> Pz(18)	714 (4.62)	640 (4.48)	504 (4.33)	351 (4.69)
CuPz(15)	675 (4.80)	618 (sh)	496 (4.23)	341 (4.66)
CuPz(18)	675 (4.79)	622 (sh)	497 (4.26)	355 (4.69)

[a] sh = shoulder.

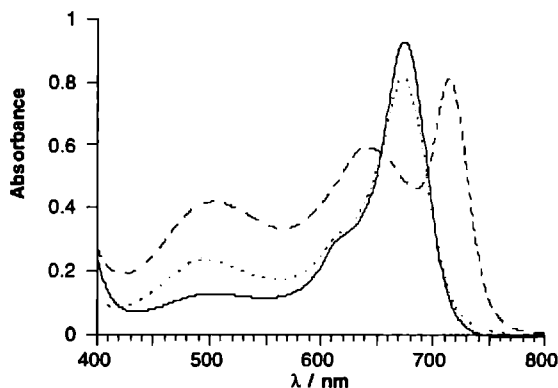


**Figure 7.4** Absorption spectra of 18-crown-6 Pz derivatives in  $\text{CHCl}_3\text{-MeOH}$  (95:5, v/v):  $\text{MgPz(18)}$  (—),  $\text{H}_2\text{Pz(18)}$  (---),  $\text{CuPz(18)}$  (.....).

#### *Influence of transition-metal ions.*

Addition of silver(I) perchlorate or mercury(II) perchlorate to solutions of the porphyrazines in chloroform-methanol caused the absorption spectra of the ligands to change. These changes varied for the different ligands and sometimes also for the different perchlorates, as will be discussed next.

As can be seen in Figure 7.5(a) the Q-band of  $\text{MgPz(7)}$  broadens and shifts to the red when  $\text{AgClO}_4$  or  $\text{Hg}(\text{ClO}_4)_2$  is added. This spectral change points to some kind of aggregation. The peak-shifts amounted to 16.5 nm and 25 nm for  $\text{Ag}^+$  and  $\text{Hg}^{2+}$ , respectively. At the same time the  $n\text{-}\pi^*$  transition at 500 nm disappeared, probably because of complexation of the metal ions to the sulfur atoms (*vide infra*). The titration curves for the two metal ions are plotted in Figure 7.5(b). In the case of  $\text{AgClO}_4$  an inflection point is visible at a metal to porphyrazine ratio of *ca* 2.5. The curve for  $\text{Hg}(\text{ClO}_4)_2$  shows two inflection points: one at a metal to porphyrazine ratio of 1 and another one at a ratio of *ca* 2.5.

$\text{MgPz(15)}$  behaved differently. No red-shift of the Q-band was observed upon titration with the perchlorates. Instead a slight blue shift, *viz.* from 675 nm to 668 nm, and a considerable broadening took place, as shown in Figure 7.6(a). The complex stoichiometry appeared to be different for the two metal ions (Figure 7.6(b)).  $\text{Hg}^{2+}$  caused a gradual decrease of the Q-band absorption during titration, up to a metal-porphyrazine ratio of about 2.5. In the case of  $\text{Ag}^+$  the spectrum was not affected up to 2 equivalents of the metal ion. Hereafter, a decrease of the Q-band

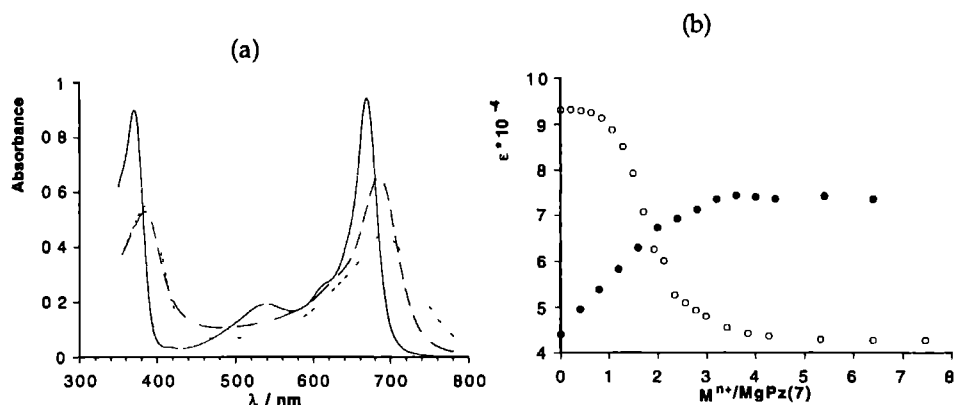


**Figure 7.5** Absorption spectra of MgPz(7) in CHCl<sub>3</sub>-MeOH (95:5, v/v): without metal salt (—), in the presence of 4 equiv. of AgClO<sub>4</sub> (---), idem, 4 equiv. of Hg(ClO<sub>4</sub>)<sub>2</sub> (.....) (a). Plot of the molar extinction coefficient versus the metal-porphyrazine ratio: Ag<sup>+</sup> (λ = 686 nm) (•), Hg<sup>2+</sup> (λ = 669 nm) (o) (b).

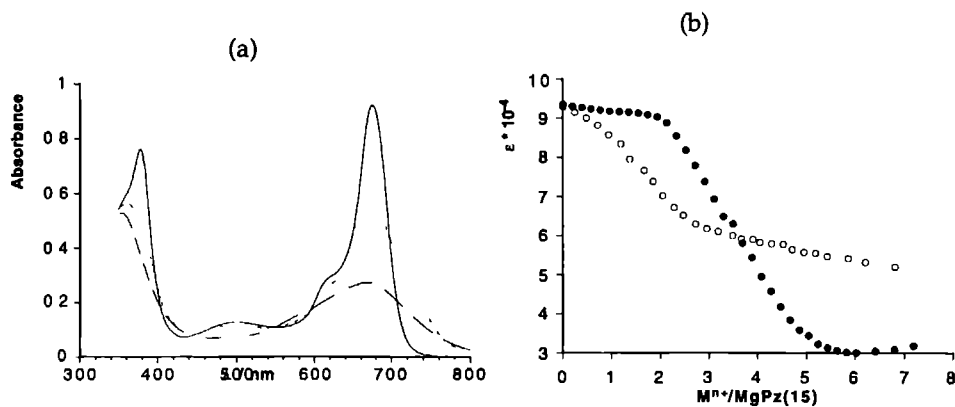


**Figure 7.6** Absorption spectra of MgPz(15) in CHCl<sub>3</sub>-MeOH (95:5, v/v): without metal salt (—), in the presence of 6 equiv. of AgClO<sub>4</sub> (---), idem, 4 equiv. of Hg(ClO<sub>4</sub>)<sub>2</sub> (.....) (a). Plot of the molar extinction coefficient at 675 nm versus the metal-porphyrazine ratio: Ag<sup>+</sup> (•), Hg<sup>2+</sup> (o) (b).

absorption took place up to a metal-porphyrazine ratio of ca. 5. Further addition of Ag<sup>+</sup> did not change the spectrum.

Porphyrazine MgPz(18) displayed a remarkable behavior. Some of the spectra that were recorded during its titration with AgClO<sub>4</sub> are shown in Figure 7.7(a). The titration curve is presented in Figure 7.7(b). Addition of AgClO<sub>4</sub> first caused a

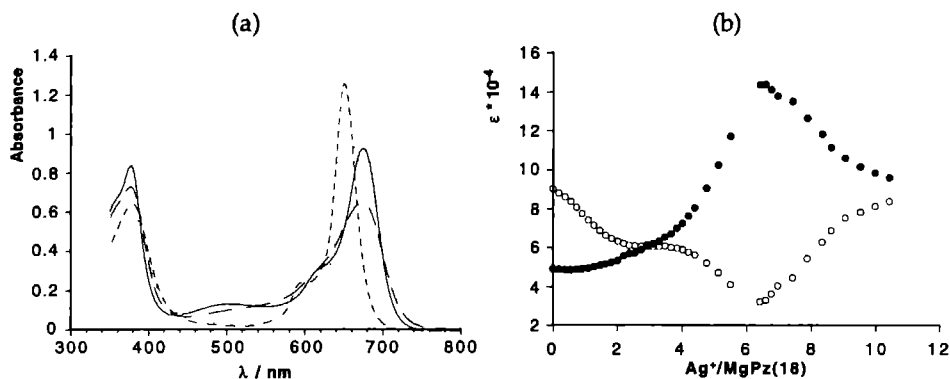


**Figure 7.7** Absorption spectra of MgPz(18) in CHCl<sub>3</sub>-MeOH (95:5, v/v) in the presence of various amounts of AgClO<sub>4</sub>: 0 equiv. (—), 2 equiv. (---), 6 equiv. (----), 12 equiv. (.....) (a). Plot of the molar extinction coefficient versus the Ag<sup>+</sup>-porphyrizine ratio at different wavelengths: 675 nm (o), 650 nm (•) (b).

decrease and broadening of the Q-band up to a metal-porphyrizine ratio of *ca* 2. At least five isosbestic points were present during this stage of the titration. With increasing amounts of AgClO<sub>4</sub> the color of the solution changed from purple to blue. A further decrease of the 675 nm band was accompanied with the development of a sharp peak at 650 nm and the appearance of new isosbestic points. The absorption at the latter wavelength reached a maximum at a metal-porphyrizine ratio of 6. Further addition of AgClO<sub>4</sub> caused this peak to decrease slightly and to shift to 661 nm. A third set of isosbestic points was now observed. The  $n-\pi^*$  transition disappeared gradually between 0 and 6 equivalents of AgClO<sub>4</sub>. Hg(ClO<sub>4</sub>)<sub>2</sub> gave virtually the same results, except that the second peak-shift beyond 6 equivalents was less distinctive (results not shown).

The behavior of the metal-free derivative H<sub>2</sub>Pz(18) was even more complex. Four stages could be distinguished during the titration with AgClO<sub>4</sub>. Each stage had its own set of isosbestic points. The results are shown in Figure 7.8. During the addition of the first two equivalents of AgClO<sub>4</sub> the two Q-bands subsided and broadened, and the  $n-\pi^*$  transition shifted to the red (Figure 7.8(a)). On further addition of AgClO<sub>4</sub>, up to 6 equivalents, the latter transition disappeared completely, and two new bands appeared, *viz.* at 676 and 626 nm with a shoulder at about 575 nm (Figure 7.8(b)). Between 6 and 8 equivalents these two new peaks slightly shifted to the red and broadened. Finally, at a metal to porphyrizine ratio

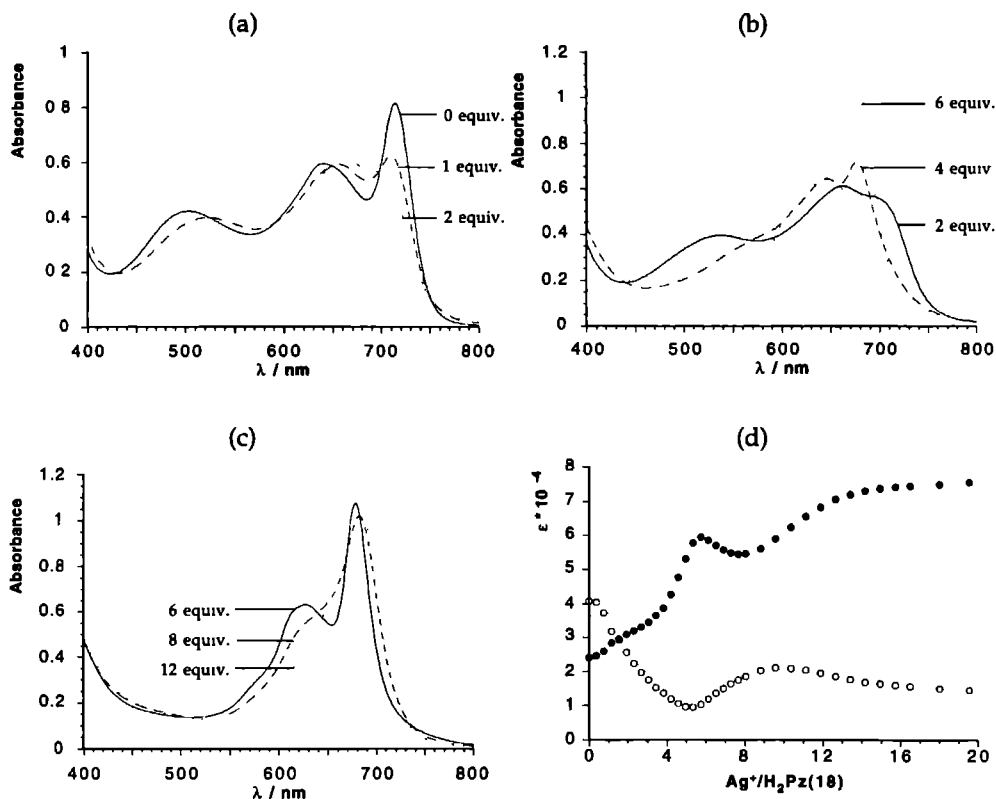


**Figure 7.8** Absorption spectra of  $\text{H}_2\text{Pz}(18)$  in  $\text{CHCl}_3$ - $\text{MeOH}$  (95:5, v/v) in the presence of various amounts of  $\text{AgClO}_4$  (a-c). Plot of the molar extinction coefficient versus the  $\text{Ag}^+$ -porphyrazine ratio at different wavelengths: 714 nm (○), 676 nm (□) (d).

of about 12, only one broad band at 676 nm with a shoulder at *ca.* 620 nm was left (Figure 7.8(c)). Further addition of  $\text{AgClO}_4$  did not affect the spectra appreciably. The plots of the molar extinction coefficient at 676 and 714 nm *versus* the  $\text{Ag}^+$  to porphyrazine ratio are presented in Figure 7.8(d).

The copper porphyrazine  $\text{CuPz}(18)$  behaved similarly as the corresponding magnesium derivative when  $\text{AgClO}_4$  was added, except that the blue shift of the Q-band at the metal-porphyrazine ratio of 6 was larger, *i.e.* to 640 nm instead of 650 nm.  $\text{CuPz}(15)$  reacted with  $\text{AgClO}_4$  in a similar way as the magnesium derivative  $\text{MgPz}(15)$  with  $\text{Hg}(\text{ClO}_4)_2$ , as could be concluded from the broadening of the Q-

band, which was observed up to a metal-porphyrzine ratio of about 3 (results not shown).

The results presented above indicate that the metal binding behavior of the crowned porphyrzines is rather complex, and at this stage it is not possible to fully explain the results obtained by the UV-Vis absorption experiments. Some conclusions can nevertheless be drawn. In most of the experiments, the addition of the perchlorates results in an immediate spectral change. Exceptions are the reaction of MgPz(7) with  $\text{Hg}(\text{ClO}_4)_2$  and the reaction of MgPz(15) with  $\text{AgClO}_4$ . It is possible that in the case of these porphyrzines some kind of cooperative binding process is operative. The reason why these compounds differ from the rest is unclear at present.

The most striking difference between the porphyrzines is the shift of the Q-band which takes place upon complexation of the metal perchlorates. The porphyrzine with the smallest crown-ether rings, MgPz(7), shows a red-shift of this band, whereas MPz(18), which has the largest crown-ether rings, shows a considerable blue-shift. The behavior of the 15-crown-5 derivative is intermediate, because no appreciable shift is observed. These spectral shifts will be discussed below in terms of the aggregation and deaggregation behavior of the porphyrzine molecules.

A remarkable phenomenon of all the experiments is the disappearance of the  $n-\pi^*$  absorption around 500 nm. This is probably caused by binding of the metal ions to the  $n$ -orbitals of the peripheral sulfur atoms. A similar effect has been reported to take place when the sulfur atoms of tetrakis(1,4-dithiacyclohexeno) Pz are protonated [28b]. Of interest is the broadening of the Q-band which is observed in the experiments with the 7-crown-2 and the 15-crown-5 porphyrzines. Also in the case of the 18-crown-6 derivative a broadening occurs when the first two equivalents of the metal perchlorate are added. These effects may be related to the formation of aggregates. In order to get further insight in the aggregation behavior of the porphyrzines, we carried out EPR experiments. The results are presented in the next section.

### 7.3.3 *Electron paramagnetic resonance*

The EPR spectra of the copper derivative CuPz(18), and the  $\text{AgClO}_4$  complexes of this porphyrzine and of CuPz(15) were recorded using a porphyrzine concentration of *ca* 1 mM. Figure 7.9(A) shows the spectra of CuPz(18) recorded at

various temperatures in  $\text{CHCl}_3$ . Large variations with temperature are observed. The spectrum at 216 K is clearly axial and characteristic of a powder spectrum of a monomeric copper complex ( $g_{\parallel} = 2.135$ ,  $g_{\perp} = 2.052$ ,  $A_{\parallel} = 205$  G). Upon heating a gradual change towards an isotropic spectrum occurred, which can be explained from a more rapid tumbling of the molecules at higher temperatures, resulting in

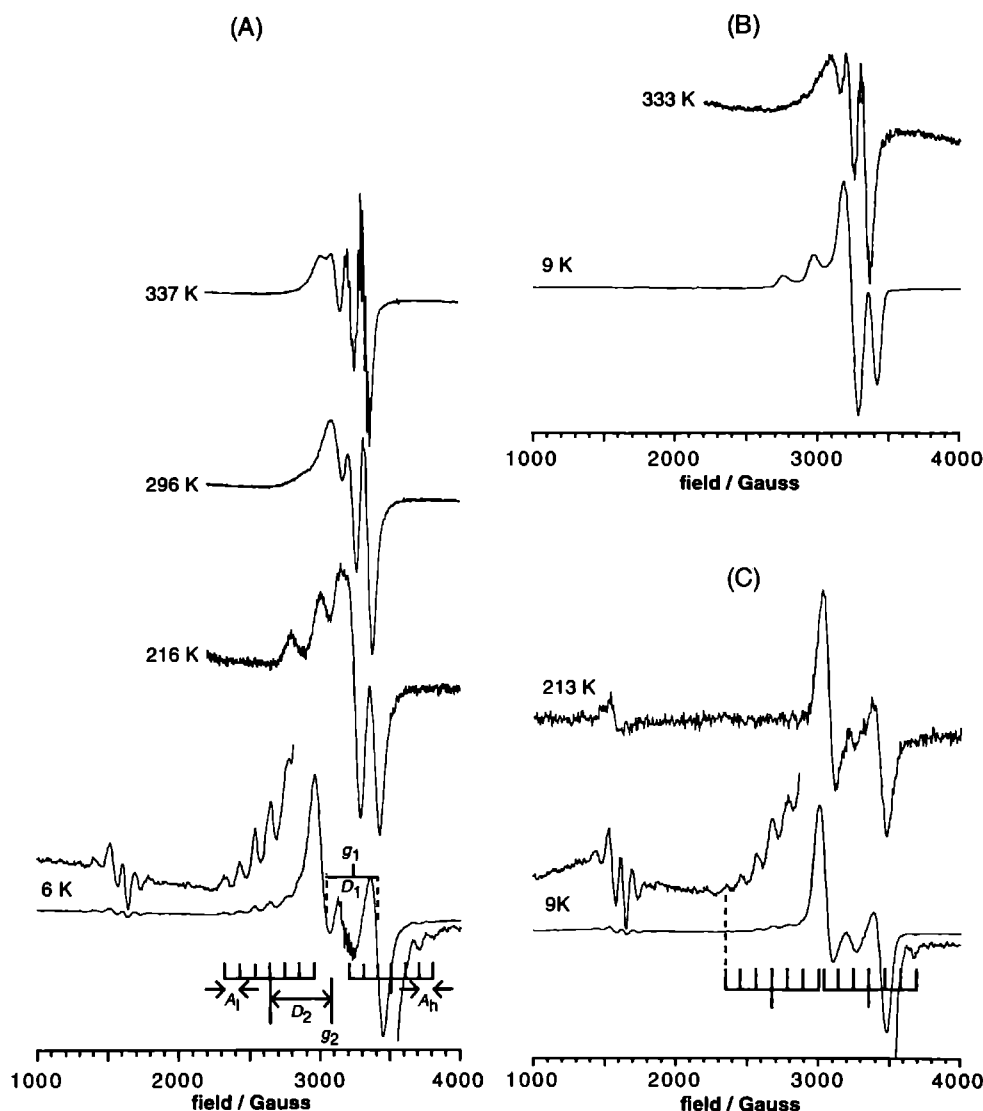


**Figure 7.9** EPR spectra of copper Pzs in  $\text{CHCl}_3$ - $\text{MeOH}$  (95:5, v/v) at various temperatures: CuPz(18) (A), CuPz(18) in the presence of 6 equiv. of  $\text{AgClO}_4$  (B), and CuPz(15) in the presence of 6 equiv. of  $\text{AgClO}_4$  (C).

an averaging of the  $g$ -tensor anisotropy. Similar effects have been reported in the literature for copper tetraphenylporphyrine [31]. When the solution was cooled below the freezing point of the solvent (210 K), a sudden change in the spectrum took place. The spectrum at 6 K (Figure 7.9(A)) is a triplet spectrum characteristic of two coupled copper nuclei, indicating that in the frozen solution dimers are present [32]. Two strong perpendicular transitions each containing seven lines are visible in the  $g = 2$  region, as well as small signals at half field. It is possible to calculate from the EPR data the distance between the two copper nuclei, using the formula [32b]:

$$D_2 = 0.65g_2^2/r^3 \quad (7.1)$$

where  $g_2$  is the average  $g$ -value of the two perpendicular transitions,  $D_2$  is the difference between  $g_2$  and the  $g$ -values of the transitions in  $\text{cm}^{-1}$ , and  $r$  is the Cu-Cu distance (see also Figure 7.9(A)). The calculated values of  $D_2$  and  $g_2$ , from which a distance of  $r = 4.1 \text{ \AA}$  can be derived, are given in Table 7.V.

Next the effect of the addition of 6 equivalents of  $\text{AgClO}_4$  on the EPR spectra of CuPz(15) and CuPz(18) was studied. The two compounds appeared to behave differently. At all temperatures between 6 and 333 K, *i.e.* both in frozen solution and in the liquid, CuPz(15) gave an EPR spectrum characteristic of a dimeric species (Figure 7.9(C)), whereas that of CuPz(18) was clearly indicative of a monomeric species (Figure 7.9(B):  $g_{\parallel} = 2.18$ ,  $g_{\perp} = 2.06$ ,  $A_{\parallel} = 206 \text{ G}$ ). In the case of CuPz(15) only a small temperature dependence was observed. The increased size of the dimeric species probably prevents the development of a fully isotropic spectrum at elevated temperatures. The spectrum recorded at 9 K was sufficiently resolved to calculate the Cu-Cu distance. We assume that the small peak which is observed at approximately 3700 G, is the outmost of the seven lines of the corresponding transition, and that the line separation is equal for the two transitions (see Figure 7.9(C)). Then a distance of  $r = 4.5 \text{ \AA}$  can be calculated from the values of  $D_2$  and  $g_2$  given in Table 7.V. The EPR spectrum of CuPz(18) in the presence of 2 equivalents of  $\text{AgClO}_4$  was

**Table 7.V** Parameters and Calculated Cu-Cu Distance ( $r$ ) from EPR Spectra of Dimeric Porphyrazines at Low Temperatures [a]

Compound	$g_1$	$g_2$	$A_{\parallel} / \text{G}$	$A_{\text{h}} / \text{G}$	$D_1 / \text{G}$	$D_2 / \text{G}$	$r / \text{\AA}$
CuPz(18)	2.045	2.136	112	105	346	424	4.1
CuPz(15)+6AgClO <sub>4</sub>	2.058	2.226	108	108	343	335	4.5

[a] See Fig. 7.9(A) for explanation of the symbols.



less well-resolved. It suggested that between 213 and 333 K a mixture of monomeric and dimeric complexes was present, as a small signal was observed at half field (results not shown).

## 7.4 Discussion

The presence of two sulfur atoms in our crown-ether porphyrazines affords the possibility of binding transition-metal ions. The X-ray structures and spectroscopic studies presented in the Results section indicate that such a binding indeed takes place. In a number of cases this leads to aggregation of the porphyrazines, *e.g.* when  $\text{AgClO}_4$  or  $\text{Hg}(\text{ClO}_4)_2$  is added to solutions of  $\text{MgPz}(7)$  and to the 15-crown-5 porphyrazines. The EPR data and the broadening of the *Q*-bands in the UV/*vis* spectra suggest that dimers are formed. Dimerization also occurs when 2 equiv. of the metal perchlorates are added to solutions of the 18-crown-6 porphyrazines. Remarkably, further addition of perchlorate to the latter compounds results in a complete dissociation of the dimers and the formation of monomeric complexes with the stoichiometry  $[\text{MPz}(18)]\cdot[\text{metal perchlorate}]_6$ . These complexes display a sharp *Q*-band which is blue-shifted with respect to the *Q*-band of the uncomplexed monomeric porphyrazine. This shift is probably caused by strong interactions of the transition-metal ions with the aromatic cores of the macrocycles [33]. The changes in the absorption spectra which occur upon addition of more than 6 equivalents of metal perchlorate to the 18-crown-6 Pzs suggest that re-aggregation takes place.

The remarkably different complexation behavior of the 15-crown-5 and 18-crown-6 porphyrazines towards silver ions can be explained as follows. As shown by the single-crystal structure of the silver complex of **2(1)**, the silver ion does not fit in the cavity of the 15-crown-5 macrocycle and one coordination site of the ion is connected to a perchlorate ion or to a neighboring ligand. A similar situation may be present in the dimeric silver complexes of  $\text{MPz}(15)$ , where the silver ions can form bridges between the two porphyrazine molecules. On the contrary, the cavity of the 18-crown-6 macrocycle is large enough to accommodate a silver ion and the coordination sites of the latter ion can be completely filled by the atoms of a single macrocycle. Any formed dimer will break up easily when more silver perchlorate is added. The fact that  $\text{MPz}(18)$  eventually forms a 6:1 guest-host complex with  $\text{AgClO}_4$  is remarkable. We tentatively propose the following structure for this species: four metal ions are bound in the crown-ether rings, while two ions are complexed to the aromatic core (Figure 7.10(A)).

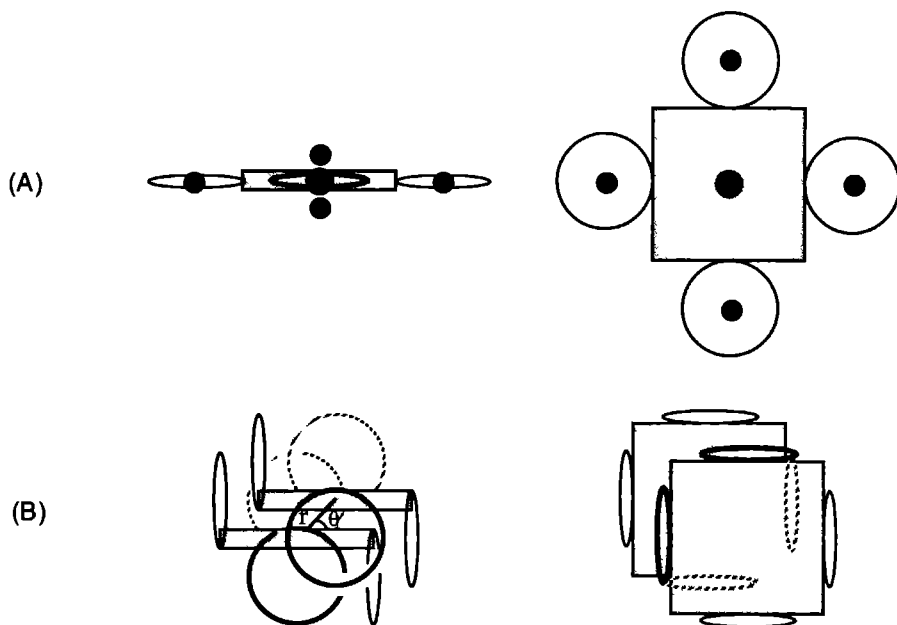


**Figure 7.10** Side view and top view of the proposed structure of the monomeric complexes between MPz(18) and 6  $\text{Ag}^+$  ions (A) and of the dimeric complex of MPz(15) and  $\text{Ag}^+$  ions with  $r = 4.5 \text{ \AA}$  and  $\theta \approx 54.7^\circ$  (B). The squares and rectangles represent the aromatic cores, the open circles are the crown-ether rings, and the filled circles are the silver ions (the latter are omitted in the complex of MPz(15) because the exact number and positions of these ions are not known).

The Q-band maxima of the dimeric complexes of MPz(15) and MPz(18) are almost unshifted when compared with the maxima of the monomeric porphyrazines. This suggests that the molecules in the dimers are not cofacially stacked, but have a slipped-stacked orientation with a tilt angle (angle between the normal of the porphyrazine plane and the center-to-center line) of approximately  $35.3^\circ$  [34]. The dimeric  $\text{AgClO}_4$  and  $\text{Hg}(\text{ClO}_4)_2$  complexes of MgPz(7) display Q-bands that are slightly red-shifted with respect to the monomer. The tilt angle of the porphyrazine moieties in these dimers must therefore be larger than  $35.3^\circ$ . From the EPR data we know that the copper-to-copper distance  $r$  in the complex of CuPz(15) with  $\text{AgClO}_4$  amounts to  $4.5 \text{ \AA}$ . From this value the interplanar distance can be calculated to be approximately  $r \times \cos 35.3 = 3.67 \text{ \AA}$ . The centers of the porphyrazine rings are shifted  $r \times \sin 35.3 = 2.60 \text{ \AA}$  along the molecular planes. The single-crystal structure of the  $\text{AgClO}_4$  complex of 15-crown-5 ether 2(1) shows that the crown-ether rings are oriented approximately perpendicular to the plane of the dicyanoethylene unit.

This makes it likely that the crown-ether rings in the  $\text{AgClO}_4$  complex of  $\text{CuPz}(15)$  also have a perpendicular orientation. Based on this assumption, and the above presented structural data from the EPR spectra we propose that the dimeric  $\text{CuPz}(15)$  complex has the structure shown in Figure 7.10(B). The porphyrazine molecules are held together by silver ions which are sandwiched between neighboring crown-ether rings.

Both the oxygen and sulfur atoms of the crown-ether rings as well as the aromatic cores of the porphyrazine rings are potential binding sites for the silver and mercury ions. This may explain why our compounds display such a great variety in complexation behavior. This feature is of great interest in view of the possible applications of our molecules in the field of molecular ionoelectronics. As postulated by Simon [2,3] a nonlinear complexation of ions is a prerequisite for developing a reliable molecular device which switches between two states. Several of our compounds meet this criterion, as can be concluded from the titration curves of  $\text{MgPz}(7)$  with  $\text{Hg}^{2+}$  (Figure 7.5(b)),  $\text{MgPz}(15)$  with  $\text{Ag}^+$  (Figure 7.6(b)),  $\text{MgPz}(18)$  with  $\text{Hg}^{2+}$  and  $\text{Ag}^+$  (Figure 7.7(b)), and from the curves of  $\text{H}_2\text{Pz}(18)$  and  $\text{CuPz}(18)$  with  $\text{Ag}^+$  (Figure 7.8(d)). The aggregation or deaggregation processes in all these cases take place above a critical concentration of ions. As will be published elsewhere [11] we also observed a difference in conducting properties between uncomplexed  $\text{H}_2\text{Pz}(18)$  and its  $\text{Ag}^+$  complex. If it would be possible to change the conductivity in a nonlinear way, then a switching device can be developed. Work along this line is in progress.

**Appendix** Summary of Crystal Data and Structure Refinement for 2(2), the AgClO<sub>4</sub> complex of 2(1), and MgPz(18)

Compound	2(2)	2(1)·AgClO <sub>4</sub>	MgPz(18) [a]
Formula	C <sub>14</sub> H <sub>20</sub> N <sub>2</sub> O <sub>4</sub> S <sub>2</sub>	C <sub>24</sub> H <sub>36</sub> Ag <sub>2</sub> Cl <sub>2</sub> N <sub>4</sub> O <sub>14</sub> S <sub>4</sub>	C <sub>56</sub> H <sub>82</sub> MgN <sub>8</sub> O <sub>17</sub> S <sub>8</sub>
Molecular weight	344.46	1015.44	1420.14
Crystal system	monoclinic	triclinic	triclinic
Space group	P2 <sub>1</sub> /c	P-1	P-1
<i>a</i> , Å	10.9310(13)	8.0687(8)	9.584(3)
<i>b</i> , Å	19.383(3)	15.793(2)	17.672(2)
<i>c</i> , Å	8.6976(14)	16.051(3)	19.620(4)
$\alpha$ , deg		116.537(11)	84.904(14)
$\beta$ , deg	108.898(11)	102.370(11)	85.21(2)
$\gamma$ , deg		90.391(9)	89.29(2)
<i>V</i> , Å <sup>3</sup>	1743.5(5)	1775.1(5)	3298.4(14)
<i>D</i> <sub>calc</sub> , g·cm <sup>-3</sup>	1.312	1.900	1.430
<i>Z</i>	4	2	2
<i>F</i> (000)	728	1016	1500
$\mu$ , cm <sup>-1</sup>	3.1	15.6	3.48
Crystal size, mm	0.30×0.50×0.80	0.28×0.28×0.55	0.10×0.10×0.63
Final <i>R</i> [b]	0.0366	0.0607	0.926
	[ <i>I</i> > 2.5σ( <i>I</i> )]	[ <i>F</i> <sup>2</sup> > 4.0σ( <i>F</i> <sup>2</sup> )]	[ <i>F</i> <sup>2</sup> > 4.0σ( <i>F</i> <sup>2</sup> )]
Final <i>R</i> <sub>w</sub> [c], no. of data	0.0504 [3056]		
Final <i>wR</i> <sub>2</sub> [d], no. of data		0.1745 [7934]	0.2525 [8608]

[a] excluding additional H<sub>2</sub>O.

[b]  $R = \sum ||F_o| - |F_c|| / \sum |F_o|$

[c]  $R_w = [\sum w (|F_o| - |F_c|)^2 / \sum w (F_o^2)]^{1/2}$

[d]  $wR_2 = [\sum w (F_o^2 - F_c^2)^2 / \sum w (F_o^2)]^{1/2}$

## References

- [1] J.-M. Lehn, *Angew. Chem.* **100** (1988) 91; *Ibid, Int. Ed. Engl.* **27** (1988) 89.
- [2] J. Simon, M.K. Engel, C. Soulié, *New J. Chem.* **16** (1992) 287.
- [3] T. Toupance, V. Ahsen, J. Simon, *J. Am. Chem. Soc.* **116** (1994) 5352.
- [4] C.C. Leznoff, A.B.P. Lever (eds.), *Phthalocyanines, Properties and Applications*, Volumes 1-3; VCH Publishers: New York, 1989-1993.
- [5] (a) O.E. Sielcken, M.M. van Tilborg, M.F.M. Roks, R. Hendriks, W. Drenth, R.J.M. Nolte, *J. Am. Chem. Soc.* **109** (1987) 4261. (b) N. Kobayashi, A.B.P. Lever, *J. Am. Chem. Soc.* **109** (1987) 7433. (c) E. Musluoglu, V. Ahsen, A. Gül, Ö Bekâroglu, *Chem. Ber.* **124** (1991) 2531. (d) G. Gümüş, Z.Z. Öztürk, V. Ahsen, A. Gül, Ö Bekâroglu, *J. Chem. Soc. Dalton Trans.* (1992) 2485. (e) A. Gürek, V. Ahsen, A. Gül, Ö Bekâroglu, *J. Chem. Soc. Dalton Trans.* (1991) 3367. (f) E. Musluoglu, A. Gürek, V. Ahsen, A. Gül, Ö Bekâroglu, *Chem. Ber.* **125** (1992) 2337. (g) M. Koçak, A.I. Okur, Ö Bekâroglu, *J. Chem. Soc. Dalton Trans.* (1994) 323. (h) A.G. Gürek, Ö Bekâroglu, *Helv. Chim. Acta* **77** (1994) 1616. (i) A.I. Okur, A. Gül, A. Cihan, N. Tan, Ö Bekâroglu, *Synth. React. Inorg. Met.-Org. Chem.* **20** (1990) 1399. (j) S. Sarigül, Ö Bekâroglu, *Chem. Ber.* **122** (1989) 291. (k) N. Kobayashi, T. Ohya, M. Sato, S.-I. Nakajima, *Inorg. Chem.* **32** (1993) 1803.
- [6] (a) O.E. Sielcken, H.C.A. van Lindert, W. Drenth, J. Schoonman, J. Schram, R.J.M. Nolte, *Ber. Bunsenges. Phys. Chem.* **93** (1989) 702. (b) O.E. Sielcken, W. Drenth, R.J.M. Nolte, *Recl. Trav. Chim. Pays-Bas* **109** (1990) 425.
- [7] (a) V. Ahsen, E. Yilmazer, A. Gül, Ö Bekâroglu, *Makromol. Chem. Rapid Commun.* **8** (1987) 243. (b) V. Ahsen, E. Yilmazer, Ö Bekâroglu, *Makromol. Chem.* **189** (1988) 2533. (c) E. Musluoglu, Z.Z. Öztürk, V. Ahsen, A. Gül, Ö Bekâroglu *J. Chem. Res. (S)* (1993) 6.
- [8] O.E. Sielcken, L.A. van de Kuil, W. Drenth, J. Schoonman, R.J.M. Nolte, *J. Am. Chem. Soc.* **112** (1990) 3086.
- [9] A. Davison, R.H. Holm, *Inorg. Synth.* **6** (1967) 8.
- [10] C.J. Pedersen, *J. Org. Chem.* **52** (1972) 66.
- [11] C.F. van Nostrum, F.B.G. Benneker, H. Brussaard, H. Kooijman, N. Veldman, A.L. Spek, J. Schoonman, M.C. Feiters, R.J.M. Nolte, to be published.
- [12] H.-J. Holdt, J. Teller, *Z. Chem.* **28** (1988) 249.
- [13] C.J. Schramm, B.M. Hofmann, *Inorg. Chem.* **19** (1980) 383.
- [14] F. Lelj, G. Morelli, G. Ricciardi, A. Roviello, A. Sirigu, *Liq. Cryst.* **12** (1992) 941.
- [15] G. Märkl, R. Vybiral, *Tetrahedron Letters* **30** (1989) 2903.
- [16] H. Hartung, R. Ahnert, D. Schollmeyer, H.-J. Holdt, J. Teller, *J. Prakt. Chem.* **334** (1992) 155.
- [17] H.-J. Holdt, *Pure Appl. Chem.* **65** (1993) 477.
- [18] J.W. Sibert, S.J. Lange, C. Stern, B.M. Hoffman, A.G.M. Barrett, *J. Chem. Soc. Chem. Commun.* (1994) 1751.
- [19] R.E. Wolf, J.R. Hartmann, J.M.E. Storey, B.M. Foxman, S.R. Cooper, *J. Am. Chem. Soc.* **109** (1987) 4328.
- [20] S.R. Cooper, S.C. Rawle, *Struct. Bonding* **72** (1990) 1.
- [21] (a) R.M. Izatt, R.E. Terry, L.D. Hansen, A.G. Avondet, J.S. Bradshaw, N.K. Dalley, T.E. Jensen, J.J. Christensen, *Inorg. Chim. Acta* **30** (1978) 1. (b) M.-T. Lai, J.-S. Shih, *Analyst* **111** (1986) 891. (c) J. Casabó, L. Mestres, L. Escriche, F.

- Teixidor, C. Pérez-Jiménez, *J. Chem. Soc. Dalton Trans.* (1991) 1969. (d) M. Sato, M. Kubo, S. Ebine, S. Akabori, *Tetrahedron Letters* **23** (1982) 185. (e) M. Oue, K. Akama, K. Kimura, M. Tanaka, T. Shono, *J. Chem. Soc. Perkin Trans. I* (1989) 1675. (f) Z. Brzozka, P.L.H.M. Cobben, D.N. Reinhoudt, J.J.H. Edema, J. Buter, R.M. Kellogg, *Anal. Chim. Acta* **273** (1993) 139. (g) H. Takeshita, B.Z. Yin, K. Kubo, A. Mori, *Bull. Chem. Soc. Jpn.* **66** (1993) 3451.
- [22] (a) N.K. Dalley, S.B. Larson, *Acta Cryst. Section B* **37** (1981) 2225. (b) R.M. Izatt, G. Wu, W. Jiang, N.K. Dalley, *Inorg. Chem.* **29** (1990) 3828. (c) F. Teixidor, J. Casabó, C. Vinas, E. Sanchez, L. Escriche, R. Kivekäs, *Inorg. Chem.* **30** (1991) 3053. (d) A.J. Blake, G. Reid, M. Schröder, *J. Chem. Soc. Dalton Trans.* (1990) 3849.
- [23] A.J. Blake, G. Reid, M. Schröder, *J. Chem. Soc. Chem. Commun.* (1992) 1074.
- [24] A.L. Spek, *Acta Crystallogr.* **A46** (1990) C34.
- [25] H.-C. Chow, R. Serlin, C.E. Strouse, *J. Am. Chem. Soc.* **97** (1975) 7230.
- [26] (a) A. Agostiano, P. Cosma, M. Della Monica, *J. Photochem. Photobiol. A: Chem.* **58** (1991) 201. (b) A. Agostiano, M. Della Monica, G. Palazzo, M. Trotta, *Biophys. Chem.* **47** (1993) 193.
- [27] N. Kobayashi, in ref. 4, Vol. 2, pp. 97-161.
- [28] (a) C.S. Velázquez, G.A. Fox, W.E. Broderick, K.A. Andersen, O.P. Anderson, A.G.M. Barrett, B.M. Hoffman, *J. Am. Chem. Soc.* **114** (1992) 7416. (b) G.P. Shaposhnikov, V.P. Kulinich, Y.M. Osipov, R.P. Smirnov, *Chem. Heterocycl. Comp.* (1986) 1036.
- [29] P. Doppelt, S. Huille, *New J. Chem.* **14** (1990) 607.
- [30] C. Weiss, H. Kobayashi, M. Gouterman, *J. Mol. Spectr.* **6** (1965) 415.
- [31] A. Pezeshk, M. Pasenkiewicz-Gierula, W.K. Subczynski, W.E. Antholine, *J. Phys. Chem.* **94** (1990) 451.
- [32] (a) N. Kobayashi, A.B.P. Lever, *J. Am. Chem. Soc.* **109** (1987) 7433. (b) M. Chikira, H. Kon, R.A. Hawley, K.M. Smith, *J. Chem. Soc. Dalton Trans.* (1979) 246.
- [33] E.A. Hall Griffith, E.L. Amma, *J. Am. Chem. Soc.* **96** (1974) 743.
- [34] (a) M. Kasha, H.R. Rawls, M. Ashraf El-Bayoumi, *Pure Appl. Chem.* **11** (1965) 371. (b) E.G. Rae, M. Kasha, in *Physical Processes in Radiation Biology*, L. Augenstein, R. Mason, B. Rosenberg (eds.); Academic Press: New York, 1964.

# ***Phthalocyanines as Gas Sensing Materials***

## **8.1 Introduction**

The semiconducting properties of phthalocyanines (Pcs) can be increased by doping the material with electron accepting or electron donating agents, thereby creating mobile holes and electrons, respectively. Also various gases are able to influence the conductivity of Pcs in this way. For this reason Pcs have been extensively studied in recent years as gas sensing materials [1]. High sensitivities have been reported. For example, the conductivities of unsubstituted Pcs are sensitive to even ppb concentrations of NO<sub>2</sub> in air [2]. There are, however, some serious draw-backs. Relatively high operating temperatures (typically 150-200 °C) are required and even then the response usually is very slow. It can take several hours to reach a saturation level [3]. Similar high temperatures are also needed for the desorption of the gas. Moreover, the gas sensor characteristics are highly dependent on the film morphology and the film thickness.

It is generally accepted that a Pc based gas sensor operates according to the following mechanism. When the sensor is exposed to an electron accepting gas such as NO<sub>2</sub>, the oxygen molecules that are initially bound to the Pc are replaced by NO<sub>2</sub> molecules. This process is followed by a charge transfer between the gas and the Pc molecules. The energy ( $\Delta E$ ) required to generate a charge carrier is given by

$$\Delta E = IP - EA - P^+ - P^- \quad (8.1)$$

where  $IP$  is the ionization potential,  $EA$  is the electron affinity, and  $P^+$  and  $P^-$  are the polarization energies of the charged species. The latter values are highly dependent on the local environment and therefore on the film morphology. The oxygen molecules adsorbed at sites with a more favorable polarization energy will be much more difficult to displace than molecules at other sites.

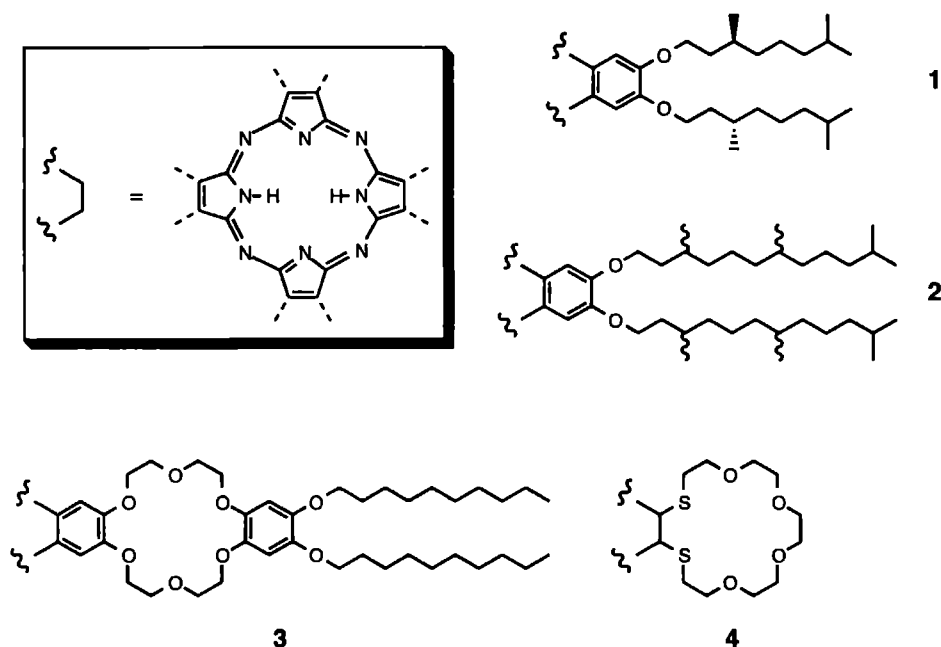
The gas sensing properties of various crown-ether substituted Pcs have recently been studied by Wright and coworkers [4]. The responses and recoveries were surprisingly good. Solution-cast films on interdigitated electrodes showed excellent and highly reversible conductivity changes at room temperature for NO<sub>2</sub> concentrations measured in the range of 1 to 5 ppm. This high reversibility can be explained from the fact that the chemisorption of NO<sub>2</sub> is only weak due to the low polarizability of the crown-ether rings ( $P^+$  in formula (8.1)). The 15-crown-5 derivative gave the best results. This may be the result of the fact that lateral electrostatic repulsions between the large surface dipoles at sites where NO<sub>2</sub> is adsorbed and neighboring adsorbed oxygen species increase the desorption rate of the latter; larger crown-ether rings lead to a greater separation of adjacently adsorbed species, which reduces the lateral repulsion, resulting in a slower response and poorer reversibility. The response and recovery rates could be further increased by treating the films with an aqueous KCl solution. This phenomenon was explained by assuming that favorable changes in the molecular assembly and the surface uniformity occurred due to the binding of the potassium ions in the crown-ether rings. As a result the number of strong adsorption sites is reduced and a slow diffusion of gases into the bulk of the film is prevented. In contrast with the untreated films, the conductivity decreased on exposure to NO<sub>2</sub>, indicating that the films had changed from a p-type to an n-type conductor. This was shown to be caused by a humidity effect [5]. The gas-sensing characteristics of the crown-ether phthalocyanine complexes are the best reported to date for an organic semiconductor film.

The use of optical sensors has certain advantages when compared to conductometric techniques. Optical sensors require only low electrical power, and they are often very sensitive, small in size, cheap, and safe. Surface plasmon resonance (SPR) potentially is a very sensitive technique for gas sensing [6]. Details regarding this technique will be presented in the next section. We used SPR to screen some of the metal free Pc derivatives that have been described before in this thesis for their gas sensing potentialities. The compounds that have been studied are given below (1-4). The SPR results will be described in section 8.5.

As outlined in chapter 2 of this thesis (section 2.5.2), Langmuir-Blodgett (LB) films have frequently been used as gas sensing materials. We have however chosen to prepare films of compounds 1-4 by spin coating from solution. Although the LB technique may provide better control over the molecular organization in the films (see previous chapters), spin coating offers some



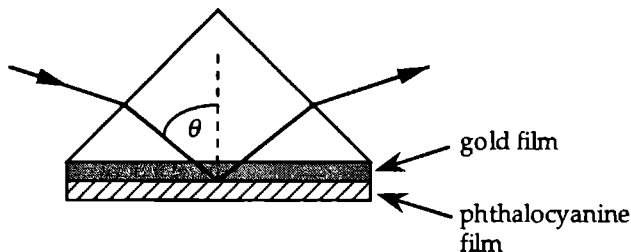
advantages over the former technique [8]. The range of compounds that can be handled with spin coating is larger, the time required for deposition is smaller, and the equipment is cheaper. Ordering is induced during deposition by forces that are associated with the circular motion and viscous flow of the material [9]. The characterization of the spin coated films of compounds 1-4, which were deposited on gold substrates, is presented in section 8.4.



## 8.2 Surface plasmon resonance

Surface plasmon polaritons (SPP) are p-polarized electromagnetic - charge density oscillations which may propagate along an interface between two media that have dielectric constants of opposite sign (*e.g.* a metal and a dielectric) [10]. When incident p-polarized light is brought into resonance with the SPP a decrease of the reflected intensity is observed. This so-called surface plasmon resonance (SPR) effect can be achieved via the Kretschmann-Raether technique of attenuated total reflection [11]. As shown in Figure 8.1, one face of a prism, with refractive index  $n_p$ , is coated with a thin metal film (with  $n_1$ ), which in turn

**Figure 8.1** Kretschmann configuration for SPR excitation.



is covered with a film of the material to be studied, having a refractive index  $n_2$ . The component of the photon wavevector parallel to the interface,  $k_x$ , depends on the angle of incidence  $\theta$  according to

$$k_x = n_p k_o \sin \theta \quad (8.2)$$

where  $k_o$  is the wavevector of light in free space. When  $k_x > n_2 k_o$ , i.e. for  $\theta$  greater than a critical angle, the radiation couples to a SPP on the outer surface of the metal film. By changing the angle of incidence it is possible to tune the wavevector of the light to equal the wavevector of the SPP on the outer metal surface. The latter value depends on the optical permittivities of the metal,  $\epsilon_1$ , and the dielectric,  $\epsilon_2$ , according to

$$k_{\text{SPP}} = \frac{\omega}{c} \sqrt{\frac{\epsilon_1 \epsilon_2}{\epsilon_1 + \epsilon_2}} \quad (8.3)$$

Formula (8.3) holds for an overlayer of infinite thickness. For a finite overlayer the optical permittivity of the environment has to be taken into account [6f]. Changes in the optical permittivity and thickness of the overlayer, for example caused by the adsorption of gas molecules, influence the momentum of the SPP and therefore the incident angle at which SPR occurs. In conclusion, the shape of the SPR curve and the angle of the reflectance minimum will depend on the optical permittivities of the prism, the metal film, the overlayer, and the environment, as well as on the thickness of the metal film and the overlayer. It is furthermore dependent on the wavelength of the incident light.

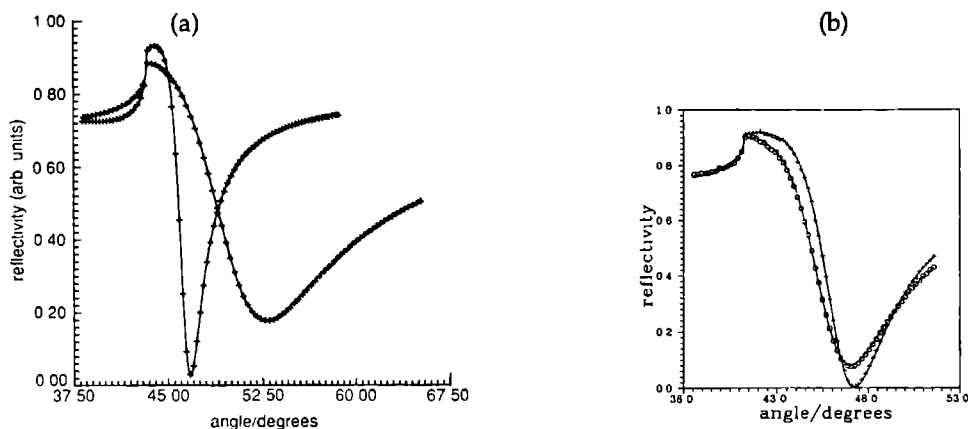


**Figure 8.2** SPR plots obtained using *p*-polarized light at 632.8 nm: for gold and gold/crown-ether-Pc films (taken from reference 6e) (a); the latter film before exposure (circles), and after 10 min. exposure to 100 ppm NO<sub>2</sub> (crosses) (taken from reference 6f) (b). The solid lines are computer fits of the data points.

Wright *et al.* have performed SPR studies on spin coated films of crown-ether substituted Pcs [6e-g]. They found (see Figure 8.2a) that the presence of a Pc layer on the gold film causes an increase of the resonance angle, and a broadening and shallowing of the reflectivity curve. Computer fitting of the SPR curves revealed that the thickness of the Pc film is inversely proportional to the rotation speed of the substrate during the spin coating process [6e]. The dielectric parameters of the Pc were found to be the same for different spin speeds, suggesting that the molecular packing and orientation are independent of the spin speed. Exposure to NO<sub>2</sub> caused an increase of the SPR angle and a decrease of the reflectivity at this angle (see Figure 8.2b) [6f]. The depth of the SPR minimum is related to the imaginary part of the permittivity (*i.e.* the optical absorption), while an increase of the angle is related to an increase in the thickness of the overlayer or an increase in the refractive index of the film (or both). Fitting the post-exposure data revealed changes in the optical permittivity as well as an 8% increase in the overlayer thickness due to the adsorption of NO<sub>2</sub> molecules onto the surface and the diffusion of these molecules into the film [6f]. Recently, a hand held sensor was developed based on SPR, which is capable of sensing NO<sub>2</sub> at sub ppm levels using crown-ether Pc films [6g].

### 8.3 Experimental section

Glass slides were cleaned by placing them in chromic acid for some hrs. Subsequently, they were washed with diluted HCl, placed in concentrated HCl for a couple of min., washed with milli-Q water, placed in a detergent solution, and finally washed again with milli-Q water and dried in a desiccator. The slides were then coated with *ca.* 40 nm of gold by vacuum sublimation. Pc films were deposited onto the gold layer as follows. The substrate was vacuum-held onto a rotating disk whose speed of rotation could be selected. A single drop of a Pc solution in chloroform was then allowed to fall onto the center of the rotating substrate. The droplet spread out and the solvent evaporated to leave a thin film of the Pc on the gold.

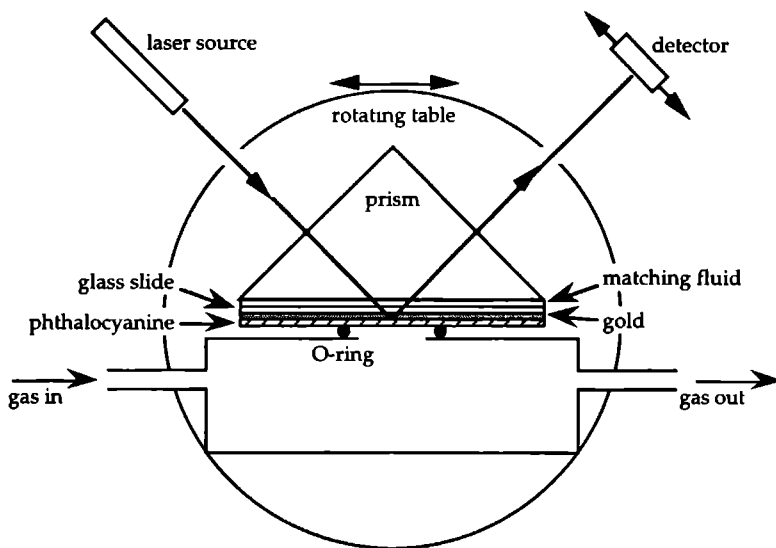


**Figure 8.3** *Experimental set-up for the SPR measurements.*

The experimental set-up for the SPR measurements is shown schematically in Figure 8.3. The substrate was placed with the Pc covered side over the hole of a gas cell using an O-ring seal. The cell contained inlet and outlet ports for the gas. A prism was clamped on top of the uncovered side of the substrate with a drop of a refractive index matching fluid (methyl benzoate) inbetween. The prism, slide, and gas cell were all mounted on a motorized rotating table with the gold-Pc interface roughly centered over the axis of rotation. P-polarized monochromatic

light (632.8 nm) was made incident onto the gold film through the prism. A photodiode detector was mounted on a table which rotated concentrically at twice the rate of the prism. Fluctuations in laser beam intensity were corrected for by ratioing the photodiode output with the output of a similar photodiode measuring the intensity of incident light via a beam-splitter inserted before the prism. Effects of ambient light variations were minimized by using a chopper in the laser beam, with lock-in amplifiers for the photodiode signals. The reflectivity  $R$  was measured against the angle of incidence on alternating exposures to dry air and 100 ppm NO<sub>2</sub>. The critical angle was found at 25.8°. The recorded SPR curves were, if necessary, shifted along the  $x$ -axis to adjust the critical angles to this value. The measured reflectivity was normalized to the reflectivity at the critical angle,  $R_c$ .

Scanning electron microscopy (SEM) was performed using a JEOL JSM-T300 scanning microscope. Ellipsometry experiments were carried out with a Gaertner L117-C single-wavelength ellipsometer ( $\lambda = 632.8$  nm). Grazing incidence reflection (GIR) Fourier-transform Infrared (FT-IR) spectra were recorded on a Bruker IFS-88 FT-IR spectrometer at 4 cm<sup>-1</sup> resolution with 1000 scans per measurement.

## **8.4 Characterization of the spin coated films**

Solutions of compounds 1-4 (*ca.* 3.0 mg·mL<sup>-1</sup>) were spin coated at a spin speed of 8000 rpm. In order to obtain different film thicknesses, the mesogenic Pc 2 was additionally deposited at spin speeds of 6000 and 4000 rpm, and crown-ether Pc 3 was also deposited using a phthalocyanine concentration of 0.3 mg·mL<sup>-1</sup>.

As could be judged by the eye almost all the substrates were fully covered with a Pc film, at least near the centers of the substrates. Only the film of 2 spun at the lowest speed was spread less homogeneously on the gold surface than the other samples.

Samples of compounds 2 and 3 spun from a solution of 3.0 mg·mL<sup>-1</sup> at 8000 rpm were investigated with the help of scanning electron microscopy (SEM) (results not shown). The sample of the former compound showed a smooth, structureless surface, whereas that of compound 3 displayed a very irregular film. This difference can be attributed to the different solubilities of the compounds. Compound 2 is completely solvated in chloroform. Phthalocyanine 3 is also

**Table 8.I.** *Relative Layer Thicknesses of Spin Coated Pc Films as Measured by Ellipsometry [a].*

Entry	Compound	Spin speed / rpm	Thickness / nm	
			Before annealing	After annealing
1	1	8000	13±1	13±2
2	2	8000	13±1	13±2
3	2	6000	18±1	16±2
4	2	4000	26±1	12±2

[a] Layer thicknesses were calculated assuming a complex refractive index of  $n = 1.50 + 0.08i$ .

soluble in this solvent but is highly aggregated (see chapter 6). Compound **3** will therefore be deposited as large aggregates, which prevents the formation of a homogeneous film.

Samples of compounds **1** and **2** were studied by ellipsometry and infrared spectroscopy. The results of the ellipsometry measurements are given in Table 8.I. The layer thicknesses were calculated assuming a complex refractive index of the film of  $n = 1.50 + 0.08i$ . As the latter value only is a rough approximation, the layer thicknesses are not absolute values. It can be concluded from Table 8.I that compounds which are spun at the same speed using the same concentration give similar film thicknesses (entries 1 and 2). Table 8.I furthermore shows that the film thickness is inversely proportional to the spinning speed (entries 2-4). The latter conclusion is in agreement with the literature [6e].

The samples that were used for the ellipsometry measurements were also investigated with the help of GIR infrared spectroscopy in order to determine the orientation of the molecules in the films. The peak intensities (results not shown) were approximately inversely proportional to the spin speed, which is in accordance with the ellipsometry results. The IR spectra were similar for different spin speeds, which suggests that the molecular orientation is independent of the spin speed. The spectra were almost similar to the solution spectra of the compounds, except for the absence of peaks at 850 and 743  $\text{cm}^{-1}$  in the spin coated films. These peaks are assigned to the out-of-plane vibration of the hydrogen atoms attached to the Pc core, and to a Pc ring deformation mode, respectively [12]. As in the GIR measurements the electromagnetic field is polarized perpendicular to the substrate, this suggests that the molecular planes are oriented perpendicular to the film plane. This is in agreement with literature data [8].

The samples were subsequently annealed for half an hour at 150 °C, whereupon the IR measurements were repeated. The spectra were similar to those before the heat treatment, except for the film of compound **2** spun at 4000 rpm. In

the latter case the out-of-plane vibrations now appeared in the spectrum. As can be seen in Table 8.I, ellipsometry measurements reveal a considerable decrease in the film thickness (or a change in the refractive index, or both) of this particular sample (entry 4). This suggests that the orientation of the molecules is lost when the sample is spun at a low speed. As mentioned above, the Pc layer of this particular sample appeared to be inhomogeneous. Defects were probably present, which allowed the molecules to change orientation at high temperatures.

## 8.5 SPR results

### 8.5.1 Compound (S)-Pc(8,2) (1)

SPR measurements on compound **1** were carried out using a film spin coated at 8000 rpm from a solution of  $3.06 \text{ mg}\cdot\text{mL}^{-1}$  in chloroform. The film was mounted in the measuring equipment, and dry air was passed over the Pc film for one hour before exposure to the  $\text{NO}_2$  gas. The SPR curves that were recorded before and during the first exposure to 100 ppm of  $\text{NO}_2$  are shown in Figure 8.4. The reaction with  $\text{NO}_2$  caused a slow decrease of the minimum reflectivity  $R_{\min}$ , and a negligible decrease of the resonance angle,  $\alpha_{\min}$ , from  $19.75^\circ$  to  $19.55^\circ$ . Figure 8.5 shows the normalized minimum reflectivity against time for the first exposure (filled circles). As can be seen from this plot the response time amounts

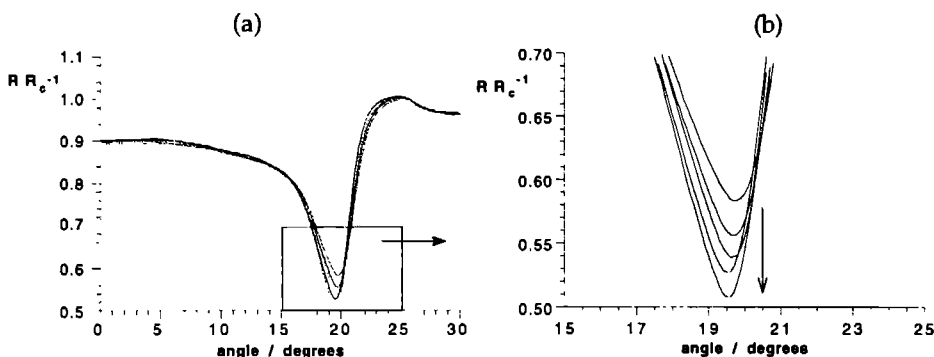


**Figure 8.4** Change of the SPR curve of a freshly prepared film of **1** during exposure to  $\text{NO}_2$  (a). Expanded view of the boxed area (b). The curves are recorded after 0, 1, 4, 7, and 20 min. of exposure (arrow in (b) indicates increasing time).

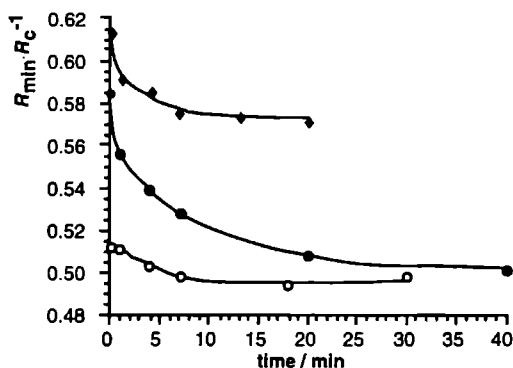


**Figure 8.5** Normalized minimum reflectivity versus time on exposure of 1 to  $\text{NO}_2$ : 1<sup>st</sup> exposure to a freshly prepared film (●); idem, 2<sup>nd</sup> exposure (○); 1<sup>st</sup> exposure to an annealed film (◆).

to approximately 20 min., during which a 14% decay of  $R_{\min}$  takes place. This decay is caused by a decrease of the optical absorption at the measuring wavelength due to the chemical reaction of the Pc with  $\text{NO}_2$  [6c,f,g].

On subsequent overnight exposure of the sample to clean air, only 14% of  $R_{\min}$  was recovered, indicating that most of the  $\text{NO}_2$  was still bound to the Pc molecules. However,  $\alpha_{\min}$  had increased to  $20.3^\circ$ . This implies a decrease in film thickness or a decrease in refractive index (or both). Probably only the surface-bound gas molecules had been removed. A second exposure of the sample to 100 ppm  $\text{NO}_2$  resulted in an immediate ( $\leq 1$  min.)  $0.35^\circ$  decrease of the resonance angle, but only a minor decrease of  $R_{\min}$  (see Figure 8.5, open circles). This result is probably due to the fast re-occupation of the binding sites on the surface of the film. However, the binding of  $\text{NO}_2$  now appeared to be irreversible. On exposure to clean air for a period of 4 hours no change occurred. The sample was therefore heated to  $120^\circ\text{C}$ , slowly cooled down, and the SPR was again measured at room temperature. When compared to the freshly prepared film, this treatment resulted in a steeper curve, a larger  $\alpha_{\min}$ , and a lower  $R_{\min}$ . Apparently, by heating the  $\text{NO}_2$  had been fully desorbed and the packing of the molecules in the film had been improved. The latter is in accordance with the observations described in chapter 4. Exposure of this annealed film to  $\text{NO}_2$  caused a faster (ca. 7 min.) but smaller response, *viz.* a decay of  $R_{\min}$  of 7%, as compared to the freshly prepared film (see Figure 8.5, filled lozenges). However, the change in  $R_{\min}$  was



now completely irreversible even after one night exposure to clean air, and a subsequent second exposure to  $\text{NO}_2$  gave hardly any response.

### 8.5.2 Compound (R,S)-Pc(12,3) (2)

A film of compound 2 was spin coated at 8000 rpm from a solution of  $3.3 \text{ mg}\cdot\text{mL}^{-1}$  in chloroform. The SPR curve of the freshly prepared sample is shown in Figure 8.6, together with the SPR curve of 1. The curve of 2 is less shallow than that of 1, which suggests that the film of the former compound is thinner. This is in contrast with the ellipsometry measurements which showed that the thicknesses of the two films were similar (*vide infra*). The latter measurements are, however, less reliable because we assumed the same refractive index for the calculation of the thicknesses of the two films.

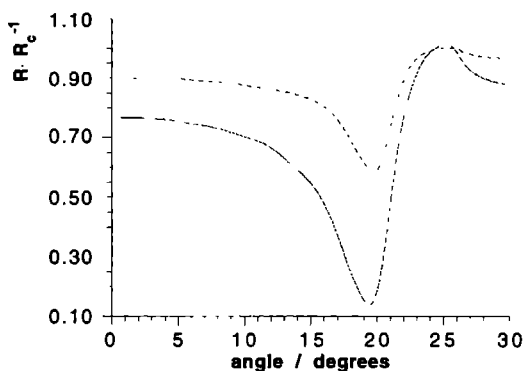


**Figure 8.6** SPR curves of freshly prepared films of compound 2 (—) and compound 1 (---).

On the first exposure to  $\text{NO}_2$  and on overnight recovery, the changes in the SPR curves of 2 were similar to those of compound 1, except that the response and reversibility were better for 2: 44% decrease of  $R_{\min}$  in 25 min. and 63% recovery in clean air (see Figure 8.7). Subsequently, a series of exposures and recoveries were applied. The results are plotted in Figure 8.7. It can be seen that

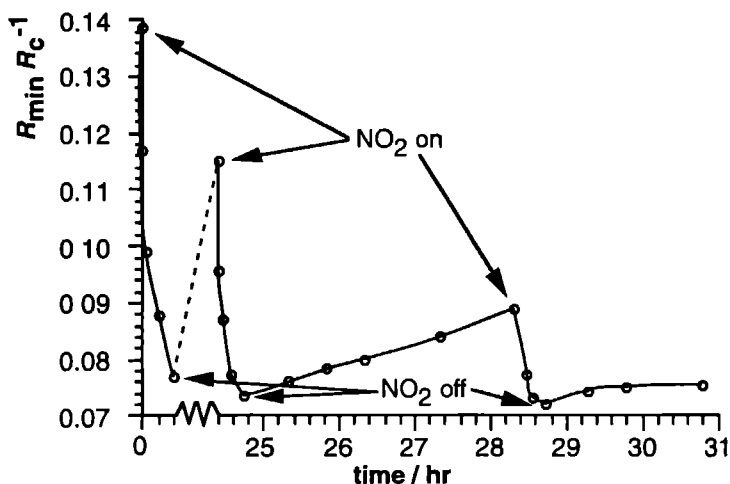


**Figure 8.7** Normalized minimum reflectivity versus time on alternating exposures of 2 to  $\text{NO}_2$  and clean air. The broken line corresponds to overnight recovery.

the recoveries are very slow and worsen in the course of the experiment. As a result the responses decrease. After a total of 5 exposures, recovery and response could no longer be observed. Apparently, saturation of the sample had occurred.

### 8.5.3 Crown-ether phthalocyanine (3)

Measurements on compound **3** were carried out using two film thicknesses, which were obtained by spin coating solutions of  $0.3 \text{ mg mL}^{-1}$  and  $3.7 \text{ mg mL}^{-1}$  of **3** at 8000 rpm. The thicker film showed a more shallow SPR curve and a lower resonance angle than the thinner film. Moreover, its response to the first  $\text{NO}_2$  exposure was much faster. The response times for the thin and thick films amounted to *ca.* 25 hours and 30 min, respectively (Figure 8.8). During these periods an 11% decrease of  $R_{\text{min}}$  was observed for both films. Interestingly, first a decrease of the resonance angle  $\alpha_{\text{min}}$  was observed and subsequently a sudden increase, as illustrated in Figure 8.8. This behavior is opposite to what has been reported for ordinary crown-ether substituted Pcs [6g]. Our results can be explained by assuming that first an increase of the film thickness occurs, due to

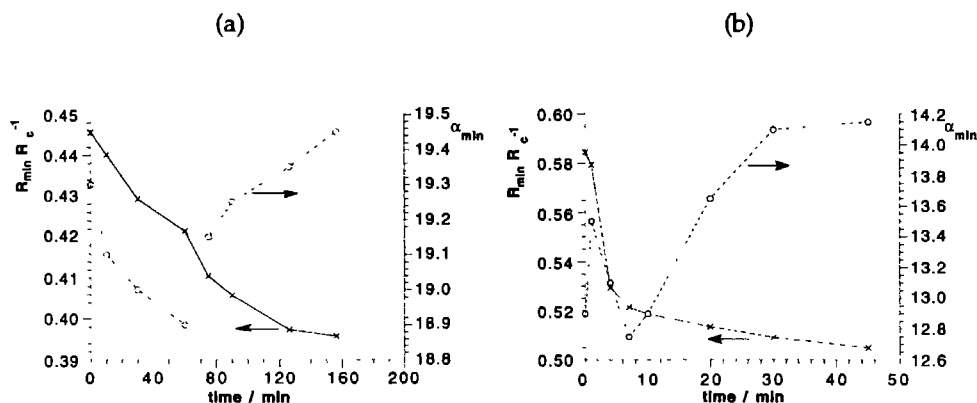


**Figure 8.8** Normalized minimum reflectivity and resonance angle versus time on exposure of freshly prepared films of 3 to NO<sub>2</sub>: thin film (a), thick film (b).

binding of NO<sub>2</sub> on the surface of the material, followed by reaction of NO<sub>2</sub> in the bulk of the film. The latter probably causes a decrease in the refractive index.

Next, both films were exposed to clean air for one night, which resulted in a further increase of the resonance angles. The thicker film showed a 48% recovery of  $R_{\min}$ , which indicates desorption of NO<sub>2</sub> from the surface of the film. On the contrary, the thinner film displayed a further slight decrease of  $R_{\min}/R_c$  to 0.3884 and an increase of  $\alpha_{\min}$  to 20.0°, which suggests that the overnight exposure to clean air had allowed NO<sub>2</sub> molecules to diffuse from the surface into the bulk of the film. This behavior was further developed by annealing the film at 155 °C. The SPR curve recorded at room temperature after this treatment showed values of  $\alpha_{\min} = 20.25^\circ$  and  $R_{\min}/R_c = 0.3350$ .

A second exposure of the thicker film to NO<sub>2</sub> caused a small but very fast response. In less than 4 min.  $R_{\min}$  decreased by 6.5%, accompanied with a 0.85° shift of  $\alpha_{\min}$  to lower angle. This result can be attributed to binding of NO<sub>2</sub> molecules on the surface of the film. Subsequent exposure of the thick film to clean air resulted in a slow, but distinct (30% in 2 hours) recovery of the reflectivity. The resonance angle shifted towards its value before the second exposure to NO<sub>2</sub>. The third exposure to NO<sub>2</sub> gave the same response as the previous one, but the recovery was rather poor. Therefore, this film was also heated to 155 °C.

Both annealed films were again exposed to NO<sub>2</sub> at room temperature. A rather fast response was observed (ca. 10 min.) with a small decrease of  $\alpha_{\min}$ , which indicates that only reaction of NO<sub>2</sub> on the surface of the film had occurred.

Probably the binding sites in the bulk of the film were still occupied. Unfortunately, the process appeared to be irreversible: three days of exposure to clean air at room temperature, followed by a second exposure to NO<sub>2</sub> gave no response at all. Apparently, the heat treatment changed the morphology of the film in such a way that NO<sub>2</sub> molecules were not only bound strongly on sites in the bulk material, but also on the surface.

#### **8.5.4 Crown-ether porphyrazine (4)**

A solution of 2.44 mg·mL<sup>-1</sup> of compound 4 in chloroform was prepared and spin coated at 8000 rpm, and SPR curves were recorded before and during exposure to 100 ppm of NO<sub>2</sub>. After 20 min. of exposure no response could be observed. The oxidation potentials of porphyrazines are known to be larger than those of phthalocyanines [13]. Electron transfer reaction between porphyrazine 4 and NO<sub>2</sub> molecules may therefore be an unfavorable process.

### **8.6 Conclusions**

Three mesogenic Pcs and one crown-ether substituted porphyrazine have been screened for their gas sensing properties with the help of the SPR technique. The crown-ether compound showed no response on exposure to 100 ppm NO<sub>2</sub>, probably as the result of its large ionization potential. This feature, which needs further study, may however be useful for selectively sensing other gases than NO<sub>2</sub>. A common feature of the mesogenic Pcs is their poor reversibility at room temperature after exposure to NO<sub>2</sub>. The sensor containing compound 1 was fully reversible only when it was heated for some time. After this treatment it exhibited a relatively fast response. Compound 2 showed better responses and recoveries at room temperature than 1, but only for a few measuring cycles. The reason for this behavior is unclear. It is possibly caused by a different morphology of the samples, about which too little is known at present.

A thick film of compound 3 absorbed NO<sub>2</sub> irreversibly in the bulk of the material, which can be attributed to the proposed heterogeneity of the film. The gas molecules that were bound on the surface of the film could be removed at least once by heating the sample in air. The slow reversibility at ambient temperature is probably due to the size of the substituents: the large separation of

the pc cores reduces the lateral repulsion between absorbed NO<sub>2</sub> molecules and hence their desorption. The thinner film of the same compound behaved differently. Its response on the first exposure to NO<sub>2</sub> was much slower than that of the thicker film. Moreover, NO<sub>2</sub> was not desorbed on subsequent exposure to clean air at ambient or elevated temperature. Instead diffusion of molecules from the surface into the bulk of the sample occurred. Probably, the film morphology of the two samples is very different.

The studies described in this chapter are preliminary in character and more work is required to completely understand the relation between molecular structure, film morphology, and gas sensing characteristics of the materials. A well-defined organic film is a prerequisite for obtaining reliable and reproducible gas sensing properties. This is a challenge for chemists that are active in the field of supramolecular chemistry.

## References

- [1] J.D. Wright, *Prog. Surf. Sci.* **31** (1989) 1.
- [2] T.A. Jones, B. Bott, *Sensors Actuators* **5** (1984) 43.
- [3] A. Wilson, J.D. Wright, *Mol. Cryst. Liq. Cryst.* **211** (1992) 321.
- [4] P. Roisin, J.D. Wright, R.J.M. Nolte, O.E. Sielcken, S.C. Thorpe, *J. Mater. Chem.* **2** (1992) 131.
- [5] J.D. Wright, P. Roisin, G.P. Rigby, E. Erkizia, R.J.M. Nolte, S.C. Thorpe, *Sensors Actuators B* **15-16** (1993) 301.
- [6] (a) P.S. Vukusic, G.P. Bryan-Brown, J.R. Sambles, *Sensors Actuators B* **8** (1992) 155. (b) C. Nylander, B. Liedberg, T. Lind, *Sensors Actuators* **3** (1982/1983) 79. (c) J.P. Lloyd, C. Pearson, M.C. Petty, *Thin Solid Films* **160** (1988) 431. (d) J. O'Donnell, C.L. Honeybourne, *J. Phys. Cond. Mat.* **3** (1991) S337. (e) P.S. Vukusic, J.R. Sambles, J.D. Wright, *J. Mater. Chem.* **2** (1992) 1105. (f) M.J. Jory, P.S. Cann, J.R. Sambles, *J. Phys. D. Appl. Phys.* **27** (1994) 169. (g) S.J. Peacock, V. Rivalle, J.D. Wright, H.C. Jagers, in *Sensors VI: Technology, Systems and Applications*, K.T.V. Grattan (ed.); Hilger: Bristol (1993), p. 15.
- [7] P.G. Schouten, J.F. van der Pol, J.W. Zwikker, W. Drenth, S.J. Picken, *Mol. Cryst. Liq. Cryst.* **195** (1991) 291; *ibid* **208** (1991) 109.
- [8] G.C. Bryant, M.J. Cook, C. Ruggiero, T.G. Ryan, A.J. Thorne, S.D. Haslam, R.M. Richardson, *Thin Solid Films* **243** (1994) 316.
- [9] S.M. Critchley, M.R. Willis, Y. Maruyama, S. Bandow, M.J. Cook, J. McMurdo, *Mol. Cryst. Liq. Cryst.* **229** (1993) 47.
- [10] E. Burstein, W.P. Chen, Y.J. Chen, A. Hartstein, *J. Vac. Sci. Technol.* **11** (1974) 1004.
- [11] E. Kretschmann, H. Raether, *Z. Naturforschung* **23a** (1968) 2135.
- [12] T. Sauer, T. Arndt, D.N. Batchelder, A.A. Kalachev, G. Wegner, *Thin Solid Films* **187** (1990) 357.
- [13] E. Ortí, M.C. Piqueras, R. Crespo, J.L. Brédas, *Chem. Mater.* **2** (1990) 110.

## Summary

Molecular materials are composed of molecular units that are synthesized separately and subsequently organized to form a so-called supramolecular structure. To obtain *functional* materials which can find application in *e.g.* the field of molecular electronics, the molecular units must have specific electronic, optical, or catalytic properties. In addition, these units must contain structural or physical information to allow them to self-organize into ordered structures. A class of compounds which exhibits these properties is that of the phthalocyanines. These molecules are disc-like, have a high stability, and possess interesting electronic and optical properties. Previous work in our group has shown that one-dimensional transport of energy and charge can take place in columns formed by stacked liquid-crystalline phthalocyanines.

This thesis describes the synthesis, characterization, and self-organizing properties of a number of novel phthalocyanine derivatives. In order to induce organization, these molecules were modified in such a way as to give them liquid-crystalline properties. Another method used to achieve a degree of organization involved the use of the Langmuir-Blodgett technique.

Phthalocyanines containing long flexible side-chains are thermotropic liquid-crystalline, *i.e.* they display a transition from the crystalline to the liquid-crystalline phase (or mesophase) at elevated temperatures. When branched side-chains are connected to the phthalocyanine core, the compounds become liquid-crystalline at room temperature, as was shown for a chiral phthalocyanine with (*S*)-3,7-dimethyloctoxy substituents. Due to these chiral substituents the molecules in the mesophase are stacked in left-handed helical columns. The effect of the helical structure on the intracolumnar charge and energy migration was investigated. Solid-state NMR techniques were used to obtain information on the molecular dynamics of these systems.

Other phthalocyanines that were synthesized possess thermotropic as well as lyotropic liquid-crystalline properties. Because of this combination of properties they are called amphotropic. One of these amphotropic phthalocyanines contained tertiary amino groups at the end of the side-chains, which made this compound soluble in diluted aqueous acetic acid. Small columnar aggregates were found to be present in this solvent. Extremely large aggregates were formed in chloroform solution by a crown-ether substituted liquid-crystalline phthalocyanine. These aggregates could be visualized with the help of electron microscopy, which showed

the presence of single strands of micrometer length and diameters that equal the diameter of a single molecule. These strands, which consist of more than  $10^4$  molecules, can be considered to be multiwired molecular cables. They contain a central electron wire composed of stacked phthalocyanine units, and four ion channels formed by stacked crown-ether rings, surrounded by an "insulating" hydrocarbon mantle.

The Langmuir-Blodgett (LB) technique is a method to construct well-defined multilayers. Molecules are spread on a water surface to form a film, which is transferred in steps onto a substrate. The phthalocyanines previously mentioned are capable of forming transferrable monolayers at the air-water interface. In the case of the chiral phthalocyanine the most stable film was a bilayer in which the molecules are oriented with their planes perpendicular to the water surface. A derivative of the crown-ether phthalocyanine was shown to form a monolayer in which the molecular units are lying horizontally on the water surface with their substituents oriented vertically. This monolayer can bind alkali metal ions from the subphase. The phthalocyanine with tertiary amino substituents can adopt various orientations at the air-water interface as was concluded from experiments at different surface pressures in a LB trough. We also investigated the formation of monolayers and LB films from a polymethacrylate with phthalocyanine units in its side-chains. A monolayer of this polymer expanded slowly when a constant surface pressure was applied. This expansion is due to a slow conformational change of the alkoxy chains present in the polymer.

Porphyrazines are a class of compounds related to the phthalocyanines. In continuation of previous studies in our group on crown-ether substituted phthalocyanines, we synthesized novel porphyrazines with sulfur containing crown-ether substituents. The structure of one of these compounds was determined by single-crystal X-ray diffraction. The presence of the sulfur atoms allowed the binding of transition metal ions. It was found that the addition of silver ions induced aggregation of the porphyrazines.

Finally, we investigated the application of some of the afore mentioned compounds as gas-sensor materials. Preliminary experiments on spin coated films showed that especially the liquid-crystalline phthalocyanines are potentially interesting materials for use in sensors, which detect  $\text{NO}_x$  gases by the surface plasmon resonance technique.



## Samenvatting

Moleculaire materialen zijn opgebouwd uit moleculaire eenheden die afzonderlijk worden gesynthetiseerd en vervolgens worden geordend tot een supramoleculaire structuur. Om *functionele* materialen te verkrijgen, voor toepassing in bijvoorbeeld de moleculaire elektronica, moeten de moleculaire eenheden specifieke eigenschappen bezitten, bijvoorbeeld elektronische, optische of katalytische eigenschappen. Daarnaast moeten deze eenheden structurele of fysische informatie bevatten om zichzelf te kunnen organiseren tot geordende structuren. Een klasse van verbindingen met zulke kenmerken is die van de ftalocyaninen. Deze moleculen zijn schijfvormig, zeer stabiel en uit elektronisch en optisch oogpunt interessant. Eerder werk in onze groep heeft aangetoond dat één-dimensionaal transport van energie en lading kan plaatsvinden in kolommen die gevormd worden door gestapelde vloeibaar-kristallijne ftalocyaninen.

Dit proefschrift beschrijft de synthese, karakterisering en de zelf-organiserende eigenschappen van een aantal nieuwe ftalocyaninederivaten. Om deze moleculen te assembleren is gebruik gemaakt van vloeibaar-kristallijn gedrag, aggregatie in oplossing en de vorming van langmuir-blodgett-films.

Ftalocyaninen waaraan lange flexibele zijstaarten zijn bevestigd, bezitten thermotroop vloeibaar-kristallijne eigenschappen, dat wil zeggen dat ze bij verhoogde temperatuur een overgang van een kristallijne naar een vloeibaar-kristallijne fase (ofwel mesofase) vertonen. Indien de zijstaarten vertakt zijn bevindt het materiaal zich al bij kamertemperatuur in de mesofase, zoals kon worden aangetoond voor een chiraal ftalocyanine met (S)-3,7-dimethyloctoxy zijketens. De moleculaire chiraliteit zorgt ervoor dat de moleculen in de mesofase gestapeld zijn in de vorm van kolommen met een linksdraaiende schroef. Het effect van deze structuur op de migratie van lading en excitonen door de kolommen is onderzocht. De moleculaire dynamica van de systemen is bestudeerd met behulp van vaste-stof-NMR-technieken.

Andere ftalocyaninen die in dit proefschrift worden beschreven, vertonen zowel thermotroop als lyotroop vloeibaar-kristallijn gedrag. Dit laatste betekent dat ze ook in oplossing kolomnaire aggregaten vormen. Deze combinatie van eigenschappen wordt aangeduid met de term amfotroop. Een van de ftalocyaninen bezit tertiaire aminogroepen aan het eind van zijn zijstaarten, waardoor de verbinding oplosbaar is in verdund azijnzuur, maar daarbij slechts kleine aggregaten vormt. Zeer grote aggregaten ontstaan wanneer een kroonether-

gesubstitueerde ftalocyanine wordt opgelost in chloroform. Deze aggregaten konden zichtbaar worden gemaakt met behulp van elektronenmicroscopie. Hierbij zijn afzonderlijke strengen van moleculen te zien die een lengte bezitten van enkele micrometers (meer dan  $10^4$  moleculen) en een diameter die gelijk is aan de diameter van één enkel molecuul. Deze strengen kunnen beschouwd worden als moleculaire coaxkabels. Ze bezitten een centrale elektronendraad bestaande uit gestapelde ftalocyanine-eenheden en vier ionenkanalen gevormd door gestapelde kroonether-ringen. Het geheel is omgeven door een "isolerende" koolwaterstof-mantel.

De langmuir-blodgett (LB)-methode is een bekende manier om goed-gedefinieerde multilagen te construeren. Daarbij wordt een stabiele monomoleculaire laag van een verbinding op een wateroppervlak laag voor laag overgebracht op een substraat. De drie tot dusver genoemde ftalocyaninen zijn in staat om stabiele, overdraagbare films te vormen op het grensvlak van lucht en water. In het geval van het chirale ftalocyanine is de meest stabiele film een bilaag waarin de vlakken van de moleculen vertikaal staan ten opzichte van het wateroppervlak. Een derivaat van het kroonetherftalocyanine vormt een monolaag waarbij de moleculen zich in horizontale positie op het wateroppervlak bevinden met de staarten loodrecht op dit oppervlak. Deze monolaag is in staat om kationen uit het water te binden en wel in de kroonetherringen. Het ftalocyanine met de tertiaire aminosubstituenten doorloopt bij geleidelijke verkleining van het monolaagoppervlak verschillende fasen waarbij de moleculen steeds andere orientaties innemen. De vorming van monolagen en LB-films werd ook bestudeerd in het geval van een polymethacrylaat met ftalocyanine-eenheden in de zijketens. Een monolaag van dit polymeer bleek langzaam te expanderen bij een constante oppervlaktedruk, hetgeen kon worden toegeschreven aan een conformatieverandering van de aanwezige alkoxyketens.

Porfyrzinen zijn aan ftalocyanine verwante verbindingen. In het verlengde van eerdere studies in onze groep aan kroonethergesubstitueerde ftalocyaninen hebben we nieuwe porfyrzinen gesynthetiseerd met kroonethersubstituenten die zwavelatomen bevatten. De structuur van één van deze verbindingen kon worden bepaald met röntgendiffractie. De aanwezigheid van de zwavelatomen in de kroonetherringen maakt dat de moleculen in staat zijn om overgangsmetaalionen te binden. Gevonden werd dat bij binding van zilverionen in oplossing aggregatie van de porfyrzinen optreedt.

Tenslotte hebben we de mogelijkheden onderzocht om een aantal van bovengenoemde verbindingen toe te passen in gassensoren. Oriënterende

experimenten met behulp van surface-plasmon-resonantie aan films die verkregen zijn met de spin-coating-techniek hebben aangetoond dat met name vloeibaar-kristallijne ftalocyaninen geschikt zijn om te worden gebruikt in sensoren voor NO<sub>x</sub>.



## *Curriculum Vitae*

De schrijver van dit proefschrift werd geboren op 28 maart 1966 te Vinkeveen en Waverveen. In juni 1984 behaalde hij het diploma gymnasium- $\beta$  aan het Mgr. Zwijsen College te Veghel. In hetzelfde jaar werd begonnen met de studie scheikunde aan de Katholieke Universiteit Nijmegen. Het propaedeutisch examen werd afgelegd in juli 1985. In februari 1990 werd het doctoraal examen behaald met als uitgebreid hoofdvak Organische Chemie (Prof. B. Zwanenburg) en als uitgebreid bijvak Biochemie (Prof. H.P.J. Bloemers).

Van maart 1990 tot en met februari 1994 was de schrijver werkzaam aan de Katholieke Universiteit Nijmegen als Assistent in Opleiding bij de vakgroep Organische Chemie. Aldaar werd onder leiding van Prof. Dr. R.J.M. Nolte het in dit proefschrift beschreven onderzoek uitgevoerd.



